

INVESTIGATION OF THE RECHARGE AND DISCHARGE MECHANISMS
OF A COMPLEX AQUIFER SYSTEM BY USING ENVIRONMENTAL
ISOTOPES AND NOBLE GASES

A THESIS SUBMITTED TO
THE GRADUATE SCHOOL OF NATURAL AND APPLIED SCIENCES
OF
MIDDLE EAST TECHNICAL UNIVERSITY

BY

ŞEBNEM ARSLAN

IN PARTIAL FULFILLMENT OF THE REQUIREMENTS
FOR
THE DEGREE OF DOCTOR OF PHILOSOPHY
IN
GEOLOGICAL ENGINEERING

FEBRUARY 2008

Approval of the thesis:

**INVESTIGATION OF THE RECHARGE AND DISCHARGE MECHANISMS OF
A COMPLEX AQUIFER SYSTEM BY USING ENVIRONMENTAL ISOTOPES
AND NOBLE GASES**

submitted by **ŞEBNEM ARSLAN** in partial fulfillment of the requirements for the degree of **Doctor of Philosophy in Geological Engineering Department, Middle East Technical University** by,

Prof. Dr. Canan Özgen
Dean, Graduate School of **Natural and Applied Sciences**

Prof. Dr. Vedat Doyuran
Head of Department, **Geological Engineering**

Prof. Dr. Hasan Yazıcıgil
Supervisor, **Geological Engineering Dept., METU**

Prof. Dr. Peter Schlosser
Co-Supervisor, **Earth and Envr. Sci. Dept., Columbia University**

Examining Committee Members:

Prof. Dr. Serdar Bayarı
Geological Engineering Dept., HÜ

Prof. Dr. Hasan Yazıcıgil
Geological Engineering Dept., METU

Prof. Dr. Nilgün Güleç
Geological Engineering Dept., METU

Prof. Dr. Mehmet Ekmekçi
Geological Engineering Dept., HÜ

Assoc. Prof. Dr. Zeki Çamur
Geological Engineering Dept., METU

Date: 06/02/2008

I hereby declare that all information in this document has been obtained and presented in accordance with academic rules and ethical conduct. I also declare that, as required by these rules and conduct, I have fully cited and referenced all material and results that are not original to this work.

Name, Last name: Şebnem Arslan

Signature :

ABSTRACT

INVESTIGATION OF THE RECHARGE AND DISCHARGE MECHANISMS OF A COMPLEX AQUIFER SYSTEM BY USING ENVIRONMENTAL ISOTOPES AND NOBLE GASES

Arslan, Şebnem

Ph.D., Department of Geological Engineering

Supervisor : Prof. Dr. Hasan Yazıcıgil

Co-Supervisor: Prof. Dr. Peter Schlosser

February 2008, 180 pages

This study aims to determine the recharge, discharge and the mixing mechanisms of a complex aquifer system located above the Kazan trona ore field using the environmental isotopes of deuterium, oxygen-18, carbon-13 and carbon-14, chlorofluorocarbons (CFC-11, CFC-12 and CFC-113) and the noble gas isotopes (He, Ne, Ar, Kr and Xe).

The groundwater system consists of three different aquifers: shallow, middle and deep. The Akpınar formation lying between deep and middle systems acts as an aquitard.

Oxygen-18 and deuterium data showed an isotopic contrast between the shallow and deeper aquifer systems and even between the unconfined and confined parts of the middle and deep aquifers. The Noble gas temperatures indicated the average yearly air temperatures in shallow aquifer system whereas the recharge temperatures came out to be lower than today's in deep groundwater system. This finding is also supported by the dissolved inorganic carbon's radiocarbon activities being close to the detection limits in the same system. These activities together with the stable isotope data revealed there might be evidence of recharge to the middle and deep aquifer systems under colder climate conditions during the late Pleistocene

CFC concentrations indicated modern recharge to the shallow aquifer system, whereas the concentrations were close to the detection limits therefore CFC's were unable to date the middle and deep aquifer systems however proved the existence of modern recharge to this system.

Mantle-He escape to shallow aquifer system is believed to be along a deep buried fault system located in downgradient areas.

Keywords: Kazan Trona Basin, Complex Aquifer System, Recharge and Discharge Mechanisms, Environmental Isotopes, Noble Gases.

ÖZ

KOMPLEKS AKİFER SİSTEMLERİNDE BESLENİM VE BOŞALIM MEKANİZMALARININ ÇEVRESEL İZOTOPLAR VE ASAL GAZLAR ARACILIĞIYLA BELİRLENMESİ

Arslan, Şebnem

Doktora, Jeoloji Mühendisliği Bölümü

Tez Yöneticisi : Prof. Dr. Hasan Yazıcıgil

Ortak Tez Yöneticisi: Prof. Dr. Peter Schlosser

Şubat 2008, 180 sayfa

Bu çalışmanın amacı, doğal bir mineral olan ve Kazan Havzasında bulunan trona rezervi üstünde oluşmuş kompleks bir akifer sisteminin beslenme ve boşalım mekanizmalarının oksijen, hidrojen ve karbon elementlerinin çevresel izotopları, kloroflorokarbonlar ve asal gazlar aracılığıyla belirlenmesidir. Bu kompleks sistem sığ, orta ve derin olmak üzere üç akiferden oluşmaktadır. Orta ve derin sistemleri ayıran Akpınar formasyonu akitard özelliği taşımaktadır.

Oksijen-18 ve döteryum sonuçları sığ ve derin akifer sistemleri ve aynı akifer sistemi içerisinde serbest ve basınçlı bölgeler arasında güçlü bir izotopik zıtlık olduğunu ortaya koymuştur. Asal gaz sıcaklıkları sığ akifer sistemde yıllık ortalama hava sıcaklıklarını gösterirken, derin sistemde günümüz koşullarından daha düşük sıcaklıklar ortaya çıkmıştır. Bu sonuç, çok düşük olan radyokarbon aktiviteleriyle de desteklenmiştir. Bu aktiviteler kararlı izotop verileriyle birlikte orta ve derin akifer sistemlerine farklı iklim koşullarında beslenme olduğunu göstermektedir. Bu beslenme günümüz koşullarından daha soğuk bir ortamda gerçekleşmiştir.

Kloroflorokarbon konsantrasyonları sığ akifer sisteminde günümüz koşullarında beslenim olduğunu göstermektedir. Bu teknik ile orta ve derin akifer sistemlerinde sağlıklı bir yaşlandırmaya yapmak mümkün değildir fakat bu sistemlerde ölçülebilir miktarda kloroflorokarbon bulunması sistemlere modern beslenimi kanıtlar.

Sığ akifer sisteminde ölçülen toplam helyum konsantrasyonlarında manto katkısı bulunduğundan dolayı bu gazın mantodan kaçıışı ve sığ akiferde gözlenmesi derin bir fay sisteminin varlığını ispatlamaktadır.

Anahtar Kelimeler: Kazan Havzası, Kompleks Akifer Sistemi, Beslenim ve Boşalım Mekanizmaları, Çevresel İzotoplar, Asal Gazlar.

TO MY BELOVED FAMILY...

ACKNOWLEDGMENTS

This thesis would have been impossible without the tremendous support, encouragement, trust and help from many people. To begin with, the author would like to express her deepest gratitude to Fulbright Commission of Turkey. The journey to Lamont- Doherty Earth Observatory of Columbia University (L-DEO) starting with Fulbright fellowship made this research and this thesis possible.

The author is thankful to her supervisor, Prof. Dr. Hasan Yazıcıgil for directing her according to her interests, guiding her to the field of isotopes, letting her to explore how to solve the puzzles of an aquifer system by the help of environmental isotopes. His help to organize the field trips are also appreciated.

During the research, the author had the honor of working with a variety of tremendously smart, motivated and gracious people. The support, guidance and advices of the co-supervisor of this study Prof. Dr. Peter Schlosser and Prof. Dr. Martin Stute are gratefully acknowledged. Being the primary advisor at L-DEO, Prof. Dr. Peter Schlosser provided the author with every possibility for this study. His contribution in every each step of the research is deeply appreciated.

Saying thank you to Prof. Dr. Martin Stute will never be enough. He was the inspiration of the author during research with his unique talent, ability and enthusiasm to teach and his success in the field of isotope hydrogeology. He made all the sampling feasible by providing the necessary equipment and backup. His guidance and his help during the interpretation of the results are also deeply appreciated.

The author would like to thank Prof. Dr. Richard Fairbanks and Richard Mortlock for their help during stable isotope measurements, Bill Smethie and Eugene Gorman for valuable assistances during chlorofluorocarbon measurements, Lex Van Geen, and Zhongqi Cheng for their help with the water chemistry measurements. Martin Stute and

Linda Baker are appreciated for noble gas measurements. Debbie Criscione offered help whenever the author needed. Her advices and encouragement are appreciated.

The author wishes to express her deepest gratitude to the committee member of this thesis Prof. Dr. Mehmet Ekmekçi for his guidance, advice and criticism. Comments, suggestions and encouragement of Prof. Dr. Nilgün Güleç are appreciated. The author also expresses her gratitude to examining committee members of the thesis Prof. Dr. Serdar Bayarı and Doç Dr. Zeki Çamur for their valuable suggestions.

The field assistances of Faruk Suluki, Ömer Kahraman, Uğur Öztürk, Lütfü Şimşek, Necip Ökten and the technical assistances of Jale Şakıyan Ateş and N. Nur Özyurt are gratefully acknowledged.

Funding for the radiocarbon and stable isotope analyses are provided by The Scientific and Technological Research Council of Turkey (TUBITAK) Grant No: 106Y310.

The author would also like to express grateful appreciation to her husband Orhan Arslan, to her parents Prof. Dr. İlker Ökten and Prof. Dr. Feyhan Ökten, to her father-in-law Osman Arslan and mother-in-law Sevim Arslan, her grandparents and to her sister Buket Ökten for their patience, unconditional love, and encouragement during the preparation of this thesis. Having such a family is a life-time privilege.

Last but not least, sincere thanks to my friends and colleagues M. Deniz Küstü, Selin Süer, Ceren Küçükuysal, Burcu Erdemli and Müge Akın for their tremendous support and encouragement throughout the study.

TABLE OF CONTENTS

ABSTRACT.....	iv
ÖZ.....	vi
ACKNOWLEDGEMENTS.....	ix
TABLE OF CONTENTS.....	xi
LIST OF TABLES.....	xiv
LIST OF FIGURES.....	xvi
CHAPTER	
1. INTRODUCTION.....	1
1.1 Purpose.....	1
1.2 Location and Extent of the Study Area.....	3
1.3 Previous Studies in Kazan Basin.....	3
1.4 Groundwater Age Concept.....	5
2. LITERATURE REVIEW.....	8
3. DESCRIPTION OF THE STUDY AREA.....	25
3.1 Physiography.....	25
3.2 Climate.....	25
3.3 Geology.....	28
3.3.1 Geology of Kazan Basin.....	28
3.3.2 Geology of the Study Area.....	30
3.3.2.1 Stratigraphy.....	34
3.3.2.2 Structural Geology.....	36

3.4 Hydrogeology of the Study Area.....	37
3.4.1 Water Resources.....	37
3.4.1.1 Surface Water Resources.....	37
3.4.1.2 Springs and Seeps.....	38
3.4.1.3 Groundwater.....	39
3.4.2 Hydrogeologic Classification of Units.....	39
3.4.2.1 Shallow Groundwater System.....	39
3.4.2.2 Middle Groundwater System.....	43
3.4.2.3 Akpınar Aquitard.....	45
3.4.2.4 Deep Groundwater System.....	45
3.4.3 Hydrogeochemical Classification of Waters.....	48
3.4.4 Conceptual Groundwater Flow Model of the Study Area.....	64
4. METHODOLOGY.....	69
4.1 Field Sampling.....	69
4.2 Laboratory Analyses.....	74
4.2.1 Oxygen-18 and Deuterium.....	74
4.2.2 Chlorofluorocarbons.....	77
4.2.3 Carbon-13 and Radiocarbon.....	81
4.2.4 Noble Gases.....	83
5. RESULTS AND DISCUSSION.....	86
5.1 Relationship of Oxygen-18 (^{18}O) and Deuterium (^2H).....	86
5.1.1 Groundwater Mixing.....	91
5.1.2 Relationship of Oxygen-18 (^{18}O) and Deuterium (^2H) in the springs...94	
5.1.3 Relationship of Oxygen-18 (^{18}O) and Deuterium (^2H) in the Shallow Groundwater System.....	95

5.1.4 Relationship of Oxygen-18 (^{18}O) and Deuterium (^2H) in the Middle and Deep Groundwater Systems.....	96
5.2 Relationship of Elevation and Oxygen-18 ($\delta^{18}\text{O}$) for Precipitation.....	98
5.3 Interpretation of Recharge Temperatures by Using Noble Gas Data.....	100
5.4 Calculation of Groundwater Ages with Chlorofluorocarbons.....	105
5.4.1 The CFC content variations in the study area.....	107
5.4.2 The CFC ages in the shallow, middle and deep aquifer systems.....	109
5.4.2.1 Processes affecting the CFC ages.....	113
5.4.2.2 Sensitivity analyses of the CFC ages in the study area.....	117
5.4.2.3 The estimated CFC ages in the study area.....	120
5.5 Calculation of Groundwater Ages with Radiocarbon.....	123
5.5.1 Natural and Anthropogenic Variations in Atmospheric ^{14}C	123
5.5.2 The ^{14}C pathway of groundwater.....	124
5.5.3 Groundwater dating by carbon-14.....	125
5.5.3.1 Geochemical reactions modifying carbon-14 activity.....	127
5.5.3.2 Carbon-13 in the Carbonate System.....	129
5.5.3.3 Correction of ^{14}C ages for Carbonate Dissolution.....	130
5.6 Evaluation of Helium-4 and Helium-3/Helium-4 ratio data.....	137
5.6.1 Helium Isotope Components.....	139
5.7 Hydraulic Age Calculations.....	143
5.8 Conceptual Model of the Groundwater Flow by using Isotope Data.....	145
6. CONCLUSIONS.....	162
REFERENCES.....	165
CURRICULUM VITAE.....	181

LIST OF TABLES

TABLES

Table 3.1 Monitoring well data.....	40
Table 3.2 Average concentrations of various species in springs and groundwater monitoring wells (SRK, 2004).....	49
Table 3.3 The groundwater budget of the aquifer systems obtained from the calibration of the groundwater model (Yazıcıgil et al., 2007).....	67
Table 4.1 The sampling program.....	70
Table 5.1 Oxygen-18 ($\delta^{18}\text{O}$) and deuterium results ($\delta^2\text{H}$) of the groundwater and spring samples within the study area.....	89
Table 5.2 Measured concentrations of Xenon and Neon, the recharge elevations (m) (recharge elevations for the shallow wells calculated from $\delta^{18}\text{O}$ data, for D-68R and D-8 see text for details) and the calculated recharge temperatures ($^{\circ}\text{C}$) by using graphical method.....	104
Table 5.3 Results of CFC measurements done at L-DEO.....	107
Table 5.4 Constants for calculation of K_H (Warner and Weiss, 1985; Bu and Warner, 1995).....	111
Table 5.5 The average CFC-11, CFC-12 and CFC-113 recharge years and the recharge temperatures and the recharge elevations used in the calculations together with the dissolved oxygen amounts obtained during field sampling.....	112
Table 5.6 Summary of processes that can modify apparent age (Modified from Plummer and Busenberg, 2000).....	114
Table 5.7 The CFC-11, CFC-12 and CFC-113 age sensitivity analyses for wells S-23, S-4 and D-57A.....	119
Table 5.8 The final recharge years assigned to each sample together with the CFCs used in the calculation of these years.....	121
Table 5.9 The radiocarbon, $\delta^{13}\text{C}$, DIC, alkalinity data and the unadjusted ^{14}C ages.....	128
Table 5.10 The unadjusted and the corrected radiocarbon ages in Years Before Present (yr. BP) for different $\delta^{13}\text{C}_{\text{soil}}$ values.....	136

Table 5.11 The dissolved Helium (He), Neon (Ne), Argon (Ar), Krypton (Kr) and Xenon (Xe) data and the $^3\text{He}/^4\text{He}$ and $^{40}\text{Ar}/^{36}\text{Ar}$ ratios.....	138
Table 5.12 The calculated ^3He concentrations and the components of the ^3He (atmospheric, crustal and mantle) with the percentages of these components for all samples.....	141
Table 5.13 The components of ^4He (atmospheric, radiogenic and mantle) and the percentages of these components for all samples.....	141
Table 5.14 The different meteoric water lines and the samples used to construct these lines together with their equations and coefficient of determinations.....	149
Table 5.15 Groundwater budget of the aquifer systems obtained from the combination of calibration of the groundwater model (Yazicigil et al., 2007) and the isotope data.....	159

LIST OF FIGURES

FIGURES

Figure 1.1 Location map of the Kazan Basin.....	4
Figure 1.2 Figure showing the mixing phenomenon which can cause a groundwater sample to contain waters with completely different ages (Modified from Kazemi et al., 2006).....	7
Figure 3.1 Relief map of the study area (SRK, 2004).....	26
Figure 3.2 The distribution of annual precipitation at Ankara station and the cumulative deviation from average annual precipitation.....	27
Figure 3.3 Regional setting of the Kazan Basin (SRK, 2004).....	29
Figure 3.4 Simplified geological map of the Kazan Basin (Toprak and Rojay, 2000)....	31
Figure 3.5 Columnar section of the study area (Toprak and Rojay, 2001).....	32
Figure 3.6 Geological map of the study area (Toprak and Rojay, 2001).....	33
Figure 3.7 Surface waters and reservoirs in the Kazan Basin.....	38
Figure 3.8 Location of the monitoring wells.....	41
Figure 3.9 Groundwater level contour map for the shallow aquifer system for March, 2003 (SRK, 2004).....	42
Figure 3.10 Groundwater level contour map for the middle aquifer system for March, 2003 (SRK, 2004).....	44
Figure 3.11 Groundwater level contour map for the deep aquifer system for March, 2003 (SRK, 2004).....	47
Figure 3.12 Average major ion concentration distribution of springs on trilinear diagram (Piper diagram) (SRK, 2004).....	56
Figure 3.13 Average major ion concentration distribution of shallow groundwater system on trilinear diagram (Piper diagram) (SRK, 2004).....	57
Figure 3.14 Stiff diagram showing the relative proportions of ions in water from selected shallow wells (SRK, 2004).....	58

Figure 3.15 Average major ion concentration distribution of middle groundwater system on trilinear diagram (Piper diagram) (SRK, 2004).....	59
Figure 3.16 Average major ion concentration distribution of deep groundwater system on trilinear diagram (Piper diagram) (SRK, 2004).....	60
Figure 3.17 Total Dissolved Solids (TDS) distribution in the shallow aquifer system (SRK, 2004).....	61
Figure 3.18 Total Dissolved Solids (TDS) distribution in the middle aquifer system (SRK, 2004).....	62
Figure 3.19 Total Dissolved Solids (TDS) distribution in the deep aquifer system (SRK, 2004).....	63
Figure 3.20 Conceptual hydrogeological model of the study area (SRK, 2004).....	66
Figure 3.21 Ground water budget obtained from calibration of the model under steady-state conditions (SRK, 2004) (The units are expressed as m ³ /day).....	68
Figure 4.1 Sampling for Dissolved Oxygen.....	71
Figure 4.2 The equipment used to take noble gas samples.....	73
Figure 4.3 The Fisons Prism III Mass Spectrometer at L-DEO.....	76
Figure 4.4 Simplified diagram showing the working principle of a CFC gas chromatograph drawn by Eugene Gorman.....	79
Figure 4.5 The Hewlett Packard 5890 Gas Chromatograph at L-DEO.....	80
Figure 4.6 Schematic overhead view of the NOSAMS AMS system. (modified from WHOI, 1989).....	82
Figure 4.7 Two views (top and side) from the MAP 215-50 noble gas mass spectrometer at L-DEO.....	85
Figure 5.1 The plot of Deuterium versus Oxygen-18 data for springs and wells (Ankara LMWL equation calculated from data in IAEA/ WMO, 2004).....	88
Figure 5.2 Deuterium versus Oxygen-18 graph showing two different mixing lines explaining the formation of M-74C and S-9.....	93
Figure 5.3 Deuterium versus Oxygen-18 graph for springs (Ankara Meteoric Water Line (AMWL) equation calculated from data in IAEA/ WMO, 2004).....	95

Figure 5.4 Deuterium versus Oxygen-18 graph for shallow groundwater wells in the study area.....	96
Figure 5.5 Deuterium versus Oxygen-18 graph for middle and deep groundwater wells in the study area Ankara Meteoric Water Line (AMWL) equation calculated from data in IAEA/ WMO, 2004.....	97
Figure 5.6 Recharge Elevation (m) versus Oxygen-18 (‰, V-SMOW) graph for the springs, shallow, middle and deep groundwater systems. The recharge elevations were calculated by using equation $\delta^{18}\text{O} = -0.0044 * (\text{Elevation}) - 4.811$ (Apaydin, 2004). Group I represents the elevations exceeding the maximum topographical elevation in the study area (1400 m).....	99
Figure 5.7 Xenon versus Neon concentrations also showing the noble gas temperatures calculated by using a recharge elevation of 1100 m.....	103
Figure 5.8 Atmospheric mixing ratios of CFC-11, CFC-12, CFC-113 and SF ₆ based on measurements from Niwot Ridge, Colorado.....	106
Figure 5.9 Concentration versus depth graph for CFC-11, CFC-12 and CFC-113 measured in the samples from the study area.....	109
Figure 5.10 The CFC age contour map for the shallow aquifer system.....	122
Figure 5.11 The pathway and associated fractionation of ¹⁴ C in CO ₂ during photosynthesis, respiration in soils and dissolution by groundwaters (Modified from Clark and Fritz, 1997).....	125
Figure 5.12 The decay of ¹⁴ C for two cases where A ₀ = 100 pmc and A ₀ =70 pmc.....	127
Figure 5.13 Logarithm of Carbon-14 activity versus oxygen-18 (‰, VSMOW).....	128
Figure 5.14 $\delta^{13}\text{C}_{\text{DIC}}$ versus Dissolved Inorganic Carbon graph showing the evolution of DIC in the groundwaters of Kazan Trona Basin.....	132
Figure 5.15 Oxygen-18 values versus unadjusted and corrected radiocarbon ages for different $\delta^{13}\text{C}_{\text{soil}}$ values. The oxygen-18 content of modern precipitation is also shown ($\delta^{18}\text{O}=-9.65$ ‰).....	137
Figure 5.16 The percentages of different ³ He components in the samples.....	142
Figure 5.17 The percentages of different ⁴ He components in the samples.....	142
Figure 5.18 Sources of helium in the aquifers of Kazan Trona Basin and the transport mechanisms of the mantle helium to the shallow aquifer system.....	144

Figure 5.19 Deuterium excess versus estimated groundwater age graph also showing the global and Ankara deuterium excesses which are 10‰ and 11.42‰ respectively (Global Deuterium Excess, Craig (1961b), Ankara Deuterium Excess calculated from data in IAEA/ WMO, 2004).....	146
Figure 5.20 Deuterium versus oxygen-18 graph for middle and deep aquifer systems and different meteoric water lines representing different water vapor sources.....	148
Figure 5.21 Map showing the lines of cross sections.....	150
Figure 5.22 Cross-section along line A-A' also showing the results of oxygen-18, deuterium, carbon-13 and carbon-14 measurements.....	151
Figure 5.23 Cross-section along line B-B' also showing the results of oxygen-18, deuterium, carbon-13 and carbon-14 measurements.....	152
Figure 5.24 Cross-section along line C-C' also showing the results of oxygen-18, deuterium, carbon-13 and carbon-14 measurements.....	153
Figure 5.25 Deuterium content, sulphate, chloride and sodium concentration versus distance from the recharge area graph for shallow aquifer system.....	156
Figure 5.26 CFC-11, Dissolved Oxygen, sulphate, chloride and sodium concentration versus distance from the recharge area graph for shallow aquifer system.....	157

CHAPTER 1

INTRODUCTION

1.1 Purpose

During the last three decades, environmental isotope techniques have commonly been applied to solve the hydrogeological problems that can not be solved by conventional methods alone. Environmental isotopes contribute to the investigations related to the origin of groundwater, its renewability and the subsurface processes affecting its quality (Clark and Fritz, 1997). Meteoric processes often modify the stable isotopic signature of water, meanwhile affecting the characteristic isotopic composition of the recharge waters. This composition serves as a natural tracer for the origin of groundwater, the recharge processes, geochemical reactions and reaction rates (Clark and Fritz, 1997). In addition to the environmental isotopes of hydrogen, oxygen and carbon, other tracers of anthropogenic origin like chlorofluorocarbons and sulfur hexafluoride are extensively used in studying the residence times of groundwater in aquifers together with the noble gas isotopes. Noble gas concentrations in groundwater, besides providing information on residence times in aquifers, have also been employed to find out the paleotemperatures in aquifers (Stute et al. 1992, 1995 and 1995a; Fontes et al., 1993).

The primary aim of this study is to determine the recharge, discharge and also the mixing mechanisms of a complex aquifer system located above the Kazan trona ore field using the environmental isotopes of deuterium, oxygen-18, carbon-13 and carbon-14, chlorofluorocarbons (CFC-11, CFC-12 and CFC-113) and the noble gas isotopes (He, Ne, Ar, Kr and Xe).

Trona, a naturally occurring mineral that is refined to soda ash by means of dissolution and recrystallization, is chemically known as sodium sesquicarbonate ($\text{Na}_2\text{CO}_3 \cdot \text{NaHCO}_3 \cdot 2\text{H}_2\text{O}$). Soda ash is one of the oldest known and largest volumes of

inorganic chemicals produced and used to make glass, paper, laundry detergents and many other products and chemicals, including baking soda. Although trona is a rare mineral throughout the world, there are two discovered deposits in Turkey. The discovery of the first Turkish trona deposit was in the Beypazarı Basin, the second discovery was made by Rio Tinto in 1998 in the Eocene deposits of the Kazan basin.

Kazan trona deposit is located at 35 km northwest of Ankara, Turkey. The deposit is planned to be extracted by solution mining method. There can be groundwater-related problems affecting the solution mining development and operation; therefore hydrogeological investigations have been conducted since 2000 to characterize the groundwater resources in the area and the impact of solution mining activity on the water resources (Yazıcıgil et al., 2001; SRK, 2001 and 2004).

In Turkey, there are some applications of the environmental tracers to solve the complicated hydrogeology related problems one of which is “Study of Recharge Conditions of Çakıloba- Karadoruk Aquifer System (Western Beypazarı-Ankara)” by Apaydın (2004). In this study, the isotope techniques were applied to find out the recharge conditions of the aquifers. There has also been a multi- tracer approach applied to a site located near Antalya, Turkey for the separation of groundwater flow components in a karstified aquifer by Nativ et al. (1999). In addition, there has been a very detailed study by Özyurt (2005) in which the stable isotopes, noble gas isotopes, CFC’s, tritium (^3H), tritiogenic helium-3 ($^3\text{He}^*$) were used to investigate the groundwater residence time distribution in the Aladağ karstic aquifer of Eastern Taurids Range. Özyurt (2005) developed a computer code for unsteady state lumped parameter modeling applications, applied plug-exponential flow model to all the springs in the study area and compared the model residence times with the ones calculated by $^3\text{H}/^3\text{He}^*$ method. This study can be considered as another application of isotope techniques in which stable isotopes of oxygen and hydrogen, CFCs and the environmental isotopes of carbon together with the noble gases are employed to solve the discharge and recharge mechanisms of the three aquifers of Kazan Basin and the mutual connection between them.

The system consists of three different aquifers which were identified above a trona deposit near Kazan, Ankara, Turkey. To establish the hydraulic interaction between the

aquifers, chlorofluorocarbons (CFC-11, CFC-12 and CFC-113), the environmental isotopes of deuterium, oxygen-18, carbon-13 and carbon-14 and the noble gas isotopes (helium, neon, argon, krypton and xenon) were utilized. Xenon and Neon concentrations were used to find out the recharge temperatures. The relationship of oxygen-18 and topographic elevation was used to reveal out the recharge elevations of different aquifers.

1.2 Location and Extent of the Study Area

The study area is located within the Kazan Basin, 35 km northwest of Ankara, Turkey. It lies between latitudes 32°24'-32°50' and longitudes 39°56'-40°28' (Figure 1.1). Kazan Basin is situated within the provincial boundary of Ankara. The main districts in the study area are Kazan in the north and Sincan in the south. İlyakut, Mülk, İncirlik, Dutluca, Fethiye and Kınık are the villages located in the study area.

1.3 Previous Studies in Kazan Basin

In Turkey, General Directorate of the State Hydraulic Works (DSİ in Turkish acronym) is the main investing institution responsible for the utilization of all water resources of Turkey. DSİ is empowered by the law No. 167 to perform all studies for surveys, investigation, conservation and utilization of ground water. The first detailed hydrogeological survey of the basin was carried out by DSİ in 1964 although the hydrogeological investigations in Kazan Basin started in 1960 by Erol (1960). 26 exploration wells at 14 locations were drilled by DSİ and electrical resistivity sounding surveys were conducted at 100 points. The results of chemical analyses of 59 different water samples from Mürted Plain, the plain area of Kazan Basin, together with a 1:100000 hydrogeological map prepared by DSİ were published in 1976 in the report "Hydrogeological Investigation Report for Mürted Plain".

No other detailed hydrogeological investigations were conducted in the study area until 2000 except for drilling wells for water supply purposes by the Bank of Provinces and

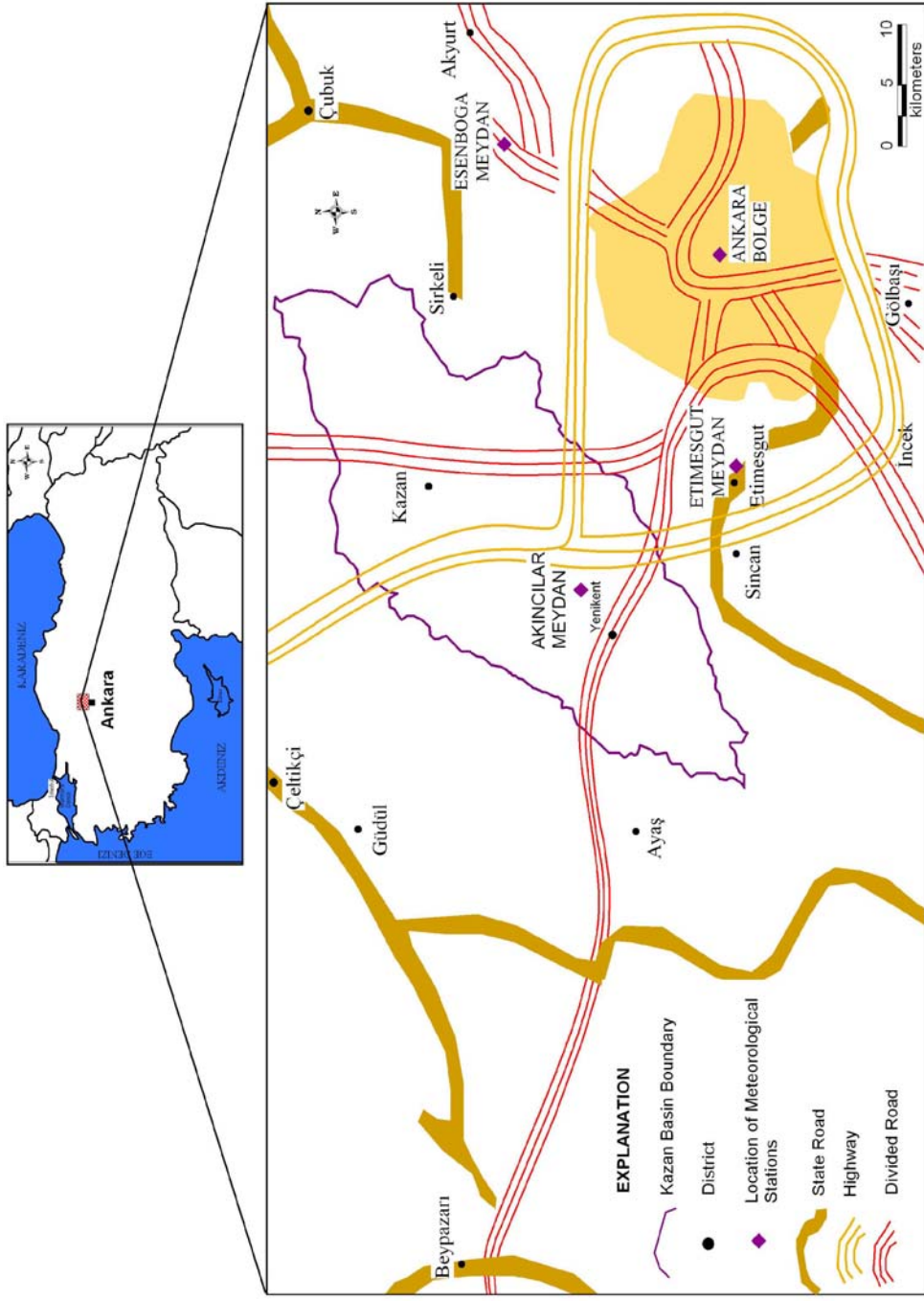


Figure 1.1 Location map of the Kazan Basin.

the General Directorate of the Rural Services. Yazıcıgil et al. (2001), together with SRK Consulting (SRK) started investigating the hydrogeological site conditions at the study area in 2000. Toprak and Rojay (2000, 2001), Rojay et al. (2002) studied the geology and Yazıcıgil et al. (2001) studied the hydrogeology and hydrogeochemistry of the area. Middle East Technical University and SRK was contracted by RioTur Madencilik A.Ş. (Riotur) which is a wholly owned subsidiary of the Rio Tinto. Riotur holds an operation license for the trona deposit located in the study area and is planning a solution mining operation to extract the deposit. In order to prevent the groundwater-related problems that can affect the solution mining development and operation, Yazıcıgil et al. (2001) and SRK (2001) started the exploration to characterize the groundwater resources in the study area and to better understand the potential impacts of solution mining activity on the water resources. Yazıcıgil et al. (2001) compiled and reviewed existing hydrological, hydrogeological, meteorological and geological data in the study area. Besides, SRK installed surface water monitoring stations and totally 58 groundwater wells, conducted aquifer tests to assess the hydraulic conductivity and storativity of the water bearing units, and developed a conceptual hydrogeological model of the study area (SRK, 2004).

1.4 Groundwater Age Concept

In this study, different approaches were used to determine the groundwater ages in shallow, middle and deep aquifer systems. There are a lot of different terms in the groundwater literature representing age and lifetime of a groundwater molecule. Throughout the thesis most of these terms will be used therefore they should be defined properly.

To begin with, “groundwater age” is used to define the amount of time passed since a water molecule was recharged into the subsurface environment until this molecule reaches a specific location in the system. Modica et al. (1998) defined the “groundwater residence time” as the time passes during the journey of the water molecules from the recharge area to the discharge area of the aquifer. If the water molecule is sampled physically then it is the age of the groundwater that is identified. As defined by Kazemi et al (2006) the date of birth of a groundwater molecule is the date in which the water

molecule enters to the subsurface environment. Accordingly, groundwater molecules die when they leave subsurface environments through natural or artificial discharge.

As stated before in this section, there are a large number of terms to address the groundwater age concept. Isotopic age is another term which is the age measured by isotopic methods and this age can well be different from the true age due to the reason that the isotopes used to measure the age of groundwater are not part of the water molecule except for tritium (Kazemi et al., 2006). Hydraulic age is another concept which is based on Darcy's law and involves the knowledge of hydraulic conductivity, effective porosity and hydraulic gradients in the aquifer. In addition, Kazemi et al. (2006) stated that if it is assumed that the groundwater movement is by advection only, likewise the displacement of the groundwater molecules are assumed to be displaced by the overall velocity field and the diffusion, dispersion and mixing is insignificant, this way a piston-flow age can be determined. Piston-flow age approach assumes that the travel of the groundwater molecule between the recharge area of the aquifer to the discharge area is as an isolated parcel (Kazemi et al., 2006).

Lastly, two other definitions should also be mentioned herein which are the model age and the apparent age concepts. Apparent age concept is used to state that the reported ages are not the true ages of the water molecules and there exists approximate average of the many real ages existing in a single sample (Kazemi et al., 2006). On the other hand, as stated by Kazemi et al., (2006), model ages are referred to ages obtained after adjusting models have been applied to correct the ages based on isotope techniques.

There are some complexities that should be taken into consideration when age- dating a groundwater sample. One of the major challenges is the mixing phenomenon. It is a high possibility that a groundwater sample consists of portions having different ages from different sources as presented in Figure 1.2 (Kazemi et al., 2006). In addition, hydrodynamic dispersion and heterogeneous groundwater velocities can also cause the cluster of numerous fractions of different ages at a microscale level as suggested by Weissmann et al (2002).

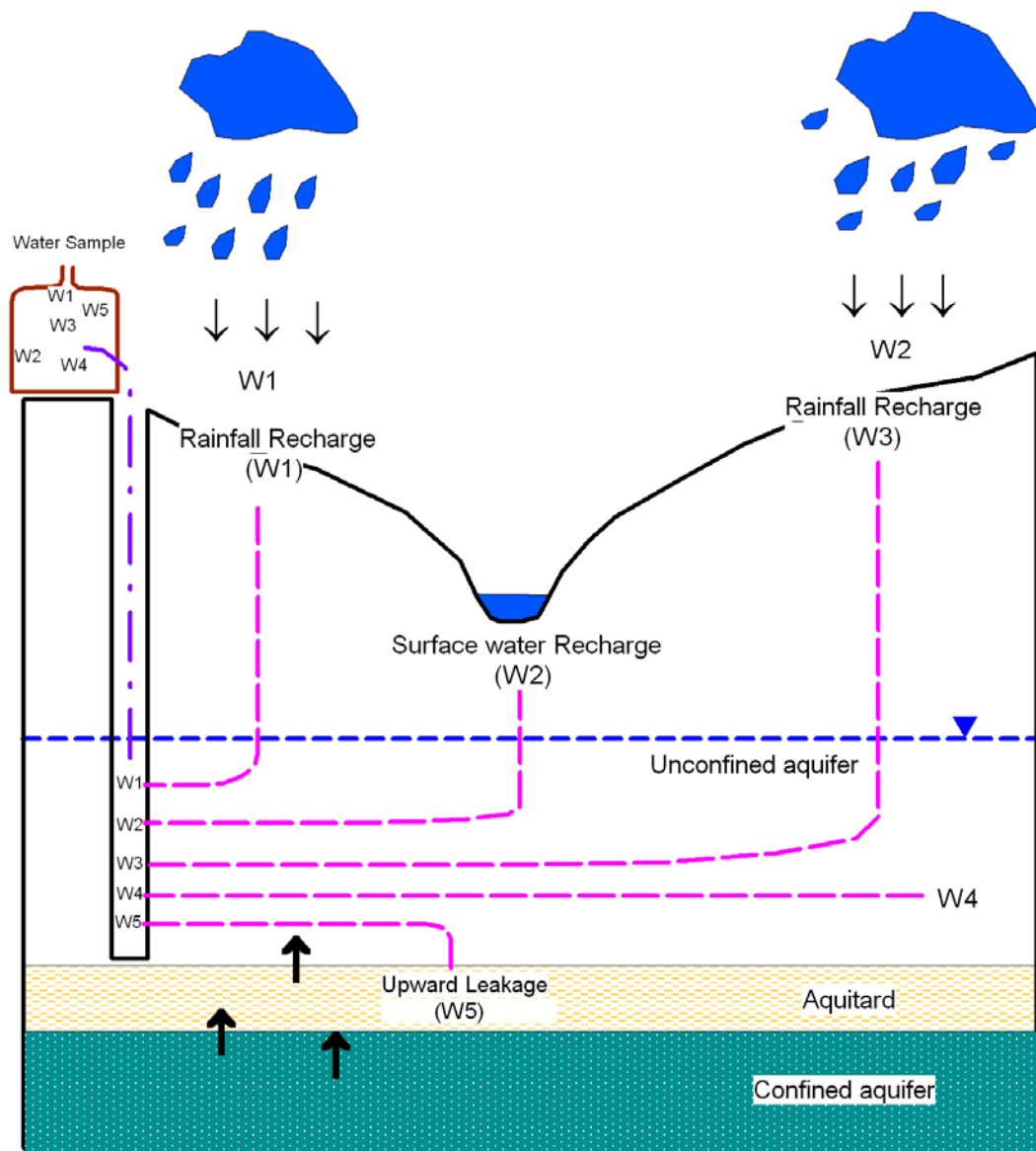


Figure 1.2 Figure showing the mixing phenomenon which can cause a groundwater sample to contain waters with completely different ages (Modified from Kazemi et al., 2006).

CHAPTER 2

LITERATURE REVIEW

An intimate literature survey was conducted before deciding on the purpose and main objectives of this study. Many scientists from all over the world proved the efficiency of the environmental tracers in the studies such as groundwater flow and evolution investigations, groundwater renewability, dating of groundwater from very young to very old, tracing the water circulation, differentiating the recharge and dispersion in groundwater systems, calculating the groundwater velocity, and distinguishing the subsurface processes affecting the quality of groundwater by utilizing the techniques in different sites for more than 40 years. In fact, the first time that “groundwater age” term introduced to the literature was in 1957 by Begemann and Libby. Since then, extensive studies were carried out about the age dating of groundwater by using environmental tracers such as tritium (^3H), helium-3, chlorofluorocarbons (CFC-11, CFC-12, CFC-113) and carbon-14 (^{14}C).

The techniques to date young groundwaters ages ranging between 0 to 60 years old includes tritium (^3H), tritium(^3H)/tritogenic helium-3(^3He), helium-4 (^4He), krypton-85 (^{85}Kr), chlorofluorocarbons, and sulphur hexafluoride. Tritium is an excellent tracer in groundwater systems because it is present in the water molecule and can be used to directly trace water movement. It is a radioactive isotope of hydrogen undergoing radioactive decay to ^3He with a half-life of 12.3 years. It can be produced in different ways like cosmic-ray bombardment of nitrogen and deuterium in the upper atmosphere, through thermonuclear tests, which terminated in 1963 and by neutron radiation of lithium in rocks. One of the earliest studies using tritium as a dating tracer is on a few New Mexican aquifers by von Buttlar (1959). Through this study, groundwater samples were collected in different months in 1956 and 1957 were analyzed for tritium content. The data showed that tritium content of some of the samples is much lower than that of the surface samples. Therefore, it has been concluded that according to the tritium

contents the aquifer did not receive substantial recharge from the recent rainfalls or surface waters. There was a sharp increase in the tritium content of one sample from May to November 1957 indicating that some recharge has occurred during this period.

The weak parts of the tritium dating method have led the scientists to revive an old technique, namely $^3\text{H}/^3\text{He}$, to replace it. This dating method, although proposed long time ago by Tolstikhin and Kamensky in 1969, was not widely recognized until 1990 because of the difficulty in sampling and in measuring the ^3He content of the groundwater samples (Kazemi et al., 2006). Before applying this method, all the sources of ^3He in the groundwater should be identified. There are four sources of ^3He in the groundwater. Atmospheric ^3He includes the excess air component and it is the solution of atmospheric ^3He in percolating water. ^3He can also be produced from the fission of ^6Li by neutrons. This is called crustal helium-3. If ^3He is generated by the disintegration of tritium it is called tritiogenic helium. The fourth source of ^3He is the mantle helium released from mantle. All these different sources have their own particular $^3\text{He}/^4\text{He}$ ratio leading to specific $^3\text{He}/^4\text{He}$ ratios in groundwater. This is how helium of different sources is differentiated.

In 1988, Schlosser et al. (1988) demonstrated the potential of combined $^3\text{H}/^3\text{He}$ measurements for studies of shallow groundwater circulation. In this study, combined $^3\text{H}/^3\text{He}$ data from three multi-level sampling wells located at West Germany were presented. The data showed the excess ^3He produced by radioactive decay of bomb tritium which is released between years 1952 and 1963. The results revealed out that there is a deviation of 15% between the apparent $^3\text{H}/^3\text{He}$ and true age attributed to the incomplete confinement of the tritiogenic ^3He (i.e. $^3\text{He}^*$), the dispersive mixing of water with different tritium and helium concentrations and the non-linear behavior of the $^3\text{H}/^3\text{He}^*$ upon mixing. This deviation was concluded to be tolerable. In 1989, Schlosser et al. (1989) presented and discussed new tritium, helium isotope and neon data from the same site. In this study, the $^3\text{H}/^3\text{He}^*$ distributions were simulated for the years 1987, 2000 and 2025. The model results showed that under favorable conditions the $^3\text{He}^*$ peak would be detectable in shallow aquifers for at least the next 4 decades. Further, this study demonstrated that it is possible to apply the $^3\text{H}/^3\text{He}^*$ method even under conditions complicated by the presence of radiogenic helium.

In 1988, Poreda et al. used the measurements of ^3H and ^3He in groundwater to calculate the age of groundwater. The tritium and helium isotope measurements on waters were reported from an unconfined aquifer associated with a low-level nuclear waste storage area. The groundwater ages, the preferred pathways for fluid migration and the hydraulic conductivities were obtained. The hydraulic conductivity results showed agreement with the hydraulic conductivities obtained from conventional aquifer tests.

In 1998, a $^3\text{H}/^3\text{He}^*$ study of ground water flow in a fractured bedrock aquifer located near New York City was published by Aeschbach-Hertig et al. In this study, the concentrations of tritium, helium isotopes, and neon have been measured in ground water by using the samples obtained from commercially exploited wells. It is emphasized in this study that the transient tracer data are valuable in fractured rock systems as they provide constraints on groundwater flow parameters that are difficult to obtain otherwise. It was observed that the relationship between tritium- $^3\text{He}^*$ ages revealed that there are age-related changes in mineralization of groundwater although the details of this connection remained to be studied. It was observed that there was a decrease of mineralization with increasing age reflecting changes in the recharge water. These changes were due to the correlations obtained between $^3\text{H}/^3\text{He}^*$ ages and concentrations of total dissolved solids and total CO_2 . In this study, it was also found out that the distribution of $^3\text{H}/^3\text{He}$ ages is related to the topography of the study area and the depth of the wells.

The release of chemicals into the atmosphere from anthropogenic sources has increased over the past 60 years. As a result, concentrations of a range of atmospheric trace gases increased continuously. Chlorofluorocarbons (CFCs) are stable, synthetic, halogenated alkanes, developed in the early 1930s as safe alternatives to ammonia and sulphur dioxide in refrigeration. Production of CFC-12 (dichlorodifluoromethane, CF_2Cl_2) began in 1931 followed by CFC-11 (trichlorofluoromethane, CFCl_3) in 1936. Many other CFC compounds have since been produced, most notably CFC-113 (trichlorotrifluoroethane, $\text{C}_2\text{F}_3\text{Cl}_3$). CFCs are nonflammable, noncorrosive, nonexplosive, very low in toxicity, and have physical properties conducive to a wide range of industrial and refrigerant applications (Plummer and Busenberg, 2000). Release of CFCs to the atmosphere and subsequent incorporation into the Earth's hydrologic cycle has closely followed

production rate. Current estimates of the atmospheric lifetimes of CFC-11, CFC-12, and CFC-113 are 45 ± 7 , 87 ± 17 , and 100 ± 32 years (Volk et al., 1997). CFCs provide excellent tracers and dating tools of young water (50 year time scale) because the atmospheric mixing ratios of these compounds are known over the past 50 years and the concentrations in air and young groundwater are relatively high and can be measured. There are some processes that can add or remove CFC-11 and CFC-12 beyond that of equilibration of infiltration water with soil air. CFC concentrations can be modified by microbial degradation, sorption and desorption, entrainment of excess air during recharge, mixing in the well casing, hydrodynamic dispersion, and contamination (Busenberg and Plummer, 1992).

The feasibility of using CFCs as tracers of recent recharge and indicators of groundwater age was first recognized in the 1970s (Thompson et al., 1974; Schultz et al., 1976; Randall and Schultz, 1976; Thompson, 1976; Hayes and Thompson, 1977; Randall et al., 1977; Thompson and Hayes, 1979; Schultz, 1979). Thompson et al. (1974) discussed the effectiveness of CFC-11 as a tracer in both groundwater and surface water hydrology. They were able to find a good agreement between CFC-11 data and tritium age data.

In 1993, Dunkle et al. used CFC-11 and CFC-12 as dating tools and hydrologic tracers in shallow groundwater at a site in United States. In this study, the recharge temperatures determined from dissolved nitrogen and argon concentrations came out to be varying from 9 ± 2 °C to 14 ± 2 °C. The potential uncertainties in CFC dating at the study site were evaluated. CFC modeled ages for totally 109 different shallow wells calculated independently for CFC-11 and CFC-12 agreed each other. The ages were evaluated in relation to the known hydrogeology, water chemistry and tritium data. The groundwater ages were seen to be increasing with depth in multilevel sampling sites throughout the study area. The vertical component of recharge was calculated to be 30- 60 cm/year in recharge zones and less than 30 to 60 cm/year in areas with low hydraulic gradient and low permeability. The results of this study supported the use of CFCs for dating shallow, aerobic groundwater.

One year after the study of Dunkle et al., in 1994, Cook et al. (1995) published another study which is “Chlorofluorocarbons as tracers of groundwater transport processes in a

shallow, silty sand aquifer". In this study, the chlorofluorocarbon profiles from a well-characterized field site in Central Ontario, Canada were described. Concentrations of CFC-11, CFC-12 and CFC-113 were measured at 14 sampling depths. Vertical groundwater profiles of chlorofluorocarbons all showed decreases in concentration with depth, reflecting increases in their concentrations in the atmosphere. At this site, degradation of CFC-11 has resulted in apparent ages which greatly overestimate groundwater travel times at all depths but there were no evidence for degradation of CFC-12 and CFC-113. The measured concentrations of neon and nitrogen were used to estimate the recharge temperature which came out to be 2 °C. Tritium measurements have also been made in 1986, 1990 and 1991 and the position of the 1963 bomb peak was determined for each year. According to this position, a mean vertical velocity was determined to be between 0.35 and 0.43 m/year. The decrease in tritium concentration observed between 1986 and 1991 was found out to be consistent with radioactive decay of tritium over a 5-year period. One- and two- dimensional groundwater flow and solute transport modeling is used to estimate chlorofluorocarbon transport parameters.

In 1996, Oster et al. published another study of groundwater age dating with chlorofluorocarbons. In this study, seven anoxic environments were investigated to examine the stability of CFC-12 relative to CFC-11. It has been found out that natural CFC-11 and CFC-12 degradation occurs under strictly anoxic conditions. The CFC-11 degradation rate was determined to be faster than CFC-12 degradation by a factor of about 10. Local CFC excesses were observed in and down wind of industrial area, which concluded to create an excess input signal to the groundwater and lead to young or even future CFC age calculations. The high local and temporal variability of the excess signal was found out to be compensated by molecular diffusion in the vadose zone. The scientists of this study concluded that local CFC soil air measurements can provide a valuable local correction factor for CFC dating. The decrease in CFC emissions was concluded to affect CFC age dating especially in systems with small turnover times. It was stated that in the future, the decrease in continental CFC concentration will make the technique insensitive to young groundwater components and this difficulty can be overcome by using trace gases not being restricted in production.

After verifying the affects of CFC degradation under anoxic conditions, a lot of studies have been carried out to further understand the stability of CFCs in certain environments. In 1997, Shapiro et al. used tritium and tritiogenic helium to determine CFC degradation and vertical mixing rates in Framvaren Fjord, Norway. In this study, concentrations of CFC-11 and CFC-12, as well as tritium and helium isotopes were measured in the super-anoxic, sub-surface waters of Framvaren Fjord. This fjord is said to provide an ideal environment to study the degradation of CFCs because of its relatively simple dynamics and the narrow zone in which chemical reactions and biological activity, relevant to CFC degradation, occur in the water column. CFCs and tritium enter the fjord at the surface and were transported into the deep water primarily by turbulent vertical mixing. The turbulent mixing rate was determined as 0.006- 0.008 cm²/s by fitting a 1D model to the vertical distributions of tritium and tritium with tritiogenic helium. Using these values, the degradation rates for CFC-11 and CFC-12 were obtained by comparing model simulations including first-order degradation rates to the observed CFC profiles. CFC-11 is degraded at a rate of 6-9 yr⁻¹ below 19 m depth where oxygen concentrations are zero. CFC-12 is found to have a maximum degradation rate of 0.01 to 0.03.

In 1998, Özyurt and Bayarı (1998) published a study in which CFCs were used to determine the groundwater age in the Aladağ karstic aquifer. It is the first application of the CFCs to reveal out the groundwater ages in a Dinarid type karstic system in the world. In this study, the CFC ages of groundwater from the springs located along the regional groundwater flow path were calculated and CFC-11 and CFC-12 ages of groundwater discharges were found to vary between 1 and 26 years. There has been a difference between CFC-11 and CFC-12 ages which was attributed to the sorption of some of the CFC-11 in groundwater to the syngenetic organic material present in carbonate rocks. Çakır et al. (1999) also applied CFCs to date the groundwater in the springs of Beydağları (Finike) karstic aquifer. According to the findings of the study, the oldest water discharged in the Taurids on the basis of CFC-12 ages and tritium content is 40 years/ 0.7 TU. The youngest springs CFC-12 ages were calculated to be between 1 to 10 years.

Another interesting study was again published by Özyurt and Bayarı (1999) about the relationship between the CFC ages and the physical, chemical and isotopic parameters in

the Aladağ aquifer (Yahyalı- Kayseri). In this study it has been demonstrated that the calculated groundwater ages by using CFCs are concordant with those parameters in concern. In addition, the tritium contents along the regional groundwater flow path are well-matched with the CFC contents.

Although CFCs are nontoxic, nonflammable, and noncarcinogenic, they are one of the prime contributors to stratospheric ozone depletion. In 1987, through signing of the Montreal Protocol on Substances That Deplete the Ozone Layer, 37 nations agreed to limit release of CFCs and soon after a global ban started in 1996 by industrialized countries. Groundwater age dating by using CFCs started losing some credibility due to the declining trend in the CFCs atmospheric concentrations after global ban since the early 1990s. Sulphur hexafluoride, SF₆, which is a colorless, odorless, nontoxic, and stable gas has now got the advantage that its concentration in the atmosphere continues to rise unlike CFCs. It is used as an electrical insulator in high-voltage switches and transformers and as a blanket gas in the melting operations of magnesium metal production. Industrial production of SF₆ began in 1953 and it has been used as a hydrologic tracer since 1993. Because of its high rate of increase in the atmosphere which is approximately 7 % per year, its known atmospheric history, its apparent stability in soils and the relatively simple analytical and sampling procedures, SF₆ is being studied as a potential environmental tracer for dating young groundwater (0 to 30 years old) (Busenberg and Plummer, 2000). It should be noted that the method is being recently introduced and more information should be gathered about possible causes that can restrict and reduce the applicability of the method like microbiological degradation of SF₆. There are not many studies involving this method as it is the latest method in the literature but the most relevant studies are as follows.

Busenberg and Plummer (2000) carried out a comprehensive study of SF₆ in groundwater in Atlantic Coastal Plain sand aquifers of the United States and springs issuing near the top of the Blue Ridge Mountains of Virginia. According to the results of SF₆ measurements from 44 samples taken from various depths the SF₆ groundwater ages were found out to be between 2.6 to 47 years. Not surprisingly, it was seen that SF₆ ages showed increase with depth. SF₆ ages were compared with CFC-12 and CFC-113 ages. This comparison showed good correlation except for very young waters with ages less

than 10 years old and old waters with ages more than 30 years old. This inconsistency was explained by two facts. As stated before, the concentration of CFCs in the atmosphere stopped rising after the Montreal Protocol therefore CFCs method is unable to date the groundwater recharged after 1993 and SF₆ method can not date groundwater older than 30 years old because of its low atmospheric concentration prior to 1970s. According to the results of Busenberg and Plummer in 2000, a large excess of SF₆ was detected, exceeding the maximum atmospheric concentrations, in many springs issuing from igneous rocks at or near fault contacts separating crystalline and sedimentary rocks in Virginia, West Virginia and New Mexico.

Within the same year of Busenberg and Plummer's study, Ho and Schlosser (2000) published another study about atmospheric SF₆ near a large urban area. They stated out that although SF₆ has the potential to be a valuable transient tracer for dating of young groundwater, there can be numerous point sources of it which can have a significant impact on the temporal evolution of its atmospheric mixing ratio and complicating its use as an age-dating tool. They presented and discussed a 12-month record of atmospheric SF₆ from a location near New York City. The data were obtained by gas chromatographic analyses performed at intervals of about 10 minutes yielding about 40,000 data points for the time series. Measurements at Lamont- Doherty Earth Observatory showed that near large urban regions, atmospheric SF₆ mixing ratios are influenced by strong local emissions, as well as regional-scale atmospheric mixing causing SF₆ mixing ratios to be higher than those in the remote atmosphere. These effects may cause regional baseline trends to deviate from those measured at remote atmosphere stations. It has been stated out that in such environments, the input function needs to be explicitly defined so as to use SF₆ as a dating tool. If not, using SF₆ to date groundwater assuming the remote atmosphere input function would produce ages that are younger than the actual age, or sometimes even prevent the determination of an age.

In 2004, Katz measured the concentration of SF₆ in 22 samples from 12 large karstic springs in Florida, USA. The SF₆ ages came out to be 2.8 to 16.3 years. These ages were found out to agree the CFC-113 ages but both tracers had sources other than atmosphere. Therefore the ages obtained from these two methods were not consistent with the ³H/³He ages which proved to be the most reliable method for these karstic springs.

Another recent study combining CFCs and SF₆ to characterize groundwater movement and residence time in a lowland Chalk catchment in the UK was carried out by Gooddy et al. in 2006. Data collected from groundwater and surface water from the study area suggest that groundwater movement can be divided into three regimes: on the interfluvies of the catchment, 'piston' flow dominates, with a bulk groundwater age of several decades; at the valley bottom, there is mixing between shallow groundwater and stream water; and in an intermediate zone between the top and the bottom of the valley there is approximately 3 parts modern water to 1 part pre-tracer water. Adjacent to the stream, groundwater- surface water interaction was found out to take place to depths more than 10 m. A conceptual model of groundwater movement has been developed to describe the catchment processes with a combined use of CFC and SF₆.

Up to this point, only the literature related to the investigation of young shallow groundwater has been mentioned. The methods used in age dating of old groundwater less than 50,000 years old include mostly carbon-14 (¹⁴C) but silicon-32, argon-39, oxygen-18 and deuterium can also be used indirectly. Herein, literature related to only ¹⁴C will be touched on.

Carbon occurs in all forms of organic life and is the basis of organic chemistry. There are two stable carbon isotopes: carbon-12 and carbon-13. Carbon-14, or radiocarbon, was discovered by Martin Kamen and Sam Ruben in 1940. It is produced naturally in the atmosphere by interactions of nitrogen and cosmic rays that bombard the Earth constantly. During this bombardment a small number of nitrogen nuclei are transformed into radioactive nuclei of ¹⁴C. A large amount of ¹⁴C was produced during the thermonuclear testing in 1950s and 1960s increasing the concentration of ¹⁴C in the atmosphere. Radiocarbon dating of dissolved inorganic carbon (DIC) in groundwater began over 45 years ago after the discovery by Libby (1955). This dating method uses the principle that atmospheric ¹⁴C dissolved in the percolating precipitation reaches the groundwater table and starts decaying to nitrogen. If no ¹⁴C exchange occurs, measurement of the remaining ¹⁴C atoms can be used to date groundwater allowing the dating of ages up to 40,000 years. When this method was first utilized Libby half-life which is 5568 ±30 years were used, however later a more accurate value was determined as 5730±40 years known as the Cambridge half-life. There are some advantages and

disadvantages of dating groundwater by ^{14}C method. The advantages are the sampling and analyses of this method are routine and it is an old and well established method that has been proved. The disadvantages include assigning a correct initial value to the water to be dated being hard as there are various processes that can modify ^{14}C signature of the percolating precipitation and the final concentration of ^{14}C in the groundwater can be modified by geochemical reactions and corrections lead to uncertainties.

In 1991, Drimmie et al. published their study about the radiocarbon and stable isotopes in water and dissolved constituents in Milk River aquifer located in Canada. To find out information about the origin and age of groundwater in the study area wells in the aquifer were sampled and deuterium (^2H) and oxygen-18 (^{18}O) in water, carbon-13 (^{13}C) and ^2H in methane, sulphur-34 (^{34}S) and ^{18}O in SO_4 , ^{13}C and ^{14}C in dissolved inorganic carbon (DIC) and dissolved organic carbon (DOC), and tritium contents determined. Herein, only some of the results will be presented. According to the results of stable isotope analyses on groundwater three different zones within the aquifer were recognized. For the first few kilometers, starting at the recharge zone, modern-type groundwaters are encountered. These are followed by groundwater with higher ^2H and ^{18}O contents which do not show a glacial signature and were probably recharged under warmer climatic conditions. Groundwater in the third zone is characterized by higher salinities and a pronounced oxygen isotope shift. They show the gradual admixture of far more saline formation waters from an adjacent basin. Radiocarbon was found out to be measurable only in the first 20 km from the recharge zone, however, it has been stated out that transformation of measured concentrations to "water ages" was very difficult because of the complexity of the geochemical system. The DIC dates and DOC dates were compared and DIC dates came out to be much older than DOC dates and the DOC dates led to the conclusion that the initial DIC radiocarbon content was as low as 30% modern when the water entered the aquifer. The age of the water 20 km from the recharge zone was assessed to be approximately 20,000 years old, resulting in a velocity of 1 m/y. This result was much higher than estimates by other techniques.

Another interesting study involving ^{14}C method was undertaken by Kazemi in 1999 in Buckinbah Creek Watershed located in eastern Australia. The watershed experienced some degree of dry-land salinization. Groundwater occurs in a shallow, locally saline

regolith and in an underlying, deep, regional fractured aquifer. According to the previous studies these two aquifers have no interaction. Groundwater samples were collected from both aquifers and analyzed for ^{14}C and CFCs contents. The sample from the shallow aquifer dated as modern by ^{14}C method and it was dated as older than 1975 by CFCs method. The sample from the deep aquifer dated as 970 years of with ^{14}C method and no CFCs were detected in this sample showing that the two dating methods fully support and complement each other. A negative correlation between the ages of deep groundwater samples and their salinity levels were also pointed out. The reason for this was explained as the precipitation of some minerals such as kaolinite and gypsum in addition to the dilution by recharging low- salinity water as groundwater travels along the flow path.

A recent study by Mahlkecht et al. published in 2006, should also be mentioned herein. This study is about the geochemical and isotopic investigations on groundwater residence time and flow in the Independence Basin located in Mexico. This basin is facing serious groundwater resources deficiency due to an increasing demand linked to a rapid population growth and agricultural development therefore the geochemistry and isotopic tracers were used in order to investigate the groundwater flow system and estimate the groundwater residence time. The groundwater was characterized by low salinity with some exceptions associated to a contribution of more saline groundwater from deep formations. High ^{14}C values were observed at the basin margins indicating recent recharge, whereas a trend to lower ^{14}C values was observed along the modern groundwater flow paths. A trend of decreasing ^{14}C activity associated with a change toward heavier $\delta^{13}\text{C}$ values indicates that geochemical reactions are affecting the ^{14}C concentration along the groundwater flow system. The groundwater residence time calculated by radiocarbon data after correction ranged between recent and 11,000 years old.

Helium isotopes, particularly radiogenic ^4He , have been used in the past as natural tracers to estimate mean residence times of groundwater. Helium was discovered in 1868 by J. Norman Lockyear. It is an inert and nontoxic gas. There are four different sources of ^4He in groundwater. Atmospheric helium is dissolved in rain water and carried into the groundwater. Radiogenic or crustal helium is the helium-4 produced from aquifer matrix

and from the sediments grains by alpha decay of uranium and thorium. Helium produced with the Earth's crust through decay reactions enters groundwater system. Mantle or terrigenous helium is produced deep in the Earth's mantle finding its way to enter groundwater. It is a proven fact that seismicity and fracturing are important transport of mantle helium through fault zones to the upper crust and shallow-level groundwaters. Ancient helium is another type of helium which is entrapped in the crystal lattices of sediments or rock strata in the course of deposition entering groundwater through solid-state diffusion process. A detailed analysis of both the He concentrations and the $^3\text{He}/^4\text{He}$ ratios measured in groundwaters allows the separation of the different components (Stute et al., 1992b). After separation of the individual He components, radiogenic ^4He can then be used to estimate mean residence times of groundwater.

In 1996, Solomon et al. investigated the source of radiogenic ^4He of groundwater at sites and discussed the implications of this method for dating young groundwater. At the Sturgeon Falls site located at Ontario, groundwater travel times and fluid velocities were well documented because of detailed profiling of tritium, $^3\text{H}/^3\text{He}$ ratios, and CFCs. Metamorphic rocks of the Canadian Shield that contain large quantities of ^4He are the protolith of the unconsolidated aquifer of this site. Observed radiogenic ^4He values increase linearly with distance along a flow path and with increasing groundwater age. A simple model of ^4He diffusion from spherical grains suggested that aquifers derived from old protoliths may leak ^4He into groundwater at rates greater than can be supported by U/Th decay up to 50 million years meaning that the accumulation rate of ^4He can be 100 times greater than accumulation rate of ^4He by U/Th decay. Results from the Sturgeon Falls site suggested that it is possible to estimate the in situ radiogenic ^4He rate using laboratory measurements. The radiogenic ^4He accumulation at two other sites from North America were also presented in this study. About these sites, it has been hypothesized that as downward velocities were too great to allow upward diffusion of deep ^4He the source of ^4He should be old aquifer solids. The data illustrated that ^4He accumulation rate at the Sturgeon Falls site was not anomalous but rather may be common.

In 2000, Castro et al. carried out a study in which comparison of ^4He ages and ^{14}C ages in simple aquifer systems involved and the implications for groundwater flow and chronologies were discussed. ^4He concentrations in excess of the solubility equilibrium

with the atmosphere by up to two to three orders of magnitude are observed in the Carrizo Aquifer in Texas, the Ojo Alamo and Nacimiento aquifers in the San Juan Basin, New Mexico, and the Auob Sandstone Aquifer in Namibia. A simple ^4He accumulation model is applied to explain these excess ^4He concentrations in terms of both in situ production and a crustal flux across the bottom layer of the aquifer. The contribution of in-situ produced ^4He to the measured concentrations was estimated for each site. The contribution was found out to be negligible for the Auob Sandstone Aquifer. In the Carrizo aquifer, in-situ produced ^4He came out to contribute 27.5% at the top and 15.4% to the total ^4He observed at the bottom of the aquifer. For San Juan Basin aquifers in-situ production dominates the ^4He concentrations at the top whereas the internal production is negligible at the bottom. The mean residence times were estimated from the measured ^4He concentrations agreed reasonably well with ^{14}C ages. The calculated ^4He ages allowed the identification of three different climate periods which are the Holocene period (0- 10,000 years BP), the Last Glacial Maximum (18,000 years BP), and the preceding period (30,000- 150,000 years BP).

Multi-tracer dating greatly increases the scientists' confidence dealing with groundwater age dating as it can provide a cross-check of the behavior of the other transient tracers. In literature it is possible to find a lot of studies in which direct comparison of different methods. For instance, in 1994, Ekwurzel et al. carried out a study about dating of shallow water and they compared the transient tracers $^3\text{H}/^3\text{He}$, CFCs and Krypton-85 (^{85}Kr). ^{85}Kr is a radioactive noble gas that beta decays to stable ^{85}Rb with a half-life of 10.76 years. It is affected only by radioactive decay and hydraulic properties of the aquifer since it is chemically inert in groundwater. Ekwurzel et al. (1994) concluded that their comparison showed close agreement between results obtained by the individual methods. In 1997, Cook and Solomon compared these three methods that previous study used and they pointed out that in simple, piston flow systems these methods can be used to estimate groundwater recharge rates with an accuracy of 20% or less, better than can be achieved with traditional hydraulic-based methods.

Plummer et al. (2001) carried out another multi-tracer study to reveal out the groundwater residence times in Shenandoah National Park located in Virginia, USA. In this study, multiple environmental tracers, including $^3\text{H}/^3\text{He}$, chlorofluorocarbons, SF_6 ,

and stable isotopes of water, were used to estimate the residence times of shallow groundwater discharging from 34 springs and 15 wells. For springs, the most reliable ages appeared to be based on SF₆ and ³H/³He, with most ages in the range of 0–3 years. This range was also consistent with apparent ages estimated from concentrations of CFCs; however, CFC-based ages concluded to have large uncertainties owing to the post-1995 leveling-off of the CFC atmospheric growth curves. The groundwater from wells and deep springs in the vicinity of the study area came out to have ages between 0 to 25 years. The data indicated that some water samples from wells were mixtures of young water (0 to 10 year old) with older, pre-CFC water.

A study from Syrian Jezireh was published in 2001 by Kattan demonstrating the use of hydrochemistry and environmental isotopes for evaluation of groundwater in a Paleogene limestone aquifer. In this study, the chemical ratios and isotopic compositions were used to differentiate the groundwater bodies into three main groups. The first group was fresh, cold and shallow groundwater, the second group is the brackish, thermal and deep groundwater and the last group is the admixed groundwater. The groundwater emerging from different springs were separated according to their origins and the mixing ratios were identified. Based on tritium content of the atmospheric precipitation, the simulation results of mean residence time agreed completely with the ¹⁴C groundwater ages. The ¹⁴C ages of the cold springs were smaller than 6,000 years and they were in a good agreement with the paleoclimatic humid conditions that prevailed during the Holocene period. The ages of thermal groundwaters were found out to be between 9,000 to 18,000 years corresponding to the paleoclimatic conditions of the Pleistocene.

Another recent study published in 2006 by Pilla et al. used hydrochemistry and isotope geochemistry as tools for groundwater hydrodynamic investigation in a multilayer aquifer located in northern Italy. In the study area, there three different aquifers, one a shallow phreatic aquifer, and two groups of confined aquifers, one in the alluvial sequence, and the other one in the lacustrine sequence have been identified. Oldest water was found in the confined aquifers because the buried structures prevent natural discharge. This water was concluded to infiltrate at the end of the cold dry climatic period of the LGM. The oldest waters were found out to be acting as a piston through the lithological and granulometric discontinuities of aquicludes and aquitards and the upward

pressure of deep groundwater avoiding the downward mass transfer of shallow groundwater. Data suggested that, the water pumped in the shallow aquifer was mixed therefore the results were older than they should be.

Last but not least, some of the recent studies in the literature used noble gases dissolved in groundwater (Ne, Ar, Kr, Xe) in selected confined aquifers to derive continental paleoclimate archive. Since the basic work of Mazor (1972) paleotemperatures were estimated by using noble gas measurements in groundwater. In 1993, Stute and Schlosser demonstrated the principles and applications of the noble gas paleothermometer. It has been proven that, the noble gas concentrations of recent groundwater closely reflect the mean annual temperature of the ground at the groundwater table since the temperature at which a water parcel was equilibrated with the atmosphere can be calculated from its noble gas concentrations using noble gases sensitivity to temperature. As the sensitivity of solubility to temperature increases with atomic mass Xe has the highest sensitivity whereas Ne solubility shows a very small temperature effect (Weiss 1970, 1971). Stute and Schlosser stated out that the quality of groundwater as paleoclimate archive depends critically on the extent to which the initial noble gas concentrations are changed by dispersion and mixing processes. There are several processes affecting noble gas concentrations measured in recent groundwater. The components which are solution of air according to Henry's law, dissolution of small air bubbles, and addition of non-atmospheric noble gases have to be separated for determination of noble gas temperature. It should be noted that the measured noble gas temperatures can only reveal paleoclimate information if the groundwater can be correctly dated using one of the established dating tools like ^{14}C .

Before Stute and Schlosser (1993) published their paper in which they discuss the principals of paleothermometer, in 1989, Stute and Deak carried out an environmental isotope study on deep groundwater circulation system in Great Hungarian Plain located in Hungary with reference to paleoclimate. Two hydrogeological crosssections were selected in the plain and groundwater samples were collected. The ^{14}C groundwater ages were corrected hydrochemically and compared with age information derived from excess helium due to ^4He from the α -decay of U and Th and their daughter nuclides within the aquifer and to He accumulation from the crustal (and mantle) He flux. In correcting the

^{14}C groundwater ages, carbonate dissolution under open and closed system conditions in the infiltration areas were considered. ^{14}C ages, after correction, fall into the last global cold period, are supported by significantly lower heavy stable isotope values as well as lower temperatures derived from the noble gases Ne, Ar, Kr and Xe.

Another study about deriving paleotemperature record derived from noble gases dissolved in groundwater was carried out by Stute et al. in San Juan Basin, New Mexico published in 1994. The results of this study indicated that there is a difference of $5.5 \pm 0.7^\circ\text{C}$ between the Holocene and Last Glacial Maximum (LGM) mean annual temperatures in the basin. The same approach had been applied to the Carrizo aquifer located in Texas. The combined results indicating uniform cooling suggested that the inland temperature gradient during the LGM must have been very close to the present one. The noble gas paleotemperatures were found out to be consistent with paleoecological evidence like plant remains, pollen and fossil vertebrates also supporting the efficiency of the method.

One other recent study published in 2002 by Aeschbach-Hertig et al. derived a paleotemperature record by using dissolved noble gases in groundwater of the Aquia Aquifer located in Maryland, USA. In the confined part of this aquifer, low ^{14}C activities in groundwater suggested that this water infiltrated at least 30,000 years ago. The radiocarbon contents of the dissolved inorganic carbon seemed to be affected by isotopic exchange; leading to overestimated ^{14}C ages, therefore for establishing a chronology an alternative method, the accumulation of radiogenic He, was used after measuring the U and Th concentrations in Aquia sand. Concentrations of dissolved atmospheric noble gases, used to derive mean annual ground temperatures at the time of infiltration, showed again the presence of water that infiltrated under much cooler conditions than at present. For this site, the temperature difference ($9.0 \pm 0.6^\circ\text{C}$) between Holocene and LGM came out to be lower than estimates derived from pollen data for this region but larger than the uniform cooling of about 5°C indicated by noble gas studies in southern locations of North America. This larger cooling was attributed to the influence of an ice sheet which at its maximum extension reached as close as 250 to the study site.

There are several other detailed studies in the literature that can not be included here, in which aforementioned methods for dating shallow and deep groundwaters with ages varying from decades to thousands of years were applied successfully. Besides age dating, paleoclimate information can also be derived and the origin of the groundwater can be understood. All these studies show and prove the necessity, capability and power of these modern methods since these techniques are efficient to solve the hydrogeological problems that can not be solved by conventional methods alone. This multi-tracer approach study will hopefully make further contributions and will provide a good case study demonstrating the application of these methods to a very complex aquifer system to determine the recharge and discharge mechanisms.

CHAPTER 3

DESCRIPTION OF THE STUDY AREA

3.1 Physiography

The study area is located on the flanks of Kazan Basin which is drained by the Ova Stream and its tributaries. Kazan Basin is an elongated NE-SW trending depression with an average width of 10 km and length of 40-45 km. It is morphologically divided into two distinct parts: a plain and a mountainous region. The flat part is called the Mürted Plain covering an area of 320 km² and being 10 km wide and 30 km long. Mürted Plain is an elevated plateau that ranges in elevation from 950 meters above sea level (masl) in the north to about 800 masl in the south (SRK, 2004). The average elevation is approximately 875 m. The highest elevation in the mountainous region is 1408 m decreasing gradually to 850 m toward the southeast. The relief map of the study area is shown in Figure 3.1 (SRK, 2004).

3.2 Climate

The study area, located in Central Anatolia, has a continental semi- arid climate with moderate to hot, dry summers and moist, cold winters. The average annual temperature recorded at Ankara Station between years 1930- 2006 is 11.8 °C with monthly averages changing from 0.1 °C in January to 23.3 °C in July. Long term meteorological records are available from Ankara, Esenboğa, Etimesgut and Akıncılar Stations whose locations can be seen in Figure 1.1. These stations belong to Turkish State Meteorological Service and the data was obtained from the institution.

The long-term average annual precipitation data is available between 1930- 2006 for Ankara Station. According to the long term measurements, the amount of precipitation received is low with an annual average of 389.1 mm (Figure 3.2).

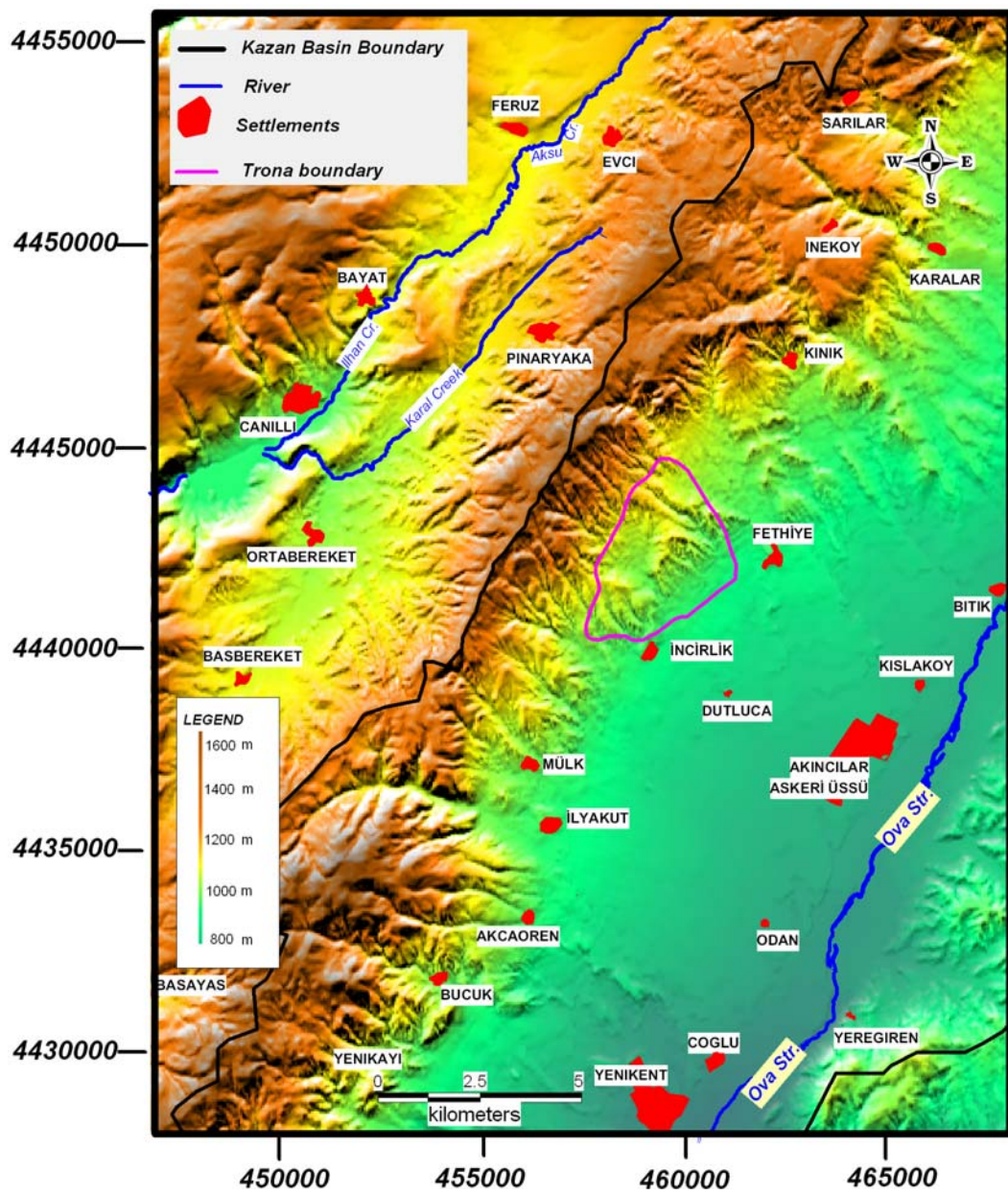


Figure 3.1 Relief map of the study area (SRK, 2004).

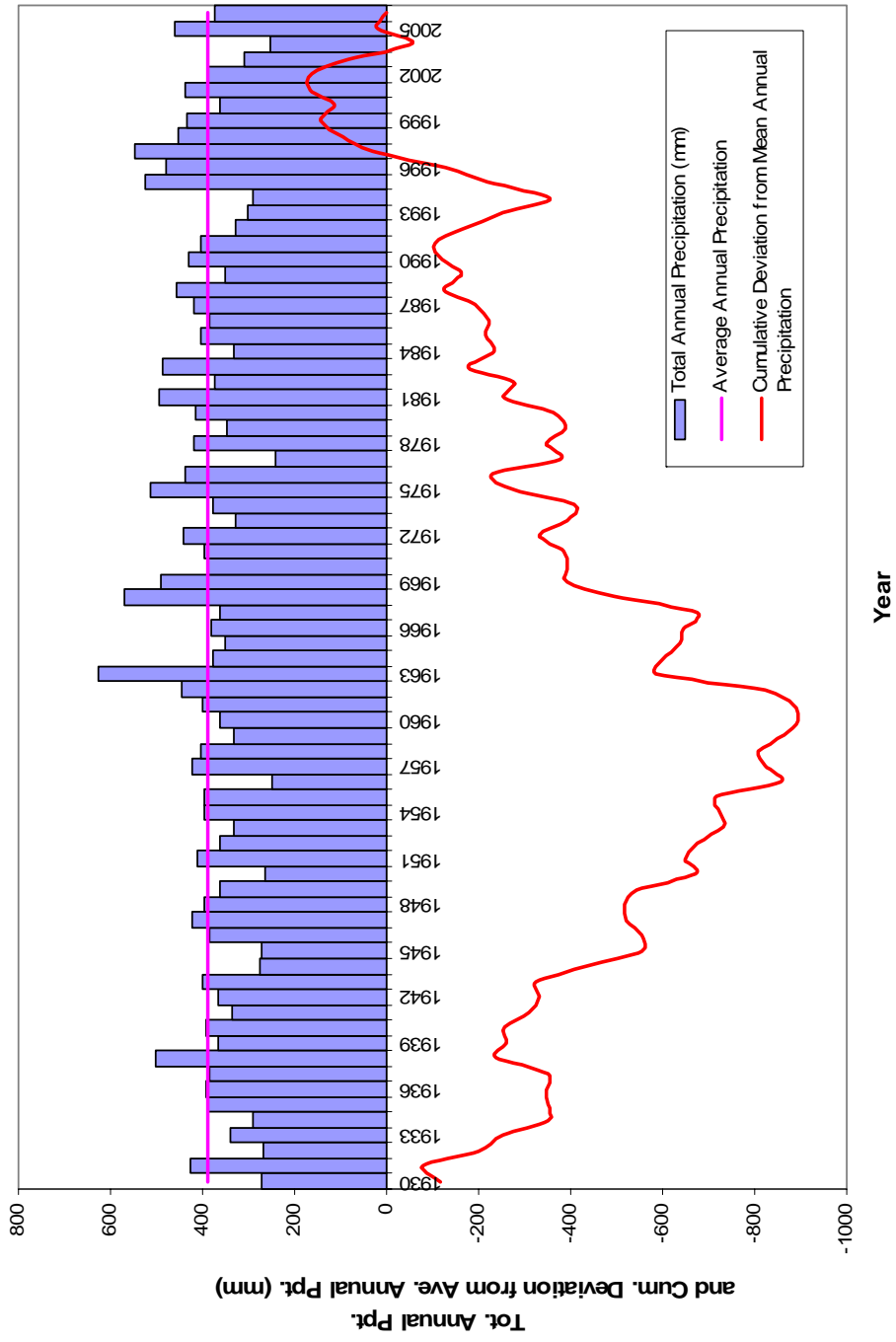


Figure 3.2 The distribution of annual precipitation at Ankara station and the cumulative deviation from average annual precipitation.

The precipitation data from Ankara station shows that the maximum annual precipitation was measured as 627.74 millimeters (mm) in 1963 and the minimum annual precipitation was recorded as 242.0 mm in 1977. In addition to Ankara Station there is another on-site meteorological Station, K-41. The total annual precipitation recorded at K-41 was 372 mm in 2001 and 351 mm in 2002 (SRK, 2004). The monthly distribution of precipitation data shows that two-thirds of the annual precipitation occurs during the winter and spring seasons (December and May) whereas the rest occurs in the summer and fall seasons.

According to the measurement of evaporation at the Ankara Station (1981-1999) average annual evaporation was 1112.2 mm. The annual average evaporation at the Ankara Station ranged from 904.3 mm in 1982 to 1526.9 mm in 1994. The average monthly evaporation varied from 19.8 mm in November to 238.5 mm in July.

The average monthly relative humidity values obtained from Ankara Station between years 1930- 2006 varies from 44.1 % in August to 77.5% in December with an average annual relative humidity of 60.5%.

3.3 Geology

3.3.1 Geology of Kazan Basin

Kazan Basin is one of several neotectonic depressions located in northwest of Ankara, Turkey, which is elongated in NE-SW direction with an average width of 10 km and length of 40-45 km. It is connected to Çubuk Basin at the northeast and is drained to other Neogene basins at the south. Kazan Basin is regionally situated to the north of the Izmir- Ankara- Erzincan Suture (IAES) and south of the North Anatolian Fault Zone (NAFZ) (Figure 3.3).

The NAFZ, which is the longest active fault zone in Turkey, is composed of closely spaced, parallel faults of right lateral strike slip character. (Tokay, 1973, 1982; Yılmaz et al. (1981); Hancock and Barka, 1983; Barka, 1984; Öztürk et al., 1985; Barka & Gülen 1988). It extends in NEE- SWW direction and passes north of Kazan basin (Figure 3.3).

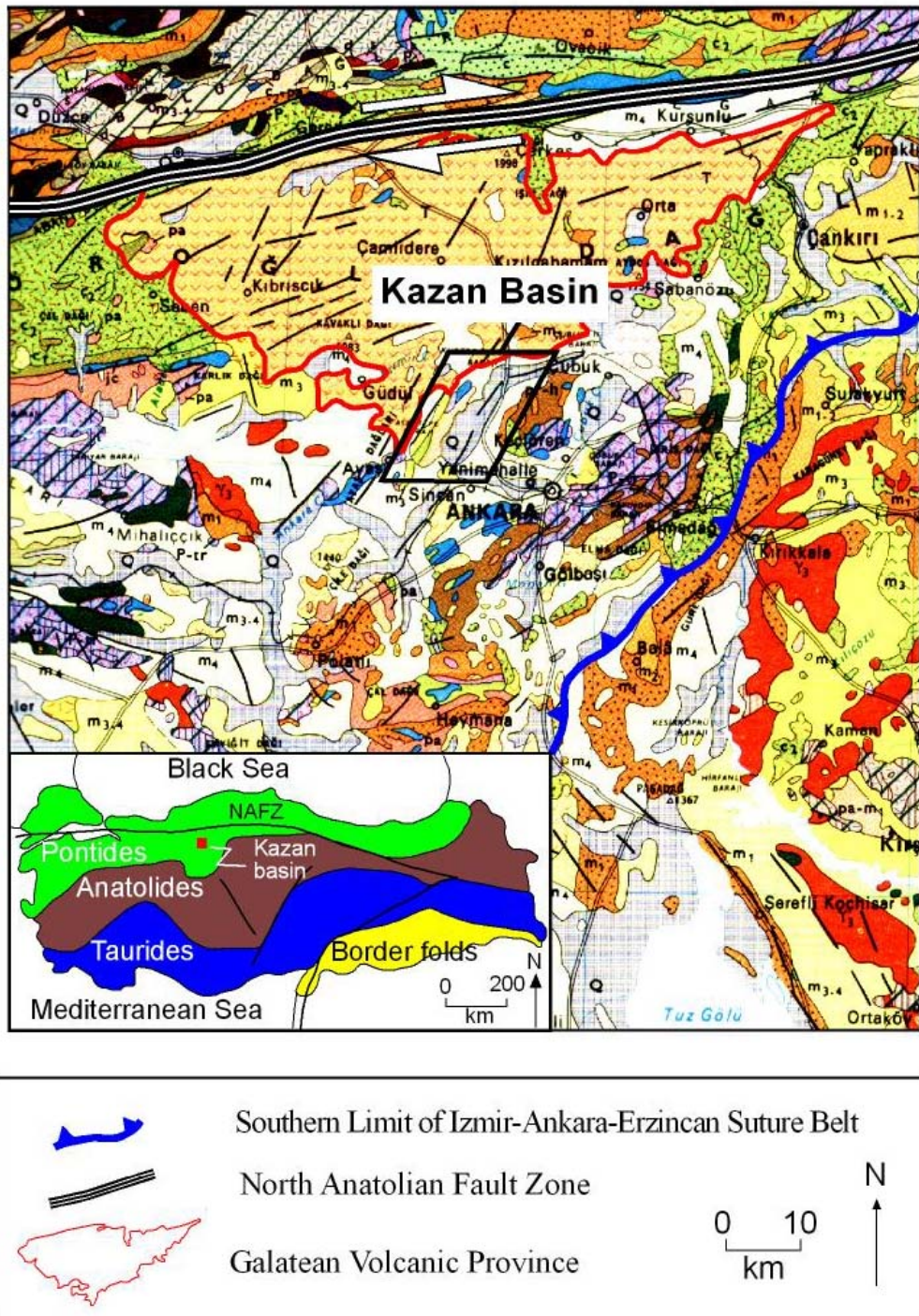


Figure 3.3 Regional setting of the Kazan Basin (SRK, 2004).

IAES defines the boundary of two major tectonic units of Turkey: Pontides to the north and Anatolides to the south. Kazan Basin is located in the Pontide Belt which is an orogenic belt evolved since Triassic by progressive accretion of continental terrains with oceanic fragments during the closure of Paleo- and Neo- Tethyn oceans (Şengör and Yılmaz, 1981; Şengör, 1984). With the closure of the northern branch of the Neotethys, the Galatean Volcanic Complex formed which is one of the major Neogene volcanic belts located in the central northwestern part of Turkey (Şengör and Yılmaz, 1981; Koçyiğit et al., 1988; Koçyiğit, 1991a). The wedge- shaped volcanic province is oriented in ENE-WSW direction for a length of about 280 km and is located within the Pontide belt to the north of IAES (Figure 3.3).

Kazan Basin is bounded by the Orhaniye uplift to the east, the Kınık uplift to the west, the Kızılcahamam volcanic terrain to the north, and the Zir volcanic terrain to the south (Figure 3.4). The rock units present in the basin are the Paleozoic Metamorphics, Jurassic- Cretaceous Carbonates, Cretaceous North Anatolian Ophiolitic Mélange which are categorized as allochthonous,, Cretaceous-Paleocene Units Eocene Mülk Formation, Middle Eocene Akpınar Limestone, post- Eocene Orhaniye Syenite which are classified as paraautochthonous, Miocene sedimentary and volcanic units, Pliocene units and Plio-Quaternary deposits which are categorized as autochthonous (Koçyiğit and Lünel, 1987; Kazancı and Gökten, 1988; Koçyiğit et al 1988).

3.3.2 Geology of the Study Area

The study area is located to the west of İncirlik and Fethiye villages, in the western margin of the Kazan basin. The detailed geological investigation of the study area was carried out by Toprak and Rojay (2000 and 2001) and Rojay et al. (2002). There are four basic rock sequences exposed in the study area which are, from bottom to top, Paleozoic Metamorphics, Eocene sequences (Mülk formation and Akpınar Limestone), Neogene Units and Plio-Quaternary deposits (Figure 3.5). The stratigraphic sequences are shown in the columnar section of the study given in Figure 3.5. In Figure 3.6, a geological map showing the distributions of the units observed in the study area can also be seen. There is also evidence of restricted volcanic input since the Eocene.

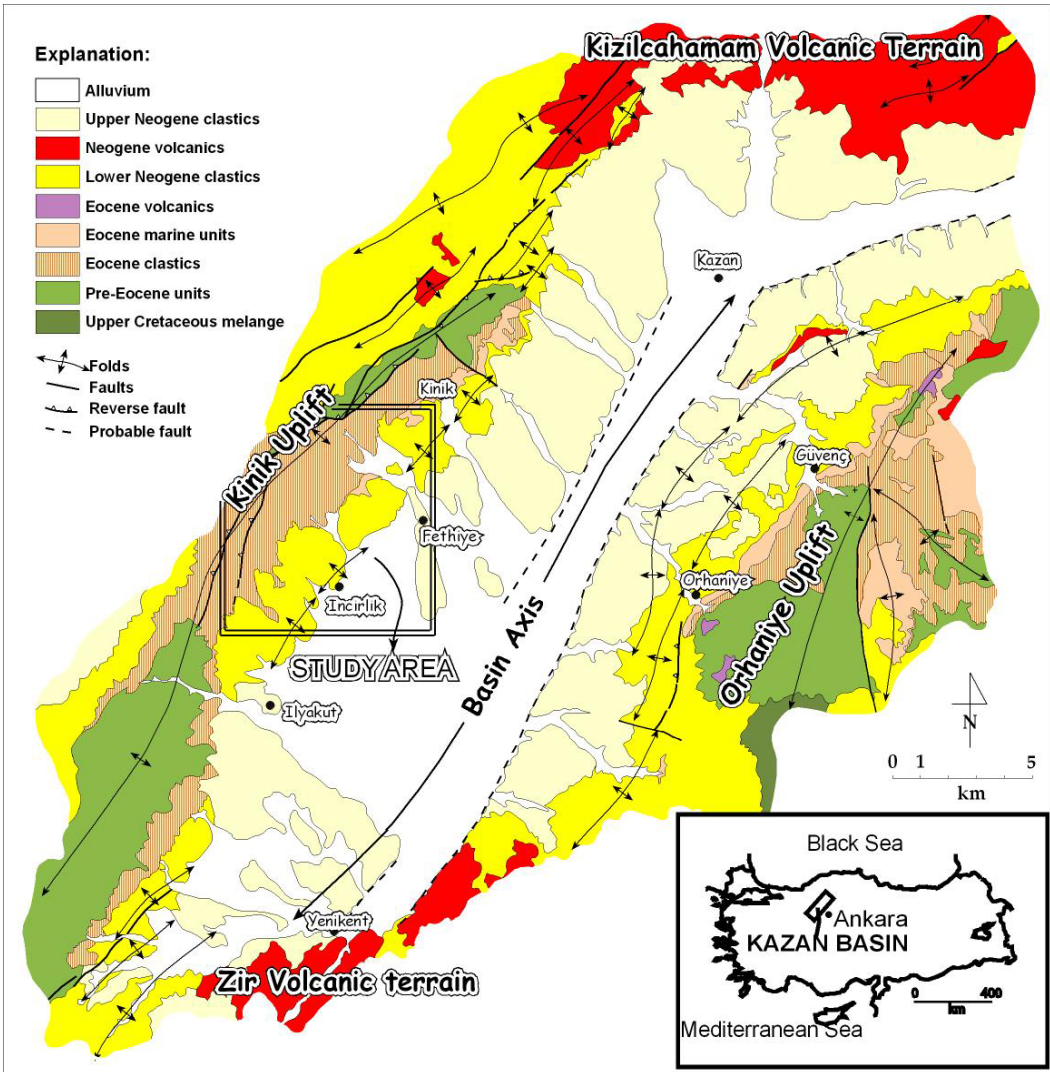


Figure 3.4 Simplified geological map of the Kazan Basin (Toprak and Rojay, 2000).

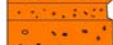
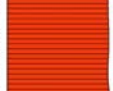
Age	Unit	Lithology	Physical Properties	Hydrogeologic Unit
Neogene	Plio-Quat.		U Colluvium-talus, alluvium, alluvial fan, slope deposits	Shallow Groundwater System
			U Red, thick bedded to massive coarse clastics	
			White, medium bedded limestone with silica beds, green sandstones-conglomerates with tuffaceous clastics	Neogene Aquitard
			Variegated clastics (mudstones, cross-bedded sandstones and conglomerates)	
Early - Middle Eocene	M Ü L K F O R M A T I O N		I - Orange, reddish brown, porous conglomerates with angular pebbles F - Gray, well-rounded, sorted, pebble supported, highly porous conglomerate	Middle Groundwater System
			U Cream-beige, medium to thick-bedded, clayey-cherty limestones-mudstones	
	Fethiye member		Yellow, medium to thick bedded, sandy Nummulitic limestone "Sarkaya member": Reddish brown, cross bedded clastics	Aquitard
			Light green-green marls with pinkish clayey limestone beds	Deep Groundwater System Fractured Fethiye, Asmalıdere and İncirlik Members
Asmalıdere member		Light brown-beige-cream, thin bedded marls, mudstones		
İncirlik member		"Clastic wedge" Yellow-yellowish brown, medium to thick bedded sandstone-conglomerate-siltstone sequence with cream, thin bedded marls		
		Dark brown, thin bedded marls, yellowish brown, thin bedded clayey limestones-marls with black laminated organic-rich beds		
Paleozoic	Taşın msh.		T Brownish yellow mudstones-siltstones-sandstones with green volcanics	Basement
			Black graphitic schists enclosing gray-blackish gray, thick bedded dismembered, intensely fractured, recrystallized limestones	

Figure 3.5 Columnar section of the study area (Toprak and Rojay, 2001).

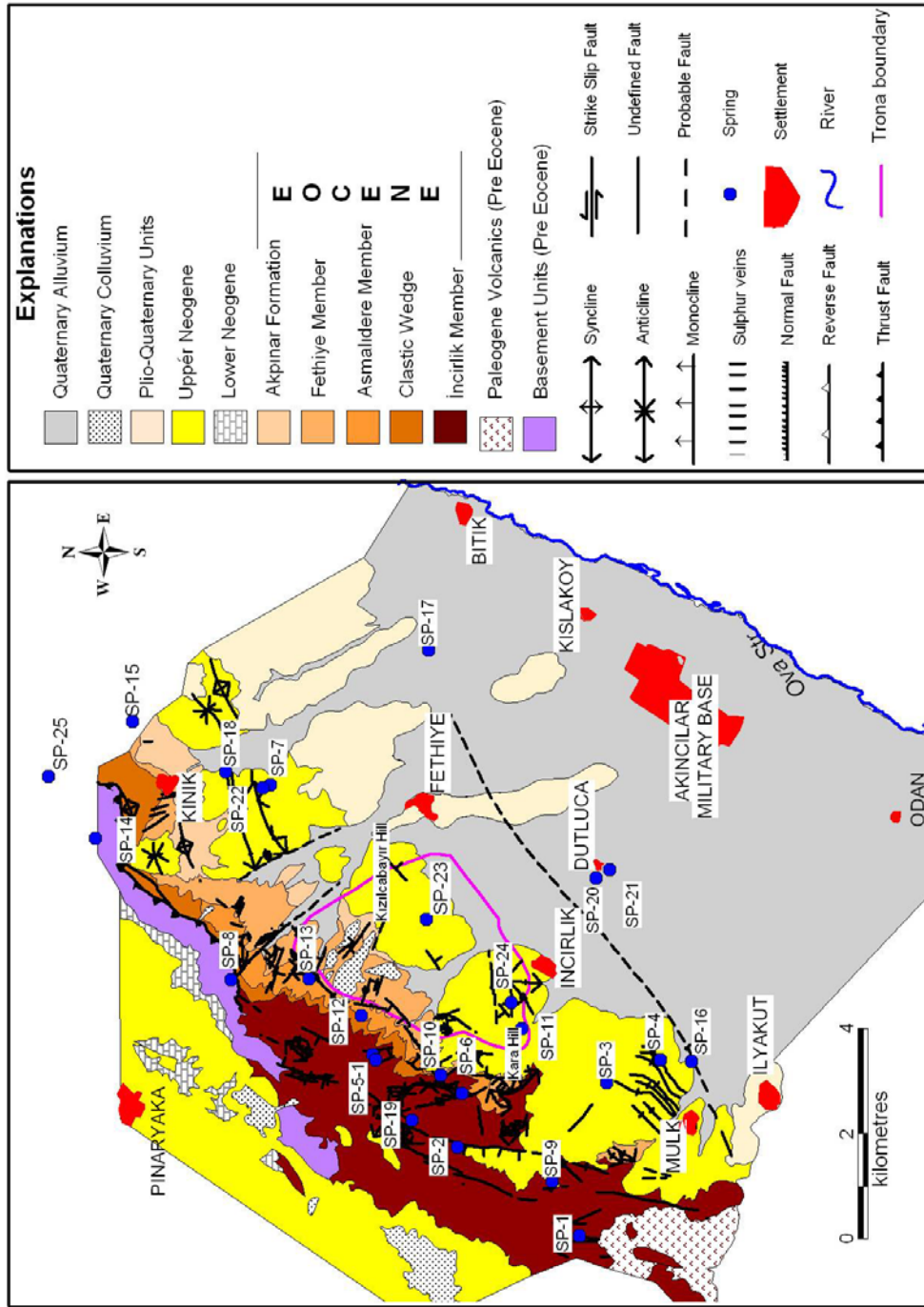


Figure 3.6 Geological map of the study area (Toprak and Rojay, 2001).

3.3.2.1 Stratigraphy

Paleozoic metamorphics, which are the basement rocks in the study area, crop out in a small area to the NW of Fethiye village. They thrust over the clastics of Eocene sequences and are unconformably overlain by Neogene units. The basement rocks are made up of black intensely deformed graphitic schists enclosing gray-grayish black, thick bedded, dismembered and intensely fractured recrystallized limestones (Figure 3.5).

Eocene units, conformably underlying volcano-sedimentary sequence of Paleocene and unconformably overlain by Neogene conglomerates, crops out as a NE-SW trending belt in the project area. The sequence is developed as a transgressive sequence from a lacustrine to a shallow marine depositional setting. Age of the sequence is well documented and an age of Early Eocene to Lutetian is assigned (Koçyiğit et al., 1988, Kazancı and Gökten, 1988).

Eocene units are lithostratigraphically divided into two sequences. The lower sequence is named as Mülk Formation and the upper sequence as Akpınar Limestone (Figure 3.5). The Mülk formation is composed of lacustrine sedimentary rocks. The formation is divided into four lithostatigraphic sequences which are, from bottom to top, Taban member, İncirlik Member, Asmalidere Member and Fethiye Member. Taban Member consists of intensely deformed and dismembered brownish yellow mudstones, siltstones and sandstones with green volcanic inclusions. İncirlik Member is comprised of dark brown, thin-bedded marls, yellowish brown, thin-bedded clayey limestones-marls with black laminated thin-bedded, carbonaceous, organic- rich dolomitic mudstone beds (Toprak and Rojay, 2000). Asmalidere Member consists of a yellow yellowish- brown-gray, medium- to thick-bedded, highly- porous sandstone- conglomerate- siltstone sequence with cream, thin- bedded marls at the bottom. This sequence is named as clastic wedge. The upper part consists of light brown-beige-cream, thin-bedded marls and mudstones. Fethiye Member consists of light- green to green marls with minor pinkish clayey limestone beds at the top of the sequence. These intensely jointed and faulted marls grades into fossiliferous sandy limestones of Akpınar Formation.

The Akpınar formation is unconformably overlain by the Neogene clastics whereas the unit has a conformable contact with the underlying green marls. At the bottom, it consists of reddish- brown, cross-laminated siltstones- sandstones- conglomerates. In the middle blueish- green marls to yellow- light- green, fossilifereous sandstones- conglomerates are present followed by yellow- gray, medium- to thick- bedded, highly porous, fossiliferous sandy limestones at the top. Based on the macrofossils of these shallow marine carbonates an age of Early Eocene to Lutetian was given by Toprak and Rojay (2001).

The Neogene units, unconformably overlapping the Paleozoic metamorphics, Mülk and Akpınar formations, consist of conglomerates of different lithologic components. There is an unconformity between the Neogene unit located in the northwestern part of the study area and the overlying Neogene sequence. These two sequences are different from each other in lithologic character and deformation pattern, therefore the lower unit is referred as the “older Neogene sequence or Lower Neogene” by Toprak and Rojay 2001. The Lower Neogene sequence consists of cream to beige, medium- to thick- bedded, clayey and cherty limestones and mudstones that are fractured and deformed compared with the younger Neogene sequences. The age of the older Neogene sequence was suggested to be early Miocene by Toprak and Rojay (2001).

The younger Neogene sequences display different depositional characteristics in different parts of the study area therefore two different sequences are labeled as Fethiye section (F in Figure 3.5) and the İncirlik section (I in Figure 3.5). The Neogene sequence in the Fethiye section consists of gray, well- rounded and sorted, highly porous, almost pebble-supported conglomerate to the northwest of Fethiye in the Kizilcabayir Hills (Toprak and Rojay, 2000). The pebbles of conglomerates are derived from graphitic schists, mafic volcanics, Eocene limestones, black cherts, recrystallized limestones-marbles and rarely from clastics of Mülk Formation. The conglomerates display first an upward fining sequence, and then towards the top of the Neogene, grades from mudstones to highly porous sandstone- conglomerate sequence. The sequence unconformably overlaps the underlying Akpınar Formation. To the northwest of İncirlik, the Neogene sequence overlaps underlying Mülk formation with orange- reddish- brown, massive, angular, pebbly, porous conglomerates. On the contrary to the conglomerates present in Fethiye section, pebbles in İncirlik section are derived almost only from Mülk formation (Toprak

and Rojay, 2000). The conglomerates continue with light green mudstones-marls and white, thick bedded cherty limestones. Brown, cross-bedded conglomerate interrupts the sequence for approximately 3 meters. This part is followed by a variegated part that consists of red mudstones - pink, thin-medium bedded limestones and green mudstones, grades into pink limestones and green mudstones and to green volcanigenic sandstones and mudstones. Top of the sequence is characterized by white, medium bedded, highly porous-light limestones, white, silica-rich limestones, green mudstones with green silica beds, green sandstones-conglomerates and white, highly porous tuffaceous clastics. The lacustrine units that define uppermost part of the Neogene sequence are interbedded with andesitic volcanics and have a considerable thickness to the far north and south of the study area (north and south of Kazan basin) (Figure 3.4). The younger Neogene sequences are known as the Kocadoruk Formation and unconformably overlain by Pliocene clastics (Toprak and Rojay, 2000).

The Pliocene clastics outcrop to the south and northeast of the Fethiye Village (Figure 3.6). They are also known as Kirmir formation and they consist of reddish, highly porous, poorly compacted and cemented, well- rounded, poorly sorted conglomerates, and sandstone- siltstone- mudstone alternations (Toprak and Rojay, 2000).

The Quaternary deposits consist of various isolated conglomerates separated from each other. These are the colluvium/talus accumulations, alluvium, alluvial fans and slope deposits. The colluvium and talus accumulations consist of yellow colored, angular to subangular, pebbly, semiconsolidated conglomerates. Alluvial fans that are on the edges of Kara hill to Kızılcabayır hills consist of yellow to white, loose, angular to subrounded pebbles. Alluvium covers the flat lying surfaces and consists of loose pebbles, sands and silts (Toprak and Rojay, 2001).

3.3.2.2 Structural Geology

The study area is bounded by a major N25E trending anticline that is truncated by a fault parallel to its axis on west and Quaternary boundary fault on the east. This anticline is asymmetrical in the vicinity of the study area. Along the core, oldest Eocene sequences (İncirlik Member) and tectonically overlying Paleozoic Metamorphics are exposed. More

than 40 folds, a monocline and various faults are developed in the area. The major structural elements are also given with the geological map of the study area in Figure 3.6. Most of the folds are parallel to each other and are NE-SW trending. They range in length from a few hundred meters to several kilometers (SRK, 2004).

3.4 Hydrogeology of the Study Area

3.4.1 Water Resources

3.4.1.1 Surface Water Resources

The Ova Stream and its tributaries constitute the major component of surface water resources in Kazan Basin. The Ova Stream flows in a NE- SW direction about 5 km to the southeast of the study area (Figure 3.7). Kurtboğazı Creek is the largest tributary to the Ova Stream joining the stream to the east of Kazan. Several other creeks also join the Ova Stream but most of them are ephemeral and dry up during the summer months. Kurtboğazı Dam is the main surface water reservoir in the Kazan Basin located 19 km north of the project area. Water from the Ova Stream has been diverted to this dam. The Mülk Reservoir is another surface water body located near Mülk Village (Figure 3.7).

Three streamflow gauging stations were established on the Ova Stream by the State Hydraulic Works (DSİ) and the Electrical Power Resources Survey and Development Administration (EİEİ) which are Eybek, Zir and Kurtboğazı stations. Currently, only one of these gauging stations (No: 1239-Eybek) is active (Figure 3.7). According to the measurements from this station, the lowest discharges occur in the months of summer and fall (July through October) whereas the highest discharges occur in March and April. Based on long-term data, the average annual discharge is 2.51 m³/s for Eybek station (SRK, 2004). The stream flow during July, August and September generally represent the base flow of the Ova Stream.

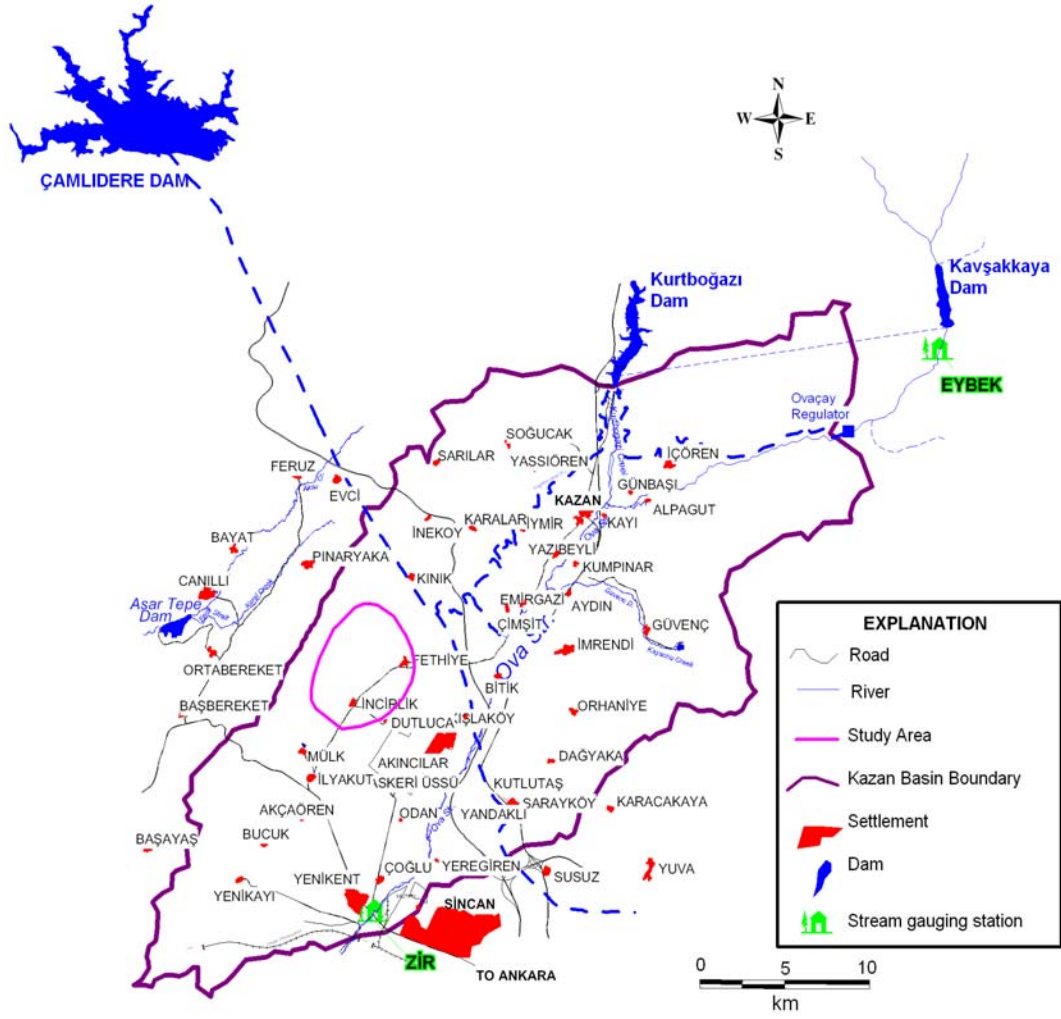


Figure 3.7 Surface waters and reservoirs in the Kazan Basin.

3.4.1.2 Springs and Seeps

According to the hydrogeological investigation studies conducted by the State Hydraulic Works (1976) between 1968 and 1970 there are several springs present in the Kazan Basin most of which are located along the faults or at the contacts between various units in the basin. During the field survey carried out by Yazıcıgil et al. in July 2000 twenty-six springs were identified (Figure 3.6) (Yazıcıgil et al., 2001). These springs were

monitored for discharge and field parameters. Measured discharges varied from 0 to 5.88 l/s. Most of the springs responded to precipitation.

3.4.1.3 Groundwater

According to the inventory of SRK Consulting about the private wells in the study area totally 46 wells are present. 33 of them are located in Fethiye Village, 4 in Mülk Village, 5 in Dutluca village, 2 in İncirlik and the rest in İlyakut Villages. Most of private wells are used for domestic and irrigation purposes. Most of them are shallow dug or driven wells (SRK, 2001).

So as to characterize the site hydrogeological conditions, fifty-eight groundwater monitoring wells have been completed in the study area. The locations of the monitoring wells are given in Figure 3.8 (SRK, 2004). Wells whose depths range from 7 to 850 m below ground surface were installed to monitor the groundwater systems at different depths (Table 3.1). In order to determine the hydraulic conductivity and storativity of the water-bearing units, several aquifer tests were conducted at selected piezometers in the study area.

3.4.2 Hydrogeologic Classification of Units

The significant water-bearing units are grouped as shallow (alluvium), middle (Neogene) and deep (Eocene) groundwater systems. The Akpınar formation lying between deep and middle systems acts as an aquitard (SRK, 2004).

3.4.2.1 Shallow Groundwater System

SRK (2004) stated that the shallow groundwater system occurs under unconfined conditions in the Quaternary alluvial deposits. The alluvial deposits form a regional unconfined aquifer in the Kazan Basin. The uppermost weathered and fractured sections of the Neogene form a local perched aquifer to the southwest of the trona deposit area. The shallow Neogene wells are S-19 through S-24 in Figure 3.8. The alluvium is penetrated by several wells in the vicinity of the Fethiye village and along the Ova stream

Table 3.1 Monitoring well data.

Well ID	Coordinates		Ground Elevation (m)	Completion Depth (m)	Formation/ Member Tapped	Depth to Screened Zone (m)		System Monitored
	Northing	Easting				Top	Bottom	
D-8	458803.4	4442308.8	985.84	194.69	Asmalidere	158.99	188.74	Deep
D-13	461261.3	4444346.2	961.35	397.49	Fethiye	361.79	391.54	Deep
D-20	458931.9	4444438.2	1073.45	227.66	İncirlik	191.96	221.71	Deep
M-31	459587.5	4442257.2	1023.93	80.81	Neogene	47.46	77.31	Middle
D-33	457656.3	4439808.0	948.32	169.33	Fethiye	151.43	163.33	Deep
D-37	460556.8	4444364.9	986.44	247.48	Fethiye	211.78	241.53	Deep
D-47	458608.2	4441977.3	980.51	378	Fethiye, Asmalidere, İncirlik	72.00	372.00	Deep
I-50	459607.5	4441948.1	991.06	826.5	İncirlik	808.50	820.50	İncirlik
D-53	461207.0	4442103.7	904.73	582	Fethiye	546.00	576.00	Deep
D-57-A	458876.9	4439740.0	907.03	324.64	Fethiye	300.71	318.62	Deep
M-57-B	458875.4	4439742.4	907.61	150.6	Neogene	132.09	144.03	Middle
A-58-A1	461568.2	4443300.1	931.97	307	Akpınar	289.00	301.00	Akpınar
A-58-A2	461568.2	4443300.1	931.97	226	Akpınar	208.00	220.00	Akpınar
S-58-A3	461568.2	4443300.1	931.97	34	Alluvium	10.00	34.00	Shallow
D-60-A	457814.6	4440764.3	976.29	298	İncirlik	280.00	292.00	Deep
M-60-B	457814.6	4440764.3	976.29	127	Neogene	114.00	126.00	Middle
D-63-A	459207.3	4443039.4	1021.06	211	Asmalidere	199.00	211.00	Deep
D-63-B	459207.3	4443039.4	1021.06	122.5	Fethiye	110.50	122.50	Deep
D-65-A	458254.2	4441658.1	1060.69	197	Fethiye	173.00	191.00	Deep
M-65-B	458254.2	4441658.1	1060.69	117	Neogene	101.00	117.00	Middle
D-68R	458768.0	4442660.0	1002.91	84	Fethiye	63.00	83.00	Deep
I-74-A	459431.0	4441041.0	937.30	550	İncirlik	520.00	544.00	İncirlik
D-74-B	459431.0	4441041.0	937.30	300	Fethiye	282.00	294.00	Deep
M-74-C	459431.0	4441041.0	937.30	98	Neogene	78.00	96.00	Middle
S-1	458389.7	4438691.6	904.26	20	Alluvium	8.00	20.00	Shallow
S-2	458866.8	4439755.7	907.93	20	Alluvium	8.00	20.00	Shallow
S-3	459986.4	4438608.1	868.47	20	Alluvium	8.00	20.00	Shallow
S-4	461000.0	4439113.0	862.27	9	Alluvium	5.00	9.00	Shallow
S-5	460231.6	4440080.6	891.53	20	Alluvium	8.00	20.00	Shallow
S-9	461520.5	4439964.2	864.85	15	Alluvium	7.00	15.00	Shallow
S-11	463142.2	4441246.7	875.28	14	Alluvium	4.00	12.00	Shallow
S-13	462230.8	4442793.2	913.55	12	Alluvium	4.00	12.00	Shallow
S-16	459264.3	4441443.7	943.48	23	Alluvium	7.00	23.00	Shallow
S-19	457306.5	4439795.9	974.32	20	Neogene	4.00	20.00	Shallow
S-20	457763.0	4439650.9	943.25	20	Neogene	4.00	20.00	Shallow
S-21	458023.7	4439202.8	927.54	20	Neogene	4.00	20.00	Shallow
S-22-A	457680.0	4439963.3	953.25	21	Neogene	13.00	21.00	Shallow
S-23	457920.9	4439664.4	939.88	20	Neogene	4.00	20.00	Shallow
S-24	457526.8	4439709.6	956.26	20	Neogene	4.00	20.00	Shallow

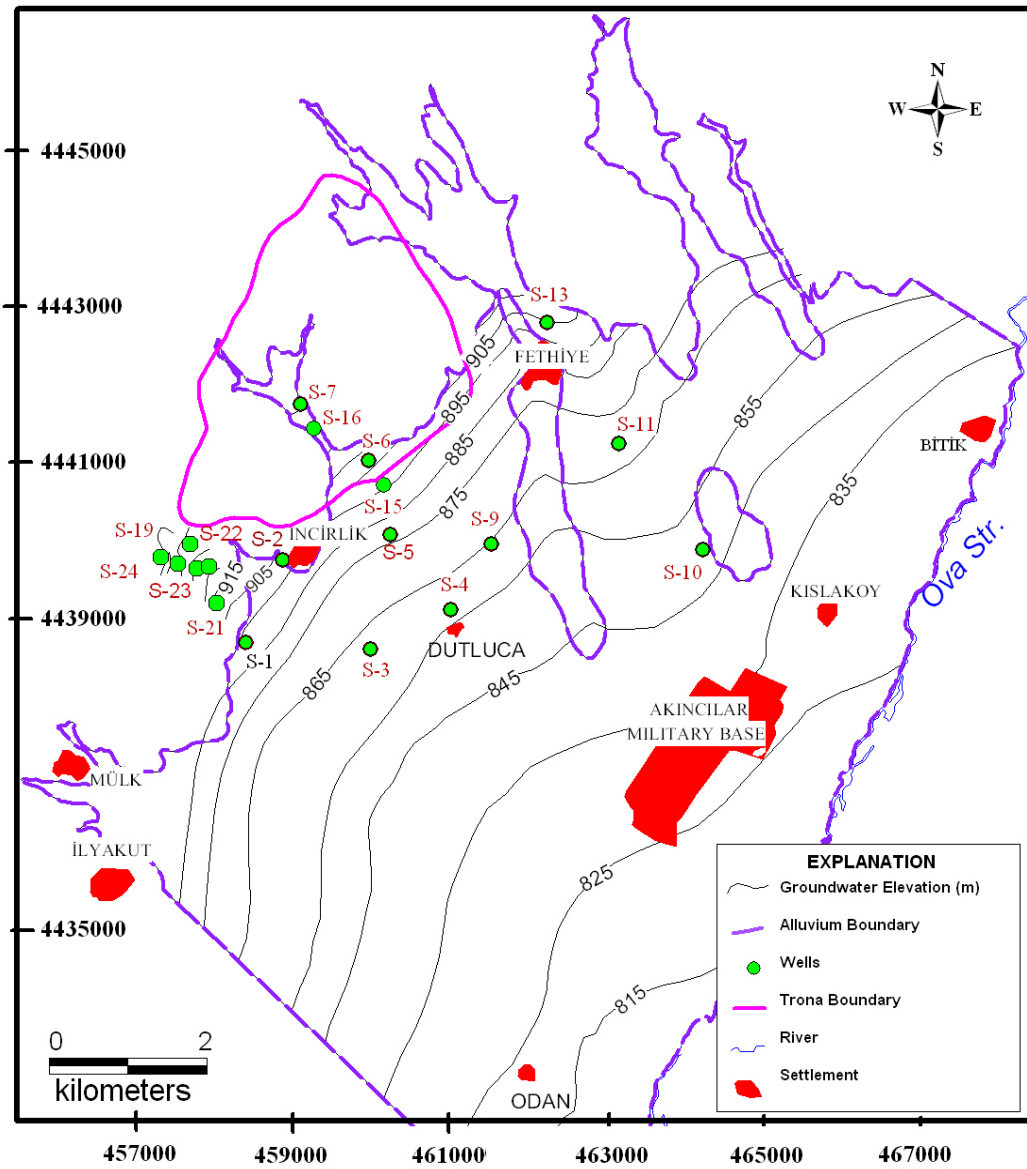


Figure 3.9 Groundwater level contour map for the shallow aquifer system for March, 2003 (SRK, 2004).

southeasterly toward the Ova Stream. The hydraulic gradient is around 0.03 along the margins of the plain in the west whereas it is about 0.007 to the southeast (SRK, 2004). In the alluvium, the depth to water table varies from 1 meter to 15 meters (SRK, 2004). Monthly monitoring data show groundwater levels rise during the wet season at

monitoring wells S-1, S-2, S-7, S-12 and S-13 which are located in front of the mountain range at the edge of the basin (Figure 3.9) (SRK, 2004).

According to the results of slug tests performed by SRK Consulting, the hydraulic conductivity of the alluvium ranges from 1×10^{-6} m/sec to 7.7×10^{-5} m/sec whereas the hydraulic conductivity in the shallow Neogene system ranges from 5.4×10^{-7} m/sec to 1×10^{-5} m/sec. These results suggest that the uppermost Neogene is not as permeable as the alluvium (SRK, 2004).

3.4.2.2 Middle Groundwater System

The middle aquifer system is present in the fractured network developed as a result of faulting and in the basal conglomerates of the Neogene unit. The groundwater system is under confined conditions away from the outcrops (SRK, 2001).

The Neogene unit is exposed in the middle of the project area between İncirlik and Fethiye Villages whereas it underlies the alluvial unit to the east of the project area. The system becomes deeper toward the east. It is separated from the underlying deep aquifer by a thick aquitard consisting of the Akpınar Formation to the north of İncirlik village. To the south of the village, the middle aquifer system, however, lies directly above the deep aquifer system (SRK, 2001). According to SRK Consulting, the average vertical thickness of the aquifer is 50 m.

The groundwater table contour map of middle aquifer system prepared by SRK for March 2003 is given in Figure 3.10. According to this map, the groundwater flow is to the southeast towards the Ova Stream. The horizontal hydraulic gradients vary between 0.07 and 0.1. Considering the hydraulic heads of deep and middle aquifer systems there is a strong vertical hydraulic gradient between these two systems away from the outcrop area. At wells M-60-B and M-65-B, the vertical gradient is almost 0 whereas it becomes 0.21 at wells M-57-B and M-74-C according to SRK (2004) (Figure 3.10).

During the previous study by Yazıcıgil et al. (2001), it was observed that the monitoring wells M-31 and M-65-B located in the area where the aquifer is unconfined respond to

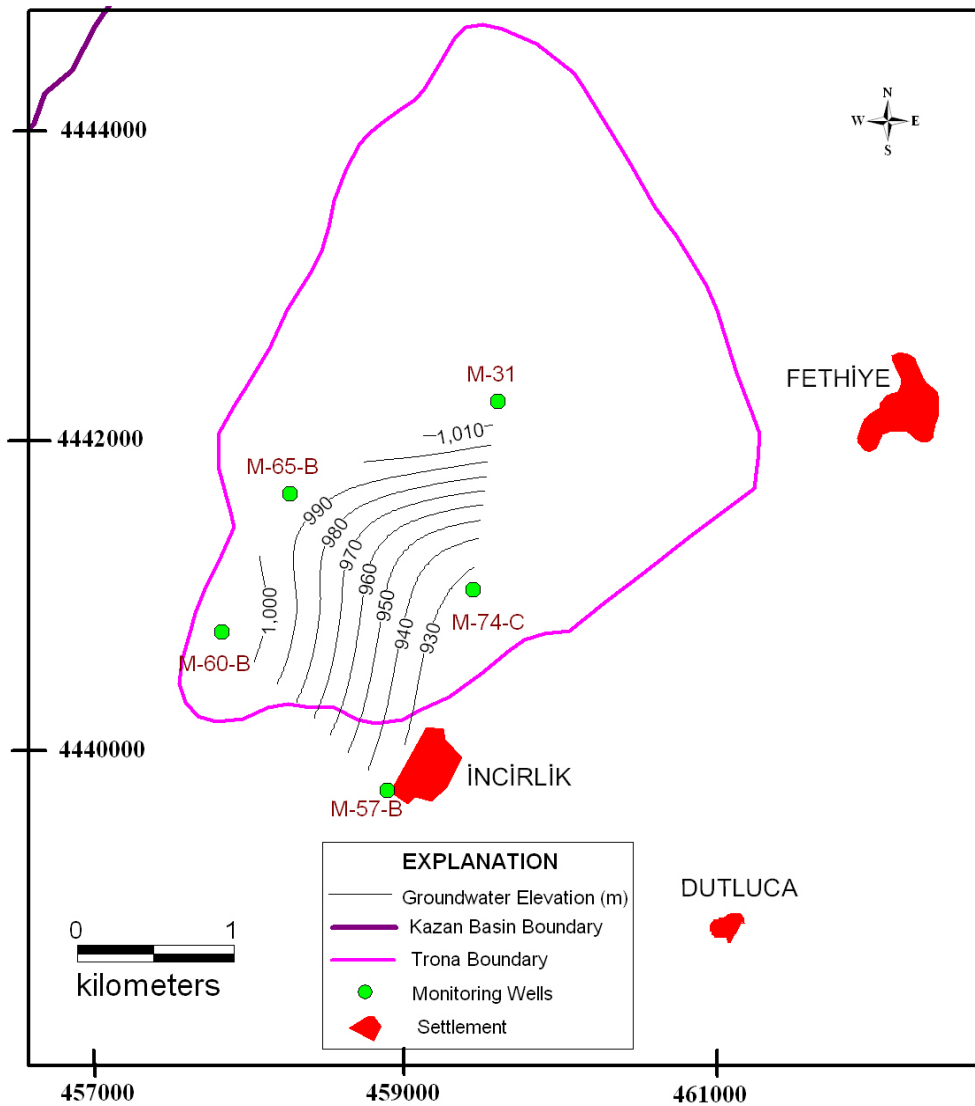


Figure 3.10 Groundwater level contour map for the middle aquifer system for March, 2003 (SRK, 2004).

precipitation directly and indicate recharge from precipitation. The artesian wells (M-57-B and M-60-B) do not show any immediate response to precipitation although the water levels showed an increase since December 2001 (SRK, 2004). These wells show free-flowing conditions with varying discharges. The flow rate in M-60-B showed a continuous decrease since its installation from a discharge rate of 0.055 l/s to 0.015 l/s.

On the other hand, M-57-B shows seasonal variations with an average discharge rate of 0.016 l/s (SRK, 2004).

According to SRK Consulting, the hydraulic conductivity values for this system ranged from 9.4×10^{-9} to 4.9×10^{-8} m/s. The aquifer behaves as a confined aquifer away from the outcrop area (SRK, 2004).

3.4.2.3 Akpınar Aquitard

The Akpınar unit is not a significant water-bearing unit although groundwater exists within it. This unit underlies the Neogene unit whenever it is present and acts as an aquitard between middle and deep groundwater systems. The monitoring wells completed in this formation reveals that all wells are under confined conditions, the groundwater levels are above the ground surface and the groundwater flow rates are too small to measure (SRK, 2004).

The hydraulic conductivity values are low and range from 6.2×10^{-9} to 8.3×10^{-9} m/s. There is an upward vertical gradient (about 0.2) from deep aquifer to Akpınar (SRK, 2004).

3.4.2.4 Deep Groundwater System

The deep groundwater system occurs under confined conditions in the fractured sections of the Fethiye, Asmalıdere and İncirlik members of the Eocene aged Mülk formation. These members are the most fractured units in the study area. As a result, groundwater flows through a deep fractured-rock system. The presence of a saline zone in the deep aquifer system at the southern half of the trona deposit area has a significant impact on groundwater quality (SRK, 2001).

The top and the bottom elevations of the fractured zone representing the top and bottom elevations of the deep aquifer system were determined using the fracture- frequency versus depth information obtained from borehole studies (SRK, 2004). Accordingly, the thickness of the fractured aquifer exceeds 400 m in the west of the deposit area decreasing progressively toward east to about 100- 150 m. The degree of fracturing

increases towards west where these rock units outcrop. The fracturing decreases towards east and almost vanishes in İncirlik and Asmalıdere Members toward the middle of the trona deposit area. Fracturing in the Fethiye Member can be observed in all the boreholes (SRK, 2004).

There are twenty- two monitoring wells in the deep fractured aquifer system. Besides, two monitoring wells were installed below the bottom of the fracture system; one is below the trona zone (I-50) another is above the trona zone (I-74-A) (SRK, 2004). Most wells completed in the system indicate groundwater under confined conditions although some wells in the outcrop area indicate groundwater under unconfined conditions. The groundwater contour map for March 2003 showing the groundwater flow direction and the water levels in the deep aquifer system prepared by SRK (2004) is given in Figure 3.11. This map indicates a groundwater mound at the north end of the trona deposit. The elevated groundwater levels in this particular area are stated to be related to a series of faults that intensely fractured the area and bring a significant amount of water into the project area from the NE- SW oriented fault zone by SRK. The groundwater flow direction is to the southeast and northeast from this mound with an average horizontal gradient of 0.04 (SRK, 2004).

There is an upward vertical gradient between the deep aquifer system and overlying units observed in the wells D-57-A, D-58-B, D-59-A, D-65-A and D-74-B with an increasing magnitude in the direction of flow to values as high as 0.25- 0.3 (SRK, 2004).

Most of the monitoring wells completed in the deep aquifer system show free-flowing conditions with varying discharge rates from a minimum of 0.005 l/s at D-53 to a maximum of 7.3 l/s at D-47 (SRK, 2001).

According to the aquifer testing conducted by SRK, the hydraulic conductivity ranges from 2.0×10^{-10} m/s in the matrix rock to 3.0×10^{-4} m/s in the most fractured sections (SRK, 2004). The system is proved to be more permeable near the outcrop zone where it is intensely fractured. The hydraulic conductivity stated out to be lower (about 10^{-9} m/sec) at wells D-59A, D-53, D-58B, D-13, which are located downstream on the eastern edge of the trona zone. The deep aquifer system is more permeable near the outcrop zone

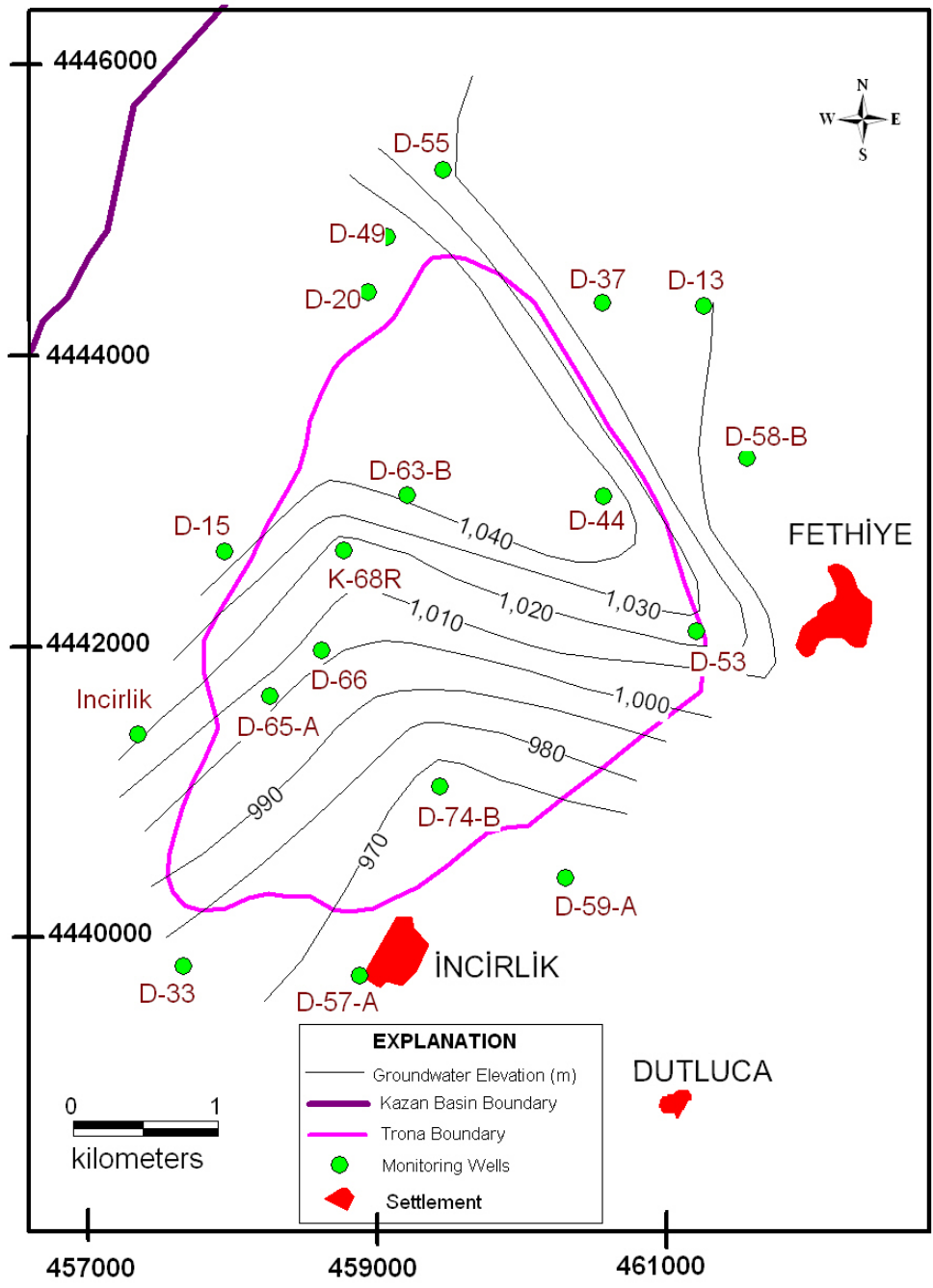


Figure 3.11 Groundwater level contour map for the deep aquifer system for March, 2003 (SRK, 2004).

where it is intensely fractured. The hydraulic conductivity is significantly higher (10^{-4} to 10^{-7} m/sec) at wells D-33, D-47, D-63-A, D-63-B, D-65-A, D-8 and D-68R located on the western part. The calculated storativities are very low (10^{-6} to 10^{-9}) which indicates a highly confined behavior for the deep aquifer (SRK, 2004).

3.4.3 Hydrogeochemical Classification of Waters

SRK Consulting collected samples from surface waters, springs and groundwater monitoring wells and the samples have been tested for a full suite of parameters, including general chemistry and metals since year 2000. The average chemical concentration values calculated from the quarterly monitoring data taken from SRK (2004) are presented in Table 3.2. The piper diagrams of the data presented can also be seen in Figures 3.12, 3.13, 3.15, and 3.16 for springs and for shallow, middle and deep groundwater system respectively. This trilinear diagram (piper diagram) representation of the waters indicated different types. SRK found out that although the discharges of the springs showed increase from dry to wet seasons the concentrations of metals and major ions did not change significantly with the fluctuation of spring flows. According to the piper diagram there are four chemically distinct groups of springs in the study area (Figure 3.12). These are Na-HCO₃ type (SP-7), Mg-SO₄ type (SP-17, SP-18 and SP-22), Na-Mg HCO₃ type (SP-16 and SP-21) and the remaining springs are Ca-Mg HCO₃ type. Na-HCO₃ and Mg-SO₄ type springs are located to the north of the study area. SP-7, with elevated concentrations of arsenic, boron, sodium and bicarbonate similar in type to the water observed in some of the fractured bedrock, is believed to be originating from deeper units and to be connected through a geological structure such as a fault or a joint (SRK, 2004). Mg-SO₄ type springs elevated concentrations of sulfate, boron, fluoride and potassium. The third group of springs, Na-Mg HCO₃ type, is concluded to be a mixed type. These springs are located in the alluvium, contain elevated levels of arsenic and their nature may imply a mixing of shallow and deep water. The last group of springs, Ca-Mg HCO₃ type, observed to respond to precipitation immediately, ceases to flow during the dry season, located along the faults or at the contacts between various units (SRK, 2004).

Table 3.2 Average concentrations of various species in springs and groundwater monitoring wells (SRK, 2004).

Sample ID		SP-3	SP-4	SP-5.1	SP-6	SP-7	SP-16	SP-17
Field Parameters								
Temperature	°C	12.9	14.79	14.52	14.74	16.87	14.69	14.43
pH		8.08	7.71	8.5	7.58	8.88	7.67	7.69
Electrical Conductivity	µs/cm	734.5	475.9	622.9	591.3	921.9	600.5	2017.8
Redox Potential		114.1	134.2	117.6	153.3	99.1	127.1	124.8
Dissolved Oxygen	mg/l	10.02	8.76	8.67	5.83	8.35	8.04	7.5
General Chemistry								
Alkalinity-Total CaCO ₃	mg/l	464	308.3	366.5	372.3	406.9	379.7	568.7
Carbonate	mg/l	5.63	2.57	4.5	0.13	23.99	1.4	-
Bicarbonate	mg/l	543.5	370.9	425.5	444.6	447.2	459.9	693.3
Fluoride	mg/l	0.47	0.62	0.16	0.22	1.12	0.7	1.32
Chloride	mg/l	2.92	5.19	3.67	2.86	41.73	8.13	33.9
Sulphate	mg/l	81.21	11.43	50.5	27.86	72.14	24.67	999
Nitrite/Nitrate Nitrogen	mg/l	0.7	0.22	0.16	0.74	5.12	2.61	0.33
Organic Nitrogen	mg/l	1.07	0.07	0.15	0.1	0.19	0.1	0.08
Total Phosphate	mg/l	0.034	0.005	0.012	0.003	0.152	0.097	0.011
Total Dissolved Solids	mg/l	521.1	303.7	395	386.3	630.6	413.3	1913.3
Total Suspended Solids	mg/l	0.33	-	12.5	-	-	-	-
Total Organic Carbon	mg/l	1.4	1.27	2.08	1.5	1.23	1.6	2
Dissolved Metals								
Aluminum	µg/l	-	-	13	1	-	-	-
Antimony	µg/l	0.1	-	0.1	0.03	-	-	-
Arsenic	µg/l	151	66	20	14	290	132	11
Barium	mg/l	-	-	0.06	0.06	-	0.02	0.01
Boron	mg/l	0.01	0.01	0.03	0.01	2.71	1.67	3.43
Calcium	mg/l	14.2	35.4	54	69.8	1.2	38.8	67.9
Chromium	µg/l	-	-	0.1	-	0.1	-	1
Copper	µg/l	0.3	0.5	0.5	0.33	0.2	-	1
Iron	mg/l	-	-	-	-	-	-	-
Lead	µg/l	-	0.01	0.02	0.05	0.1	-	-
Lithium	mg/l	0.107	0.032	0.008	0.015	0.084	0.069	0.283
Magnesium	mg/l	125.6	48.3	66.2	54.9	0.6	55.8	220
Manganese	mg/l	-	0.2	0.5	0.1	-	1	-
Mercury	mg/l	0.01	-	-	0.01	-	-	0.1
Molybdenum	mg/l	10	1	5	8	-	10	10
Potassium	mg/l	3.98	2.86	0.5	-	-	7	6.33
Selenium	mg/l	1	0.14	1	3	4	1	14
Silicon	mg/l	25.8	13.6	7.4	11.8	8.4	14	10.6
Sodium	mg/l	11.6	18.6	12.3	5.4	256.3	67	249
Strontium	mg/l	0.2	0.37	0.84	0.72	0.1	0.52	7.04
Uranium	µg/l	3.1	4.7	4	3	10	5	30
Zinc	mg/l	-	-	0.002	-	-	-	-

Table 3.2 Average concentrations of various species in springs and groundwater monitoring wells (SRK, 2004) (Continued).

Sample ID		SP-18	SP-21	SP-22	SP-23	S-1	S-2	S-3
Field Parameters								
Temperature	°C	15.92	13.84	14.36	14.57	13.29	14.26	14.52
pH		7.63	7.66	7.64	7.86	7.96	7.73	7.67
Electrical Conductivity	µs/cm	1876.6	863.9	2905.9	497.7	549.8	933.3	767.2
Redox Potential		125	145.7	141	121.9	100.4	115.7	116.4
Dissolved Oxygen	mg/l	8.72	3.63	7.28	8.59	8.58	5.8	5.4
General Chemistry								
Alkalinity-Total CaCO ₃	mg/l	339.5	462.8	468.2	306.5	316	366	428.8
Carbonate	mg/l	-	0.6	0.8	-	-	-	1.2
Bicarbonate	mg/l	414.2	535.8	550.3	373.5	371.3	446.5	501.6
Fluoride	mg/l	0.81	0.34	1.33	1.32	0.33	0.02	0.48
Chloride	mg/l	19.1	27.73	30.22	6.25	7.5	100.8	81.6
Sulphate	mg/l	1190	121	1810	15.1	49.1	67.4	115
Nitrite/Nitrate Nitrogen	mg/l	4.58	2.1	1.37	0.45	2.5	10.4	4.18
Organic Nitrogen	mg/l	0.16	0.14	0.25	0.17	0.32	0.26	0.16
Total Phosphate	mg/l	-	0.303	0.002	-	0.72	0.13	0.23
Total Dissolved Solids	mg/l	1970	683.3	3011.7	347	354	755	635.3
Total Suspended Solids	mg/l	-	-	1.17	-	1135	133	507
Total Organic Carbon	mg/l	2.3	1.63	3.18	1.9	2.67	2.45	2.5
Dissolved Metals								
Aluminum	µg/l	8	-	-	11	20	20	10
Antimony	µg/l	-	0.1	-	-	0.2	-	-
Arsenic	µg/l	12	142	0.4	25	69	27	81
Barium	mg/l	0.02	0.04	0.002	0.35	0.06	0.09	0.07
Boron	mg/l	0.87	1.65	4.76	0.16	0.18	0.83	0.72
Calcium	mg/l	203.5	58.1	224.5	40.8	39.4	60.4	49.3
Chromium	µg/l	-	2	-	-	0.2	1.6	8.4
Copper	µg/l	2	0.2	0.2	1	1.8	1.5	0.4
Iron	mg/l	0.05	-	-	-	0.0198	0.0025	0.001
Lead	µg/l	-	-	-	-	-	-	-
Lithium	mg/l	0.213	0.06	0.586	0.049	0.04	0.09	0.07
Magnesium	mg/l	201	72.4	236.3	47.3	47.5	68.2	68.5
Manganese	mg/l	2	-	-	1	3	3	7
Mercury	mg/l	-	-	0.03	-	0.01	-	0.05
Molybdenum	mg/l	3	10	-	2	20	20	20
Potassium	mg/l	2.65	6.25	8.98	0.6	3.1	13.5	0.3
Selenium	mg/l	10	3	2	-	3	5	7
Silicon	mg/l	6.9	18.4	5.3	11.9	12.7	13.5	12.5
Sodium	mg/l	107	96.3	388.5	20.7	35.9	77.9	121.8
Strontium	mg/l	7.61	1.06	12.9	1.04	0.72	1.31	1.08
Uranium	µg/l	10	10	20	10	4	3	5
Zinc	mg/l	0.04	-	-	0.003	0.07	0.19	0.05

Table 3.2 Average concentrations of various species in springs and groundwater monitoring wells (SRK, 2004) (Continued).

Sample ID		S-4	S-5	S-9	S-11	S-13	S-16	S-19
Field Parameters								
Temperature	°C	15.01	14.72	14.76	15.36	15.45	14.73	14.48
pH		7.72	7.77	8.34	7.73	7.79	7.59	7.81
Electrical Conductivity	µs/cm	12839	714.6	1704.9	831.6	741.6	704.5	671.5
Redox Potential		113.9	115.4	96.1	117.9	114.3	125	112.5
Dissolved Oxygen	mg/l	5.04	8.49	6.53	5.93	3.91	8.79	6.99
General Chemistry								
Alkalinity-Total CaCO ₃	mg/l	507.6	389.4	746.5	388	468.8	416	464
Carbonate	mg/l	4.7	-	4.8	-	1	-	-
Bicarbonate	mg/l	589.6	457.4	899.8	473.1	535	507.2	565.7
Fluoride	mg/l	0.77	0.23	1.97	1.06	0.47	-	-
Chloride	mg/l	2918	15.6	235	24.9	11.4	0.7	9.7
Sulphate	mg/l	6168	93.8	508.5	134.5	110.2	5	27
Nitrite/Nitrate Nitrogen	mg/l	0.32	3.08	0.95	6.53	1.9	0.12	12.4
Organic Nitrogen	mg/l	0.52	0.33	0.17	0.14	0.36	0.28	0.15
Total Phosphate	mg/l	2.37	0.81	1.84	1.11	0.87	0.08	0.31
Total Dissolved Solids	mg/l	14100	537	1950	636	536.8	546	498
Total Suspended Solids	mg/l	2183.5	1047.8	2640	2700	1118.5	10	357
Total Organic Carbon	mg/l	9.1	2.07	3.35	0.5	1.33	2.4	2.1
Dissolved Metals								
Aluminum	µg/l	20	-	140	30	90	-	-
Antimony	µg/l	-	-	-	-	0.2	-	-
Arsenic	µg/l	197	63	1255	77	58	52	14
Barium	mg/l	0.01	0.07	0.08	0.05	0.09	0.07	0.08
Boron	mg/l	22.5	1.34	8.37	0.88	0.59	1.7	0.2
Calcium	mg/l	165.8	54.3	10.7	42.5	53.7	55.4	29
Chromium	µg/l	0.4	1.7	3.8	6	4.4	-	-
Copper	µg/l	2.2	0.6	-	-	0.8	3	2
Iron	mg/l	-	-	0.065	0.02	0.0956	-	-
Lead	µg/l	-	-	-	1.5	-	-	-
Lithium	mg/l	0.58	0.04	0.15	0.07	0.06	0.03	0.11
Magnesium	mg/l	186.8	58.3	13.6	62	58.4	62.8	78.5
Manganese	mg/l	71	3	41	63	78	6	5
Mercury	mg/l	0.01	-	-	-	0.03	-	-
Molybdenum	mg/l	230	10	70	10	4	20	10
Potassium	mg/l	13	1.1	3.6	5.5	2.8	-	6
Selenium	mg/l	-	1	10	5	5	3	7
Silicon	mg/l	15.9	15.9	17.1	12.1	9.9	14.2	10.9
Sodium	mg/l	4224	62.7	694.5	98	67.7	53	54
Strontium	mg/l	6.58	0.91	0.68	1.34	1.27	0.85	0.57
Uranium	µg/l	169	3.7	60	7	3	4	17
Zinc	mg/l	0.04	0.01	0.02	0.06	0.02	0.44	0.19

Table 3.2 Average concentrations of various species in springs and groundwater monitoring wells (SRK, 2004) (Continued).

Sample ID		S-20	S-21	S-22	D-8	D-13	D-20	M-31
Field Parameters								
Temperature	°C	12.82	13.34	14.31	20.22	15.9	14.8	10.6
pH		7.81	7.8	7.65	9.45	8.6	7.57	12.3
Electrical Conductivity	µs/cm	583.2	493	733	4015.8	1075.6	754.39	1907
Redox Potential		113.8	108.8	120	-100	-77.17	-45.29	55
Dissolved Oxygen	mg/l	9.33	7.19	8.45	0.96	1.71	1.57	6.04
General Chemistry								
Alkalinity-Total CaCO ₃	mg/l	374	362	463	2130	674.3	408.8	329
Carbonate	mg/l	-	-	-	426.8	27.1	-	156.5
Bicarbonate	mg/l	456	441.4	564.5	1663.7	745.2	481.46	-
Fluoride	mg/l	-	-	-	1.58	1.08	0.21	0.75
Chloride	mg/l	8.6	9.4	17.8	151.8	18.7	2.9	392
Sulphate	mg/l	50	30	59	10.8	41.3	111.8	25
Nitrite/Nitrate Nitrogen	mg/l	2.85	7.5	5.53	0.03	0.002	0.04	0.89
Organic Nitrogen	mg/l	0.18	0.32	0.14	0.29	0.06	0.03	1.4
Total Phosphate	mg/l	0.06	0.45	0.26	3.8	0.03	0.07	0.03
Total Dissolved Solids	mg/l	430	433	532	2632	864.3	522.6	985
Total Suspended Solids	mg/l	57	793	573	3	1.7	0.6	63
Total Organic Carbon	mg/l	1.7	2.7	1.4	3.8	1.5	1.5	5.3
Dissolved Metals								
Aluminum	µg/l	-	-	-	3	5	-	1.22
Antimony	µg/l	-	-	-	-	-	-	-
Arsenic	µg/l	34	51	29	2	3	310	-
Barium	mg/l	-	-	0.03	0.07	0.025	0.04	0.35
Boron	mg/l	0.2	0.6	0.4	63.23	4.8	0.16	0.3
Calcium	mg/l	46.4	27.1	35.4	1.4	4.1	52.9	134
Chromium	µg/l	-	-	-	-	-	-	-
Copper	µg/l	2	3	-	1	0.05	0.06	-
Iron	mg/l	-	-	-	0.003	0.087	0.15	0.02
Lead	µg/l	-	-	-	0.4	-	-	-
Lithium	mg/l	0.06	0.06	0.14	0.18	0.24	0.004	-
Magnesium	mg/l	60.4	40.6	61.3	1	2.15	54.6	0.09
Manganese	mg/l	4	9	2	-	2	8	-
Mercury	mg/l	-	-	-	0.011	-	-	-
Molybdenum	mg/l	30	10	10	-	-	2	0.02
Potassium	mg/l	3	4	4	-	4	1	18
Selenium	mg/l	4	4	6	-	-	-	-
Silicon	mg/l	13.2	16.5	14.3	28.8	51	25.4	3.6
Sodium	mg/l	35	86	101	1116.3	323	71.2	247
Strontium	mg/l	0.47	0.33	0.62	0.1	0.12	1.31	1.8
Uranium	µg/l	7	11	13	0.14	-	0.04	-
Zinc	mg/l	0.07	0.1	0.02	-	0.023	0.27	-

Table 3.2 Average concentrations of various species in springs and groundwater monitoring wells (SRK, 2004) (Continued).

Sample ID		D-33	D-37	D-47	I-50	D-53	D-57A
Field Parameters							
Temperature	°C	17.3	20.9	22.2	16.9	15.9	21.4
pH		9.5	8.6	9.3	10.02	9.5	8
Electrical Conductivity	µs/cm	5030.6	1077.9	10250.6	25720	9155.2	9845
Oxidation Reduction Potential		-91.82	-93.18	-100	-17.5	-100	-95
Dissolved Oxygen	mg/l	1.27	1.53	1.2	2.51	0.81	1.22
General Chemistry							
Alkalinity-Total CaCO ₃	mg/l	2702.2	622.2	5776.3	50833.3	5658.8	5437.8
Carbonate	mg/l	639.8	38.5	1194.9	23765.4	1963.8	182.8
Bicarbonate	mg/l	1893.2	661.5	4198.2	12906.6	2774.7	5998.6
Fluoride	mg/l	3.35	0.71	5.9	11.9	8.61	4.4
Chloride	mg/l	247.3	20.1	570.5	6730	846.5	887.4
Sulphate	mg/l	19.1	38.7	2.4	124.3	32.2	4
Nitrite/Nitrate Nitrogen	mg/l	0.004	0.081	0.08	0.1	0.01	0.283
Organic Nitrogen	mg/l	0.34	0.12	0.7	6.4	2.27	0.78
Total Phosphate	mg/l	2.97	0.04	8.14	18.13	1.65	5.67
Total Dissolved Solids	mg/l	3372.2	795	6975	60633.3	7866.3	7505.6
Total Suspended Solids	mg/l	9.2	55.7	5.9	80.3	26.6	91.4
Total Organic Carbon	mg/l	2.7	1.6	7.6	44.5	11.2	8.3
Dissolved Metals							
Aluminum	µg/l	10	-	-	-	-	-
Antimony	µg/l	-	-	-	-	-	-
Arsenic	µg/l	25	1	3	-	14	6
Barium	mg/l	0.292	0.04	0.31	-	0.084	1.272
Boron	mg/l	16.3	5	173.75	138.67	309.3	94.3
Calcium	mg/l	1.9	2.3	0.8	13.7	1.3	2.7
Chromium	µg/l	-	-	-	100	-	0.2
Copper	µg/l	-	0.03	10	-	-	-
Iron	mg/l	0.069	-	-	2	-	-
Lead	µg/l	0.04	-	0.8	-	0.3	0.3
Lithium	mg/l	0.56	0.3	0.02	0.27	3.83	2.89
Magnesium	mg/l	1.68	1.35	-	26.7	-	5.19
Manganese	mg/l	2	1	-	140	2	2
Mercury	mg/l	-	0.02	0.02	-	-	0.01
Molybdenum	mg/l	-	1	-	133	-	-
Potassium	mg/l	0.6	1.8	-	35.67	16.1	6.6
Selenium	mg/l	-	-	0.3	-	0.1	0.1
Silicon	mg/l	31.1	47.6	47.3	5.3	33.8	50.9
Sodium	mg/l	1393.4	298.8	2947.5	24866.7	3060	3012.2
Strontium	mg/l	0.27	0.11	0.26	-	0.17	1.55
Uranium	µg/l	2	-	-	50	3	-
Zinc	mg/l	-	-	-	0.667	-	-

Table 3.2 Average concentrations of various species in springs and groundwater monitoring wells (SRK, 2004) (Continued).

Sample ID		M-57B	A-58A1	A-58A2	D-60A	M-60B	D-63A
Field Parameters							
Temperature	°C	15.6	18.14	18.02	15.46	15	21.55
pH		8.5	12.67	12.73	8.8	9.4	8.18
Electrical Conductivity	µs/cm	4073.7	16211	15927	613.17	745.8	907.6
Oxidation Reduction Potential							
		12.95	-100	-98	-100	-85.28	-74.17
Dissolved Oxygen	mg/l	1.55	2.04	2.07	1.65	1.45	1.78
General Chemistry							
Alkalinity-Total CaCO ₃	mg/l	2350.6	2976	2986	398	485.4	386
Carbonate	mg/l	172.2	55.4	102.3	28.42	129.7	24.2
Bicarbonate	mg/l	2413	-	-	412.54	288.54	405.5
Fluoride	mg/l	2.06	0.35	0.3	0.53	0.64	0.21
Chloride	mg/l	398.5	2122	2028	4	4.8	5.1
Sulphate	mg/l	295.7	8.4	16.2	34.2	41.4	74.6
Nitrite/Nitrate Nitrogen	mg/l	0.0148	0.25	0.03	0.01	0.02	0.01
Organic Nitrogen	mg/l	0.34	0.08	0.21	0.02	0.07	0.04
Total Phosphate	mg/l	1.52	0.03	0.02	0.2	0.18	0.03
Total Dissolved Solids	mg/l	3518.9	6706	6372	495.8	606	421.8
Total Suspended Solids	mg/l	0.9	4	3.2	6.8	1	15
Total Organic Carbon	mg/l	3.7	1.58	1.76	0.9	1.1	1.1
Dissolved Metals							
Aluminum	µg/l	-	10	-	18	540	-
Antimony	µg/l	-	-	-	-	0.06	0.04
Arsenic	µg/l	240	3	6	20	20	11
Barium	mg/l	0.07	2.6	3	0.02	0.01	0.1
Boron	mg/l	32.02	0.4	0.92	0.76	1.48	1.84
Calcium	mg/l	3.57	569.2	519.4	2.8	2.03	20.8
Chromium	µg/l	2	-	-	-	11	-
Copper	µg/l	0.5	0.2	2	-	0.2	0.1
Iron	mg/l	-	-	-	0.03	0.06	0.072
Lead	µg/l	0.04	1	3	-	0.04	0.02
Lithium	mg/l	0.75	0.59	0.67	0.12	0.14	0.06
Magnesium	mg/l	2.72	-	-	0.8	0.54	23.2
Manganese	mg/l	-	-	-	1	2.6	0.3
Mercury	mg/l	0.01	-	-	-	-	-
Molybdenum	mg/l	4	-	-	4	4	0.6
Potassium	mg/l	4.82	141.4	178.6	-	5.6	2
Selenium	mg/l	-	0.7	0.9	-	0.2	-
Silicon	mg/l	30.1	0.36	0.1	23.4	20.5	38.1
Sodium	mg/l	1231.3	2026	1964	190	253	146.8
Strontium	mg/l	0.47	34.2	46.7	0.06	0.1	0.5
Uranium	µg/l	20	-	-	-	1	0.1
Zinc	mg/l	0.04	0.39	0.27	0.021	0.04	-

Table 3.2 Average concentrations of various species in springs and groundwater monitoring wells (SRK, 2004) (Continued).

Sample ID		D-63B	M-65B	D-68R	I-74A	D-74B	M-74C
Field Parameters							
Temperature	°C	18	15.1	16.6	17.83	22.2	15.4
pH		8.8	12.7	8.5	8.22	9.4	12.4
Electrical Conductivity	µs/cm	807.5	8481.7	884.8	8178.57	23518	6020
Oxidation Reduction Potential							
		-77.22	-100	-13.33	100	-	-
Dissolved Oxygen	mg/l	1.65	3.39	1.14	1.86	1.95	3.08
General Chemistry							
Alkalinity-Total CaCO ₃	mg/l	453.4	2540	390.5	5436.67	1101.3	2503.3
Carbonate	mg/l	85.8	115.4	17.7	280.59	355.8	711
Bicarbonate	mg/l	361.1	-	400.8	5735.38	577.2	-
Fluoride	mg/l	0.38	0.54	0.25	30.15	4.03	2.44
Chloride	mg/l	5.8	56.2	81.2	505.3	9240	265.3
Sulphate	mg/l	73.2	33	70	-	363.7	164.7
Nitrite/Nitrate Nitrogen	mg/l	0.009	0.15	0.016	0.05	0.009	0.16
Organic Nitrogen	mg/l	0.04	1.6	0.03	2.61	0.64	1.37
Total Phosphate	mg/l	0.05	0.31	0.03	3.72	63.67	38.2
Total Dissolved Solids	mg/l	637.8	2835	699	7273.3	14773	3356.7
Total Suspended Solids	mg/l	67.8	82	3	19.3	10.2	171.3
Total Organic Carbon	mg/l	1.1	4.4	1.3	17.8	10.5	15.3
Dissolved Metals							
Aluminum	µg/l	58	580	-	-	-	860
Antimony	µg/l	0.1	-	-	-	-	-
Arsenic	µg/l	14	-	1	-	140	210
Barium	mg/l	0.046	1.34	0.065	0.08	-	-
Boron	mg/l	2	7.33	2.6	213.67	45.6	3.5
Calcium	mg/l	5.5	161.15	4.1	2.3	10.2	3.34
Chromium	µg/l	-	-	-	-	-	310
Copper	µg/l	0.22	-	-	-	-	40
Iron	mg/l	0.04	-	-	0.15	-	0.47
Lead	µg/l	0.1	-	-	-	-	-
Lithium	mg/l	0.13	0.82	0.17	1.07	2.85	0.82
Magnesium	mg/l	3.5	-	2.25	1.5	7.77	0.17
Manganese	mg/l	3	-	3	-	-	-
Mercury	mg/l	-	-	-	-	-	-
Molybdenum	mg/l	1	10	3	-	30	40
Potassium	mg/l	13.2	387.75	2	3.43	32	401.33
Selenium	mg/l	-	0.3	-	-	-	-
Silicon	mg/l	39.7	1.1	39.4	31.2	4.7	9.3
Sodium	mg/l	221	711.5	252.5	2923.3	5820	1062.7
Strontium	mg/l	0.2	15.08	0.12	0.29	3.58	0.49
Uranium	µg/l	1	-	0.2	-	13.3	10
Zinc	mg/l	-	-	-	-	-	-

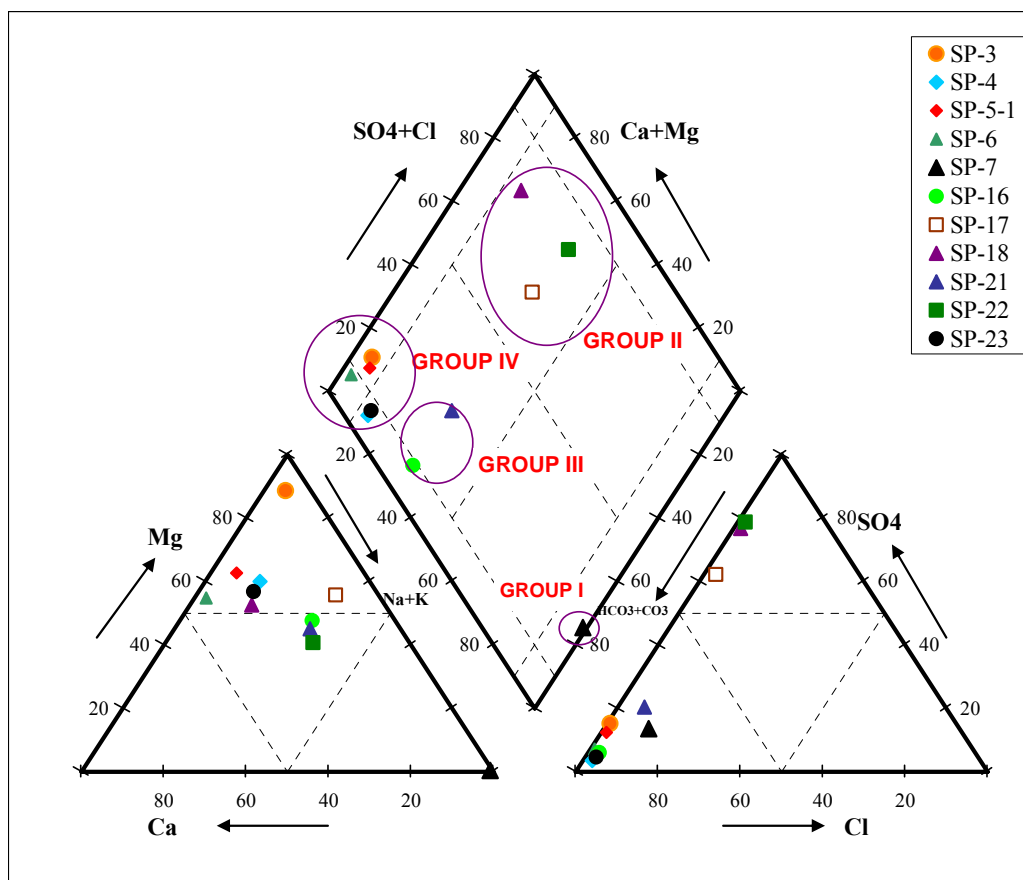


Figure 3.12 Average major ion concentration distribution of springs on trilinear diagram (Piper diagram) (SRK, 2004).

The average chemical concentrations calculated again from the quarterly monitoring data for the alluvium taken from SRK (2004) are also presented in Table 3.2. It has been observed that the concentrations didn't show significant seasonal changes. The hydrochemical characteristics of the shallow groundwater found out to reflect increasing trends along the flow direction from upgradient to downgradient (SRK, 2004).

The most striking part of these chemical data is the hydrochemical characteristics of this system reflecting increasing trends along the flow direction from upgradient to downgradient. The concentrations of various parameters increased significantly at wells S-4 and S-9 (refer to Figure 3.9 for locations) as can be seen from the Stiff Diagram

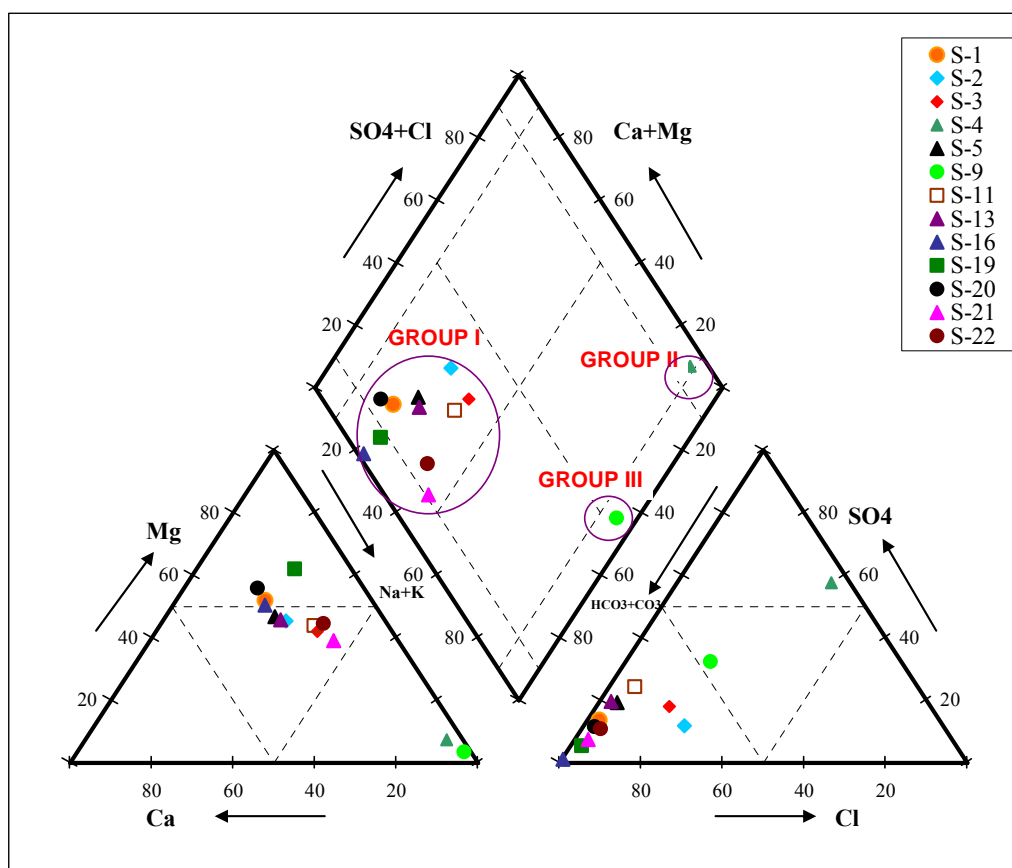


Figure 3.13 Average major ion concentration distribution of shallow groundwater system on trilinear diagram (Piper diagram) (SRK, 2004).

presented in Figure 3.14. This diagram is prepared to facilitate the comparison of the relative proportions of ions in water.

The average TDS concentrations were proven to increase in the downstream direction from about 500 mg/l to 1,950 mg/l at S-9 and 14,100 mg/l at S-4 by SRK (2004) (Figure 3.17) due to the elevated concentrations of sodium, chloride and sulphate in these two wells. Although the exact mechanism or mechanisms causing the sudden increase in some concentrations by several folds was unclear to SRK, it has been suggested that a buried fault can be present allowing the seepage of deeper groundwater into the alluvium

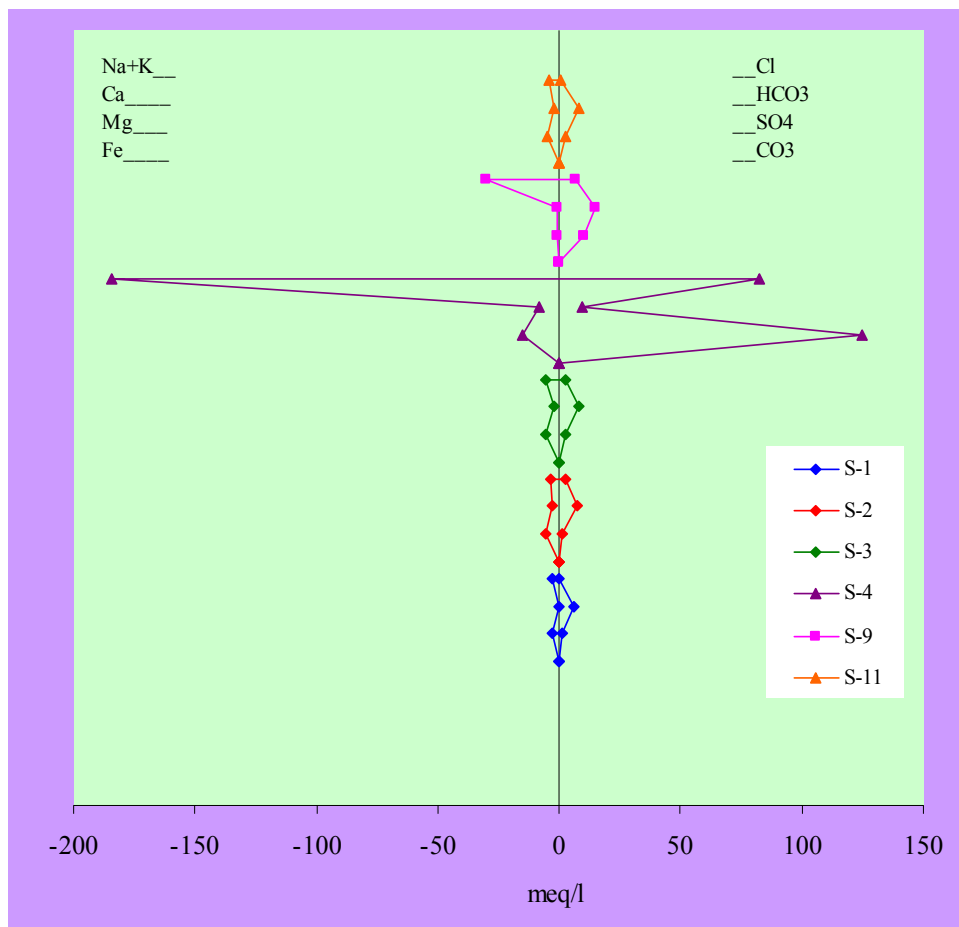


Figure 3.14 Stiff diagram showing the relative proportions of ions in water from selected shallow wells (SRK, 2004).

in these areas. As a result, although shallow groundwater is of a mixed Ca-Mg HCO₃ type in general (Group I in Figure 3.13), it is Na-SO₄ type (Group II in Figure 3.13) and Na-SO₄-Cl type (Group III in Figure 3.13) at S-4 and S-9 wells, respectively (Figure 3.13) (SRK, 2004).

For the middle aquifer system, when the data presented in Table 3.2. is examined, the average TDS concentrations show an increase in the downward direction just like the shallow system but this time from a value of 1000 mg/l to 3357 mg/l at M-74-C (Figure 3.18). According to the trilinear representation of the data presented in Figure 3.15, the

groundwaters in this system are dominantly Na-CO₃ and Na-HCO₃ (Group I in Figure 3.15), except for M-31 water which came out to be Na-Cl type (Group II in Figure 3.15) (SRK, 2004).

According to SRK (2004), geological, geochemical and sedimentological studies did not indicate the presence of any sodic (Na-HCO₃) mineral phase in the Neogene units. Since the water quality indicates Na and HCO₃ or CO₃ as dominant ions and since there is no sodic mineral phase in the Neogene, the presence of these ions may suggest that there is some mixing of the Neogene unit groundwater and the sodium-rich groundwater from

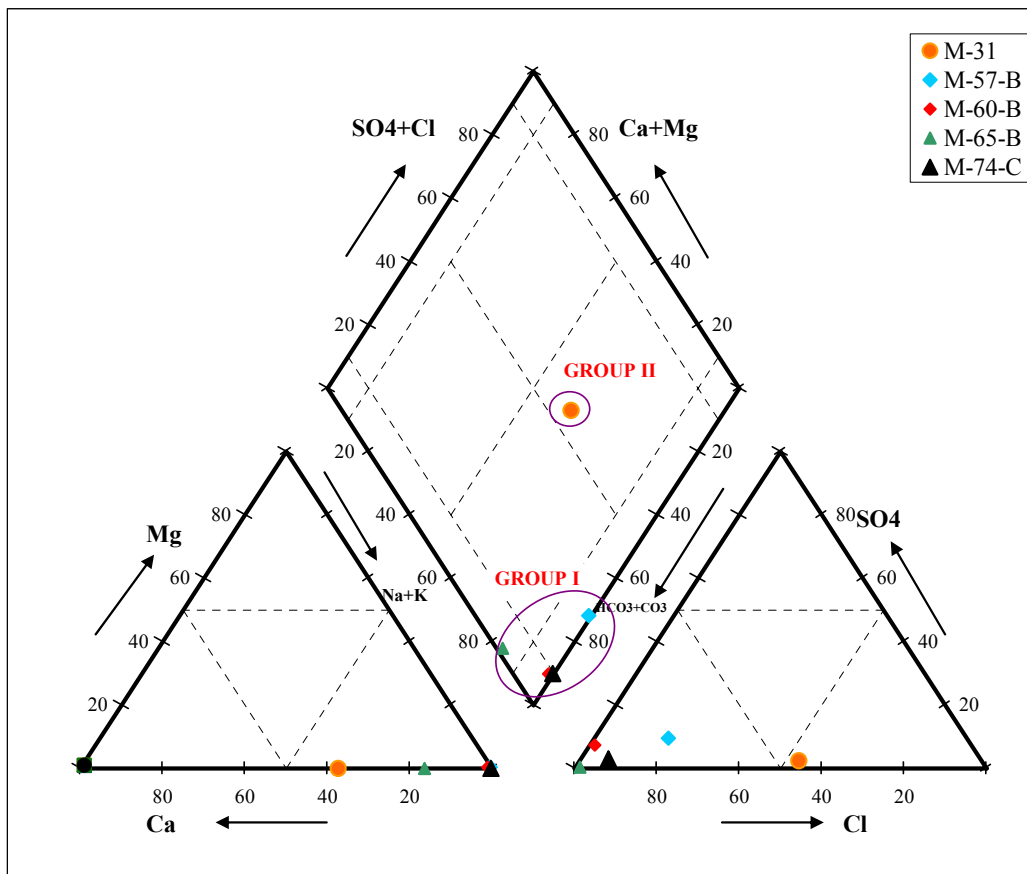


Figure 3.15 Average major ion concentration distribution of middle groundwater system on trilinear diagram (Piper diagram) (SRK, 2004).

other sources (SRK, 2004). It has been pointed out by SRK that this mixing could be possible through a fault that acts as a conduit or through an upward leakage from the bottom layers.

The average concentrations of alkalinity, boron, lithium and sodium in wells M-57-B, M-65-B and M-74-C are significantly higher than the other wells and SRK stated out that such high concentrations of these ions are present in the groundwater of the underlying deep aquifer, suggesting an upward leakage mechanism for the mixing. This is also verified by the observed vertical hydraulic gradients between the deep and middle aquifer systems.

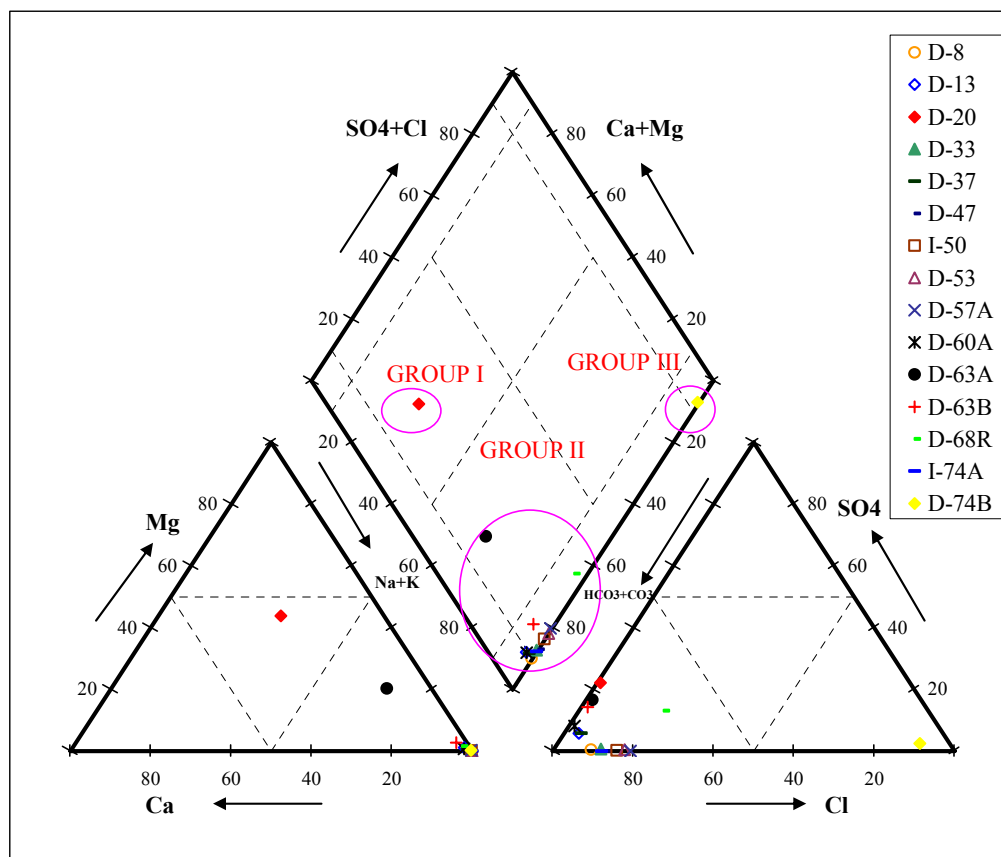


Figure 3.16 Average major ion concentration distribution of deep groundwater system on trilinear diagram (Piper diagram) (SRK, 2004).

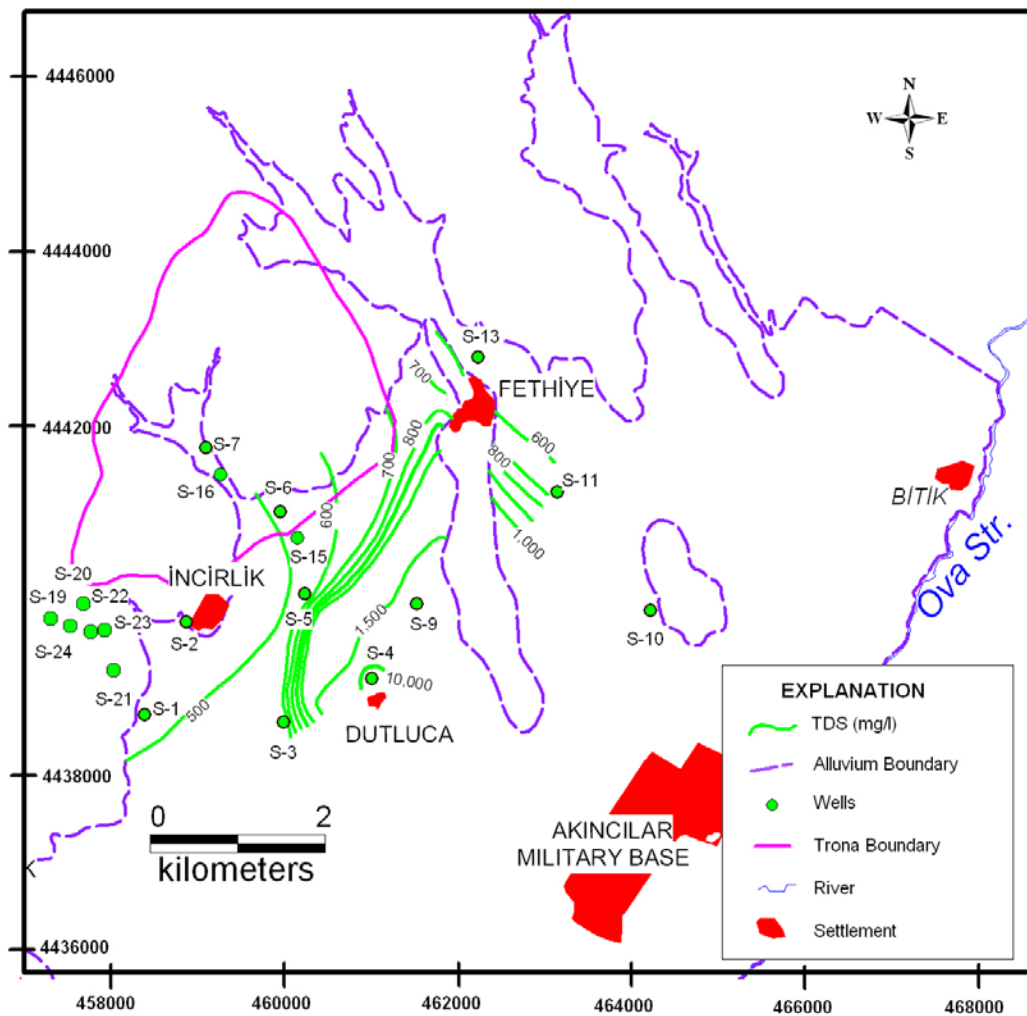


Figure 3.17 Total Dissolved Solids (TDS) distribution in the shallow aquifer system (SRK, 2004).

The groundwater present in the deep groundwater system, monitored by collecting data from 22 wells, showed that the groundwater quality is affected by the extend of the geological structures, proximity of the well to the recharge areas and the presence of veins filled with the sodic minerals. The TDS concentration values around the mound area, the presence of which was discussed in the previous section, are low, increasing in the direction of flow, reaching a value as high as 15,000 mg/l at well M-74-B (Figure 3.19) (SRK, 2004). A pattern similar to the TDS concentration distribution pattern can

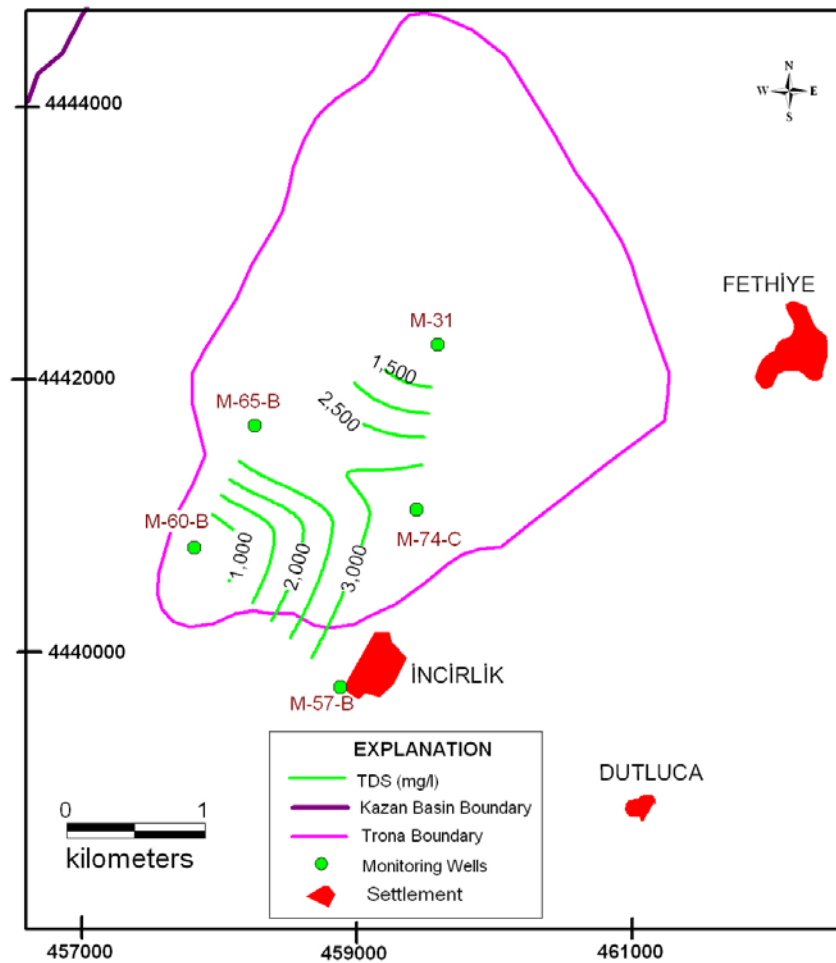


Figure 3.18 Total Dissolved Solids (TDS) distribution in the middle aquifer system (SRK, 2004).

also be seen in the Na, HCO₃, Cl and K concentration distributions (SRK, 2004). The presence of the saline zone in the deep aquifer system in the southern half of the trona deposit area found out to have a significant impact on groundwater quality (SRK, 2004). In the saline zone, some of the saline minerals are dissolved in groundwater and water quality in this area is impacted. Dissolution of minerals such as searlesite, northupite and shortite will increase the concentrations of boron, sodium, chloride and bicarbonate in the groundwater. The trilinear diagram presented in Figure 3.16 indicates that there are three different types of water occurring in the deep aquifer system. The wells located near the

outcrop zone in the west indicated a mixed type of groundwater (Group I in Figure 3.16) whereas the type changes to Na-HCO₃ (Group II in Figure 3.16) toward the east becoming a Na-Cl type (Group III in Figure 3.16) in downgradient (SRK, 2004).

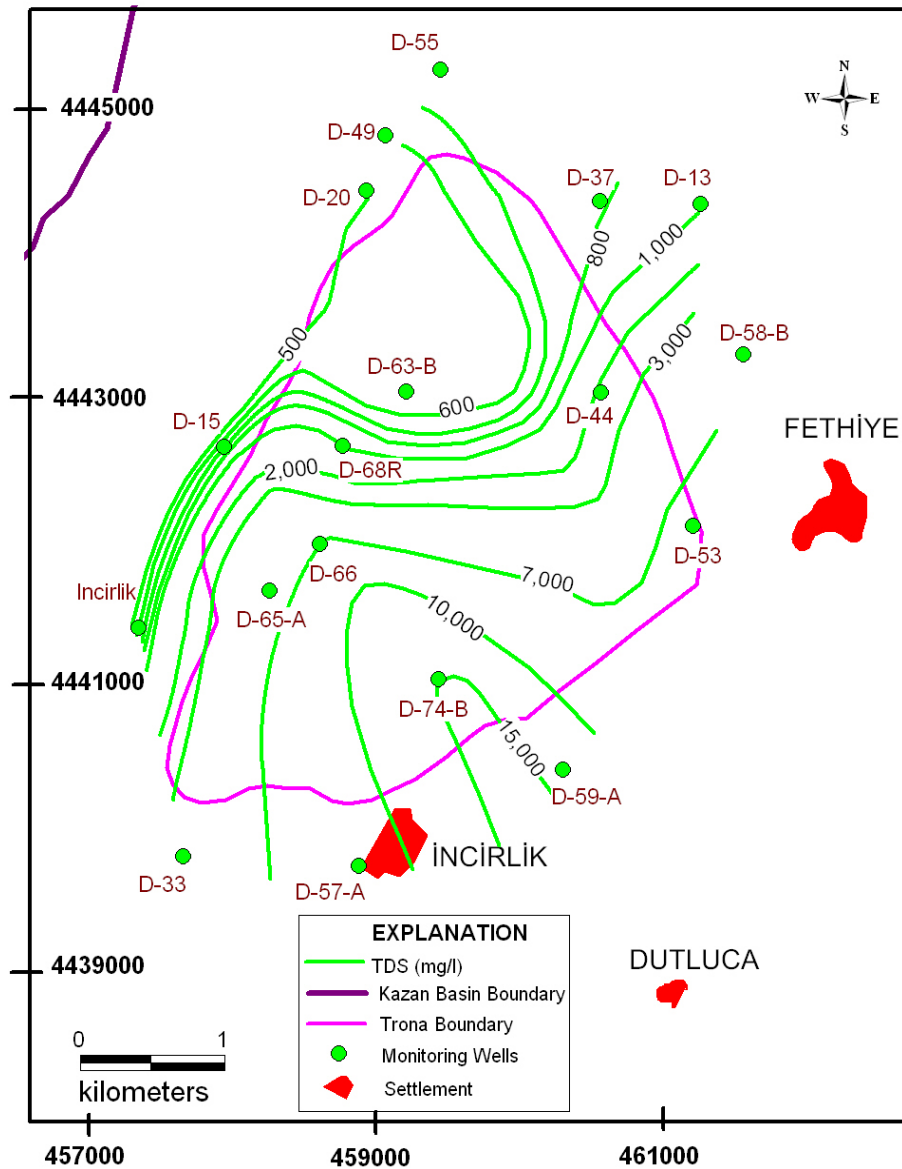


Figure 3.19 Total Dissolved Solids (TDS) distribution in the deep aquifer system (SRK, 2004).

3.4.4 Conceptual Groundwater Flow Model of the Study Area

SRK (2004) was able to conceptualize the groundwater flow in the study area as shown in Figure 3.20. In order to verify the conceptual hydrogeological understanding of the study area and to determine groundwater flow and the interaction between the three aquifer systems, a numerical groundwater flow model has also been developed. According to SRK (2004), the water bearing units from bottom to top consist of a deep groundwater aquifer system in fractured bedrock (i.e., fractured zones of İncirlik, Asmalıdere and Fethiye), a middle system at the base of the Neogene, and a shallow system in the Quaternary Alluvium and the uppermost fractured and weathered Neogene. The Akpınar Formation acts as an aquitard where it exists. Furthermore, the deep aquifer system is mainly recharged along zones that outcrop in the ridges on the western side and by line sources and the flow is mainly controlled by the shear and fracture zones. The evidence suggests that these are a series of faults, which are probably connected to the main NE-SW striking fault system at the western boundary of the Kazan Basin. The main direction of flow in the deeper fractured system appears to be towards the southeast and probably interrupted by a large graben along the Ova Stream Valley. The deeper fractured aquifer system, having a greater potentiometric surface than the middle Neogene and upper alluvial system, also sets up an upward gradient; thereby, recharging them in downgradient areas. SRK also concluded that the decrease in the intensity of fractures in the bedrock aquifer downgradient acts as a barrier to the groundwater flow forcing the flow to take place toward the alluvial system.

Elevated temperatures and higher TDS concentrations measured in downgradient alluvium wells also reflect a probable mixing of groundwater from two different origins. SRK (2004) stated out that the exact mixing mechanism was not known, whether this mixing is of diffuse type or of lineament type controlled by structural features like a fault. SRK (2004) suggested that more thorough studies supported by seismic surveys may provide information as to the type of mixing.

The groundwater budget of the aquifer systems obtained from the calibration of the groundwater model constructed by Yazıcıgil et al. (2007) is presented in Table 3.3. According to the findings of Yazıcıgil et al. (2007) about the groundwater budget

components, the shallow system is recharged from the deeper aquifer systems. This recharge contribution is about 10000 m³/day and makes up 40 % of the total recharge of 24500 m³/day to the shallow aquifer system. The remaining recharge to the shallow system is supplied by infiltration from precipitation. About 60% of this recharge in the shallow aquifer discharges into the Ova Stream as base-flow and the rest as surface runoff, evapotranspiration losses and spring discharges. The deep aquifer is mainly (about 75%) recharged from subsurface inflow from the main fault zone. The contribution of recharge from precipitation in the outcrop zones amounted 25% of the total yearly average recharge rate. Most of this recharge (89%) is lost to the upper layers in the form of upward vertical flow. Four percent of the recharge was used for water wells. The downward flow was found out to be insignificant (only about 1%) (SRK, 2004). Figure 3.21 visually shows all the groundwater budget elements, the discharge and recharge mechanisms of the aquifer systems as proposed by SRK (2004).

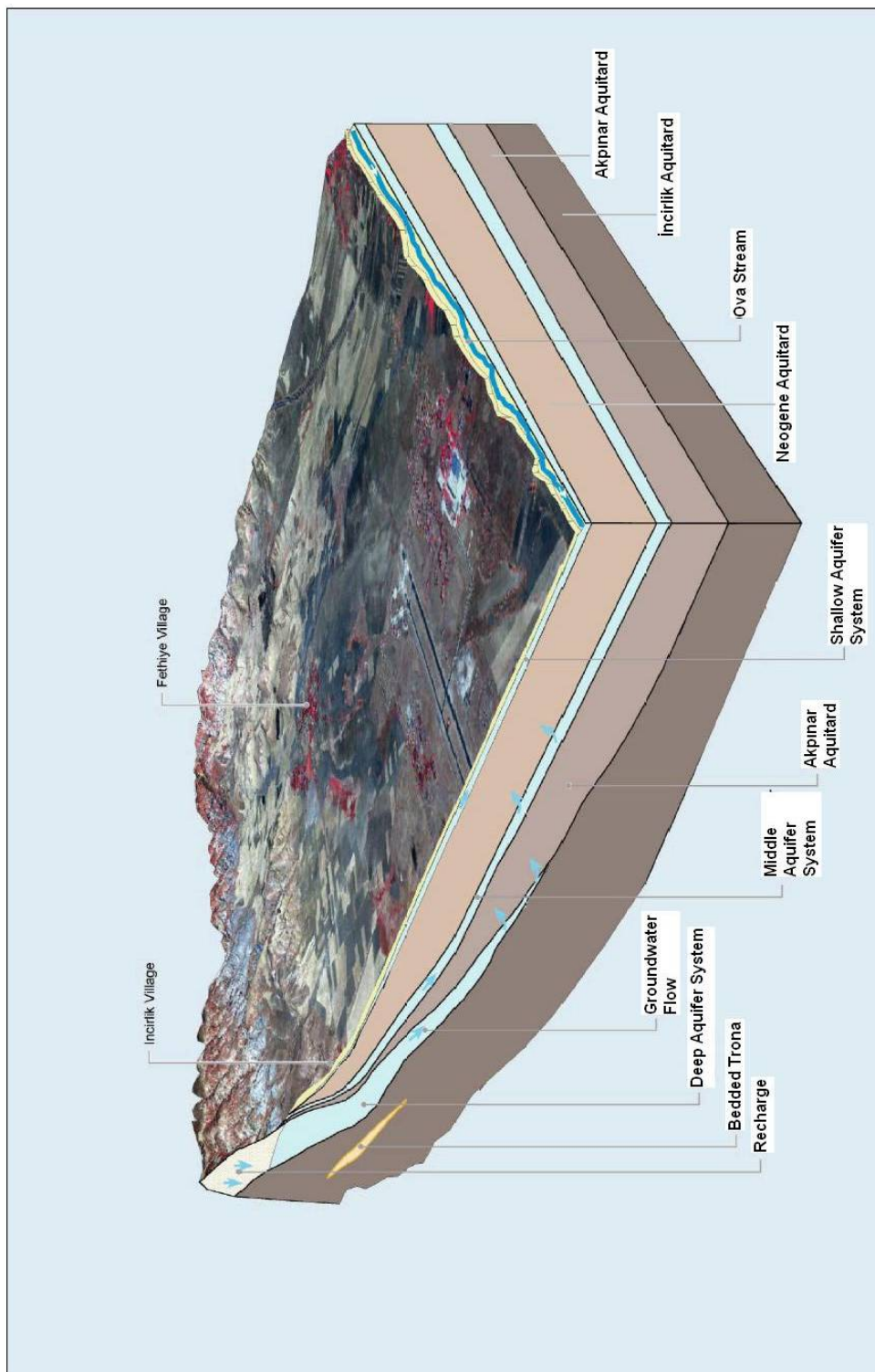


Figure 3.20 Conceptual hydrogeological model of the study area (SRK, 2004).

Table 3.3 The groundwater budget of the aquifer systems obtained from the calibration of the groundwater model (Yazıcıgil et al., 2007).

Hydrogeologic Unit	Recharge	(m³/day)	Discharge	(m³/day)
Shallow Groundwater System	Precipitation	14,504	Discharge to Ova Stream	14,822
	Recharge from Lower Aquitard	5,018	Springs (SP17, SP20 & SP21)	245
	Recharge from Deep Aquifer	5,336	Evapotranspiration Surface Runoff	4,946 4,679
Middle Groundwater System	Recharge from Deep Aquifer	3,015	Discharge to Upper Aquifer	4,106
	Recharge from Lower Aquitard	90	Discharge to Lower Aquifer	12
	Recharge from Upper Aquitard	994		
Deep Groundwater System			Discharge to Shallow Aquifer	5,336
	Precipitation	2,554	Discharge to Middle Aquifer	3,015
			Discharge to Upper Aquitard	1,056
			Discharge to Lower Aquitard	14
	Subsurface Inflow	8,280	Surface Runoff (outcrop area)	671
			Wells (K-17 & K-27)	487

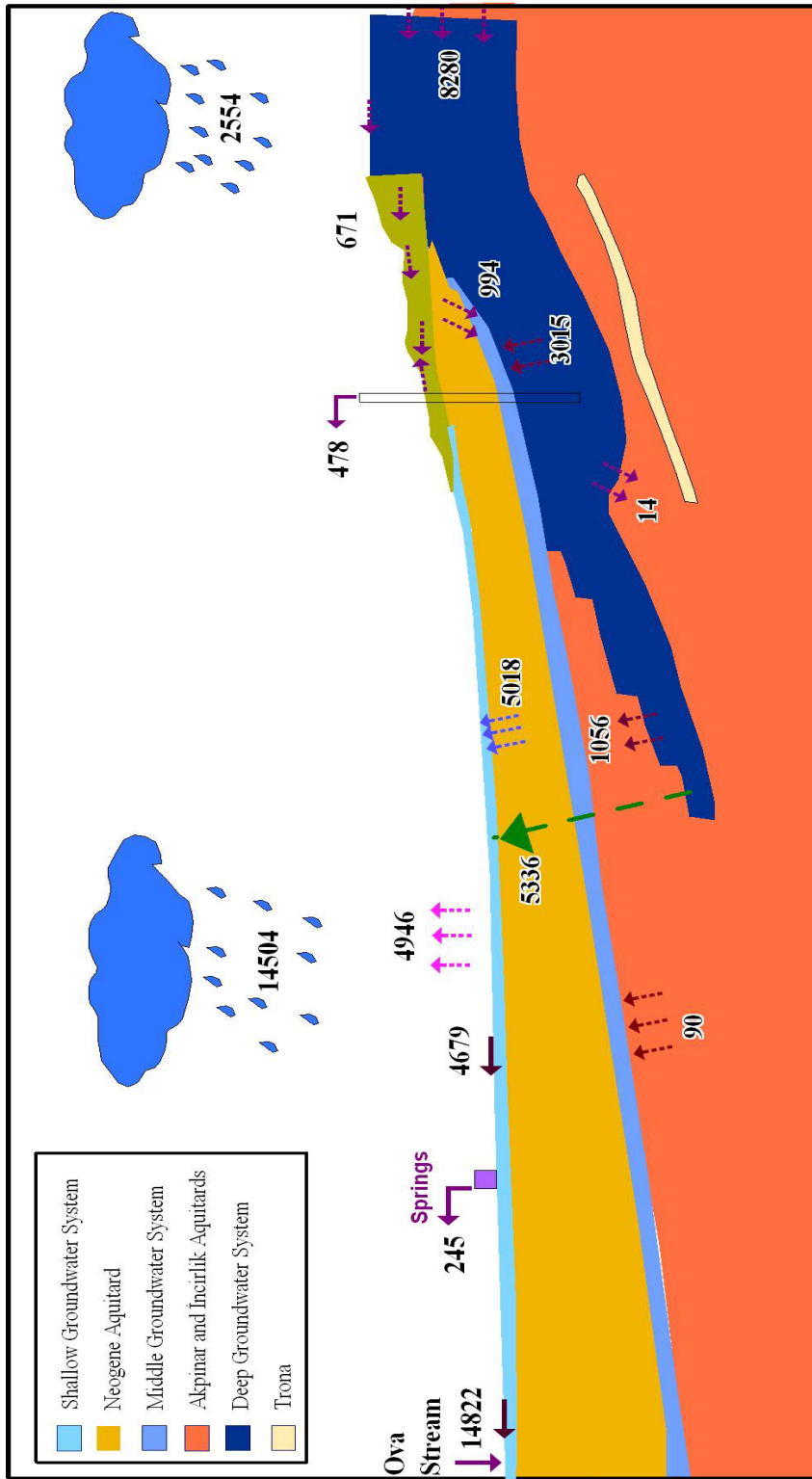


Figure 3.21 Ground water budget obtained from calibration of the model under steady-state conditions (SRK, 2004) (The units are expressed as m³/day).

CHAPTER 4

METHODOLOGY

4.1 Field Sampling

In the previous chapters, it has been emphasized that a lot of studies utilized environmental tracer techniques to solve the problems related to groundwater flow and evolution which are indeed not possible to solve with traditional methods. The Kazan Trona site can well be another representative study in which extensive hydrogeological and hydrogeochemical studies carried out since year 2000 were unable to solve the exact mixing mechanisms within a complex aquifer system. After deciding on employing an isotopic approach to find out about the unrevealed parts of the mixing in the study area four field trips were achieved. The first field trip was performed in August 2006, followed by the other in November 2006, May 2007 and June 2007. Samples from the selected springs and the wells monitoring three different aquifers were collected with special techniques. The sampling program and the number of samples collected in each trip are given in Table 4.1.

The samples for major ion analyses were collected to 20 ml deionized water- rinsed plastic bottles. The samples for trace metal analyses were collected to similar bottles with the major ion analyses bottles but this time acid-rinsed bottles were used. The samples were filtered by using a 0.45 μm filter. The dissolved oxygen measurements were performed in the field by using a colorimetric method with special ampoules; therefore no samples were collected for laboratory analyses. During the measurement, the most prominent point is to prevent the samples contact with the atmosphere. For this reason, fittings with different diameters were used to completely close the well heads or spring heads. Then, a plastic hose is connected to the fitting from one side and the other side of the hose is connected to a sampling tube (Figure 4.1). Before performing the test, the system was purged for a few minutes at the fastest possible rate. Afterwards, the flow

Table 4.1 The sampling program.

Sample	Date	August 2006	November 2006	May 2007	June 2007
		Number of samples collected			
¹⁸ O and ² H		20	24	12	31
CFC-11, CFC-12, CFC-113		7	11	-	18
Noble Gases		-	17	-	13
Carbon-13 and Carbon-14 in DIC		12	3	-	-
Major ions		-	20	-	-
Dissolved Oxygen		-	28	-	20

was reduced and a CHEMet ampoule was inserted inside the sampling tube with tapered tip facing the bottom of the tube. The ampoule tip is then pressed gently allowing snapping. The ampoule is then filled with water. The contents should be mixed by inverting the ampoule and afterwards the color inside the ampoule should be compared with the reference colors given with the CHEMet Kit set. The test employs two different methods depending on the amount of the dissolved oxygen content of the water. If the dissolved oxygen content is expected to be between 0 mg/l to 1 mg/l then the Rhodazine D Method is employed by the Oxygen CHEMets (ASMT 1984, ASMT D 1999). In this method, dissolved oxygen reacts with the pale yellow colored leuco form of Rhodazine D to produce a deep rose color. The resulting color is proportional to the dissolved oxygen concentration in the sample. The other method is called the indigo carmine method and it is utilized if the dissolved oxygen amount is expected to be between 1 mg/l to 10 mg/l (Gilbert et al., 1982). This method uses the principle that in an acidic solution, oxygen oxidizes the yellow-green colored leuco form of indigo carmine to form a highly colored blue dye. The resulting blue color is proportional to the dissolved oxygen concentration in the sample. Test results are expressed in mg/l dissolved oxygen as O₂.

For oxygen-18 and deuterium analyses, the samples were collected in 60 ml boston round clear glass bottles with 20 mm sized screw caps. The bottles were preserved after tightly taping the caps by an electrical tape to prevent possible evaporation of the samples.



Figure 4.1 Sampling for Dissolved Oxygen.

The samples for carbon-13 and carbon-14 from dissolved inorganic carbon analyses were collected in 250 ml boston round clear glass bottles with 24 mm screw caps. Post-collection biological activity can alter the carbon isotopic concentration of the samples therefore the samples were poisoned with 0.2 ml of a saturated mercuric chloride solution and possible bacteria formation were prevented.

The samples for CFC-11, CFC-12 and CFC-113 analyses were collected with CFC bottle sampling method, following the procedure described by USGS CFC laboratory. The bottles were 125 ml boston round clear glass. Special aluminum lined plastic caps were used to close the bottles after sample collection. All the samples were collected in duplicate. The filling procedure was carried out within a three liter glass beaker. For the shallow wells, a water pump was used. Normally, plastic materials can cause CFC contamination so they are not preferred however for facilitating sampling, a plastic tubing is used with one end connected to the pump and the other end connected to a copper tubing. For the deep wells, the well head was tightly closed with a suitable sized fitting to prevent the samples contact with the atmosphere and then the tubing was connected to the fitting. First the well has been purged then the sample bottle was placed in the beaker and the end of the copper tubing was inserted all the way into the bottom of the bottle. The bottle was filled with sample water until it overflows from the beaker. At least 2 liters of water was allowed to flow through the bottle and out of the beaker. Then the copper tube was removed from the bottle and the bottle was capped tightly underwater without allowing the water in the bottle to come in contact with air. The capped bottle was then removed from the beaker and the cap was retightened. Afterwards the bottle was inverted and checked for air bubbles. If there were bubbles all the procedure was repeated by using a new cap. If no bubbles were present, then the cap was taped with electrical tape. The bottles were stored upside down at room temperature until shipment. A small bubble formation after collection is considered as normal.

The noble gas samples were collected by filling a special copper sample tube (Figure 4.2). These tubes are 50-cm in length with about 9 mm outer and 7 mm inner diameters containing about 40 cc of water. These special tubes were fitted with stainless steel pinch-off clamps at each end. Before sampling, the same procedure with CFC sampling

was followed, for shallow wells; clear plastic tubing (tygon) was connected to the pump from one end and the other end was connected to the copper tube which is fixed in an aluminum channel holding the stainless steel pinch-off clamps (Figure 4.2). Clear plastic tubing is preferred to visually observe whether air bubbles are present in the water line. To make sure that the connection to the well or pump was completely airtight; the connections were secured with stainless steel hose clamps. The tube was flushed by paying special attention to the ends of the copper tube as damage to the ends of the tube may prevent proper attachment of the sample tube to the vacuum extraction line for sample preparation at the laboratory. A back pressure was applied to the discharge end of the copper tube during flushing by using a back pressure valve assembly (Figure 4.2). The tubing and the plexiglass tube were continuously inspected for bubbles. During flushing, the side of the aluminum tube was bang a couple of times to remove trapped air bubbles from the copper tube. After flushing the sample container at least 1 minute with bubble free water the pressure valve was closed completely. The clamp closer to the pressure valve (top clamp) was closed first followed by the bottom clamp while watching



Figure 4.2 The equipment used to take noble gas samples.

the plastic tubing for the bubbles. The sample containers were stored at room temperature and as the ends of the copper tube are very fragile, they were transported with special care.

4.2 Laboratory Analyses

4.2.1 Oxygen-18 and Deuterium

Stable environmental isotopes are measured in the laboratories around the world as the ratio of the two most abundant isotopes of a given element. For oxygen it is the ratio of ^{18}O to common ^{16}O . The terrestrial abundance of ^{18}O is 0.204 % and ^{16}O is 99.796, thus the $^{18}\text{O}/^{16}\text{O}$ ratio is about 0.002044 (Clark and Fritz, 1997). For hydrogen, it is the ratio of ^2H , with a terrestrial abundance of 0.015% to ^1H representing 99.985% (Coplen et al., 2000). Isotopic concentrations are expressed as the difference between the measured ratios of the sample and reference over the measured ratio of reference. For oxygen and hydrogen this reference standard is VSMOW (Vienna Standard Mean Ocean Water). To represent the difference from the reference, delta (δ) notation is used, expressed as the parts per thousand permil (‰) (Clark and Fritz, 1997).

$$\delta \text{ (‰)} = \frac{(\text{heavy / light isotope})_{\text{sample}} - (\text{heavy / light isotope})_{\text{standard}}}{(\text{heavy / light isotope})_{\text{standard}}} \times 10^3 \quad (4.1)$$

For oxygen, Equation 4.1 becomes:

$$\delta^{18}\text{O} \text{ (‰)} = \frac{(^{18}\text{O} / ^{16}\text{O})_{\text{sample}} - (^{18}\text{O} / ^{16}\text{O})_{\text{VSMOW}}}{(^{18}\text{O} / ^{16}\text{O})_{\text{VSMOW}}} \times 10^3 \quad (4.2)$$

The $\text{H}_2^{18}\text{O}/\text{H}_2^{16}\text{O}$ ratio measurements of the samples collected in August and November 2006 were done at Lamont- Doherty Earth Observatory of Columbia University (L-DEO) laboratories by using a FISIONS PRISM III Isotope Ratio Mass spectrometer (Figure 4.3). This mass spectrometer is equipped with a Micromass Multiprep automatic sample

processing system after water sample equilibration with CO₂ using standard methods described by Epstein and Mayeda in 1953. The Multiprep system uses a Gilson autosampler to automatically collect, transfer, dry and inlet gases into the mass spectrometer (Figure 4.3). Water samples are analyzed with the standard Multiprep method. 200 µl of water are placed into a 1-ml glass vial with silicone septum and pierceable screw cap. Between the septum and the glass vial an impermeable disc is placed to inhibit the diffusion of gases across septum during equilibration. The CO₂ equilibration for ¹⁸O, to determine C¹⁸O₂, was accomplished within 8 hours at 35 °C. For some samples, the pH was adjusted to 6 or lower to facilitate more rapid equilibration. The adjustment for pH was done by adding 10 µl of phosphoric acid to 200 µl of sample so as to reduce the pH from 9 or 10 to 5. After equilibration, water samples are sampled automatically by the Multiprep autosampler and subsequently analyzed on the Mass Spectrometer. Up to 60 samples can be measured in each batch using this standard method. All of the samples were run in duplicate. Precision is estimated to be ±0.03 per mil that is 1σ (standard deviation) as determined by multiple daily analyses of laboratory standard. Instrument linearity and accuracy was determined by comparison of the laboratory standard to the reference materials VSMOW, Greenland Ice Sheet Precipitation (GISP) water, and Standard Light Antarctic Precipitation (SLAP) water. The accuracy is estimated to be within 0.03 per mil by comparison of measurements of North Atlantic Bottom Water with VSMOW.

The rest of the samples collected for oxygen-18 analyses and all the deuterium samples were shipped to Environmental Isotope Laboratory of University of Waterloo, Canada. Deuterium samples were analyzed on Micromass ISOPRIME mass spectrometer. The measurements were performed on hydrogen gas produced from water reduced on hot chromium using the following procedure explained by Drimmie et al. (2001a). Water samples were pipetted into 2-ml septum vials that are placed into a Eurovector Liquid Autosampler (LAS). The autosyringe rinses itself twice with new sample, and then it samples 1 microliter (µl) of water. The water is injected into a heated inlet system on a Eurovector Euro HT/EA where helium gas carries it to a 960° C furnace packed with chromium. The chromium reduces the water to hydrogen gas, which is then carried to the mass spectrometer. The autosampler holds a batch of 110 samples, standards and repeats. The precision for this technique is better than 1 per mil approximately 0.8 per mil. All



Figure 4.3 The Fisons Prism III Mass Spectrometer at L-DEO.

samples were run in duplicate. Results were recorded and standard corrections using the international reference materials VSMOW and SLAP from the International Atomic Energy Agency were done.

Oxygen-18 determinations were achieved by CO₂ equilibration using standard procedures based on the principles in Epstein and Mayeda (1953); the principles also used at LDEO for oxygen-18 determinations. Basically, water samples in septum vials filled with a helium CO₂ mixture are placed into an aluminum bath at 40°C for more than 3 hours. The CO₂ is extracted automatically with a Gilson Autosampler connected to a Micromass Multiprep. The Multiprep contains a 50- μ l sample loop, and a column that separates CO₂, N₂, O₂ and H₂O. Helium carrier gas then transports the purified CO₂ into the Micromass IsoPrime continuous flow isotope ratio mass spectrometer system (CF-IRMS) that analyses the isotope ratios (Drimmie and Heemskerk 2001b). Quality control were maintained by placing the laboratory water standard (de-ionized water kept in stock bottle and calibrated to VSMOW and VSLAP) at the beginning and every ten samples in the 60 sample batch. Duplicates were run for every fifth sample. Standard corrections will then be performed based on the current laboratory/VSMOW/VSLAP calibration. Results were recorded and the standard corrections using the international reference materials were done.

4.2.2 Chlorofluorocarbons

CFC-11, CFC-12 and CFC-113 concentrations in water can be determined to a detection limit of about 0.3 picograms per kg of water (pg/kg) using purge and trap, gas chromatographic techniques with electron-capture detector (GC-ECD; Bullister, 1984; Bullister and Weiss, 1988; Busenberg and Plummer, 1992).

Chromatography is the separation of a mixture of compounds (solutes) into separate components. By separating the sample into individual components, it is easier to identify and measure the amount of the various sample components. There are numerous chromatographic techniques and corresponding instruments. Gas chromatography (GC) is one of these techniques. It is estimated that 10-20% of the known compounds can be

analyzed by GC. To be suitable for GC analysis, a compound must have sufficient volatility and thermal stability.

All CFC measurements were done by using a Hewlett- Packard (HP) 5890 CFC chromatograph available at L-DEO. Before determining the CFC concentration of a sample a calibration curve is run. The standard used in the calibration curve has been calibrated on **SIO** (Scripps Institute of Oceanography) 93 scale. Ten calibrated loops- from 0.1 to 0.25 cc- are used in the calibration curve. First the sample extraction system is tested for a system blank. Then one loop at a time is filled with the standard, allowed to vent down to atmospheric pressure and injected into a cold trap (Figure 4.4). The cold trap consists of Unibeads-2s and is kept at -70 °C while the sample and nitrogen pass through it at 75 cc/min for 4 minutes. After 4 minutes the cold trap and sample are heated to 100 °C for 1 minute and then injected into the Gas Chromatograph (GC) (Figure 4.4). The columns in the GC are 4 inches of mol sieve 5A (F12 only), a Porasil-B pre-column (3 feet), and 5 feet of Carbograph 1-AC. The GC oven is kept at 100 °C and the carrier has flow rate is 33 ml/min. The run time is 7 minutes for CFC-12, CFC-11, CFC-113. This procedure is repeated two to three times for each loop. The number of picomole (pmol) injected is obtained from the ideal gas law. The peak areas for each injection are corrected for the system blank and a calibration curve is fitted to the peak areas. The pmols of CFC in the sample is determined by comparing its area to the calibration curve.

Prior to GC analysis the samples are weighed full. The dimensions of the bubbles formed inside the bottles were also measured to calculate the volume of gas in the headspace. This information is to be used in the headspace correction during calculations. The bottle is then attached to a purge-and-trap extraction system and opened under a CFC- free nitrogen atmosphere. An aliquot of the sample is transferred from the ampoule to a 20 cc calibrated volume and then to a stripper chamber. The CFCs are stripped from the water sample by sparging with CFC-free nitrogen for 4 minutes at 75 cc.min. The CFCs are trapped as described above and injected into the GC the same way as the standard. The figure showing the gas chromatograph used in the measurement of CFCs at LDEO is given in Figure 4.5. The pmols of CFCs in the water are determined from the calibration curve: subsequently a blank is subtracted and the sample's pmols are divided by the calibrated volume to determine pmol/l. When the bottle dries out it is weighed again to

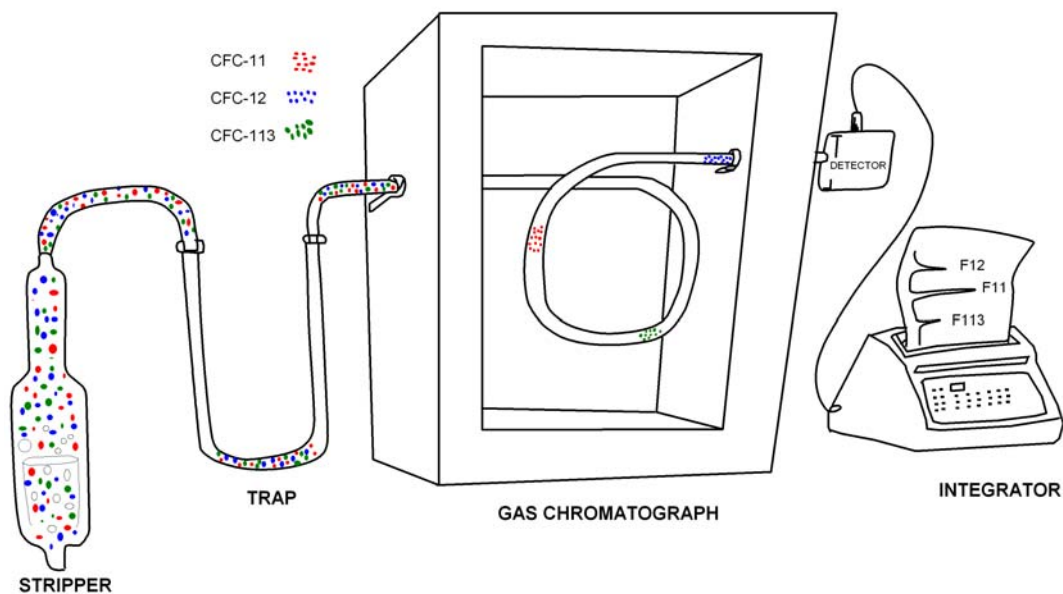


Figure 4.4 Simplified diagram showing the working principle of a CFC gas chromatograph drawn by Eugene Gorman.

determine the volume of the water in the original sample. The headspace correction is required to calculate the corrected concentrations of measured CFCs. It assumes that the CFCs in the headspace are in thermodynamic equilibrium with the water and the ratio of CFCs in the headspace to CFCs in the water is calculated using the solubility equations determined in Warner and Weiss (1985) and this ratio is applied to the concentration measured in the water.

The sources of error in the procedure explained herein include error in the headspace coefficients, handling, the standard itself, calibrated volumes, and in the calibration curve. Assuming no sample degradation the overall analytical error is estimated to be 1 to 2 per cent at one pmol/l (Mensch et al., 1998).



STRIPPER

GAS CHROMATOGRAPH



INTEGRATOR

30.08.2006

Figure 4.5 The Hewlett Packard 5890 Gas Chromatograph at L-DEO.

4.2.3 Carbon-13 and Radiocarbon

All samples for ^{13}C and ^{14}C were analyzed in the laboratories of Woods Hole Oceanographic Institution. ^{13}C analyses were done by using a VG PRISM Stable Mass Spectrometer. Before the mass spectrometer system, dissolved inorganic carbon is stripped in an automated system in the Sample Preparation Laboratory using acidification and sparging with nitrogen to strip the evolving CO_2 from the water. This way the DIC content of the water is determined. The isotopic composition of this gaseous CO_2 is then measured with the mass spectrometer. The precision of the measurements are reported to be ± 0.05 per mil. The data are represented as the per mil deviation of the ^{13}C to ^{12}C isotope ratio relative to VPDB (Vienna PeeDee Belemnite) standard. For carbon, Equation 4.1 becomes:

$$\delta^{13}\text{C} (\text{‰}) = \frac{(^{13}\text{C}/^{12}\text{C})_{\text{sample}} - (^{13}\text{C}/^{12}\text{C})_{\text{VPDB}}}{(^{13}\text{C}/^{12}\text{C})_{\text{VPDB}}} \times 10^3 \quad (4.3)$$

Radiocarbon samples were also measured from Dissolved Inorganic Carbon (DIC) in water in National Ocean Sciences Accelerator Mass Spectrometry Facility (NOSAMS) by using an accelerator mass spectrometry (AMS) system at Woods Hole Oceanographic Institution (Figure 4.6). Before the AMS system step, dissolved inorganic carbon is stripped, the same procedure followed in carbon-13 measurement. Then the carbon or “graphite” derived from the sample is compressed into a small cavity in an aluminum target which acts as a cathode in the ion source (WHOI, 1989). The detailed explanation of the system is given in Figure 4.6. This system is over 30' long and consists of a 2.5 million Volt tandem (two-stage) accelerator, sandwiched between a low-energy mass spectrometer and a high-energy mass spectrometer. Major sections of the system are labeled in the schematic. In Section a, there are two cesium sputter ion sources present. In AMS, it's critical to create negative ions in order to discriminate against the most abundant natural element of mass 14, nitrogen which does not form negative ions (WHOI, 1989). To generate a negative ion beam, the compacted solid carbon samples are bombarded with Cesium ions. Ions extracted with a 40,000 Volt electric field, move from the source (a) at a speed of more than 450 miles per second inside of a vacuum beam line

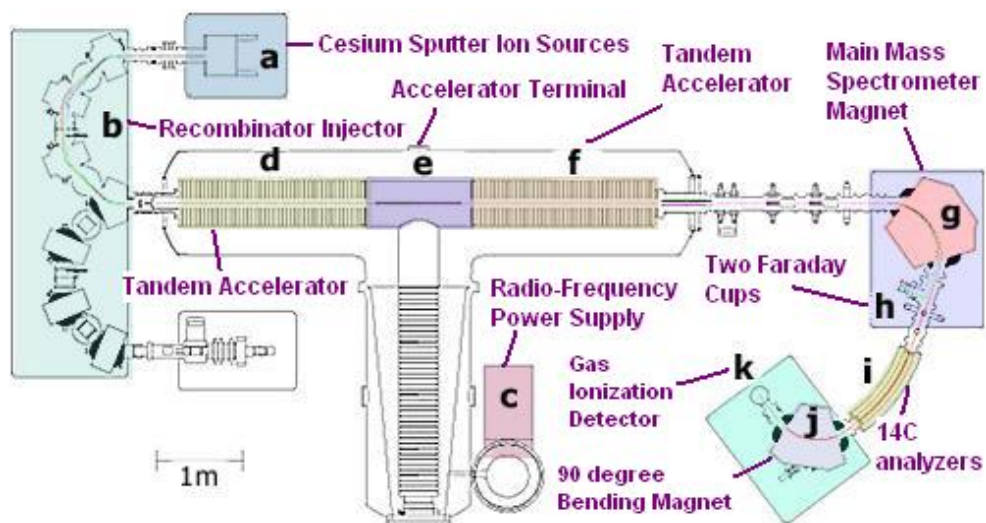


Figure 4.6 Schematic overhead view of the NOSAMS AMS system (modified from WHOI, 1989).

to the left, then into an assembly of four magnets and two electrostatic lenses. This device is called a "recombinator injector" because it serves to separate the negative ions by mass and remove ions with masses outside of the range of the carbon isotopes ($A = 12 - 14$ atomic mass units) before recombining the now mostly pure negative carbon ions for injection into the next stage, the accelerator (WHOI, 1989). A solid state radio-frequency power supply (c) provides charge to the center piece of the accelerator, the terminal (e). DC voltages over +2.5 million Volts can be reached using a capacitively fed heap of 1,600 high-voltage diodes (WHOI, 1989). The negative carbon ions entering to the first stage of the tandem accelerator (d) experience a "pull" toward the terminal and gain a speed of more than 3,600 miles per second. Accelerator terminal (e) is at 2.5 million Volt and contains an "electron stripper" canal, a tube of about 0.5 inch diameter filled with a very small amount of argon gas (WHOI, 1989). Up to half of the ions passing through this canal encounter grazing collisions with argon atoms that leave the ions "stripped" of four of their valence electrons. These carbon ions now have only three electrons left to counter their six protons and are therefore charged positive (3+) (WHOI, 1989). This process also takes care of a potentially big problem: compound ions of carbon and

hydrogen (^{12}CH , $^{12}\text{CH}_2$, ^{13}CH) which are always part of the negative ion beam coming out of (a). These compounds become dissociated during stripping, leaving the break-up products with incorrect kinetic energies for the final stretch of the system (WHOI, 1989). The now positive ions experience a "push" from the terminal and double their speed to over 7,200 miles per second in the second stage of the tandem accelerator (f). Their final kinetic energy is about 10 million electron Volts. The main mass spectrometer magnet (g) of the system bends the (3+) carbon ions 110° to the right. Here the three isotope beams are separated by mass, ^{14}C encounters the least amount of deflection, ^{12}C the most. Two Faraday cups (h) at this location collect the lighter ion beams (^{12}C , ^{13}C) and measure their current. The ^{14}C ions are allowed to travel on. The first of three remaining ^{14}C analyzers (i) is a 33° electrostatic deflector, filtering out any ions that don't have the correct energy: charge ratio. A 90° bending magnet (j) filters out scattered ions that have made it through the electrostatic deflector but have an incorrect momentum (mass x velocity). A gas ionization detector (k) analyzes the ions emerging from the last bending magnet (WHOI, 1989). In this final device, particles are identified by their energy loss due to the fact that the stopping power for particles in matter is dependent on the number of protons in the ion's nucleus. By adjusting the gas pressure in the detector, the ^{14}C ions are "selected". The ionization-charge pulses they generate in the gas are proportional to their energy. These individual charge pulses are collected and counted in the AMS detector electronics (WHOI, 1989).

The raw result of the AMS analysis is the ratio of ^{14}C particles per second detected in the ionization chamber to the particle currents measured in the Faraday cups (h). This ratio is compared with frequently measured ratios of known "standards" to arrive at the final AMS result. The results are reported as Percent Modern Carbon (pmc) (WHOI, 1989).

4.2.4 Noble Gases

Noble gas (Helium, Neon, Argon, Krypton, and Xenon isotopes) measurements were performed at L-DEO using a multi-purpose noble gas mass spectrometer (MAP 215-50) (Figure 4.7). Firstly, the noble gas sample container was attached to an evacuated extraction system. The water was then transferred from the copper tube into a glass bulb. The water was stirred continuously for 45 minutes and the copper tube heated

periodically to transfer all gases into the gas phase. Water vapor was used to transport the gases through a capillary and an alcohol/dry ice trap into an evacuated volume (1 liter), where the dry gases accumulated during the extraction. Of the extracted gas, 2.5% was then exposed to titanium sponge at 800 °C for 10 minutes to remove all chemically active gases except hydrogen (Stute and Schlosser, 2000). In order to trap hydrogen, the oven was allowed to cool down to about 100°C over a period of 30 minutes. The remaining noble gases were adsorbed quantitatively on activated charcoal held at 14 °K. The individual noble gases successively released from the charcoal by stepwise heating of the trap measured in the mass spectrometer (Stute and Schlosser, 2000). This process was continuously monitored by a spinning rotor pressure gauge. The pressure reading was used for measuring the total concentration of Helium for only in the upper concentration range and Argon, as well as for the decision if the sample could be directly admitted into the mass spectrometer or if it had to be split (Stute and Schlosser, 2000).

The mass spectrometer, MAP 215-50, is a double focusing 90° static sector field instrument with extended geometry. The system was calibrated with known quantities of atmospheric air. Calibration was checked by measuring water samples equilibrated with atmospheric air at known pressure and temperature. The precision of the measurements were about ±1 to 2 percent for noble gas abundances (Stute and Schlosser, 2000).

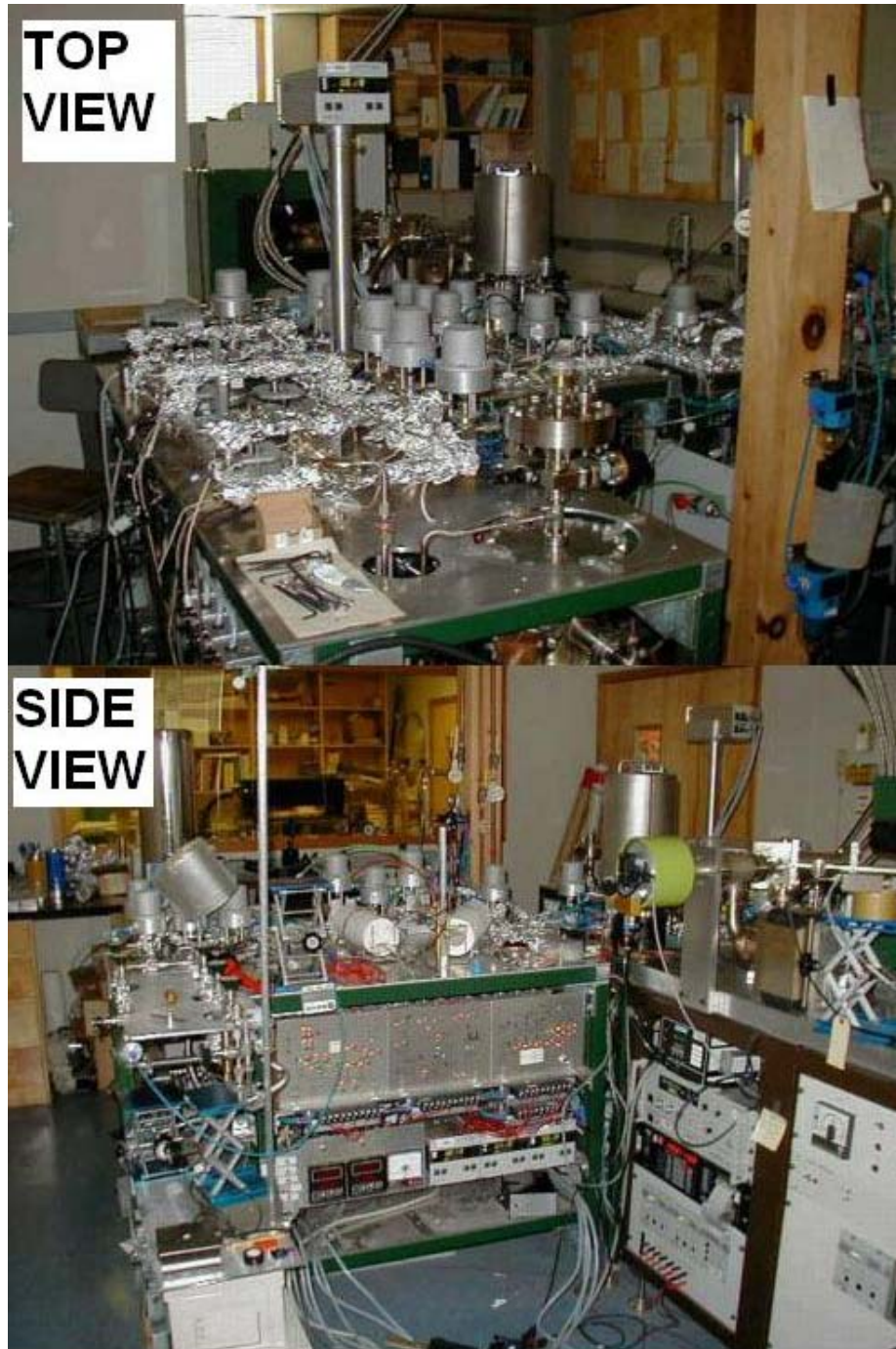


Figure 4.7 Two views (top and side) from the MAP 215-50 noble gas mass spectrometer at L-DEO.

CHAPTER 5

RESULTS AND DISCUSSION

5.1 Relationship of Oxygen-18 (^{18}O) and Deuterium (^2H)

The δD and $\delta^{18}\text{O}$ values in precipitation and fresh waters generally plot close to a straight line that is the **Global Meteoric Water Line (GMWL)**. This line, determined by Craig (1961b) and presented in Equation 5.1, defines the relationship between ^{18}O and ^2H in worldwide fresh waters.

$$\delta^2\text{H} = 8 \delta^{18}\text{O} + 10 \text{ (‰ SMOW)} \quad (5.1)$$

Local Meteoric Water Lines (LMWL) may also exist, having slightly different slopes and intercepts than the GMWL, as a result of differences in altitude, local climate and distance from the moisture source (Rozanski et al., 1993). If groundwater $\delta^{18}\text{O}$ and $\delta^2\text{H}$ values plot near the present precipitation water line for the sampling area, the waters are likely meteoric in origin, that is to say, derived from precipitation without subsequent modification. If they do not plot along this line, they have been impacted by some physical or chemical process prior to recharge, or during the groundwater's journey through the aquifer (Clark and Fritz, 1997).

For local investigations, it is important to compare surface water and ground water data with a LMWL; however it is impossible to continuously monitor precipitation over a representative period of time. Thus, Clark and Fritz emphasized that meteoric water lines must be borrowed from the closest available monitoring station. International Atomic Energy Agency (IAEA) and the World Meteorological Organization (WMO) have been surveying the content of hydrogen and oxygen isotopes in precipitation since 1961 and fortunately, IAEA has a station in Ankara, very close to the study area, where precipitation samples were collected starting from 1963 and analyzed for oxygen-18 and

deuterium contents. There is a database called **Global Network of Isotopes in Precipitation (GNIP)** constituted by IAEA where all the available data is gathered. The results of monthly measurements of oxygen-18 and deuterium in precipitation from this station starting from March 1964 until November 2006 were taken from GNIP website (IAEA/WMO, 2004) and were plotted. **Ankara Local Meteoric Water Line (ALMWL)** was produced from that plot, represented by Equation 5.2 with a coefficient of determination of 0.9484 and given in Figure 5.1.

$$\delta^2\text{H} = 8 \delta^{18}\text{O} + 11.42 (\text{‰ SMOW}) \quad (5.2)$$

Results of the oxygen-18 and deuterium analyses of the groundwater and springs from the study area are presented in Table 5.1. When all the results were examined, it has been concluded that, oxygen-18 data measured at L-DEO is approximately 0.5 per mil more positive compared to the results obtained from the measurements at University of Waterloo. This difference is believed to be related to the neutralization process carried out by using %100 H₃PO₄. This process should have affected the oxygen-18 values. To avoid the affects of this process, 0.5 per mil was subtracted from all oxygen-18 results belonging to August and November 2006. All the comments about these results will be based on the modified oxygen-18 values.

At a given location, the seasonal variations in $\delta^{18}\text{O}$ and $\delta^2\text{H}$ values of precipitation and the weighted average annual $\delta^{18}\text{O}$ and $\delta^2\text{H}$ values of precipitation remain fairly constant from year to year because the climatic conditions such as temperatures and the vapor source are almost constant (Clark and Fritz, 1997). Generally, rain in the summer is isotopically heavier (more positive values) than rain in the winter due to the seasonal temperature differences. Springs recharged by direct precipitation are expected to reflect these seasonal variations mostly. These variations often disappear during infiltration through the unsaturated zone as a function of the physical characteristics of this zone, the length of the flow path and residence time. According to Clark and Fritz (1997), a critical depth can be defined where the isotopic variation is less than the 2σ error of the $\delta^{18}\text{O}$ analysis. The critical depth can be reached at 3 to 5 m in a fine-grained soil (Zimmermann et al., 1967). If the critical depth is situated below the water table minor

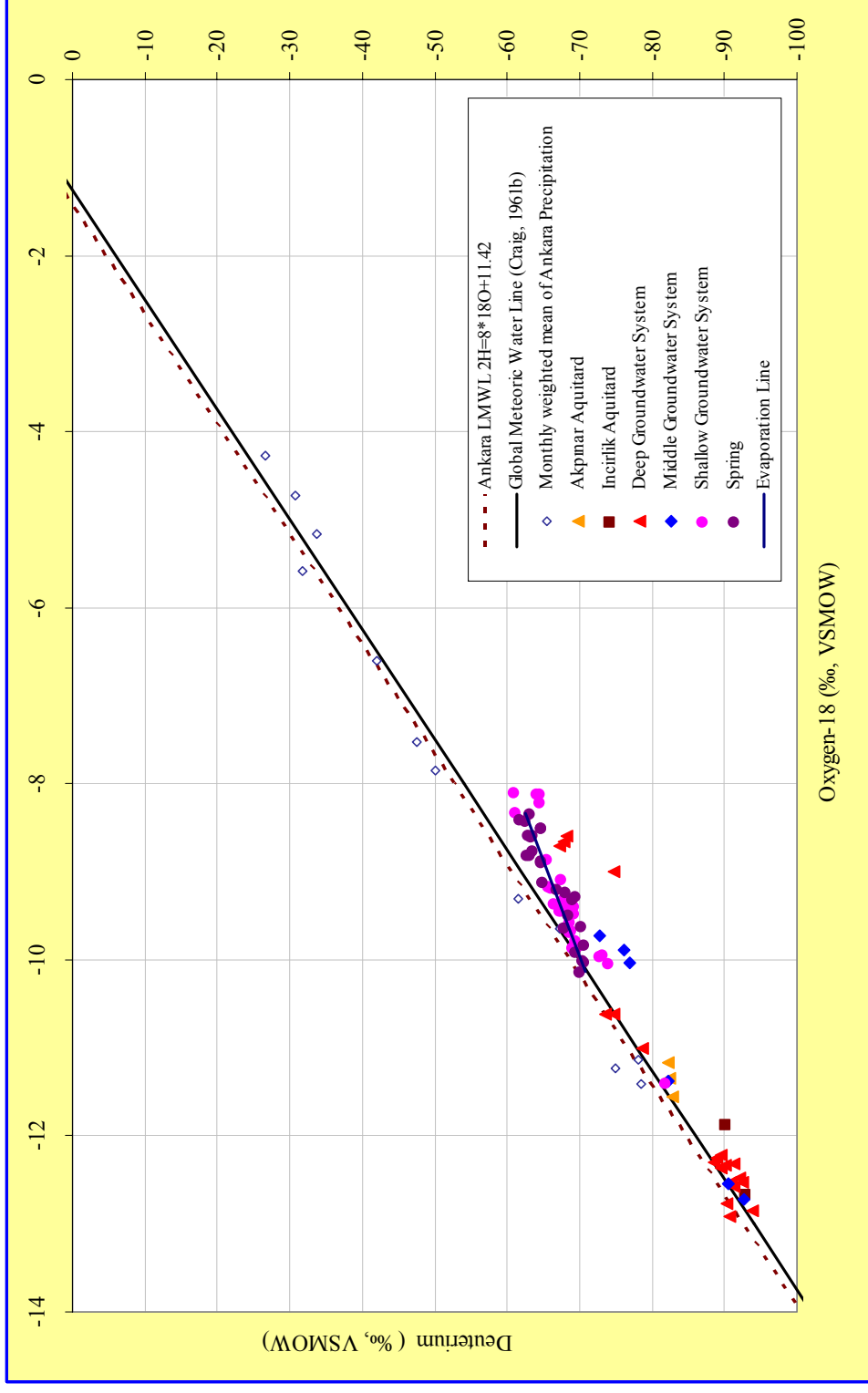


Figure 5.1 The plot of Deuterium versus Oxygen-18 data for springs and wells (Ankara LMWL equation calculated from data in IAEA/ WMO, 2004).

Table 5.1 Oxygen-18 ($\delta^{18}\text{O}$) and deuterium results ($\delta^2\text{H}$) of the groundwater and spring samples within the study area.

Sample name	Date	August 2006		November 2006		May 2007		June 2007	
	Depth/Elev. (m) *	^{18}O (‰)	^2H (‰)	^{18}O (‰)	^2H (‰)	^{18}O (‰)	^2H (‰)	^{18}O (‰)	^2H (‰)
S-1	14			-9.18	-66.02			-9.16	-65.69
S-2	14			-9.44	-67.51			-9.39	-69.21
S-3	14			-9.43	-67.32			-9.56	-68.61
S-4	7	-8.21	-64.58	-8.11	-64.05			-8.10	-64.57
S-5	14							-9.67	-68.55
S-9	11	-9.94	-73.11	-9.96	-72.77			-10.04	-73.88
S-11	8	-9.86	-69.13						
S-13	8							-9.66	-68.82
S-15	12							-9.77	-69.39
S-16	15			-9.85	-69.86			-9.88	-69.42
S-19	12			-8.32	-61.13			-8.10	-60.89
S-20	12	-9.35	-66.41					-9.30	-67.91
S-21	12							-9.08	-67.51
S-22A	17							-8.86	-65.51
S-23	12							-9.37	-68.36
S-24	10							-9.47	-69.20
D-8	174	-12.31	-88.58	-12.85	-93.82				
D-13	377			-12.33	-90.07				
D-20	207	-10.61	-73.80					-10.61	-74.66
D-33	157			-12.52	-92.49			-12.92	-90.82
D-37	227	-12.37	-89.62	-12.32	-91.31				
D-47	222			-12.47	-92.12				
I-50	815	-8.99	-74.52						
D-53	561							-8.59	-68.20
D-57A	310	-12.58	-91.37					-12.78	-90.32
M-57B	138							-12.72	-92.63
A-58A1	295	-11.17	-82.31					-11.35	-82.40
A-58A2	214							-11.55	-82.84
S-58A3	22							-11.40	-81.83
D-60A	286			-12.53	-90.99				
M-60B	120	-12.54	-90.59						
D-63A	205	-11.00	-78.73						
D-63B	117			-11.38	-82.23				
M-65B	182	-9.72	-72.88						
D-68R	73	-12.25	-89.02	-12.21	-89.52				
I-74A	532	-12.65	-92.96					-11.87	-90.09
D-74B	288	-8.71	-67.26					-8.65	-67.80
M-74C	87	-9.89	-76.08					-10.04	-76.92
SP-3	961	-8.76	-63.52	-8.8	-62.71	-8.81	-63.09		
SP-4	929			-8.41	-62.49	-8.34	-63.10	-8.40	-61.76
SP-5.1	1100	-9.11	-64.96	-9.91	-69.48	-9.63	-67.79		
SP-6	1093			-10.01	-70.52	-10.13	-70.05		
SP-7	952	-9.22	-68.11	-9.3	-69.12	-9.28	-69.36		
SP-16	914			-8.49	-64.68	-8.57	-63.55	-8.49	-64.76
SP-17	855					-9.49	-68.40		
SP-18	969					-9.20	-66.92		
SP-21	855			-9.82	-70.59	-10.00	-70.35		
SP-22	944			-8.89	-64.68	-8.87	-64.62		
SP-23	959			-8.57	-62.83	-8.59	-63.22		

* Depth for wells, elevation for springs.

seasonal variations are preserved in shallow groundwaters. On the other hand, the isotopic variability below the critical depth in a confined aquifer generally does not exceed the 2σ analytical precision. When it does, this signifies preferential pathways or mixing of different recharge waters (Clark and Fritz, 1997). Under the light of these information when Table 5.1 is examined, it can be seen that, if the results taken from the same location in different seasons are considered it is not possible to observe seasonal variations in any of the samples, not even in springs, except for SP-5.1, D-8 and I-74A. The possible reason for the seasonal variations in D-8, representing the groundwater from the deep groundwater system under confined conditions, and I-74A, representing the groundwater from the İncirlik Aquitard located below the deep groundwater system, can well be a sign of the preferential pathways in the fractured aquifer. The seasonal variations observed in SP-5.1 will be discussed together with the findings from Figure 5.1.

In order to understand the relationship between ^{18}O and ^2H , the results were plotted and also presented in Figure 5.1 together with the GMWL and Ankara LMWL. According to this plot, there is a wide range of values covered in both $\delta^2\text{H}$ and $\delta^{18}\text{O}$ values for the whole system. A strong isotopic contrast is found between shallow and deep aquifer systems. This contrast can also be observed between unconfined and the confined parts of the deep aquifer system. The samples from the shallow groundwater wells and the springs plotted in the same region, $\delta^{18}\text{O}$ values being between -8 and -10 per mil and $\delta^2\text{H}$ values between -60 and -70 per mil, whereas samples from the middle and deep groundwater system plotted in $\delta^{18}\text{O}$ values being between -9 to -13 per mil, $\delta^2\text{H}$ values being between -65 to -95 per mil, towards isotopically lighter values. The isotopic signature of modern recharge groundwaters is consistent with local precipitation whereas deeper groundwaters are depleted by up to 3 per mil in $\delta^{18}\text{O}$ and 25 per mil in $\delta^2\text{H}$. These lighter values can well be due to the reason that the recharge elevation of the deep aquifer system is higher than the shallow system (altitude effect) or owing to the reason that the recharge temperatures in the deep aquifer system are lower than the temperatures in the shallow system. In the following sections, altitude effect and the recharge temperatures will be investigated.

In Figure 5.1, some of the samples plotted along the GMWL, however most of them showed deviations from the meteoric water line. Generally, it is known that deviations from meteoric water line are caused by different processes like evaporation, condensation, water- rock interactions, mixing of waters having different origins and seasonal effects (Clark and Fritz, 1997). In high temperatures, mostly in geothermal systems, oxygen-18 exchange with rocks is possible causing a shift towards more positive values in $\delta^{18}\text{O}$. It is also possible to observe the oxygen-18 shift in the low temperature systems however this process requires a considerable amount of time over geologic time scale. Water can be lost by evaporation occurring prior to infiltration, from the unsaturated zone or from the water table causing an evaporative enrichment in the stable isotope signature of the sample considered (Clark and Fritz, 1997). The deviations from the GMWL in the samples from the springs and the shallow groundwater system are due to the evaporative enrichment of the samples, the details of which will be discussed in the proceeding sections.

5.1.1 Groundwater Mixing

Groundwater mixing can be present locally and regionally in an area under investigation. Utilization of various techniques involving isotopes helps the investigators in determining the mixing between groundwaters from different aquifers and flow systems. As stated by Clark and Fritz (1997) mixing between two distinct groundwaters can be quantified by simple algebra using $\delta^{18}\text{O}$ or $\delta^2\text{H}$ (Equation 5.3), due to the fact that ^{18}O and ^2H are conservative in mixing relationships and so will preserve the mixing ratio.

$$\delta_{sample} = \lambda\delta_A + (1 - \lambda)\delta_B \quad (5.3)$$

In the above equation, λ is the mixing percentage δ is the ^{18}O or ^2H value, A and B are the mixing components and sample is the water formed as a result of mixing.

Not surprisingly, it is possible to observe quite complex mixing between the three different aquifers in the study area. According to the hydraulic and geochemical data gathered by SRK, there is an upward groundwater mixing taking place from the deeper aquifer systems to the shallower one in study area. A recent study by Çamur et al. (2007)

aimed establishing existing hydrogeochemical relationships between groundwater environment and geological units in the area. Çamur et al. (2007) tested the processes that can cause chemical anomalies in the groundwater compositions, explained in Chapter 3. According to Çamur et al., the mineralogical distribution is homogeneous in a given unit except the presence of saline minerals (searlesite, shortite and northupite) therefore the chemical anomalies in the groundwater compositions could be attributed to three processes: chemical anomalies was formed as a result of mixing from the concentrated upgradient groundwater in the same unit due to lateral flow or from the concentrated groundwater in underlying units due to upward flow and/or these anomalies represent saline mineral interactions within the same unit without mixing.

According to Çamur et al. (2007) the formation of the groundwater composition of D-8 could be modeled by using D-63A water composition. By the inverse modeling calculations, D-8 could be derived from D-63A by dissolution of searlesite, shortite and northputite and precipitation of dolomite, calcite and quartz. The validity of this finding can be checked by utilizing the isotope data available. Because of the fact that stable isotopes are conservative in geochemical reactions, the $\delta^{18}\text{O}$ and $\delta^2\text{H}$ results of these two waters should be very close to each other. Nonetheless, the results presented in Table 5.1 shows that D-8 is about 1.3‰ depleted in oxygen-18 and 10‰ depleted in deuterium when compared to D-63A. This depletion can not be explained by precipitation or dissolution of some minerals.

In the same study, the groundwater of D-57B was proposed to be formed by mixing of 57% M-60B upgradient groundwater and 43% D-57A groundwater from the underlying unit. This result, suggested by inverse modeling calculations, is also supported by isotope data. If Equation 5.3 is utilized by using the results presented in Table 5.1 and by assuming binary mixing, it is possible to calculate the mixing percentages of D-57A and M-60B as 70.7%, and 29.3% respectively. It is not possible to calculate the mixing percentages by using the deuterium data. Likewise, according to Çamur et al. (2007), M-74C water composition was formed by mixing of 97% of the groundwater of M-60B and 3% of the groundwater of D-74B. This finding is also verified with the isotope data (Figure 5.2). The mixing percentages calculated are slightly different for oxygen-18 and deuterium data. According to oxygen-18 data, the percentage of D-74B should be 64.3%

and M-60B should be 35.7% and if the deuterium data is used the mixing percentages should be 60% and 30% for D-74B and M-60B respectively. In Figure 5.2, it is possible to observe the mixing line for the formation of M-74C.

In the same paper, Çamur et al. (2007) claimed that formation of S-9 groundwater requires 0.75 and 0.25 mixing fractions for S-5 and D-57A. As stated by Çamur et al. (2007) the mixing component from the underlying units is questionable as because there is no information about the depth of the suspected fault, the presence of which is attributed to the chemical anomalies in wells S-4 and S-9. According to Figure 5.2, if only binary mixing is assumed, S-9 is not located in the mixing line between S-5 and D-57A due to the effects of evaporative enrichment in this well which will be explained in the following section. The unmodified stable isotope signal of S-9 to be used in the calculation is not known, thus increasing the uncertainty of the calculation. The mixing fractions of S-9 water from S-5 and D-57A were not calculated.

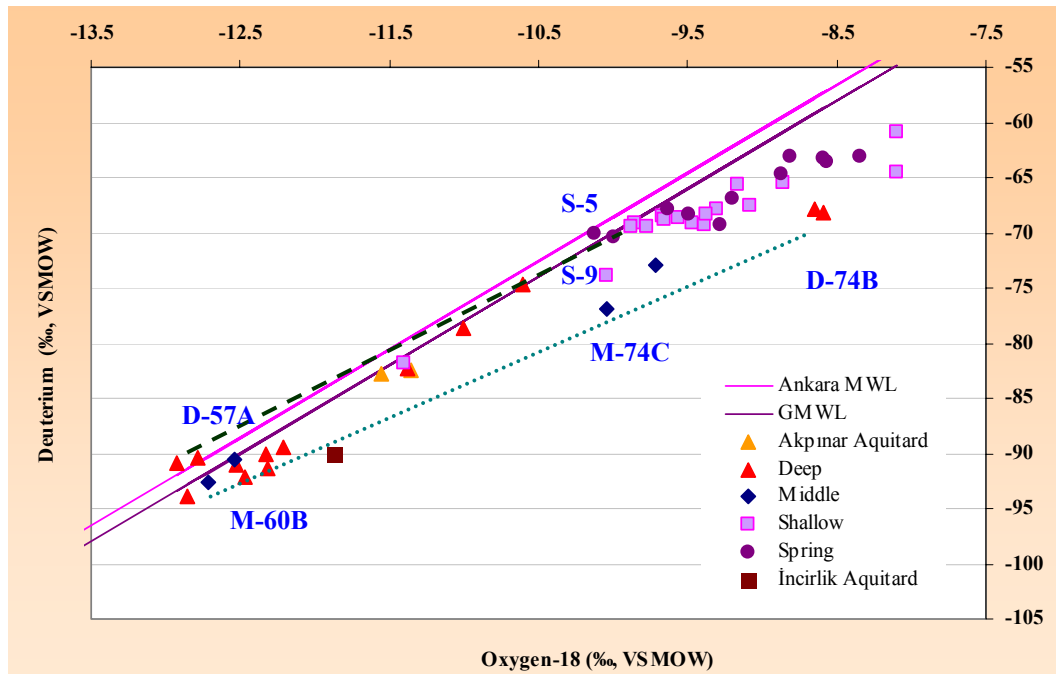


Figure 5.2 Deuterium versus Oxygen-18 graph showing two different mixing lines explaining the formation of M-74C and S-9.

5.1.2 Relationship of Oxygen-18 (^{18}O) and Deuterium (^2H) in the springs

The oxygen-18 and deuterium data from the springs in the study area suggests that there is evaporative enrichment of the stable isotopes (Figure 5.3) in some of the springs. The evaporation lines formed leads to deviation from the GMWL (Figure 5.3). The three different lines, drawn parallel to each other, have a slope of 4 proposing strong evaporation. The enrichment in both ^{18}O and ^2H for the springs can be explained by the fact that sampling for those springs were impossible to carry out from their original sources as these sources are buried underground. There was one exception, SP 5.1, which was collected right from the source therefore shows seasonal effects.

SP-4, SP-23, SP-3, and SP-22, located in the same evaporation line (Evaporation Line 1 in Figure 5.3), were in fact collected from the fountains in which the source of the spring first visits a storage reservoir and after waiting for some time discharges from the fountain. During this standby, evaporation is possible. These springs unmodified oxygen-18 signal should be approximately -9.66 ‰ and unmodified deuterium signal is about -68 ‰ from Figure 5.3. SP-16, SP-18 and SP-17 follows another evaporation line (Evaporation Line 2 in Figure 5.3) having the same slope as Evaporation Line 1. These springs were also fountains and their stable isotope signals were also modified due to the evaporative enrichment. Their original oxygen-18 and deuterium contents should be close to -10 ‰ and -70 ‰ respectively. Lastly, SP-7 is another spring showing evaporative enrichment following Evaporation Line 3. The original oxygen-18 and deuterium values for this spring should be around -10.3 ‰ and -72.5 ‰.

In Figure 5.3 it is obvious that SP-6 and SP-21, although collected through fountains like the rest of the springs except for SP 5.1, do not show evaporative enrichment. Therefore the measured oxygen-18 and deuterium contents of these springs (SP-6, SP-21 and SP-5.1) can be used directly during the interpretations. For the rest of the springs the suggested unmodified oxygen-18 and deuterium values should be taken into consideration.

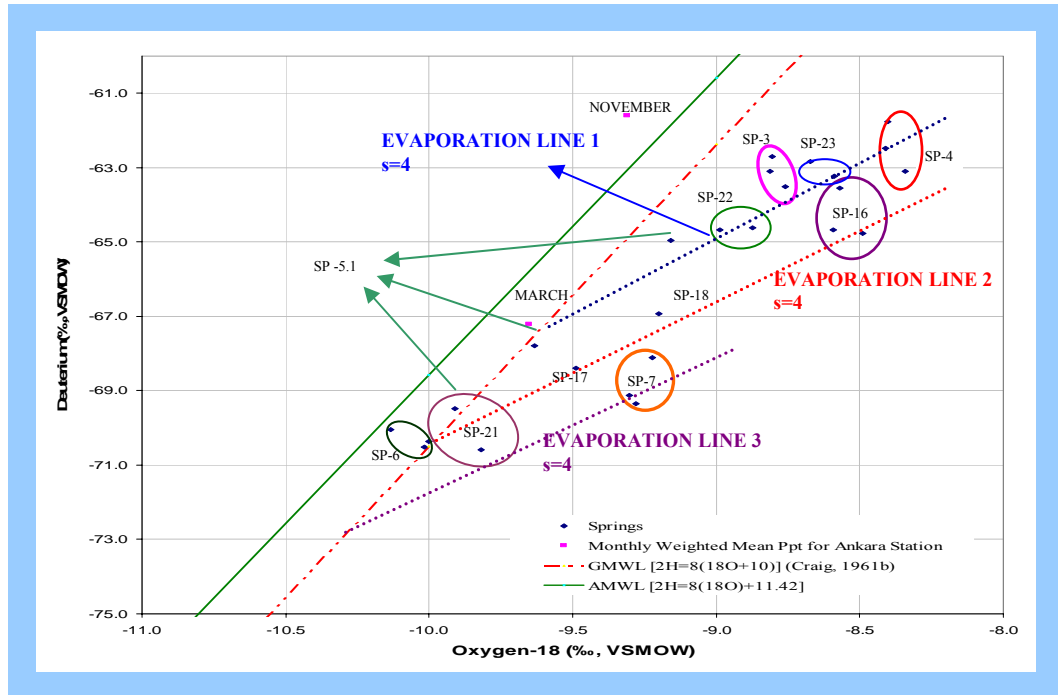


Figure 5.3 Deuterium versus Oxygen-18 graph for springs (Ankara Meteoric Water Line (AMWL) equation calculated from data in IAEA/ WMO, 2004).

5.1.3 Relationship of Oxygen-18 (^{18}O) and Deuterium (^2H) in the Shallow Groundwater System

For shallow groundwater wells, it is possible to observe evaporative enrichment during or after recharge in arid regions. The depth to groundwater is the lowest in well S-9, smaller than 2 meters; and the highest in S-5, around 15 meters. Thus, it is not surprising to observe the evaporation effect in the results. The evaporation lines 1, 2, and 3 in Figure 5.4 have slopes of 3.9 suggesting strong evaporation. According to Figure 5.4, there is no evaporation effect (or the effect is negligible) in wells S-11, S-16, S-3 and S-5. The evaporative enrichment seems to be the highest in S-19 and S-4. Most of the shallow wells follow Evaporation Line 1, S-9 follows Evaporation Line 2 and S-19, S-1 and S-20 are all along Evaporation Line 3. The wells following Evaporation Line 1 should have

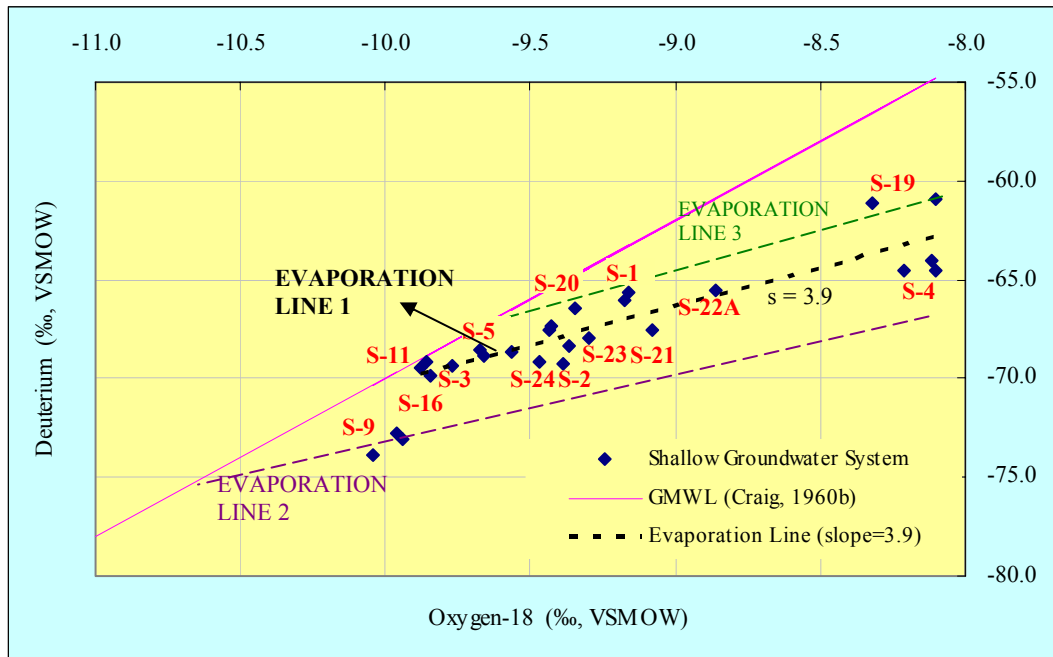


Figure 5.4 Deuterium versus Oxygen-18 graph for shallow groundwater wells in the study area.

original oxygen-18 and deuterium signals approximately -9.9 ‰ and -69‰ respectively. S-9, in case its evaporation follows Evaporation Line 2, should have a relatively depleted stable isotope content, unmodified oxygen-18 value being around -10.7‰ and deuterium value being -75‰. On the other hand, S-19, S-1 and S-20 should have started evaporation from originally -9.7‰ for oxygen-18 and -67 ‰ for deuterium. All the proceeding calculations involving stable isotope data of springs and shallow groundwater wells should be based on the original, unmodified stable isotope signals.

5.1.4 Relationship of Oxygen-18 (¹⁸O) and Deuterium (²H) in the Middle and Deep Groundwater Systems

The samples from middle and deep groundwater systems show interesting patterns. For these two systems evaporative enrichment is a low possibility unlike springs and shallow groundwater system. For the middle system, two of the samples (M-60B and M-57B)

plotted in the GMWL but the other samples plotted below the meteoric line having a deuterium excess of around +4 per mil (Figure 5.5). This shift can be an indication of a change in the vapor source affecting these samples during time of recharge. This possibility will be discussed in the following sections. Two of the samples from deep groundwater system, D-33 and D-57A plotted just above the GMWL, with a deuterium excess of around +12 per mil (Figure 5.5). This value is almost the same as the deuterium excess of today's Ankara LMWL. Combining the information gathered from other data to be discussed in the following sections, this issue will also be enlightened. The samples from the deep groundwater system plotting below the GMWL gives a deuterium excess of around +8 per mil. This shift is similar to the one observed in the samples from the middle groundwater system. Herein, more can not be concluded with the already presented data.

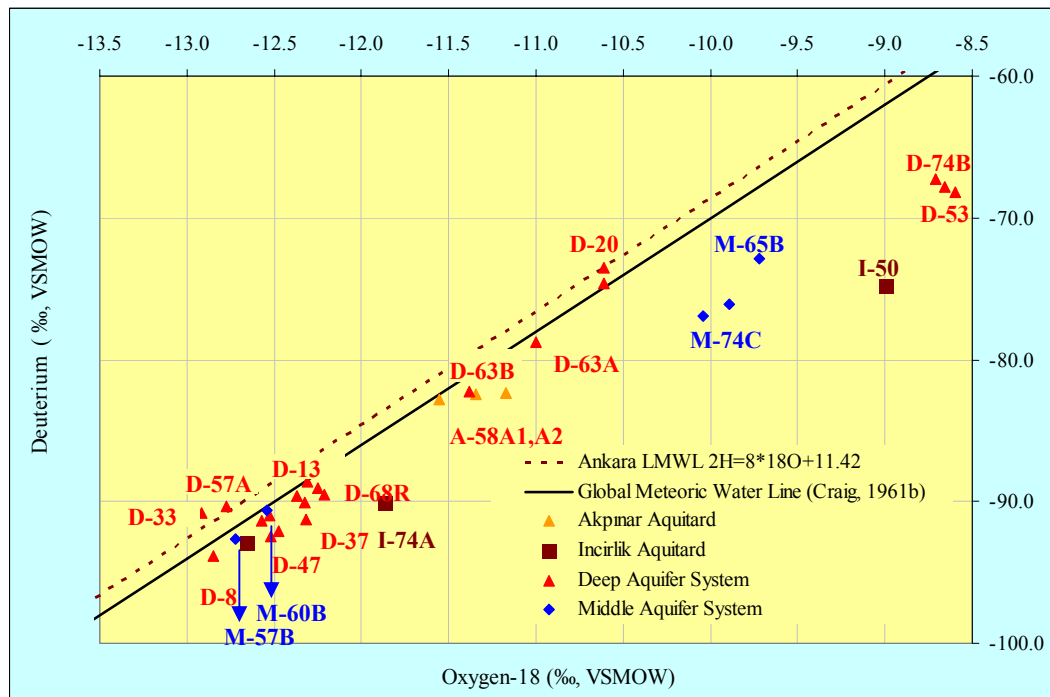


Figure 5.5 Deuterium versus Oxygen-18 graph for middle and deep groundwater wells in the study area Ankara Meteoric Water Line (AMWL) equation calculated from data in IAEA/ WMO, 2004.

5.2 Relationship of Elevation and Oxygen-18 ($\delta^{18}\text{O}$) for Precipitation

It is a known fact that $\delta^{18}\text{O}$ content of precipitation changes with changing altitude, temperature, latitude etc. At higher altitudes where the average temperatures are lower, precipitation will be isotopically depleted. For ^{18}O , the depletion varies about -0.15 and -0.5 per mil per 100-m rise in altitude. This altitude effect can be used in distinguishing groundwaters recharged from different altitudes (Clark and Fritz, 1997).

For the study area, unfortunately, there is no data available regarding precipitation from different altitudes. Normally, springs with different elevations, showing seasonal variations in discharges (being dry in summer and increasing discharges in winter) can also be used to reveal out the relationship of ^{18}O with altitude but due to the reason that springs in the study area showed evaporative enrichment and also the springs had more or less constant discharge throughout the year, it was decided that it is not feasible to use the available spring data. Therefore this relationship is borrowed from another study by Apaydın (2004) carried out in Beypazarı Trona Ore Field, located 50 km west of the Kazan Trona Ore Field. Apaydın used the data gathered from the springs fed by local precipitation with elevations changing between 800 masl to 1500 masl. According to his findings, the depletion in $\delta^{18}\text{O}$ is about -0.44 per mil per 100-m rise in altitude. The equation suggested by Apaydın for the relationship of ^{18}O and altitude for May 2000 with a coefficient of determination of 0.97 is given in Equation 5.4.

$$\delta^{18}\text{O} = -0.0044 * (\text{Elevation}) - 4.811 \quad (5.4)$$

To check the validity of this equation at the Kazan Trona Field, SP-5.1, fed by local precipitation without showing evaporative enrichment, was used. It's known that the recharge elevation of this special spring is approximately equal to its discharge elevation. Thus, according to the equation given by Apaydın, $\delta^{18}\text{O}$ for SP- 5.1 with a recharge and also a discharge elevation of 1100.6 m should be -9.654 per mil for May 2007. The measured oxygen-18 value is -9.63 per mil, very close to the calculated value, proving the validity of the equation.

Equation 5.4 was used to calculate the recharge elevations of springs and groundwaters from shallow, middle and deep groundwater systems (Figure 5.6). During the calculations, for the springs and the shallow groundwater samples showing evaporative enrichment, the unmodified oxygen-18 signals given in the preceding section were used.

For the springs, the calculations of the true recharge elevations are not easy because as stated before in Chapter 3, geochemical data (elevated concentrations of arsenic, boron, sodium and bicarbonate) suggested that some of the springs are originating from deeper units (SP-7) and some others are actually discharging water which is a mixture of

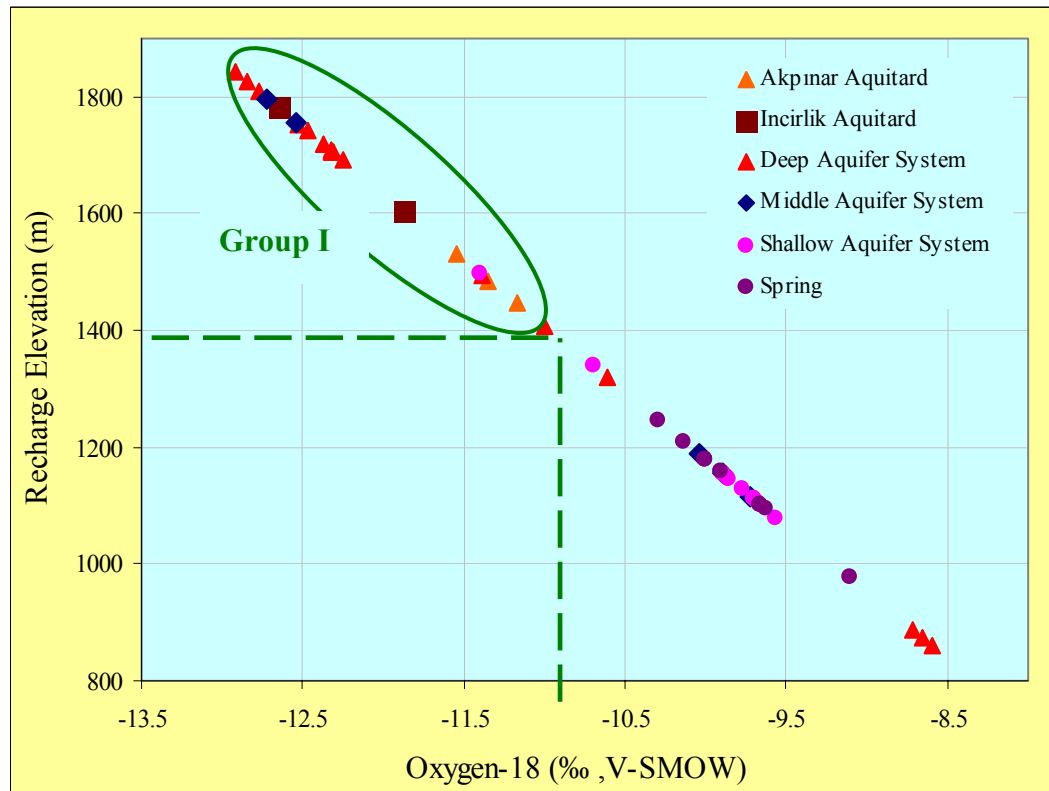


Figure 5.6 Recharge Elevation (m) versus Oxygen-18 (‰, V-SMOW) graph for the springs, shallow, middle and deep groundwater systems. The recharge elevations were calculated by using equation $\delta^{18}\text{O} = -0.0044 * (\text{Elevation}) - 4.811$ (Apaydın, 2004). Group I represents the elevations exceeding the maximum topographical elevation in the study area (1400 m).

shallow and deeper water (SP-16 and SP-21) (SRK, 2004). SP-17, SP-18 and SP-22 also had elevated concentrations of sulfate, boron, fluoride and potassium and there can also be contribution from the deeper groundwater in those springs (SRK, 2004). The remaining springs can be used for a comparison between the recharge and discharge elevations. When SP-3, SP-23 and SP-4 are considered, the discharge elevations are the same for SP-3 and SP-23 (960 m), and for SP-4 the elevation is 929 m and according to their unmodified oxygen-18 content their recharge elevations are the same for these three and is around 1100 m. Accordingly, SP-6 is recharged with the precipitation falling to 1200 m and discharges its water at around 1090 m. For SP-7, SP-16, SP-21, SP-17, SP-18 and SP-22 the situation is complicated as these springs show mixing of groundwater having higher recharge elevations. When SP-7 is taken into account, the calculated recharge elevation is around 1250 m and the discharge elevation is 950 m. For SP-16, SP-17, SP-18, SP-21, SP-22 the calculated recharge elevations are the same for all, 1180 m, and their discharge elevations are 914 m, 855 m, 969 m, 855 m, 944 m respectively.

It has been stated out in the previous chapters that the highest topographic elevation in the area is around 1408 m according to the current topography within the Kazan Basin; therefore the highest recharge elevation can be around 1400 m. However the recharge elevations calculated from the above equation came out to be between 850 m and 1842 m for shallow, middle and deep aquifer systems (Figure 5.6). It is impossible to explain the isotopically lighter values measured in samples from the deeper groundwater systems with the altitude effect (Group I in Figure 5.6). All the samples belonging to the waters from this system, except for D-20, D-53 and D-74B should have a recharge elevation greater than 1400 m according to the calculations. This arise the question, together with the shifts from the GMWL, whether these samples belong to present day recharge or they entered to the aquifer system in colder temperatures, may be in another climatic period. Before answering this crucial question, additional data should be presented and evaluated.

5.3 Interpretation of Recharge Temperatures by using Noble Gas Data

In Chapter 2, general information was given about the utilization of noble gas data to interpret the recharge temperature of a given sample. It has been stated that the solubility

of noble gases in water is a function of temperature and salinity (for groundwaters salinity can be disregarded because the dissolved salt concentrations need to exceed 1000 mg/l NaCl to reduce solubility by 1%) and noble gas solubility increases with atomic mass and decreases with temperature (Stute and Schlosser, 2000). The sensitivity to temperature increases with mass. For example, at 25 °C, the sensitivity of the solubility ranges from 0.1 %/ °C for Helium to 2.8 %/ °C for Xenon (Benson and Krause, 1976). Water percolating through the unsaturated zone equilibrates continuously with ground air until it reaches capillary fringe. For most recharge areas, the noble gases dissolved in groundwater may be assumed to reflect the ground temperature at the water table (Herzberg and Mazor, 1979; Phillips, 1981; Stute and Schlosser, 1993). There can be exceptions where the water table is very close to the surface (1 to 2 m), the recharge rates are very high or the recharge does not have sufficient time for equilibration with the ground air like in karst areas. If the water table is not far below the surface (greater than 30 m), the noble gas temperatures should be within 1°C of the surface ground temperature. Surface ground temperatures can be converted into air temperatures by using local relationships between these variables (Stute and Schlosser, 2000).

The noble gas thermometer is based on a simple physical principle, namely the temperature dependence of the solubility of noble gases in water. Different techniques can be used to delineate the recharge temperatures from noble gas data (Stute and Schlosser, 2000). These techniques are the graphical method, iterative schemes and inverse modeling method. In the iterative method the noble gas concentrations are calculated by subtracting small quantities of unfractionated air from the measured concentrations and the calculated concentrations are converted into temperatures by using the solubility data and the atmospheric pressure at the water table elevation (Andrews and Lee, 1979; Rudolph et al., 1984 and Stute et al., 1995a). The subtraction process endures when optimum agreement between the four calculated noble gas temperatures (Ne, Ar, Kr and Xe) achieved. In this procedure the role of atomic weight in the temperature sensitivity is ignored. Inverse modeling technique performs the optimization procedure providing an intense solution of the component separation as the effects of atomic weight are also taken into account (Ballentine and Hall, 1999 and Aeschbach-Hertig et al., 1999). These two techniques were proven to give similar results (Stute and Schlosser, 2000).

Herein, the graphical method suggested by Heaton and Vogel (1981) is used. In this technique, data points can be extrapolated toward the equilibrium line assuming that the excess air component is not fractionated and the temperature can be determined. Little is known about the origin or composition of the excess air component. It is probably caused by trapping of air bubbles during rapid recharge events in fractures, or by fluctuations of the water table trapping and partially or entirely dissolving small air bubbles under increased hydrostatic pressure or surface tension. In cases where excess air is unfractionated, its contribution has been expressed as cm^3STP (Standard Temperature, 0°C and Pressure, 101.325 kPa) of dry air per g of water (Stute and Schlosser, 2000).

In Figure 5.7, xenon versus neon concentrations for all samples can be seen. In this figure, the solid line corresponds to solubility equilibrium at 1100 m and the broken lines symbolize the addition of unfractionated atmospheric air. Here, the measured data plotted to the right of the expected concentrations due to solubility equilibrium alone, suggesting the presence of excess air (Herzberg and Mazor, 1979). For the sake of simplicity, Figure 5.7 was prepared by assuming a recharge elevation of 1100 m for all the samples although it is not the case. According to the recharge elevations calculated by using the relationship of $\delta^{18}\text{O}$ and elevation, it should be different for all wells as presented in Table 5.2. Unfortunately, one sample, D-68R, had air contamination, therefore the data was not used and a noble gas temperature was not calculated. It should also be noted that for D-8 and D-47, as their isotopically lighter $\delta^{18}\text{O}$ values couldn't be explained with the elevation effect, different recharge elevations were assigned for D-8 and the noble gas temperatures were calculated. This way, the sensitivity of the noble gas recharge temperatures to the recharge elevation can be seen.

When the Noble Gas Temperatures (NGT) presented in Table 5.2 are examined, it can be seen that for the shallow groundwater wells (S-11, S-3, S-16 and S-2) the NGT reflects the mean annual air temperature for Ankara which is 11.8°C . For D-8, it can be seen that the calculated NGTs increases about 0.8°C with 500 m change in the recharge elevation. For D-47 this change is 0.5°C . If the recharge elevation is taken to be the highest available topographic elevation then, for D-47 the NGT should be around 8.4°C and for D-8, it should be around 5.5°C . For these two wells the lower temperatures can be due to the fact that precipitation in higher elevations has lower temperatures or these

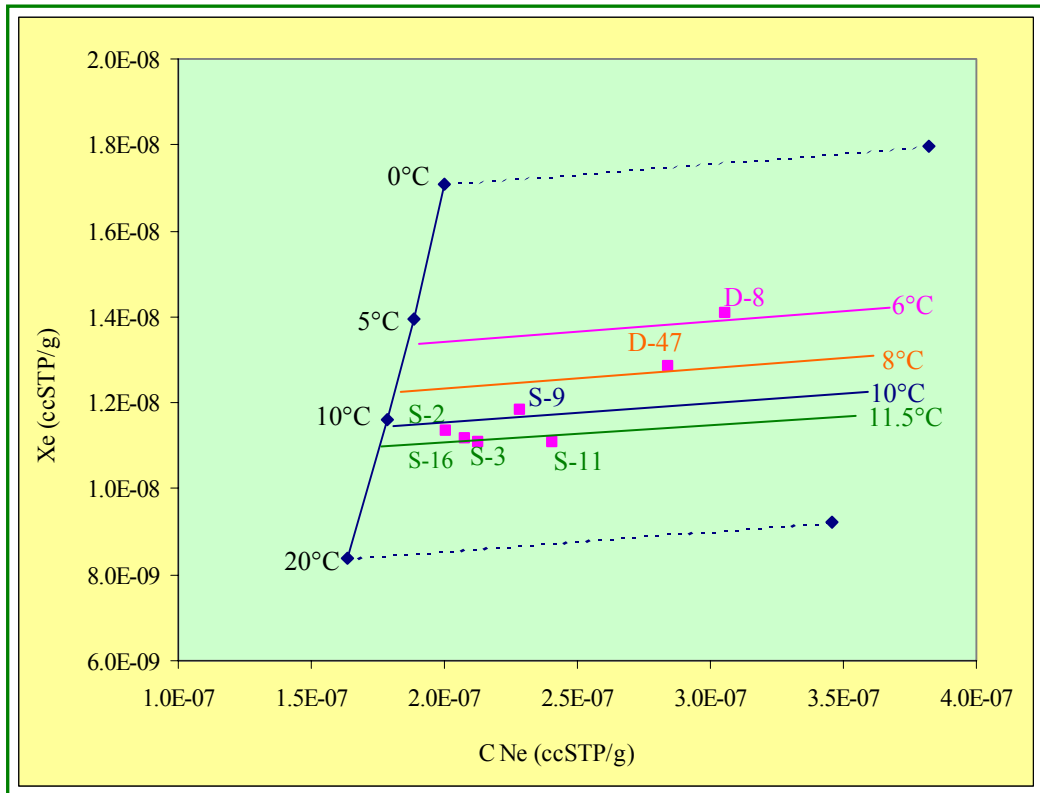


Figure 5.7 Xenon versus Neon concentrations also showing the noble gas temperatures calculated by using a recharge elevation of 1100 m.

lower temperatures can be an indication that the groundwater representing these samples entered to the aquifer system a long time ago, in a relatively colder period if this way their isotopically lighter values can also be explained which can indeed not explained with the elevation effect. Apaydın (2004) used the temperature data from six stations having topographic elevations changing between 400 m and 1400 m. According to Apaydın (2004), there is a nice correlation showing the decrease in the temperatures with rising altitude and the precipitation in 1400 m should have a temperature around 6.5 °C, whereas it should be around 9 °C in 1100 m. In this section, more can not be concluded about the reasons for the lower recharge temperatures in the deeper aquifer.

Another interesting point to be mentioned herein is that, for one well, S-9, the NGT came out to be in between the ones calculated for the shallow groundwater system and the ones

Table 5.2 Measured concentrations of Xenon and Neon, the recharge elevations (m) (recharge elevations for the shallow wells calculated from $\delta^{18}\text{O}$ data, for D-68R and D-8 see text for details) and the calculated recharge temperatures ($^{\circ}\text{C}$) by using graphical method.

Sample name	Ne [ccSTP/g]	Xe [ccSTP/g]	Recharge Elevation (m)	Recharge Temperature by Graphical Method ($^{\circ}\text{C}$)
D-68R	1.02E-06	1.80E-08	-	Not Applicable
D-8	3.06E-07	1.41E-08	1800	5
			1700	5.2
			1600	5.3
			1500	5.4
			1400	5.5
			1300	5.8
D-47	2.84E-07	1.80E-08	1800	8
			1600	8.2
			1400	8.4
			1300	8.5
S-9	2.29E-07	1.18E-08	1338	9.9
S-11	2.41E-07	1.11E-08	1146	12.2
S-3	2.13E-07	1.11E-08	1080	12
S-16	2.08E-07	1.12E-08	1152	12
S-2	2.01E-07	1.13E-08	1157	11.4

for deep groundwater system. This can be another indicator of the mixing of deep groundwater through a fault just as the geochemical data indicates. Before reaching to further conclusion, all the data should be considered in an integrated manner.

Although not enough noble gas measurements is available to find the NGTs for all samples, the data belonging to shallow groundwater wells proves that it will not be unrealistic to use the mean annual air temperature as their recharge temperature in the calculation of groundwater ages with chlorofluorocarbons. This assumption can only be valid for the wells in which mixing of deeper groundwater is not possible.

5.4 Calculation of Groundwater Ages with Chlorofluorocarbons

In order to have information about the residence times of different aquifers in the study area the groundwater samples were analyzed for their CFC-11, CFC-12 and CFC-113 contents. It was stated out in Chapter 2 that CFCs provide excellent tracers and dating tools of young groundwater over 50 year time scale. Fortunately, history of atmospheric CFC mixing ratios, making CFC age dating possible, is available for both hemispheres. Production and release of CFCs to the atmosphere rose rapidly through 1970s and 1980s (AFEAS, 1997). Annual production of CFC-11 and CFC-12 peaked in 1987 at 382000 and 425000 metric tons, respectively, and that of CFC-113 peaked in 1989 at 251000 metric tons. Total production of CFC-11 and CFC-12 in 1987 was 7.0 and 9.4 million metric tons, respectively and that of CFC-113 in 1989 was 1.7 million metric tons. In Figure 5.8 atmospheric mixing ratios of CFC-11, CFC-12, CFC-113, and SF₆ in North American air (based on measurements from Niwot Ridge, Colorado, an atmospheric monitoring station in the Rocky Mountains at 3013 m elevation near Boulder, Colorado) are given. According to this figure, the global average CFC-11 tropospheric mixing ratio peaked at 272.8 parts per trillion volume (pptv) in 1994 and has declined at about 1 pptv per year (Elkins et al., 1993, 1996). The CFC-12 mixing ratio has slowed at a rate of about 1.66 pptv each year since 1988. In 2001, CFC-12 mixing ratio peaked with a global average tropospheric mixing ratio of 546.5 pptv. For CFC-113 peak mixing ratio was observed in 1995 with a value of 83.7 pptv (Figure 5.8). CFC-11 and CFC-12 mixing ratios for air before 1976 were reconstructed from production data by McCarthy et al. (1977). Air mixing ratios of CFC-113 were compiled from Wisegarver and Gammon (1988), Tominaga (1992), Fisher and Midgley (1993), Fraser et al. (1996), Busenberg and Plummer (1993) and data from the NOAA since 1991. As most CFCs have been released to the troposphere in the northern hemisphere, CFC mixing ratios in the southern hemisphere lag behind those of the northern hemisphere (Busenberg and Plummer, 2000).

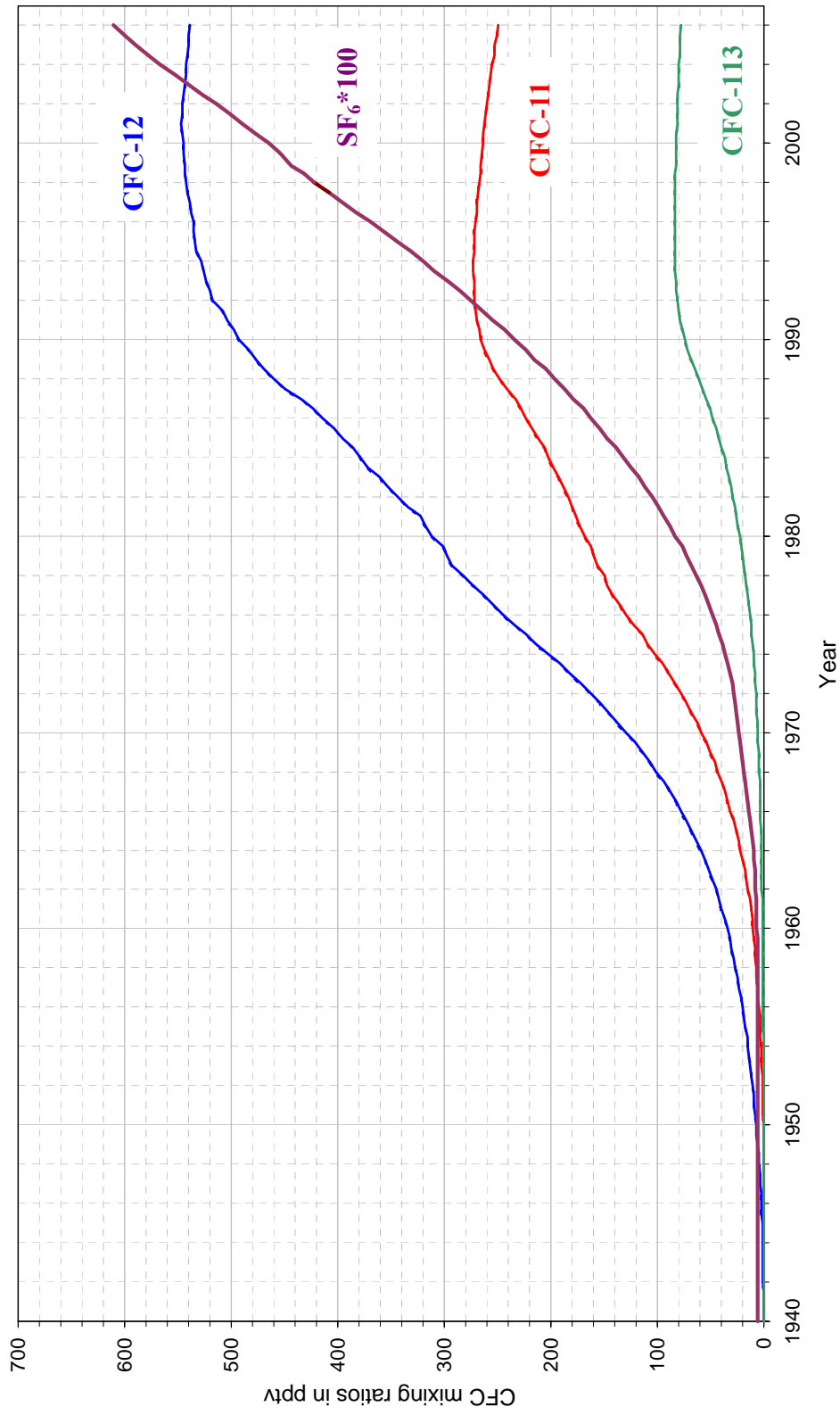


Figure 5.8 Atmospheric mixing ratios of CFC-11, CFC-12, CFC-113 and SF₆ based on measurements from Niwot Ridge, Colorado.

5.4.1 The CFC content variations in the study area

Samples collected from twenty-five different wells in three different seasons were analyzed for their CFC-11, CFC-12 and CFC-113 contents. All the samples were collected and analyzed in duplicate, and the results are presented in Table 5.3 as the average of these two consecutive measurements. According to these results, there are some minor differences in the CFC concentrations of the samples from the same wells in different seasons. As it is stated out before, there can be contamination during sampling or these differences can be attributed to the processes during the measurement of CFCs. The differences are noticeable for the samples collected in August 2006 and the rest of

Table 5.3 Results of CFC measurements done at L-DEO.

Sample name	Depth (m)	August 2006			November 2006			June 2007		
		AVERAGE CFC CONCENTRATION (pmol/l)								
		CFC-11	CFC-12	CFC-113	CFC-11	CFC-12	CFC-113	CFC-11	CFC-12	CFC-113
S-1	14.0	-	-	-	3.403	2.088	0.337	-	-	-
S-2	14.0	-	-	-	1.448	0.827	0.174	1.069	0.694	0.175
S-3	14.0	-	-	-	5.599	2.115	0.372	3.165	1.484	0.228
S-4	7.0	-	-	-	0.409	0.704	0.199	0.408	0.442	0.099
S-5	14.0	-	-	-	-	-	-	2.832	1.770	0.280
S-9	11.0	0.093	0.043	0.002	0.141	0.460	0.044	0.310	0.318	0.077
S-11	8.0	-	-	-	0.789	0.804	0.144	-	-	-
S-13	8.0	-	-	-	-	-	-	2.340	1.765	0.352
S-15	12.0	-	-	-	-	-	-	1.921	1.584	0.275
S-16	15.0	-	-	-	3.497	2.295	0.309	2.886	1.927	0.362
S-19	12.0	-	-	-	3.562	2.081	0.309	2.673	1.740	0.325
S-20	12.0	-	-	-	-	-	-	3.048	2.023	0.376
S-22A	17.0	-	-	-	-	-	-	2.467	1.843	0.333
S-23	12.0	-	-	-	-	-	-	2.980	2.005	0.380
S-24	12.0	-	-	-	-	-	-	2.186	1.532	0.256
D8	173.9	0.009	0.016	0.000	-	-	-	-	-	-
D-13	376.7	-	-	-	-	-	-	0.065	0.175	0.019
D-33	157.4	-	-	-	-	-	-	0.317	0.456	0.104
D-37	226.7	0.035	0.026	0.000	-	-	-	-	-	-
D-57A	309.7	0.012	0.035	0.085	-	-	-	0.049	0.103	0.000
M-60B	120.0	0.007	0.035	0.000	0.073	0.176	0.040	-	-	-
D-63A	205.0	0.070	0.025	0.001				0.487	0.559	0.117
D-63B	116.5	-	-	-	0.373	0.241	0.061	-	-	-
D-68R	73.0	0.005	0.018	0.018	0.272	0.195	0.054	0.483	0.231	0.045
SP-16	-	-	-	-	-	-	-	2.349	1.724	0.312

the samples: the results for the samples collected in August 2006 are lower than the rest of the results. This difference can be attributed to various mistakes. Therefore, this first set of measurements will not be used in the following calculations. Together with August 2006 samples, November 2006 measurement of S-3 should also be excluded because for that particular sample, the measured CFC-11 concentration exceeds the maximum amount of CFC-11 that can enter to the aquifer which should be around 4.5 pmol/l.

When the rest of the results presented in Table 5.3 are examined, it can be seen that the lowest CFC-11 concentration belongs to a sample from the deep aquifer system, D-57A; the highest CFC-11 concentration belongs to a sample from the shallow aquifer system, S-19 measured in November 2006. The lowest CFC-12 concentration belongs again to D-57A whereas the highest CFC-12 concentration belongs to D-16, again a sample from the shallow aquifer system. For CFC-113, the lowest concentration measured to be 0 again in D-57A and the highest concentration was measured in S-23.

The existence of the CFCs in deep groundwater system can be an indication of modern recharge to this system if and only if the CFCs entered to the system in the recharge area and traveled through preferential pathways through the deep system. Before deciding on the possibility of modern recharge to this system another possible reason for the presence of CFCs in the deeper parts should also be mentioned herein. The groundwater wells monitoring deeper systems in the study area were constructed using wet rotary drilling method which requires a fluid to be pumped down the hole. This drilling method has the disadvantage of contaminating the well with the introduced fluids (modern, CFC bearing fluids). Extensive well development is always necessary to overcome this problem. During the construction of these wells, essential well developments were carried out and the possibility of the contamination of the well with the modern, CFC bearing fluids has been prevented (personal communication with H. Yazıcıgil, 2008)

In Figure 5.9, the change of the concentrations in three different chlorofluorocarbons with respect to depth can be seen. This figure shows that for the shallow groundwater system, for which the sample depth can be taken as smaller than 50 m, the CFC-11 concentrations show a wide range between 3.5 pmol/l and 0.8 pmol/l. For the deep and

middle groundwater systems, for which the sample depth can be assumed to be greater than 50 m, all the CFC concentrations are smaller than 0.5 pmol/l.

5.4.2 The CFC ages in the shallow, middle and deep aquifer systems

Previously in Chapter 1, information about the groundwater age concept was given. It was stated by Plummer and Busenberg (2000) that groundwater age, determined by using the concentrations of CFCs in water, refers to the time elapsed since recharge and isolation of the newly recharged water from the soil atmosphere. The simplest and most common transport assumption in CFC-based dating is to assume piston flow. The interpreted recharge year assumes that the concentration of the CFC was not altered by

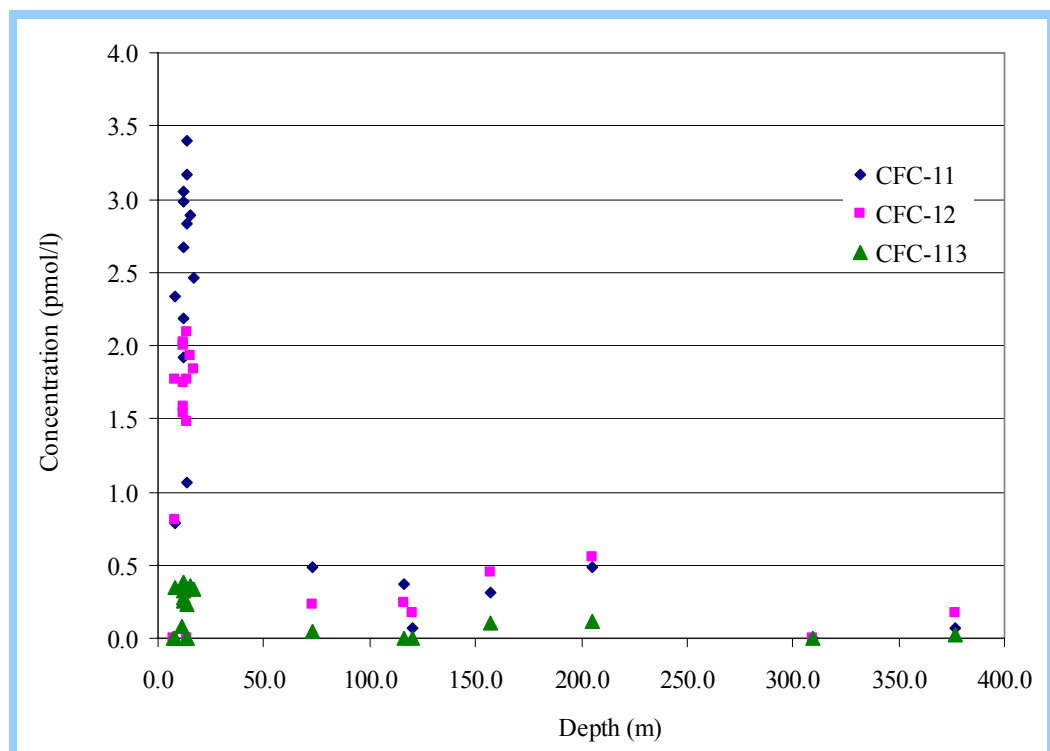


Figure 5.9 Concentration versus depth graph for CFC-11, CFC-12 and CFC-113 measured in the samples from the study area.

transport processes from the point of entry to the measurement point in the aquifer (Plummer and Busenberg, 2000). The CFC recharge years presented later in this section are based on the simplifying assumption of piston flow.

Groundwater dating with CFCs is based on Henry's law of solubility. Henry's law states that the concentration of the gas dissolved in water in equilibrium with air is proportional to the partial pressure, p_i , of the gas in air. The term p_i is defined by Warner and Weiss in 1985 given in Equation 5.5.

$$p_i = x_i(P - p_{H_2O}) \quad (5.5)$$

In this equation, x_i is the dry air mole fraction of the i^{th} CFC, P is the total atmospheric pressure and p_{H_2O} is the water vapor pressure. For ideal gases, the dry air mole fraction is replaced with the air mixing ratio, volume per volume. Henry's law then gives the CFC solubility in water, C_i with Equation 5.6.

$$C_i = K_H p_i \quad (5.6)$$

In Equation 5.6, K_H is the Henry's law constant for the i^{th} CFC. K_H has been measured in pure water and seawater for CFC-11 and CFC-12 (Warner and Weiss, 1985) and for CFC-113 (Bu and Warner, 1995) K_H can be calculated by using Equation 5.7.

$$\ln K_H = a_1 + a_2\left(\frac{100}{T}\right) + a_3 \ln\left(\frac{T}{100}\right) + S \left[b_1 + b_2\left(\frac{T}{100}\right) + b_3\left(\frac{T}{100}\right)^2 \right] \quad (5.7)$$

The constants, a_1 , a_2 , a_3 , b_1 , b_2 , and b_3 , used in the calculation of K_H are given in Table 5.4. The values given are the least square parameters to the temperature (Kelvin) and salinity (parts per thousand, ‰) dependence of K_H for concentrations in mol kg⁻¹ atm⁻¹ and mol L⁻¹ atm⁻¹, valid for temperatures of 273- 313 Kelvin (0- 40°C) and salinities of 0-40‰.

During the calculation of the CFC age of a sample, first the measured concentration is converted to a dry air atmospheric mixing ratio, x_i . This calculation requires the Henry's

Table 5.4 Constants for calculation of K_H (Warner and Weiss, 1985; Bu and Warner, 1995).

CFC	a_1	a_2	a_3	b_1	b_2	b_3
Solubilities in mol kg ⁻¹ atm ⁻¹						
CFC-11	-136.269	206.115	57.2805	-0.1486	0.095114	-0.01634
CFC-12	-124.44	185.4299	51.6383	-0.14978	0.094668	-0.016
CFC-113	-136.129	206.475	55.8957	-0.02754	0.006033	---
Solubilities in mol L ⁻¹ atm ⁻¹						
CFC-11	-134.154	203.2156	56.232	-0.14445	0.092952	-0.016
CFC-12	-122.325	182.5306	50.5898	-0.14563	0.092509	-0.01566
CFC-113	-134.243	203.898	54.9583	-0.02632	0.005874	---

law constant to be calculated at the recharge temperature, the calculation of which was shown in the previous section. The Henry's law constant is also a function of salinity, but most shallow groundwater of interest in dating with CFCs is too dilute to require corrections for salinity. Salinity corrections will be necessary for all studies involving seawater, estuaries, and saline lakes and trona waters. Therefore, in this study the deeper wells and the shallow wells (S-4 and S-9) with high electrical conductivity values also require salinity correction. The effects of salinity in the CFC ages will be examined in the proceeding section.

The recharge elevation is also needed to estimate the total atmospheric pressure, P , during recharge. These elevations were calculated by using the relationship of $\delta^{18}\text{O}$ and elevation. For recharge elevations less than 3000 m, the relation, $\ln P = -H/8300$ (List, 1949), can be used, where H is the recharge elevation in meters. It should also be considered that recharge occurs in a moist unsaturated zone; relative humidity is near 100%. The vapor pressure of water, p_{H_2O} , is subtracted from the total pressure solve for the dry air mixing ratio of the CFC. The vapor pressure of water can be calculated by using Equation 5.8 (Weiss and Price, 1980).

$$\ln p_{H_2O} = 24.4543 + 67.4509\left(\frac{100}{T}\right) - 4.8489\ln\left(\frac{T}{100}\right) + 0.000544S \quad (5.8)$$

The dry air mixing ratio for the particular CFC, x_i , is then compared to the appropriate historical atmospheric mixing ratio given in Figure 5.8 to determine recharge date. The average CFC recharge years obtained from the CFCs were calculated by following the above calculations and presented in Table 5.5. The same table also shows the recharge temperatures, obtained from the noble gas measurements, and the recharge elevations, obtained from the oxygen-18 data, both of which were used during the calculations.

Table 5.5 The average CFC-11, CFC-12 and CFC-113 recharge years and the recharge temperatures and the recharge elevations used in the calculations together with the dissolved oxygen amounts obtained during field sampling.

Sample name	Date			November 2006			June 2007		
	Rech. Temp. (°C)	Rech. Elev. (m)	DO (mg/l)	AVERAGE CFC RECHARGE YEAR					
				CFC-11 Age	CFC-12 Age	CFC-113 Age	CFC-11 Age	CFC-12 Age	CFC-113 Age
S-1	12.00	1111.1	5.00	1981.5	1986.5	1987.5	-	-	-
S-2	12.00	1156.6	2.00	1971.5	1972.5	1982.5	1969.5	1971.5	1982.5
S-3	12.00	1079.9	3.00	CONTAMINATION			1979.5	1979.5	1984.5
S-4	12.00	1156.6	0.70	1963.5	1970.5	1983.5	1963.5	1967.5	1978.5
S-5	12.00	1105.4	10.00	-	-	-	1977.5	1984.5	1986.5
S-9	10.00	1338.4	0.10	1957.5	1966.5	1972.5	1961.5	1964.5	1976.5
S-11	12.00	1146.5	0.40	1967.5	1972.5	1980.5	-	-	-
S-13	12.00	1102.1	-	-	-	-	1975.5	1983.5	1988.5
S-15	12.00	1127.1	4.00	-	-	-	1973.5	1980.5	1986.5
S-16	12.00	1152.1	5.50	1981.5	1988.5	1986.5	1978.5	1985.5	1988.5
S-19	12.00	1111.1	5.00	1982.5	1986.5	1986.5	1977.5	1983.5	1987.5
S-20	12.00	1111.1	5.00	-	-	-	1978.5	1986.5	1988.5
S-22A	12.00	1156.6	5.00	-	-	-	1976.5	1985.5	1988.5
S-23	12.00	1156.6	5.00	-	-	-	1978.5	1987.5	1989.5
S-24	12.00	1156.6	2.00	-	-	-	1974.5	1980.5	1985.5
D-13	8.00	1400.0	0.00	-	-	-	1953.5	1959.5	1968.5
D-33	8.00	1400.0	0.00	-	-	-	1961.5	1966.5	1977.5
D-57A	8.00	1400.0	0.00	-	-	-	1953	1956.5	1960.5
M-60B	8.00	1400.0	0.00	1954.5	1959.5	1971.5	-	-	-
D-63A	8.00	1400.0	0.05	-	-	-	1963.5	1968.5	1978.5
D-63B	8.00	1400.0	0.00	1962.5	1961.5	1973.5	-	-	-
D-68R	8.00	1400.0	0.00	1960.5	1959.5	1972.5	1963.5	1961.5	1972.5
SP-16	12.00	1179.0	6.00	-	-	-	1975.5	1983.5	1987.5

According to Table 5.5, there are some differences between the CFC recharge years calculated by using the CFC-11, CFC-12 and CFC-113 concentrations. The most prominent difference is, although the CFC-11 and CFC-12 recharge years are more or less close to each other, the CFC-113 recharge ages are younger than the rest. There are some processes that can affect the measured CFC concentrations in a sample and these processes should be investigated before assigning a recharge year to a sample.

5.4.2.1 Processes affecting the CFC ages

As stated before, there are several physical and chemical processes affecting the concentrations of CFCs in the aquifer that should be considered while calculating a recharge year based on CFC concentrations. Table 5.6 summarizes the most important of those processes their affect on the calculated recharge year and their relative importance. All of these processes should be considered while evaluating the CFC age data given in Table 5.5.

According to Table 5.6, over-estimation of the recharge temperature results in the CFC ages that are too young and under- estimation gives ages that are biased old. The CFC ages are extremely sensitive to uncertainties in recharge temperature especially for water recharged after 1990s (Busenberg et al., 1993). In this study, the recharge temperatures used during calculations should not affect the calculated CFC-ages for the samples from the middle and deep aquifer systems as these samples had CFC ages greater than 1970, and for those samples a ± 2 °C difference of the recharge temperature should affect the ages by ± 1 year or even less. For the rest of the samples collected from the shallow groundwater system, there should not be any inaccuracy in the recharge temperatures as they reflect the mean annual air temperature in the study area. A sensitivity analyses will be presented later to further show the affect of the recharge temperatures on the CFC ages.

Another important parameter considered in the calculations is the recharge elevation because gas solubilities are a function of total pressure. If the pressure is overestimated, this means underestimation of the recharge elevation, the interpreted CFC age will be biased old. Uncertainty in recharge elevation does not introduce significant errors in CFC

Table 5.6 Summary of processes that can modify apparent age (Modified from Plummer and Busenberg, 2000)

Property	Environment Most Affected	Description of Process	Effect on the calculated CFC Age
Recharge temperature	Shallow water table	Over-estimated.....	Too young
		Under-estimated.....	Too old
		$\pm 2^{\circ}\text{C}$, $\leq 1970 \pm 1$ year or less	
		$\pm 2^{\circ}\text{C}$, 1970-1990, $\pm 1-3$ years	
	$\pm 2^{\circ}\text{C}$, >1990, >3 years		
Excess air	Rapid, focused recharge; fractured rock.	Addition of air trapped and dissolved during recharge.	Too young Significant for post-1990 recharge.
Recharge elevation	Mountain recharge	Water recharged at high altitude dissolves less CFCs because of lower barometric pressure.	
		Over-estimated.....	Too young
		Under-estimated.....	Too old
		± 100 m not important	Significant for post-1990 recharge
± 1000 m, < 1987, \pm few years			
Thickness of unsaturated zone	Unsaturated	Air in deep unsaturated zone is older than that of the modern troposphere.	Too old
	zone >10 m	0-10 m, error < 2 years	
		30 m, error 8 - 12 years.	
Urban air	urban areas	CFC mixing ratios in urban and industrialised areas can exceed regional values.	Too young
CFC contamination	Urban and industrial areas, sewage effluent	CFCs added to water from local anthropogenic sources, in addition to that of air-water equilibrium.	Impossibly young
Microbial degradation	Anaerobic environments, sulphate-reducing, methanogenic Fluvial and glacial drift sediment	No degradation in aerobic environments.....	No effect
		Sulphate-reducing, and fermentation: CFC-11, CFC-113 degraded, CFC-12 quasi-stable..	CFC-11, CFC-113 Too old
		Methanogenic: CFC-11 \geq CFC-113 >> CFC-12	Too old
Sorpton	Organic-rich sediment, peat	Sorption of CFCs onto particulate organic carbon and mineral surfaces.	Too old
		CFC-113 >> CFC-11 \geq CFC-12	
Mixed waters	Production wells, fractured rock	Apparent age of young fraction in mixture.....	Too old
		Apparent age of old fraction in mixture.....	Too young
Hydrodynamic dispersion	All groundwater environments	1975 - 1993.....	Too old
		<1975.....	Too young

dating in areas of low relief where elevation of recharge is within a few hundred meters (Busenberg et al., 1993). In fact this is the case in the study area. If the error in the calculated recharge elevations is assumed to be ± 100 m, this error will not have an important affect on the calculated CFC ages.

Excess air, as explained before, is the air trapped and dissolved in groundwater during recharge under increased hydrostatic pressure at the capillary fringe. Introduction of excess air adds CFCs to groundwater, causing ages calculated too young. The effect is significant for post-1990 groundwater (Busenberg and Plummer, 1992). According to Table 5.5 there isn't any post-1990 water therefore these effects can be ignored.

CFC contamination is another property that can affect the calculated CFC ages. CFC contaminated water has CFC concentrations that are greater than that possible for equilibrium with tropospheric air, usually for groundwater from urban and industrial areas. The addition of contaminant concentrations of CFCs to groundwater can usually be attributed to anthropogenic point sources such as discharge from septic tanks, leakage from underground storage tanks and recharge from rivers carrying effluent from sewage treatment plants (Schultz et al., 1976; Busenberg and Plummer, 1992). When the study area is considered, there is no evidence of CFC contamination as there aren't any anthropogenic point sources available in the area.

The possibility of microbial degradation of CFCs in certain environments should also be considered in assigning a recharge date to a groundwater sample. There is no evidence for aerobic degradation of CFCs in groundwater (Dunkle et al, 1993; Katz et al., 1995; Szabo et al., 1996, Plummer et al., 1998b); however, CFCs can all be degraded under anaerobic conditions (Lovley and Woodward, 1992; Denovan and Strand, 1992; Lesage et al, 1992, Oster et al., 1996, Shapiro et al., 1997). CFC degradation can also occur in sulphate reducing conditions. In fact, Katz et al. (1995) found CFC-11 ages being 6- 12 years older than those based on CFC-12 in groundwater undergoing sulphate reduction and methanogenesis. Oster et al. (1996) observed degradation of CFC-11 and CFC-12 in various anoxic environments, with rate of CFC-11 degradation approximately 10-fold that of CFC-12. In such a situation, the calculated CFC-11 ages should be greater than that of CFC-12 ages. According to Cook and Solomon (1997), the dissolved oxygen

amount in the water should be smaller than 0.5 mg/l in order to observe the degradation of CFC-11. When the dissolved oxygen amounts presented in Table 5.4 are considered, for most of the shallow groundwater samples, DO exceeds 0.5 mg/l except for S-9 and S-11 measured as 0.1 and 0.4 mg/l respectively. For the samples from middle and deep groundwater systems DO amount is 0 mg/l. Therefore, the possibility of microbial degradation can be considered for S-9, S-11, D-13, D-33, D-57A, M-60B, D-63A, D-63B and D-68R. The CFC concentrations measured in the samples from the middle and deep groundwater systems are very close to the detection limits therefore it is not correct to reach conclusions about the degradation. However, for D-9 and for D-11, the calculated CFC-11 ages are 3 and 5 years older than the CFC-12 ages respectively. These differences can be due to the microbial degradation.

One other process that can remove CFCs from groundwater like microbial degradation is the sorption. This process causes the CFC ages to be older than they should be. Russel and Thompson in 1983 showed that CFC-11 and CFC-12 sorb to dry soils, and are released when soils wetted. Cook et al. (1995) observed retardation of CFC-113 relative to CFC-12 and ^3H at the Sturgeon Falls site, Canada. It is stated out by Plummer and Busenberg (2000) that in most groundwater environments sorption seem to be important for CFC-113 rather than CFC-11 and CFC-12. When the CFC-113 ages presented in Table 5.5 are compared to the CFC-11 and CFC-12 ages, it is obvious that the CFC-113 ages are younger than the others therefore the sorption of CFC-113 is impossible and there should be another reason for these younger CFC-113 ages.

In addition to the previously mentioned processes, there can be mixing of different aged groundwaters in the well bore producing mixed ages. When considering different waters mixing, each end-member water samples should have a unique and definable age to solve for mixing fractions and ages of end-member waters. If two young waters mix, it is possible to solve the mixing problem with measurement of CFC-11, CFC-12 and CFC-113. The problem can also easily be solved for binary mixtures of young and old waters. If the old fraction is CFC-free, and no other processes affect CFC concentrations other than air-water equilibrium, the CFC-11/CFC-12 ratio will define the age of the young fraction if recharged between the late 1940s and about 1977. Similarly, the CFC-113/CFC-12 ratio will define the age of the young fraction if recharged in the 1980s.

Dating binary mixtures of young and old water requires utilization of the $^3\text{H}/^3\text{He}$ method to determine the age of the young fraction. Unfortunately, due to the reason that the tritium data is missing in this study, it will not be applicable to carry out calculations regarding mixing.

Last but not least, hydrodynamic dispersion can also affect the calculated CFC ages. Plummer et al. (1993) simulated the transport and resulting age uncertainties for CFC-11 and CFC-12 for water recharged from 1940 through 1991. The calculations with CFC-11 and CFC-12 indicate that, if hydrodynamic dispersion were significant, waters recharged since 1975 appeared older than the advective age whereas water recharged prior to 1970 appeared to be slightly younger than the advective age. The same study showed that a dispersivity of 0.1 metres had no effect on CFC-11 and CFC-12 concentrations over the dating range of the tracers however a dispersivity of 1 m affected the CFC-11 age of the water recharged in 1960 by as much as 5 years whereas this value was 3 years for CFC-12 age of the same water.

5.4.2.2 Sensitivity analyses of the CFC ages in the study area

In order to determine the sensitivity of the calculated CFC ages to the salinity of given water, the recharge elevations and the recharge temperatures sensitivity analyses have been carried out in three selected samples. These samples are S-23 and S-4 from the shallow groundwater system and D-57A from the deep aquifer system. The salinities of the selected samples were calculated by using the relationship between the specific electrical conductance (the electrical conductivity measured at 25 °C) and the salinity. Unfortunately, in this study the electrical conductivities (EC) were measured in the field without considering the temperature of the sample so the specific electrical conductance values are not available. However to roughly calculate the salinities the EC values presented in Table 3.2 were assumed to be equal to the specific electrical conductance values to be used in Equation 5.9 suggested by USGS (Hydrolab, 1994).

$$S = 5.995 * 10^{-8} C^4 - 2.31 * 10^{-5} C^3 + 3.43 * 10^{-3} C^2 + 0.5353 C^{-1} - 0.0155 \quad (5.9)$$

In the Equation 5.9, S is the salinity in ppt (parts per trillion), C is the specific electrical conductance in milliSiemens/cm. Accordingly, the calculated salinities are smaller than 0.5 ppt for all the shallow wells except for S-4 and S-9. The salinity of S-4 is calculated to be around 7.5 ppt and the salinity of S-9 is 0.9 ppt. For the deeper wells the salinities for D-8, D-33 and D-57 came out to be 2.2 ppt, 2.8 ppt and 5.6 ppt respectively.

In Table 5.7, the sensitivity of the CFC recharge years for wells S-23, S-9 and D-57A to the recharge temperature, recharge elevation and the salinity can be seen. The calculations showed that for S-23, the calculated CFC recharge years are rather sensitive to overestimation of the recharge temperature by 2 °C as the CFC-11, CFC-12 and CFC-113 recharge years came out to be 3 years younger. The underestimation of the recharge temperature influenced the CFC-11 and CFC-113 recharge years similarly, the calculated years appeared to be 1 year older, for CFC-12 recharge year was clarified to be 2 years older. The estimation of the recharge elevation ± 100 m didn't influence the CFC recharge years at all.

When S-4 is considered, the over-estimation of the recharge temperatures had the same influence on CFC-11, CFC-12 and CFC-113 recharge years since the three ages came out to be 1 years younger. The under-estimation of the recharge temperature didn't change the CFC-11 recharge year but the CFC-12 and CFC-113 recharge years became 1-year older (Table 5.7). ± 100 m change in the recharge elevation didn't influence the CFC ages. For this well the salinity is quite high therefore the effect of the salinity was also investigated. For a salinity value of 7.5 ppt CFC-11, CFC-12 and CFC-113 recharge years were calculated to be 1 year younger proving that totally ignoring the salinity effect for the rest of the shallow wells will not lead to wrong CFC recharge years.

Lastly, a sample from the deep groundwater system is considered for the sensitivity of the CFC recharge years to three parameters. For this well, the over-estimation of the recharge temperature by 2°C didn't change the CFC-11 and CFC-113 recharge years but the CFC-12 recharge year was appeared to be 1 year younger. The under-estimation of the recharge temperature only affected CFC-11 recharge year, it was calculated to be 1 year older (Table 5.7).

Table 5.7 The CFC-11, CFC-12 and CFC-113 age sensitivity analyses for wells S-23, S-4 and D-57A.

Parameter Analysed for S-23	Error	CFC-11 Recharge Year	CFC-12 Recharge Year	CFC-113 Recharge Year
Recharge Temperature	+2°C	1981.5	1991.5	1992.5
	-2°C	1977.5	1985.5	1988.5
Recharge Elevation	+100 m	1978.5	1987.5	1989.5
	-100 m	1978.5	1987.5	1989.5
Parameter Analysed for S-4				
Recharge Temperature	+2°C	1964.5	1968.5	1979.5
	-2°C	1963.5	1966.5	1977.5
Recharge Elevation	+100 m	1963.5	1967.5	1978.5
	-100 m	1963.5	1967.5	1978.5
Salinity	0 ppt	1963.5	1967.5	1978.5
	5 ppt	1963.5	1967.5	1978.5
	7.5 ppt	1964.5	1968.5	1979.5
	10 ppt	1964.5	1968.5	1979.5
Parameter Analysed for D-57A				
Recharge Temperature	+2°C	1953.5	1957.5	1960.5
	-2°C	1952.5	1956.5	1960.5
Recharge Elevation	+100 m	1953.5	1956.5	1960.5
	-100 m	1953.5	1956.5	1960.5
	+200 m	1953.5	1956.5	1960.5
	+300 m	1953.5	1956.5	1960.5
	+400 m	1953.5	1956.5	1960.5
Salinity	0 ppt	1953.5	1956.5	1960.5
	5.6 ppt	1953.5	1957.5	1960.5

The uncertainty during the determination of the correct recharge elevations in the deeper wells was inevitable therefore the sensitivity of the CFC recharge years to a wide range of recharge elevations were investigated in well D-57A and it has been seen that the over-estimation of the recharge elevation even around 400 m did not have any influence on the calculated recharge elevations. For the deeper wells, the effect of the salinity was also taken into consideration and it was seen that the salinity, being around 5.6 ppt, only changed the CFC-12 recharge year by a year (Table 5.7).

5.4.2.3 The estimated CFC ages in the study area

In the groundwaters collected from the shallow, middle and deep aquifer systems it is very difficult to correctly identify the exact processes affecting the calculated CFC ages. In general, the inconsistency between the CFC-11, CFC-12 and CFC-113 ages indicates involvement of different processes. Unfortunately, there is no information both about the presence of the organic carbon in the alluvium sediments and yet any other adsorption surface available in the sediments allowing the sorption of these chemical substances by the sediments of the shallow system. At ordinary temperatures it is known that CFC-11 and CFC-12 are gases however CFC-113 is a liquid. Therefore, CFC-11 and CFC-12 is volatile during sampling, although CFC-113 is in liquid. This difference in their behavior at different temperatures can also lead to escape of CFC-11 and CFC-12 during sampling although sampling was carried out with special attention. For most of the samples, the difference between the CFC-11 and CFC-12 ages is greater than the difference between CFC- 113 ages. Even though there are differences in the recharge years obtained from different CFCs it is convenient to assign an average year to each sample by using two different CFCs giving similar recharge years. Herein, the purpose for using CFCs are only to obtain an estimation of a recharge year and the recharge years presented in Table 5.8 is prepared to simplify the situation complicated by these different CFC ages, these recharge years will be used to draw some conclusions. In this table, the CFCs used in the calculation of the average recharge year is also given.

According to Table 5.8, the CFC ages are greater for the deep and middle aquifer systems when compared to shallow groundwater system. Although it is possible to assign an average age to the samples of the middle and deep groundwater systems these ages can be deceptive because of the reason that the CFC concentrations measured in that samples are very close to the detection limits. For the shallow groundwater system to observe the areal distribution of the CFC ages and to compare their pattern with the groundwater flow directions a CFC age contour map is created. According to this map, presented in Figure 5.10, the CFC ages increase in the flow direction towards southeast of the study area. Generally, it is expected to observe an increase in the groundwater residence times along flow direction. There are two particular points breaking the general behaviour of

Table 5.8 The final recharge years assigned to each sample together with the CFCs used in the calculation of these years.

Sample name	Groundwater System	Recharge Year	CFCs used in the calculation
S-1	Shallow	1987	CFC-12 and CFC-113
S-2	Shallow	1970	CFC-11 and CFC-12
S-3	Shallow	1979.5	CFC-11 and CFC-12
S-4	Shallow	1965	CFC-11 and CFC-12
S-5	Shallow	1983	CFC-11, CFC-12 and CFC-113
S-9	Shallow	1963	CFC-11 and CFC-12
S-11	Shallow	1970	CFC-11 and CFC-12
S-13	Shallow	1985	CFC-12 and CFC-113
S-15	Shallow	1980	CFC-11, CFC-12 and CFC-113
S-16	Shallow	1985.5	CFC-11, CFC-12 and CFC-113
S-19	Shallow	1986.5	CFC-12 and CFC-113
S-20	Shallow	1987	CFC-12 and CFC-113
S-22A	Shallow	1987	CFC-12 and CFC-113
S-23	Shallow	1988	CFC-12 and CFC-113
S-24	Shallow	1983	CFC-12 and CFC-113
D-13	Deep	> 1953	CFC-11 and CFC-12
D-33	Deep	1963	CFC-11 and CFC-12
D-57A	Deep	> 1953	CFC-11 and CFC-12
M-60B	Middle	1960	CFC-12
D-63A	Deep	1965.5	CFC-11 and CFC-12
D-63B	Deep	1962	CFC-11 and CFC-12
D-68R	Deep	1960	CFC-11 and CFC-12
SP-16	Spring	1985	CFC-11 and CFC-12

the CFC ages along the flow direction. These points are S-2 and S-5 (Figure 5.10). In S-2, the calculated CFC age is older than it should be according to the general trend whereas in S-5, the calculated age is younger than it should be. In S-2, there can well be a line source- causing mixing of older groundwater with younger, thus affecting the CFC age. In the following sections this issue will be clarified. For S-5, since there is only one measurement available it is very hard to truly rely on the calculated age. Therefore this younger age can be attributed to many reasons. It should also be noted that for the wells

S-4 and S-9, the calculated CFC ages are close to the ones calculated for the deep aquifer system. This similarity can well be another indication of the seepage of the deeper groundwater into the shallow system as suggested by SRK (2004).

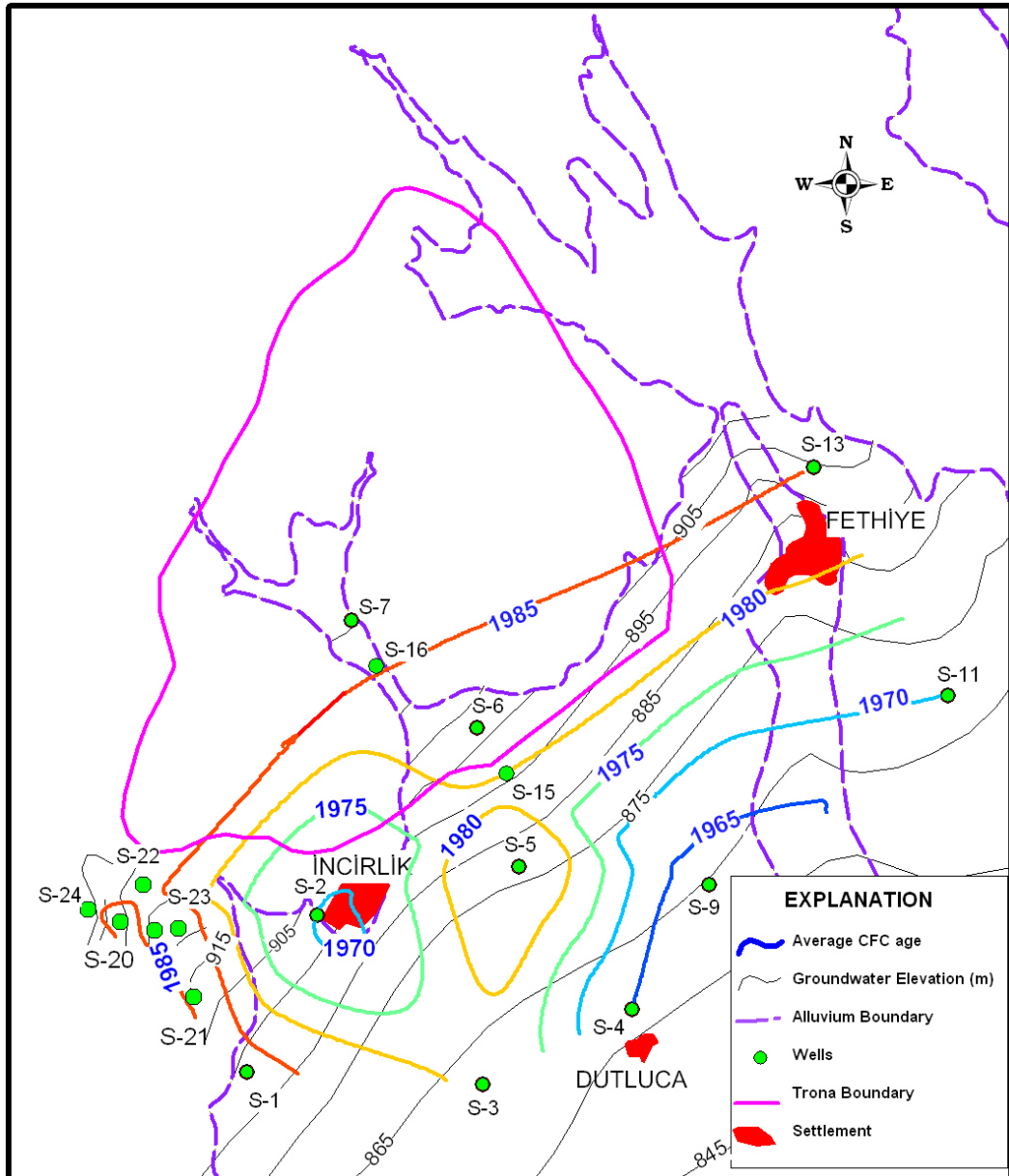


Figure 5.10 The CFC age contour map for the shallow aquifer system.

5.5 Calculation of Groundwater Ages with Radiocarbon

By using the measured CFC concentrations, the average residence times of the groundwater in shallow groundwater system was approximated. However, the measured CFC concentrations were very near to the detection limits therefore exact dating was impossible for the deeper groundwater. In order to have information about the groundwater ages in the middle and deep groundwater systems, another standard method of determining ages up to 40,000 years before present was utilized. This method requires measuring carbon-13 and carbon-14 of DIC in the groundwater. Thus, measurements were carried out for totally 12 different samples.

It has been stated in Chapter 2 that radioactive isotope of carbon, ^{14}C , is extensively used in dating of dissolved inorganic carbon (DIC) in groundwater ($\text{DIC} = \text{CO}_{2(\text{aq})} + \text{HCO}_3^- + \text{CO}_3^{2-}$) as the atmospheric ^{14}C dissolved in the precipitation reaches the groundwater table and starts decaying to nitrogen in the groundwater system. Its relatively long half-life of 5730 years allows dating of ages up to 40,000 years. As stated by Kalin (2000), the geochemistry of carbon in groundwater systems include interaction with the atmosphere, biosphere and geosphere resulting in multi sources and sinks of carbon that varies in time and space. ^{14}C is produced naturally in the atmosphere by interactions of nitrogen and cosmic rays that bombard the Earth constantly. These rays strike the Earth's upper atmosphere producing thermal neutrons as they interact with atoms and molecules. These thermal neutrons react to form ^{14}C in the upper atmosphere by the reaction given in Equation 5.10 (Kalin, 2000). The ^{14}C is quickly oxidized to CO_2 and mixes into the lower atmosphere where it is assimilated in the biosphere and hydrosphere.



5.5.1 Natural and Anthropogenic Variations in Atmospheric ^{14}C

There are natural variations in atmospheric ^{14}C because the neutron flux from cosmic radiation has not been constant. According to the dendrochronology studies, there have been strong variations in the ^{14}C activity of atmospheric CO_2 during the Holocene (Clark and Fritz, 1979). There are short- term cycles (11-year) related to variation in solar

output. These 11-year cycles are weak when compared to the long-term evolution in atmospheric ^{14}C due to the changing structure of the Earth's geomagnetic field (Damon et al., 1989) protecting the Earth from the incoming flux of charged particles. This field is internally generated by the dynamo of the rotating/ convecting Fe-Ni liquid outer core. As stated by Clark and Fritz (1997), these variations affect the initial radiocarbon activity, in turn, affecting the calculated ^{14}C ages.

In addition to these natural variations, there are also antropogenic effects on atmospheric ^{14}C over the past century. The combustion of fossil fuel diluted ^{14}C by 25% whereas; atmospheric weapons testing and nuclear power plants have been releasing additional radiocarbon to the atmosphere and biosphere since 1950s. The high neutron flux generated by thermonuclear bomb testing activated ^{14}N to produce ^{14}C (Clark and Fritz, 1997).

5.5.2 The ^{14}C pathway to groundwater

The modern activity of ^{14}C is 13.56 decays-per-minute per gram of carbon. The starting point or “zero year” for this activity is 1950 AD. This value is considered to have an activity of 100 Percent Modern Carbon (pmc) without considering the natural and antropogenic impacts on atmospheric ^{14}C explained above. Samples which have an activity greater than 100 pmc should be younger than 1950 AD whereas; all samples having an activity lower than 100 pmc are pre-1950AD. Although the modern activity of ^{14}C is assumed to be 100 pmC, evidence suggests that it can be above 100 pmC, up to 140 pmC, due to the antropogenic effects (Clark and Fritz, 1997).

Clark and Fritz (1997) stated that rainwater contains some $^{14}\text{CO}_2$ from the atmosphere however the radiocarbon signal of groundwater is given by soil zone Atmospheric ^{14}C is included into vegetation by photosynthesis and released in the soil by decay and root respiration as given in Figure 5.11. There are four dominant pathways followed by radiocarbon entering the hydrologic cycle (Kalin, 2000). First of all, formation and dissociation of carbonic acid (H_2CO_3) during gas exchange between CO_2 in surface water and groundwater with atmospheric CO_2 . Secondly, the biologic activity of plants can

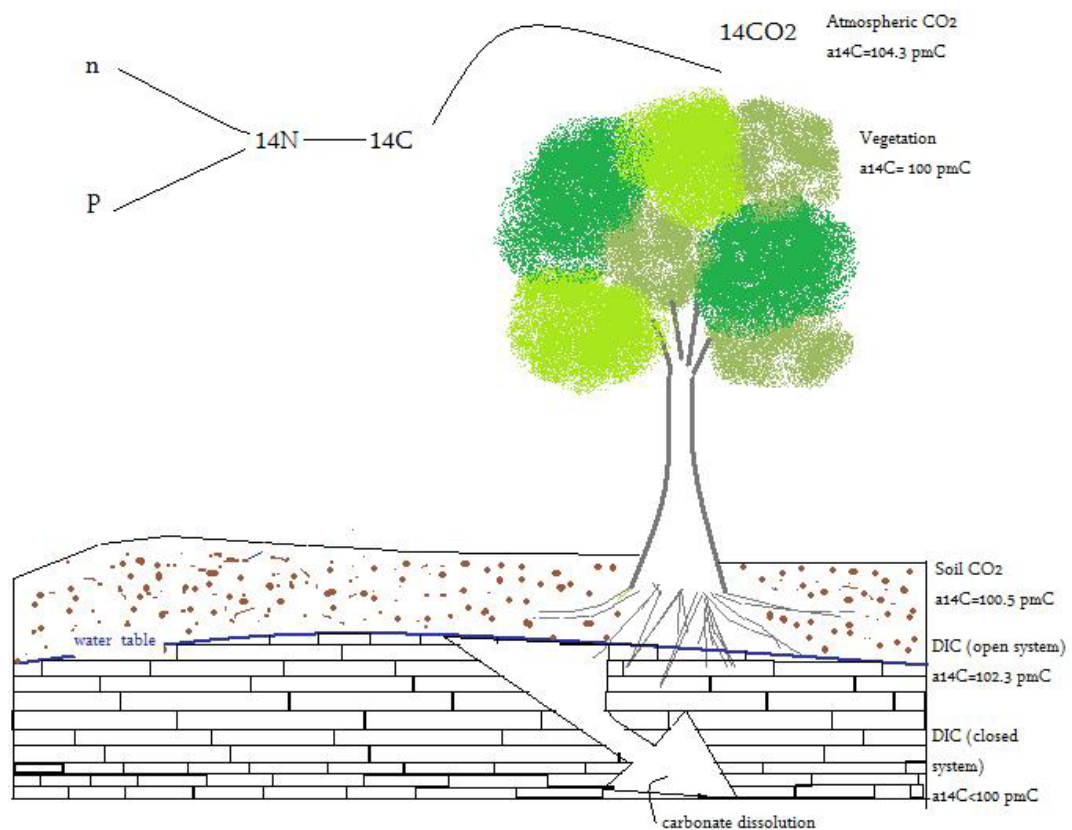


Figure 5.11 The pathway and associated fractionation of ^{14}C in CO_2 during photosynthesis, respiration in soils and dissolution by groundwaters (Modified from Clark and Fritz, 1997).

result in respired CO_2 in the soil zone dissolving in water. Thirdly, microbial utilization of organic material in soil and finally dissolution of mineral phases containing geologically young carbon can also dissolve CO_2 (Kalin, 2000).

5.5.3 Groundwater dating by carbon-14

Radiocarbon dating of groundwater is based on measuring the loss of the parent radionuclide, ^{14}C and depends on knowing the initial activity, A_0 (Clark and Fritz, 1997). The radiocarbon age of any water can be calculated by using Equation 5.11.

$$A = A_0 e^{-\lambda t} \quad (5.11)$$

In the above equation, A is the observed or measured activity of the sample, λ is the decay constant and t is time since recharge. This equation requires two key features to be known correctly. Firstly, the initial activity, A_0 , to the water to be dated should be assigned correctly. However, assigning a correct value to the initial activity is very hard as there are various processes that can modify ^{14}C signature of the penetrating precipitation. Secondly, the final concentration of ^{14}C in the groundwater, A , should have only been affected by radioactive decay although it can also be modified by isotopic exchange from recrystallisation and precipitation reactions. Equation 5.11 becomes Equation 5.12 for ^{14}C with a half-life of 5730 years.

$$t = -8267 * \ln \left(\frac{a_t^{14}\text{C}}{a_0^{14}\text{C}} \right) \quad (5.12)$$

This relationship indicates that after one half-life (5730 years) $a_t^{14}\text{C}$ is half of $a_0^{14}\text{C}$ just like it is given in Figure 5.12 prepared by using Equation 5.12. According to Figure 5.12 for a sample, if the $a_0^{14}\text{C}$ is 100 pmc, the time required to measure $a_t^{14}\text{C}$ as 40 pmc is approximately 7575 years by simple decay of ^{14}C . Whenever $a_0^{14}\text{C}$ is known and only closed system decay occurs, dating with ^{14}C is a simple calculation. However, this is rarely the case. Actually dilution and loss of ^{14}C by geochemical reactions are common which will be explained later in this chapter.

The results of the radiocarbon data are presented in Table 5.9. Radiocarbon activities presented in this table are close to the detection limits and the enrichment in $\delta^{13}\text{C}$ implies isotope exchange between groundwater and the aquifer matrix. There is a linear relationship between the logarithm of the measured ^{14}C activity presented in Table 5.9 and the oxygen-18 values (Figure 5.13). For the samples collected from the springs and shallow aquifer, the radiocarbon activities are greater and these samples are enriched in oxygen-18 whereas the samples from the deeper wells have smaller radiocarbon activities together with depleted oxygen-18 values.

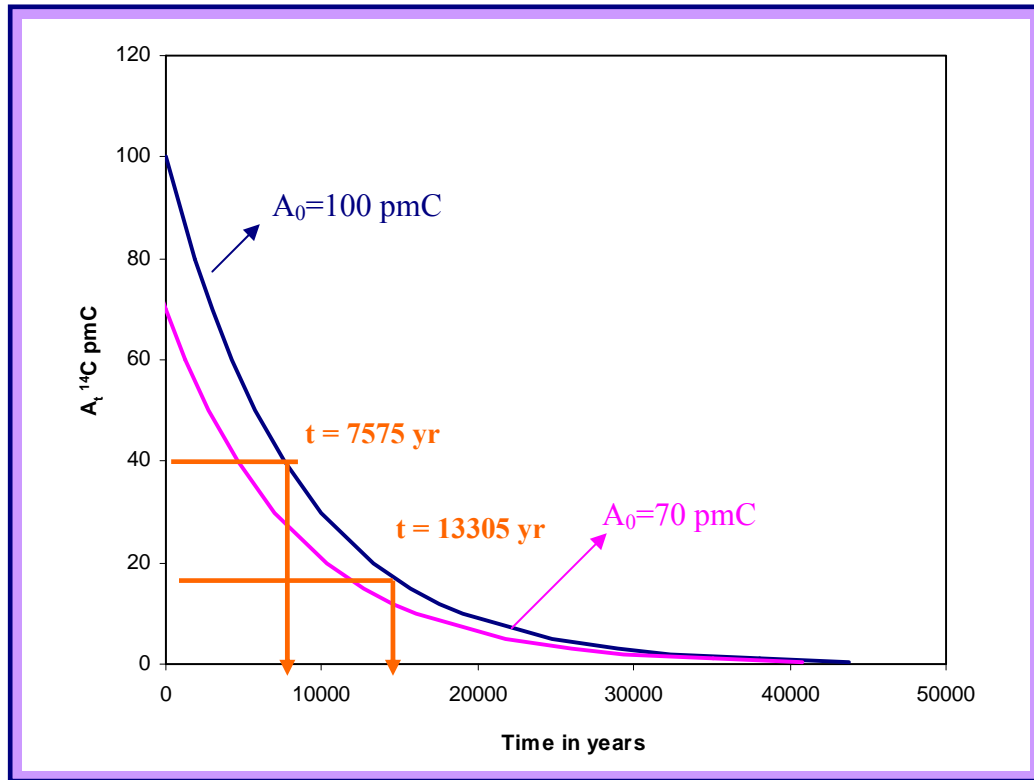


Figure 5.12 The decay of ^{14}C for two cases where $A_0 = 100$ pmc and $A_0 = 70$ pmc.

In Table 5.9, the error in the measurements, dissolved inorganic carbon and the ages calculated by assuming $a_0^{14}\text{C} = 100$ pmC and strictly closed system decay are also given. According to these unadjusted ages, two of the samples, D-47 and D-57A, exceed the limits of utilization of radiocarbon age dating. For the rest of the samples, the ages changes between 5,000 years and 51,000 years. These ages should be corrected along the flow path for geochemical reactions that involve carbon containing phases.

5.5.3.1. Geochemical reactions modifying carbon-14 activity

The most typical radiocarbon modifying reactions include the dissolution of carbonate minerals adding carbon without ^{14}C activity to the groundwater. This results in a lower $\delta^{13}\text{C}$ and DIC. Table 5.9 The radiocarbon, $\delta^{13}\text{C}$, DIC, alkalinity data and the unadjusted ^{14}C ages.

Sample name	$\delta^{13}\text{C}_{\text{DIC}}$ (‰)	ALKALINITY (meq/l)	^{14}C (pmC)	^{14}C Error (pmC)	Unadjusted ^{14}C Age	^{14}C Age Error	DIC (mmol/l)
M-60B	-6.64	9.71	0.387	0.02	44600	460	7.07
SP-7	-8.61	8.14	53.069	0.21	5090	30	7.75
S-9	-8.17	7.79	24.002	0.16	11450	55	16.39
S-4	-8.65	10.15	29.790	0.16	9730	45	9.07
D-68R	-6.33	7.81	0.796	0.03	38800	290	7.71
D-63A	-7.74	7.72	3.6988	0.05	26500	120	7.8
D-57A	3.52	108.76	0.0748	0.03	> 52000	-	95.72
D-47	2.76	115.53	0.1538	0.03	> 52000	-	69.5
D-37	-3	12.44	0.2918	0.03	46900	860	12.01
D-20	-7.01	8.18	27.814	0.14	10300	40	8.06
D-13	-2.3	13.49	0.4526	0.03	43400	530	12.51
D-8	2.28	42.60	0.1669	0.03	51400	1300	12.79

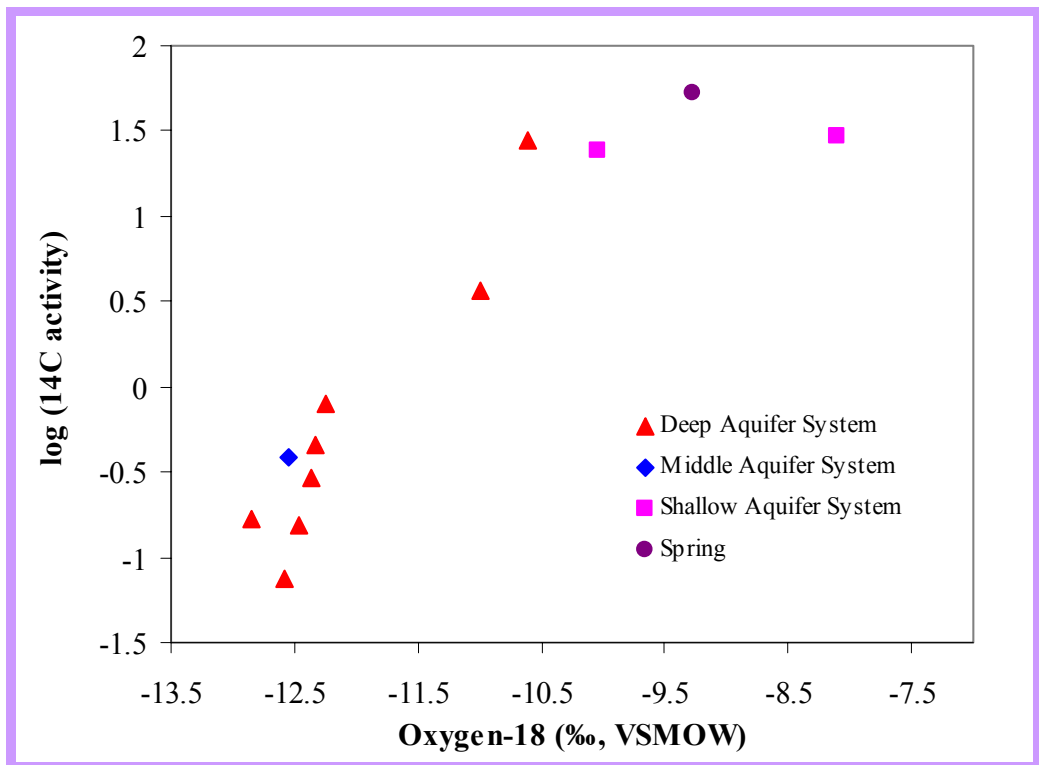


Figure 5.13 Logarithm of Carbon-14 activity versus oxygen-18 (‰, VSMOW).

¹⁴C ratio for the sample. The dissolution of carbonate minerals accompanied by the precipitation of calcite can also remove ¹⁴C. The addition of dead carbon from other sources such as the oxidation of old organic matter, sulfate reduction and methanogenesis can also reduce the ¹⁴C activity of the sample. There can also be an isotopic exchange involving CO₂ and carbonate minerals that can lower the ¹⁴C activity even though this process is negligible at normal groundwater temperatures (Kazemi et al., 2006). The dilution of ¹⁴C through different geochemical reactions can also be taken into account if Equation 5.12 is modified by adding a dilution factor, q, as given in Equation 5.13 (Clark and Fritz, 1997). It is not simple to assign a correct value to the dilution factor. The development of carbonate and ¹³C evolution provides a basis for calculating q.

$$t = -8267 * \ln \left(\frac{a_t^{14}C}{q * a_0^{14}C} \right) \quad (5.13)$$

5.5.3.2 Carbon-13 in the Carbonate System

Clark and Fritz (1997) pointed out that carbon-13 is an excellent tracer of carbonate evolution in groundwaters because of the large variations in the various carbon reservoirs. The evolution of DIC and $\delta^{13}C_{DIC}$ begins with atmospheric CO₂ with $\delta^{13}C$ being approximately -7‰ VPDB. Photosynthetic uptake of CO_{2(atm)} is accompanied by significant depletion in ¹³C. This uptake occurs during CO₂ diffusion into the leaf stoma and during carbon fixation by the leaf's chloroplast where CO₂ is converted to carbohydrate (CH₂O) (Clark and Fritz, 1997). As a result of this uptake depletion occurs in ¹³C, the amount of fractionation changes between 5 to 25 ‰ and this amount depends on the pathway followed. There are three principal photosynthetic cycles recognized: the Calvin or C₃ cycle, the Hatch-Slack or C₄ cycle and the Crassulacean acid metabolism (CAM) cycle (Clark and Fritz, 1997).

The Calvin cycle dominates in most terrestrial ecosystems functioning in about 85% of plant species. Clark and Fritz (1997) states C₃ plants fix CO₂ with the Rubisco enzyme. The diffusion and dissolution of CO₂ has a net enrichment in ¹³C whereas carbon fixation reveals 29‰ depletion on the fixed carbon. (O'Leary, 1988). Most C₃ plants have $\delta^{13}C$

values that range from -24 to -30 ‰ with an average of about -27 ‰ (Vogel, 1993). These plants dominate in tropical forests and temperate and high latitude regions. Some of the C₃ crops are wheat, rye, barley, legumes, cotton and tobacco (Clark and Fritz, 1997).

At higher temperatures and under low CO₂: O₂ conditions, increased respiration in C₃ plants interferes with their ability to fix CO₂. C₄ plants use PEP carbon fixation enzyme acting to deliver more carbon to Rubisco for fixation. As a result, C₄ plants have δ¹³C values that range from -10 to -16‰ with a mean value of -12.5‰ (Vogel, 1993). These plants dominate in hot open ecosystems and they represent less than 5% of floral species (Ehleringer et al., 1991). Sugar cane, corn and sorghum are the common agricultural C₄ plants (Clark and Fritz, 1997).

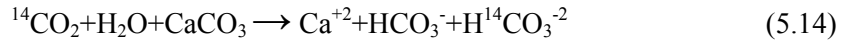
The third photosynthetic cycle is the CAM photosynthesis favored by 10% of plants dominating in desert ecosystems. During the day, they act like C₃ plants and during night they follow C₄ pathway for fixing CO₂ (Clark and Fritz, 1997).

5.5.3.3 Correction of ¹⁴C ages for Carbonate Dissolution

There are different approaches to correct apparent ¹⁴C water ages such as statistical correction (Vogel, 1967, 1970), alkalinity correction (Tamers, 1975), chemical mass-balance correction (Fontes and Garnier, 1979), and δ¹³C mixing model correction (Pearson and Hanshaw, 1970) (Clark and Fritz, 1997). Generally, in all approaches, the diluting source of carbon is assumed to be ¹⁴C-free and all approaches provide estimates of groundwater ages. The most appropriate approach to correct carbon-14 ages depends on the geochemical system and the data available.

It has been emphasized by Clark and Fritz (1997) that carbon-13 is a good tracer of open and closed system evolution of DIC in groundwaters and the large difference in δ¹³C between the soil-derived DIC and carbonate minerals in the aquifer provide a reliable measure of ¹⁴C dilution by carbonate dissolution. Under open system conditions, the DIC is continuously exchanging with the infinite reservoir of ¹⁴C- active soil CO₂. In this case, the initial ¹⁴C activity of DIC remains unchanged at 100 pmc ($a_0^{14}\text{C}_{\text{DIC}}=100$ pmc). Under

closed system conditions, the stoichiometry of calcite dissolution by carbonic acid imparts about a 50% dilution to the initial ^{14}C as given in Equation 5.14 (Clark and Fritz, 1997).



The $\delta^{13}\text{C}$ mixing model, first introduced by Pearson (1965) and Pearson and Hanshaw (1970), allows for incorporation of ^{14}C - active DIC during carbonate dissolution under open system conditions and ^{14}C dilution under closed system conditions (Clark and Fritz, 1997). This model is strongly dependent on recharge conditions affecting the ^{13}C enrichment factor during dissolution of CO_2 and the evolution of $\delta^{13}\text{C}_{\text{DIC}}$. Any process that adds to, removes or exchanges carbon from the DIC pool altering the ^{14}C concentrations will also affect the ^{13}C concentrations. It is possible to observe the evolution of DIC in the groundwaters of study area and the influence of this evolution on $\delta^{13}\text{C}$ values (Figure 5.14). Figure 5.14 indicates that the ^{14}C concentrations should highly be impacted from the processes adding dead carbon to the DIC pool in the deep aquifer system.

The dilution factor (q) can be used to dissipate the factors influencing the ^{14}C concentrations in the samples from the study area. This factor can be calculated by using Equation 5.15 as suggested by Pearson and Hanshaw (1970).

$$q = \frac{\delta^{13}\text{C}_{\text{DIC}} - \delta^{13}\text{C}_{\text{carb}}}{\delta^{13}\text{C}_{\text{soil}} - \delta^{13}\text{C}_{\text{carb}}} \quad (5.15)$$

In Equation 5.15, $\delta^{13}\text{C}_{\text{DIC}}$ is measured ^{13}C in groundwater; $\delta^{13}\text{C}_{\text{soil}}$ is $\delta^{13}\text{C}$ of the soil CO_2 (depends on the vegetation, C_3 plants -27‰, C_4 plants approximately -12.5‰); and $\delta^{13}\text{C}_{\text{carb}}$ is $\delta^{13}\text{C}$ of the calcite being dissolved (usually close to 0‰, ‰ 2 for marine carbonates).

According to the $\delta^{13}\text{C}_{\text{DIC}}$ values presented in Table 5.9, there is a dramatic evolution of $\delta^{13}\text{C}_{\text{DIC}}$ especially in D-57A, D-47 and D-8. This indicates an extensive water- rock

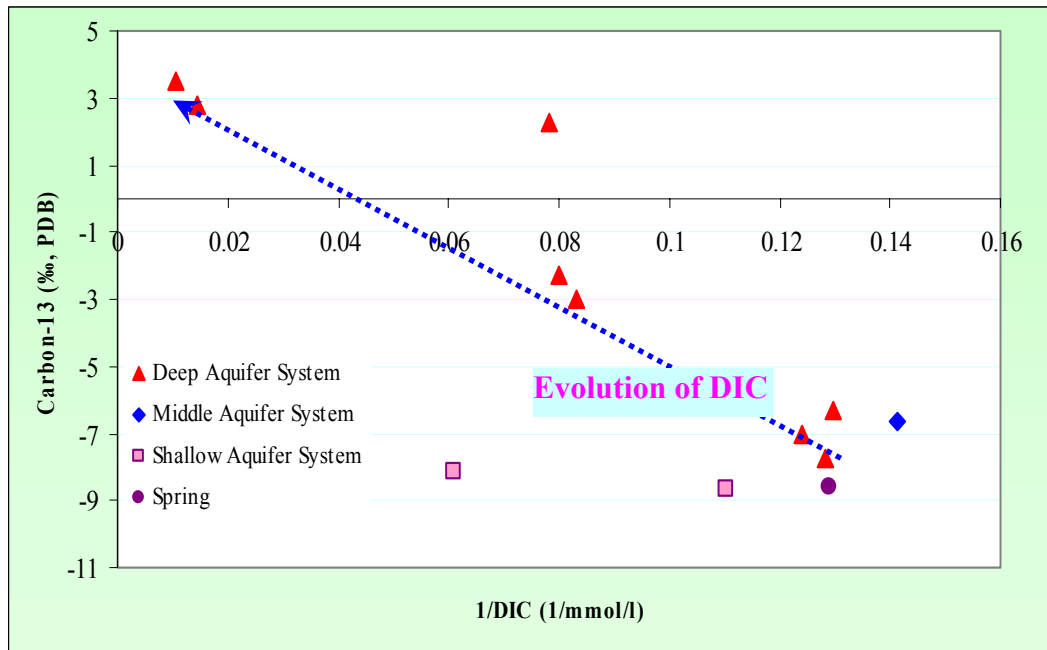


Figure 5.14 $\delta^{13}C_{DIC}$ versus Dissolved Inorganic Carbon graph showing the evolution of DIC in the groundwaters of Kazan Trona Basin.

interaction, thus the need for a major correction. In order to apply Equation 5.15 to correct the radiocarbon ages of those samples, $\delta^{13}C_{soil}$ and $\delta^{13}C_{carb}$ should be known. Although there is no information about the $\delta^{13}C_{carb}$ value of the carbonates in the study area, they should have a value similar to the value measured for the carbonates located near the study area and deposited at the same time with the Eocene carbonates in the area. In a study carried out by Genç (2006) in Kırşehir, located at Central Anatolia, Turkey, $\delta^{13}C$ values of Lutetian carbonates ranged from +2.1 ‰ to +2.2 ‰. Kırşehir is also located in Central Anatolia, just like the Kazan Basin and the carbonates in question are of the same age. This value can be greater than + 2.2‰ for some other carbonates deposited in the Central Anatolia because in a study carried out in Konya Closed Basin by Bayarı et al. (2005), the Mesozoic marine dolomitic limestones were measured to have $\delta^{13}C$ of +4.21 ‰. Therefore, it is not unrealistic to assume a value of +3 ‰ for $\delta^{13}C_{carb}$ for the carbonates in the study area to be used in Equation 5.15 although it should

be mentioned that there is a high uncertainty. However, this way, the positive $\delta^{13}C_{DIC}$ values of D-57A, D-47 and D-8 can be explained.

So as to assign a value to $\delta^{13}C_{soil}$ there should be information about the vegetation cover in the recharge area. From the field observations and other studies carried out around Ankara (Çetin et al., 2002, Elçi et al., 2005) the modern plant species should follow a C_3 pathway as their principal photosynthesis cycle. Therefore, the $\delta^{13}C_{soil}$ should be around -27‰ for today. By using these values, q- factor can be calculated for each sample. However $\delta^{13}C_{soil}$ should not be considered to be constant over time. The best estimate for vegetation cover in the recharge area should not only be considered for today but also be considered for the past because there is a high possibility that the vegetation in the study area was completely different from today's thousands of years ago. There is a nice study by Oğuz (2003) titled "Remaining tree species from the indigenous vegetation of Ankara, Turkey". In this study Oğuz stated that around 6500 B.C. the climate was warm and rainy in Central Anatolia and well-developed forest vegetation existed unlike today. However, it is hard to exactly tell the vegetation cover in the area in the last 50,000 years. Due to this fact, the high uncertainty in the $\delta^{13}C_{carb}$ is unfortunately not the only one since there is a considerable uncertainty in $\delta^{13}C_{soil}$ value also.

Before the calculation of a corrected radiocarbon age with the associated uncertainties, the value of $a_0^{14}C$ should also be estimated. Estimation of $a_0^{14}C$ requires radiocarbon data of a sample that is proven to be modern. During the hydrogeology studies for conceptual understanding of the study area, Yazıcıgil (2001) gathered isotope data from some of the springs and wells in the study area. The deuterium and oxygen-18, carbon-13 and carbon-14 results, obtained from the samples collected in February 2001, were similar to the ones presented herein for K-47 and K-57A. For SP-2, the tritium amount was measured to be 7.58 TU again in February, 2001. This indicates that SP-2 is recharged by precipitations younger than nuclear testing (before 1963). Therefore, the water discharging from SP-2 should be modern. The carbon-14 activity in this particular sample was reported to be 68 pmC and the $\delta^{13}C$ was -8.96 ‰ (Yazıcıgil, 2001). Under these circumstances, it should not be wrong to use 68 pmC as the initial activity of radiocarbon, $a_0^{14}C$, for the samples apart from D-13, D-37, D-57A, D-8 and D-47 during calculations. For these three samples the interaction with trona, having 0 pmc modern

carbon, is high as indicated by the $\delta^{13}\text{C}$ values and the dead carbon contribution is considerably elevated. If it is assumed that the modern recharge waters $a_0^{14}\text{C}$ value is 68 pmc then equal mixing of this young, recharge water with the water having trona contribution should lower the $a_0^{14}\text{C}$ by 50 %. Due to this fact, the $a_0^{14}\text{C}$ value for those samples can assumed to be equal to 34 pmc.

It is very hard to correctly estimate the radiocarbon model ages in such a complex system in which the amount of dead carbon contribution is not exactly known, the vegetation cover (C3 or C4 plants) in the area is highly uncertain for the past and the $\delta^{13}\text{C}$ value for the carbonate rocks in the study area is not precisely known. In this study, to estimate the radiocarbon model ages, NETPATH which is an interactive code for modeling net geochemical reactions along a flow path developed by Plummer et al. (1994) could have been utilized. This program is frequently used in the literature to estimate the ^{14}C age of groundwaters from various complex systems. This computer program utilizes previously defined chemical and isotopic data for waters from a hydrochemical system for a set of mineral and (or) gas phases hypothesized to be the reactive phases in the system. NETPATH calculates the mass transfers in every possible combination of the selected phases that accounts for the observed changes in the selected chemical and isotopic compositions observed along a defined flow path (Plummer et al., 1994). NETPATH uses several well-known adjustment models to obtain estimates of the initial ^{14}C activity. These adjustment models were mentioned before in this section. Each adjustment model uses the initial ^{14}C activity to compute the ^{14}C expected in the final water as if there were no radioactive decay. The adjusted ^{14}C activity is compared to the measured ^{14}C activity through the radioactive decay equation to determine the radiocarbon age of the water. These inorganic carbon adjustment models consider to varying degrees, processes including exchange of dissolved inorganic carbon with soil-zone CO_2 , dilution of inorganic carbon by carbonate- mineral dissolution etc (Plummer et al., 1994).

Accurate estimation of the radiocarbon model ages by using NETPATH requires a suitable geochemical model. The construction of this model requires considerable amount of time and data which indeed in this study is not available. Due to these adversities utilization of NETPATH was not logical and there was no attempt to use this program, instead ambiguities in various parameters lead to a tentative interpretation on

the radiocarbon ages by carrying out calculations for different $a_0^{14}C_{soil}$ values and different q-factors, the results of which are presented in Table 5.10. In this table the sensitivity of the estimated radiocarbon ages to different $a_0^{14}C_{soil}$ values can be seen. During this calculations, although the exact value is highly uncertain, the $a_0^{14}C_{soil}$ values were assumed to be + 3.6 ‰. As stated before, $a_0^{14}C$ values for D-13, D-37, D-57A, D-47 and D-8 were assumed to be 34 pmc and for the rest of the samples $a_0^{14}C$ is considered to be 68 pmc.

In Table 5.10, it is obvious that there is a major correction for wells D-57A, D-47 and D-8, the q-factor is the smallest for these two samples. Among the estimated radiocarbon ages, the oldest corrected one belongs to a sample from the middle aquifer system, M-60B being around 33000 years BP. For SP-7, S-4 and D-20, the radiocarbon ages calculated to be smaller than 0 due to the major corrections. The estimated ages calculated by using different $\delta^{13}C_{soil}$ values showed an increase of -1‰ in this value causes a decrease of 270 years in the corrected ages. This difference is about 2% of the calculated ages. Within the scope of this study, a deviation of 300 years from the actual age will not make much of a difference therefore using -27‰ for $\delta^{13}C_{soil}$ can give the average result needed herein. The calculated ages presented in Table 5.10 are plotted in Figure 5.15. In this figure, the minor effects of two different $\delta^{13}C_{soil}$ values can be seen. The same trend observed in Figure 5.13 can also be observed herein: there is depletion in the oxygen-18 values with increasing radiocarbon ages both for corrected and unadjusted ones. In the same figure, it is possible to see the oxygen-18 content of the modern precipitation in around 1100 m. The oxygen-18 content of the samples having modern radiocarbon ages are similar to the oxygen-18 content of precipitation showing that for those samples the estimated radiocarbon ages are not unrealistic. Figure 5.15 also indicates that the difference between the unadjusted age and the age estimated as a result of the correction is the highest for one sample (D-57A).

Here, it should once again be mentioned that the values presented in Table 5.10 are calculated under considerable uncertainty associated with each parameter estimated. Due to the previously explained reasons, those ages should never be considered as absolute ages.

Table 5.10 The unadjusted and the corrected radiocarbon ages in Years Before Present (yr. B.P.) for different $\delta^{13}\text{C}_{\text{soil}}$ values.

Sample	$a_0^{14}\text{C}_{\text{DIC}}$	$\delta^{13}\text{C}$	$\delta^{13}\text{C}_{\text{soil}}=-20\text{‰}$		$\delta^{13}\text{C}_{\text{soil}}=-24\text{‰}$		$\delta^{13}\text{C}_{\text{soil}}=-27\text{‰}$		$\delta^{13}\text{C}_{\text{soil}}=-29\text{‰}$	
			q-factor	Corrected ^{14}C Age	q-factor	Corrected ^{14}C Age	q-factor	Corrected ^{14}C Age	q-factor	Corrected ^{14}C Age
M-60B	68	-6.64	0.43	35821.89	0.37	34527.53	0.33	33674.51	0.31	33151.11
SP-7	68	-8.61	0.52	-3398.43	0.44	-4692.79	0.40	-5545.81	0.37	-6069.22
S-9	68	-8.17	0.50	2857.48	0.43	1563.12	0.38	710.10	0.36	186.69
S-4	68	-8.65	0.52	1402.01	0.44	107.65	0.40	-745.37	0.38	-1268.78
D-68R	68	-6.33	0.42	29612.21	0.36	28317.85	0.32	27464.83	0.30	26941.43
D-63A	68	-7.74	0.48	18010.39	0.41	16716.04	0.37	15863.01	0.35	15339.61
D-47	34	2.76	0.04	17053.69	0.03	15759.33	0.03	14906.30	0.03	14382.90
D-37	34	-3	0.28	28801.15	0.24	27506.80	0.22	26653.77	0.20	26130.37
D-20	68	-7.01	0.45	781.41	0.38	-512.94	0.35	-1365.97	0.33	-1889.37
D-13	34	-2.3	0.25	24245.56	0.21	22951.21	0.18	21375.29	0.18	21574.78
D-8	34	2.28	0.06	20114.49	0.05	18820.13	0.02	13119.89	0.04	17443.70
D-57A	34	3.52	0.0034	3574.01	0.0029	2279.65	0.0026	1426.63	0.0025	903.23

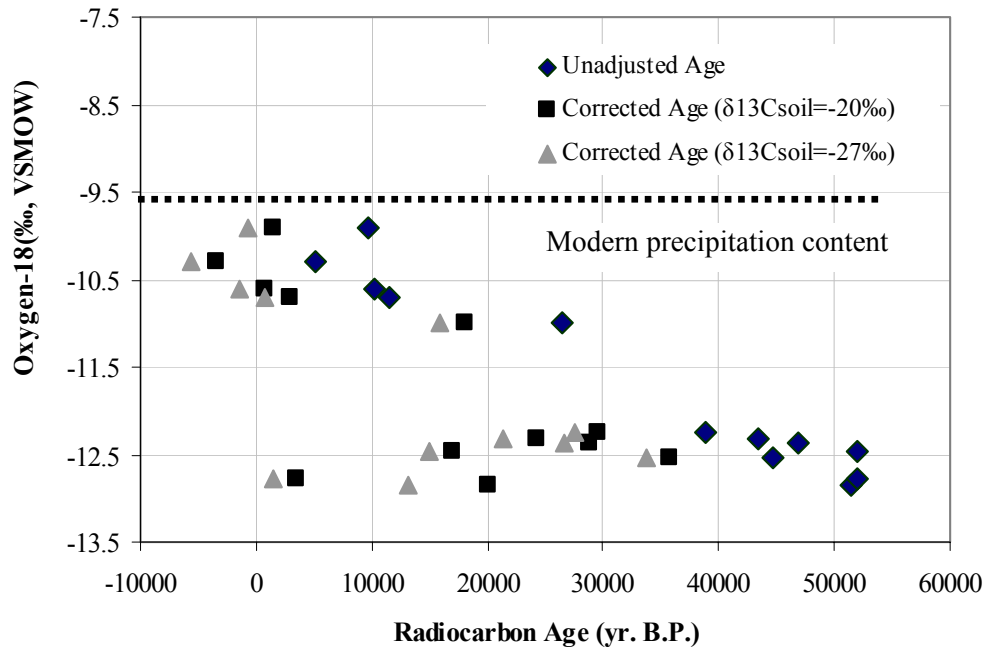


Figure 5.15 Oxygen-18 values versus unadjusted and corrected radiocarbon ages for different $\delta^{13}C_{soil}$ values. The oxygen-18 content of modern precipitation is also shown ($\delta^{18}O=-9.65$ ‰).

5.6 Evaluation of Helium-4 and Helium-3/ Helium-4 ratio data

It has been stated out in the previous sections that Xenon and Neon concentrations measured in a groundwater sample can be used to find the recharge temperature of that sample. In this study, together with Xenon and Neon concentrations, Helium, Argon, and Krypton concentrations were also measured and the $^3He/^4He$ and $^{40}Ar/^{36}Ar$ ratios were determined (Table 5.11). In this section only helium and $^3He/^4He$ ratio data will be discussed.

In Chapter 2, general information about helium isotopes was given and the different sources of 4He in groundwater were explained. The ratio of $^3He/^4He$ is a key indicator to differentiate among 4He of different sources and in groundwater dating. Helium is the second most abundant element in the known universe after hydrogen and constitutes 23%

Table 5.11 The dissolved Helium (He), Neon (Ne), Argon (Ar), Krypton (Kr) and Xenon (Xe) data and the $^3\text{He}/^4\text{He}$ and $^{40}\text{Ar}/^{36}\text{Ar}$ ratios.

Sample Name	He-4 [ccSTP/g]	Ne-20 [ccSTP/g]	Ar-36 [ccSTP/g]	Kr-84 [ccSTP/g]	Xe-132 [ccSTP/g]	$^3\text{He}/^4\text{He}$	$^{40}\text{Ar}/^{36}\text{Ar}$	R/Ra
D-68R	4.53E-07	1.02E-06	1.46E-02	1.36E-07	1.80E-08	1.24E-06	294	0.89
D-47	1.53E-05	2.84E-07	8.13E-03	9.59E-08	1.28E-08	1.96E-07	294.8	0.14
S-9	7.55E-06	2.29E-07	6.92E-03	8.41E-08	1.18E-08	2.20E-07	296.1	0.16
S-11	1.32E-06	2.41E-07	6.91E-03	8.01E-08	1.11E-08	1.15E-06	295.6	0.83
S-3	1.20E-05	2.13E-07	6.48E-03	7.82E-08	1.11E-08	2.76E-07	295.7	0.20
S-16	5.08E-08	2.08E-07	6.79E-03	8.07E-08	1.12E-08	1.43E-06	295.3	1.03
S-2	5.04E-08	2.01E-07	6.63E-03	7.95E-08	1.13E-08	1.71E-06	294.5	1.24
D-8	3.19E-07	3.06E-07	8.61E-03	1.00E-07	1.41E-08	4.04E-07	294.8	0.29

of all elemental matter measured by mass. In the Earth's atmosphere the concentration of helium by volume is 5.24 parts per million only according to Verniani (1966). There are eight isotopes of helium, however only ^3He and ^4He are stable. ^4He is an unusually stable nucleus because its nucleons are arranged into complete shells. The total concentration of helium in Earth's atmosphere is mostly ^4He . In fact, there is only one ^3He atom for every 730,000 ^4He . Therefore the $^3\text{He}/^4\text{He}$ ratio in the atmosphere is $1.384 \cdot 10^{-6}$ (Clarke et al., 1976).

In meteoric waters, two terrigenous components of helium can be found. The continental crust is dominated by isotopically heavy Helium (Helium-4) that is produced in situ by nuclear reactions (radioactive decay of Uranium, Thorium and Lithium) in crustal rocks and minerals. Therefore, this crustal component has a $^3\text{He}/^4\text{He}$ ratio of $2 \cdot 10^{-8}$ (Mamyrin and Tolstikhin, 1984; Andrews, 1985). Crustal Helium is often identified by radiogenic helium. Besides crustal He, there is another source of helium that is Earth's mantle. The mantle contains newly produced He relicts of isotopic light He inherited during planet formation. This source often has a $^3\text{He}/^4\text{He}$ ratio of $1.2 \cdot 10^{-5}$ (Ozima and Podosek, 1983; Mamyrin and Tolstikhin, 1984).

The groundwater samples from the shallow and deep aquifer systems have $^3\text{He}/^4\text{He}$ ratios varying between $1.15 \cdot 10^{-6}$ and $4.04 \cdot 10^{-7}$. Normally, the shallow groundwater samples should indicate a $^3\text{He}/^4\text{He}$ ratio close to the atmosphere, $1.384 \cdot 10^{-6}$. According to Table

5.11, only S-2 and S-16 are close to this value, together with their helium concentrations which are very close to the air-equilibrated waters concentrations ($4.61 \cdot 10^{-8} \text{ cm}^3 \text{STPg}^{-1} \text{ H}_2\text{O}$ at 12°C). The helium concentrations for the rest of the samples are different from the equilibration concentrations as an indication of addition of extra helium components.

In Table 5.11, R/Ra ratios which are the $^3\text{He}/^4\text{He}$ ratios (R) against the $^3\text{He}/^4\text{He}$ ratio in the atmosphere (Ra) for each sample are also presented. Ra is $1.384 \cdot 10^{-6}$ as stated before in this section. R/Ra value is close to 1 for the samples having atmospheric helium. At a first glance, the atmospheric helium component should be the highest in the samples from the shallow wells S-16 and S-2 as stated before and for D-68R there should have a significant amount of atmospheric helium contribution to the total helium present in this sample.

5.6.1 Helium Isotope Components

The different helium components (atmospheric, radiogenic and mantle) of the waters sampled were separated by using the equations given in a study by Imbach (1997) (Equations 5.16- 5.24). The atmospheric helium components ($^3\text{He}_{\text{atm}}$ and $^4\text{He}_{\text{atm}}$) were calculated by using Equations 5.16 and 5.17 respectively and presented in Tables 5.12 and 5.13 respectively. The components other than atmospheric Helium which can be mantle and crustal ($^3\text{He}_{\text{ex}}$ and $^4\text{He}_{\text{ex}}$) were calculated by using Equations 5.19 and 5.20 (Table 5.12 and Table 5.13 respectively). Furthermore, the excess helium calculated was separated as mantle and crustal by using the Equations 5.21- 5.24. In these equations the abbreviations atm stands for atmospheric, ex stands for excess, crus stands for crustal and meas stands for measured and calc stands for calculated. It should be noted that $^3\text{He}_{\text{calc}}$ was calculated by using the measured helium-4 concentrations and $^3\text{He}/^4\text{He}$ ratios (Equation 5.18).

$$^3\text{He}_{\text{atm}} = R_{\text{atm}} * (^4\text{He}/^{20}\text{Ne})_{\text{atm}} * ^{20}\text{Ne}_{\text{meas}} \quad (5.16)$$

$$^4\text{He}_{\text{atm}} = (^4\text{He}/^{20}\text{Ne})_{\text{atm}} * ^{20}\text{Ne}_{\text{meas}} \quad (5.17)$$

$$^3\text{He}_{\text{calc}} = ^4\text{He}_{\text{meas}} * (^3\text{He}/^4\text{He}) \quad (5.18)$$

$${}^3\text{He}_{\text{ex}} = {}^3\text{He}_{\text{calc}} - {}^3\text{He}_{\text{atm}} \quad (5.19)$$

$${}^4\text{He}_{\text{ex}} = {}^4\text{He}_{\text{meas}} - {}^4\text{He}_{\text{atm}} \quad (5.20)$$

$${}^3\text{He}_{\text{man}} = ({}^4\text{He}_{\text{ex}} - (R_{\text{rad}}^{-1} * {}^3\text{He}_{\text{ex}})) / (R_{\text{man}}^{-1} - R_{\text{rad}}^{-1}) \quad (5.21)$$

$${}^4\text{He}_{\text{man}} = ({}^3\text{He}_{\text{ex}} - (R_{\text{rad}} * {}^4\text{He}_{\text{ex}})) / (R_{\text{man}} - R_{\text{rad}}) \quad (5.22)$$

$${}^3\text{He}_{\text{rad}} = {}^3\text{He}_{\text{ex}} - {}^3\text{He}_{\text{man}} \quad (5.23)$$

$${}^4\text{He}_{\text{rad}} = {}^4\text{He}_{\text{ex}} - {}^4\text{He}_{\text{man}} \quad (5.24)$$

In the above equations, $({}^4\text{He}/{}^{20}\text{Ne})_{\text{atm}}$ was taken to be 0.24 (Benson ve Krause, 1976) and R_{atm} was equal to $({}^3\text{He}/{}^4\text{He})_{\text{atm}} = 1.384 * 10^{-6}$ as stated before in preceding section.

In Tables 5.12 and 5.13, the percentages of all the different components of ${}^3\text{He}$ and ${}^4\text{He}$ were also given. According to Table 5.11, for S-16, 95% of the total ${}^3\text{He}$ is the atmospheric ${}^3\text{He}$ as expected. The lowest percentages of ${}^3\text{He}_{\text{atm}}$ component are in S-3, D-47, S-9 and S-11. ${}^3\text{He}_{\text{man}}$ percentage is strikingly highest in a sample from the shallow aquifer system, S-11. For all samples, the mantle contribution is greater than the radiogenic contribution (Figure 5.16). This finding is not surprising because helium-3 is most abundant in mantle. When the intensely fractured sections of the deep aquifer system are considered, the mechanism transporting these huge amounts of ${}^3\text{He}_{\text{man}}$ to the shallower parts should be the fractures. In addition to the fractures, the upward mixing of the deeper groundwater enhances the dissemination of different helium components to the shallower parts.

When Table 5.16 is investigated, it can be seen that the atmospheric ${}^4\text{He}$ component is very small in D-47, S-9, S-11 and S-3, however it is remarkable at D-8 and D-68R and for S-2 and S-16 almost all of ${}^4\text{He}$ comes from the atmospheric sources. The mantle ${}^4\text{He}$ is the highest in S-11, followed by D-68R, lowest in D-8 and S-16 (Figure 5.17). The contribution of radiogenic ${}^4\text{He}$ to the total ${}^4\text{He}$ is remarkable as expected because helium-4 is most abundant in the Earths crust. The presence of even minor amounts of ${}^4\text{He}_{\text{man}}$

Table 5.12 The calculated ^3He concentrations and the components of the ^3He (atmospheric, crustal and mantle) with the percentages of these components for all samples.

Sample	$^3\text{He}_{\text{cal}}$	$^3\text{He}_{\text{atm}}$	$^3\text{He}_{\text{ex}}$	$^3\text{He}_{\text{man}}$	$^3\text{He}_{\text{crus}}$	%	%	%
	(ccSTP/g)	(ccSTP/g)	(ccSTP/g)	(ccSTP/g)	(ccSTP/g)	$^3\text{He}_{\text{atm}}$	$^3\text{He}_{\text{man}}$	$^3\text{He}_{\text{crus}}$
D-68R	5.60E-13	3.39E-13	2.22E-13	2.18E-13	3.80E-15	60.42	38.90	0.68
D-47	3.00E-12	9.44E-14	2.91E-12	2.61E-12	3.01E-13	3.15	86.84	10.02
S-9	1.66E-12	7.60E-14	1.58E-12	1.43E-12	1.47E-13	4.59	86.52	8.89
S-11	1.51E-12	8.00E-14	1.43E-12	1.41E-12	2.28E-14	5.29	93.20	1.51
S-3	3.32E-12	7.07E-14	3.25E-12	3.02E-12	2.35E-13	2.13	90.80	7.07
S-16	7.24E-14	6.90E-14	3.43E-15	3.42E-15	1.34E-17	95.26	4.72	0.02
S-2	8.63E-14	6.67E-14	1.96E-14	1.96E-14	1.20E-17	77.28	22.71	0.01
D-8	1.29E-13	1.02E-13	2.73E-14	2.24E-14	4.88E-15	78.84	17.37	3.78

Table 5.13 The components of ^4He (atmospheric, radiogenic and mantle) and the percentages of these components for all samples.

Sample	$^4\text{He}_{\text{atm}}$	$^4\text{He}_{\text{ex}}$	$^4\text{He}_{\text{man}}$	$^4\text{He}_{\text{crus}}$	%	%	%
	(ccSTP/g)	(ccSTP/g)	(ccSTP/g)	(ccSTP/g)	$^4\text{He}_{\text{atm}}$	$^4\text{He}_{\text{man}}$	$^4\text{He}_{\text{crus}}$
D-68R	2.45E-07	2.08E-07	1.82E-08	1.90E-07	54.02	4.01	41.97
D-47	6.82E-08	1.52E-05	2.17E-07	1.50E-05	0.45	1.42	98.14
S-9	5.49E-08	7.49E-06	1.20E-07	7.37E-06	0.73	1.58	97.69
S-11	5.78E-08	1.26E-06	1.17E-07	1.14E-06	4.39	8.92	86.69
S-3	5.11E-08	1.20E-05	2.51E-07	1.17E-05	0.42	2.09	97.49
S-16	4.99E-08	9.53E-10	2.85E-10	6.68E-10	98.13	0.56	1.31
S-2	4.82E-08	2.23E-09	1.63E-09	5.99E-10	95.57	3.24	1.19
D-8	7.34E-08	2.46E-07	1.87E-09	2.44E-07	23.00	0.58	76.41

indicates the heterogeneity of the whole system and the existence of pathways for ^4He from mantle to even shallower parts in the study area. This finding is supported with the CFC data also. For S-2, S-9, S-11 and S-3, for instance, as stated in the preceding sections, the CFC ages came out to be the oldest in the study area. These can be an indication of the existence of different line sources- suggested also by the mantle He presence in these shallow wells.

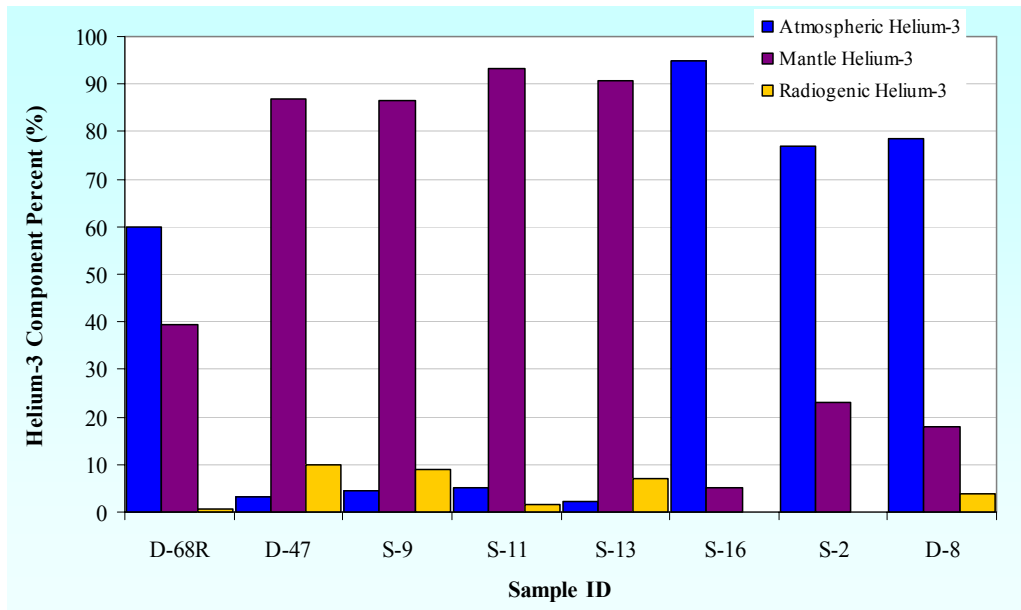


Figure 5.16 The percentages of different ^3He components in the samples.

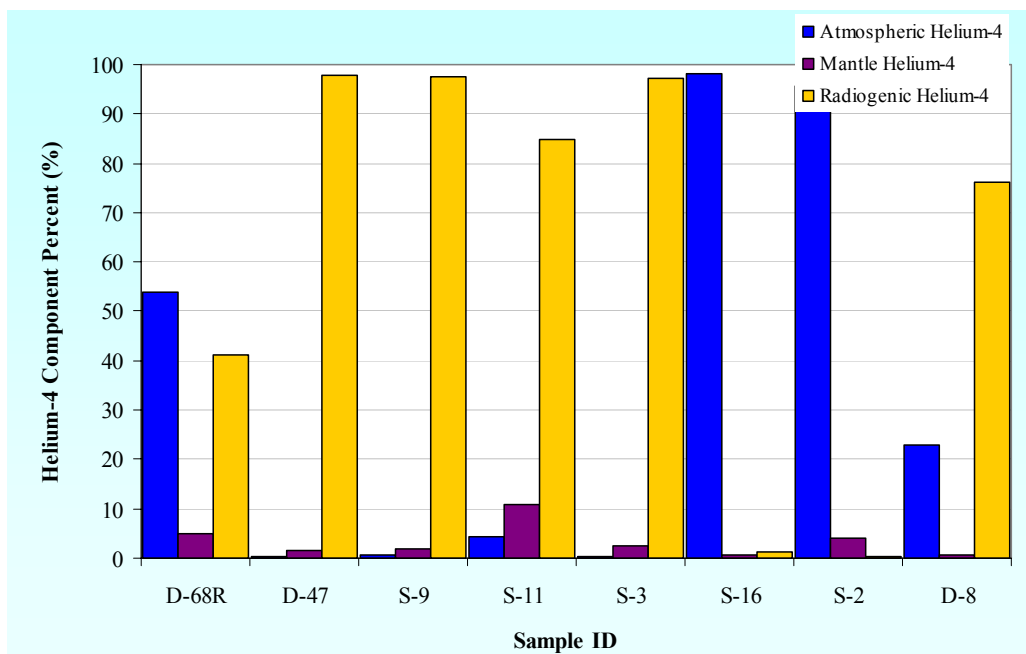


Figure 5.17 The percentages of different ^4He components in the samples.

The total quantity of ^3He is very minor when compared to the total amount of ^4He (the difference is about a million); therefore ^3He doesn't make any difference in the total helium amount. For this particular reason, ^4He data can be considered as the total helium data. Figure 5.18 shows the sources of helium in the aquifers of Kazan Trona Basin and the transport mechanisms of the helium-4 to the shallow aquifer system.

5.7 Hydraulic Age Calculations

Calculation of the hydraulic ages using simple Darcy Equation is useful to check on the accuracy of the dating results because it is based upon a different principle requiring knowledge of the recharge area (Kazemi et al., 2006). Based on Darcy's law and using measured hydraulic gradients, effective porosity and hydraulic conductivity, the hydraulic age of all groundwaters can be calculated from young to very old (Equation 5.25).

$$t = \frac{x}{-K.i/\varepsilon} \quad (5.25)$$

In Equation 5.25, t is the hydraulic age, x is the distance traveled since the entrance of the water to underground, K is the hydraulic conductivity of the porous medium, i is the hydraulic gradient and ε is the effective porosity of the medium which the water travels through.

There were two attempts to calculate the approximate hydraulic ages in the confined portions of the deep aquifer system. The first one was for D-63A. The distance from the recharge area to D-63A was estimated to be 1.7 km, the effective porosity of the medium was taken to be 0.1, a typical value for carbonate rocks, the hydraulic gradient was taken to be 0.04 (SRK, 2004). This way, two different ages can be calculated because the hydraulic conductivity of the medium changes between 10^{-4} m/s and 10^{-7} m/s (SRK, 2004). If the water reaching to D-63A travels from the parts with the highest hydraulic conductivity values, then hydraulic age should only be 1.35 years. If the effective porosity of the medium is 0.15, then the hydraulic age will be 2.02 years. If the groundwater travels from the parts with the lowest hydraulic conductivity values, then

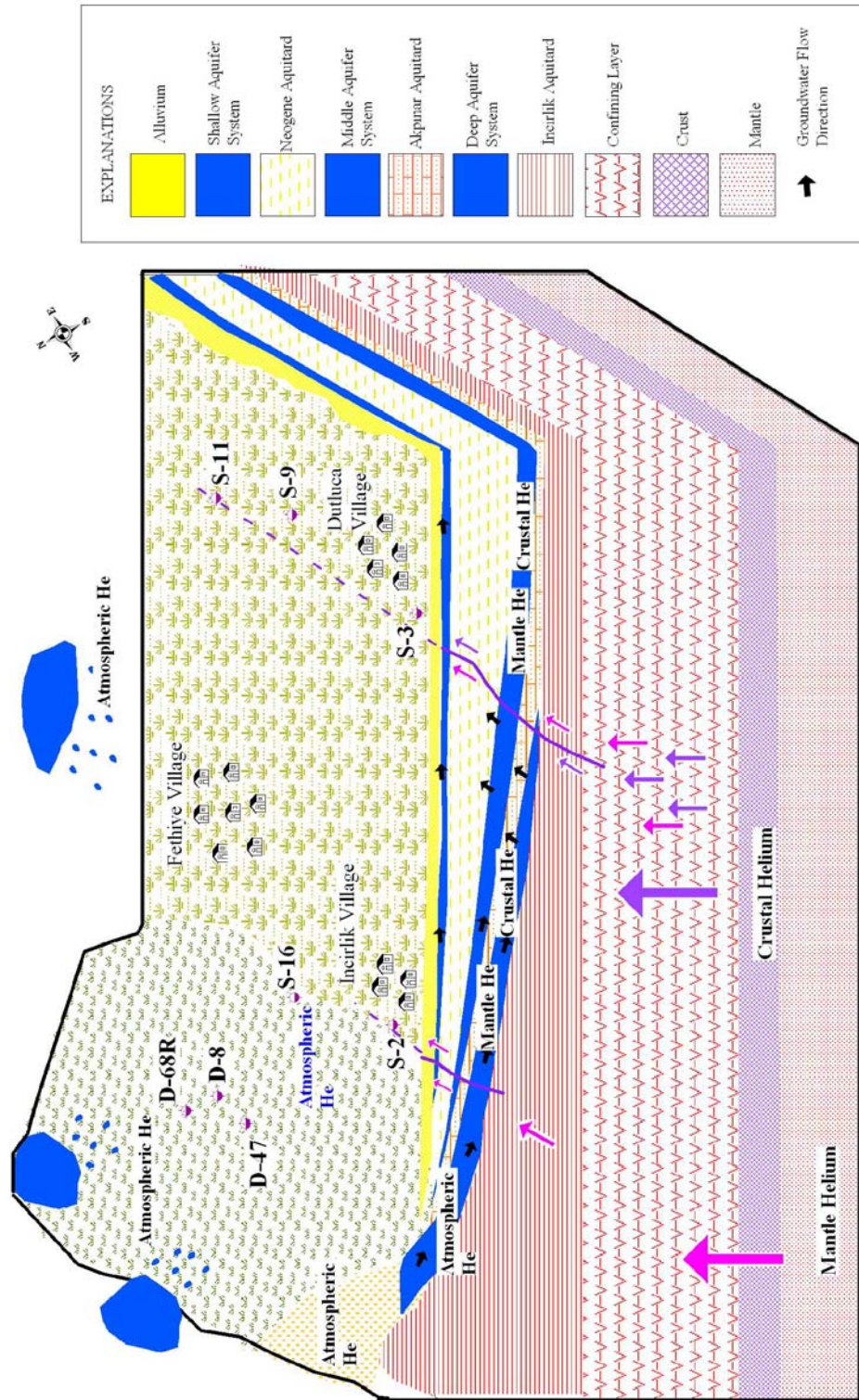


Figure 5.18 Sources of helium in the aquifers of Kazan Trona Basin and the transport mechanisms of the mantle helium to the shallow aquifer system.

the calculated hydraulic age should be around 1348 years for an effective porosity of 0.15 the hydraulic age will be 2021 years..

For D-57A, the situation is different as the hydraulic conductivity values of the medium changes between 2×10^{-10} m/s, if the water travels through the matrix rock and 3×10^{-4} m/s if the water travels through the fractured sections. For the water traveling through the fractured sections, it will only take one year to travel 3.7 km from the recharge area. If the water travels through the matrix rock, then it requires 1.47 million years to reach D-57A.

When the estimated hydraulic ages are compared with the approximated CFC and radiocarbon ages, it can be seen that for D-63A, the CFC age of this groundwater is 41.5 years old whereas the tentative radiocarbon age came out to be 15863 years old. The presence of the measurable amount of CFCs in this sample can be an indication of the groundwater traveled through the higher conductivity areas. For D-57A, the CFC age was found out to be 54 years old whereas due to extensive corrections the radiocarbon age came out to be 1426 years old. The previously calculated ages are found out to be in a harmony with the hydraulic ages proving that in the samples from the deep wells there exist different portions of waters having different ages due to mixing of modern and considerably old groundwaters.

5.8. Conceptual Model of the Groundwater Flow by using Isotope Data

So far in this chapter, up to this section, only the isotope data available was presented one by one. In this part, all data will be combined and a conceptual model of the groundwater flow will be presented based purely on the available data. This model will be used to check the validity of the available flow model constructed by SRK (2004).

To begin with, the relationship between the deuterium excess values and the corrected radiocarbon and CFC ages should be revealed out. Deuterium excess, d , is first proposed by Dansgaard (1964) to characterize the deuterium excess in precipitation. The value d is defined for a slope of 8, and is calculated for any precipitation sample by using Equation 5.26. On a global basis, d averages about 10‰, however it varies regionally due to

variations in source of humidity, wind speed and sea surface temperature (SST) (Clark and Fritz, 1997). According to Clark and Fritz (1997) when humidity is about 85% then precipitation plots very close to the global meteoric water line.

$$d = \delta^2 H - 8\delta^{18} O \quad (5.26)$$

Figure 5.19 shows deuterium excess values calculated by using Equation 5.26 versus the estimated ^{14}C ages and also some of the CFC ages belonging to the shallow samples that do not show evaporative enrichment in their stable isotope values. This figure shows that, deuterium excess values in the springs and shallow groundwater wells are around 10‰, and the data points are located near global deuterium excess for samples that are modern.

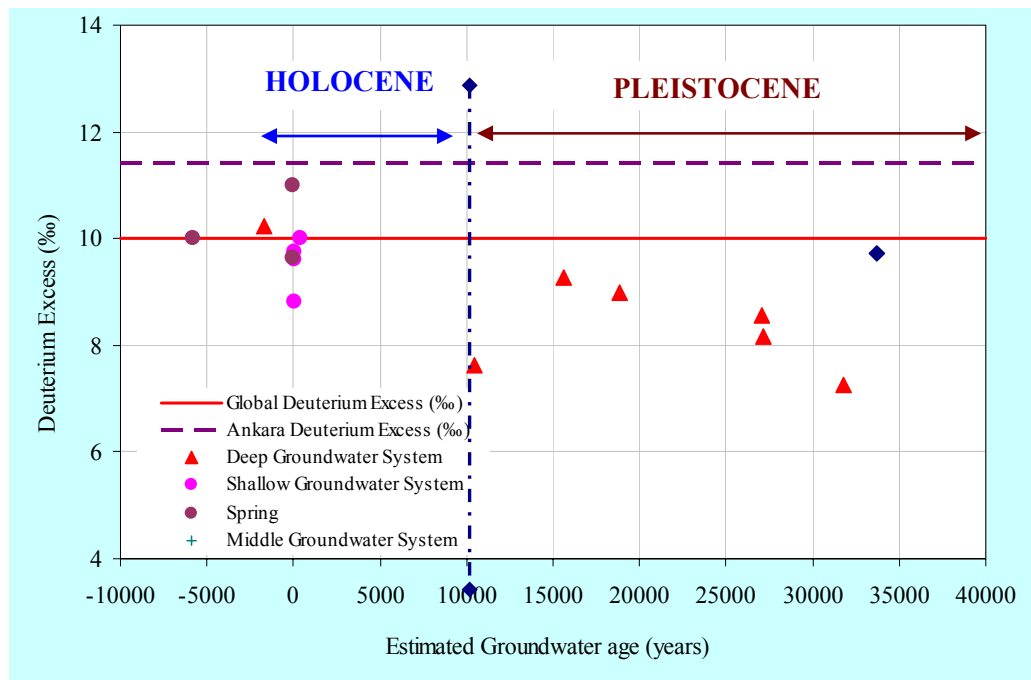


Figure 5.19 Deuterium excess versus estimated groundwater age graph also showing the global and Ankara deuterium excesses which are 10‰ and 11.42‰ respectively (Global Deuterium Excess, Craig (1961b), Ankara Deuterium Excess calculated from data in IAEA/ WMO, 2004).

Data presented in Figure 5.19 does not show a total agreement with the local (Ankara) deuterium excess except for one spring plotted close to AMWL.

When all available data, presented before in this chapter is considered it will not be wrong to state that for the deep aquifer system, there might be evidence of recharge under different climatic conditions. The depletion in heavy isotopes of the groundwaters with ^{14}C ages of about 10000 years BP and greater, in comparison to more recently recharged waters, marks the climatic transition from the Pleistocene epoch (Last ice age, the most recent glacial period in the Pleistocene epoch) to Holocene epoch (interglacial period) also shown in Figure 5.19. The youngest corrected ^{14}C age from the deep aquifer system belongs to a sample very close to the recharge area, showing the influence of modern recharge. This influence can be observed in the stable isotope values being relatively enriched when compared to the ones having greater estimated ^{14}C ages.

An important point that should be emphasized herein, as stated before in the previous sections, is calculated radiocarbon ages should not be considered as absolute ages instead should be considered as model ages. These ages can well be a mixture of various ages as stated by hydraulic ages or they can represent the groundwater entering to the aquifer system exactly at the time given by the radiocarbon age dating method. Due to this fact, it is hard to conclude on the deuterium excess values in the precipitation of Holocene epoch or Pleistocene epoch. If the latter is true, then it can be concluded that during the passage from Pleistocene to Holocene, the deuterium excess values decreased by about 2‰. However, in general, the deuterium excess is more or less uniform throughout the record suggesting a constant circulation regime of the atmosphere over the study area for the past 35000 years as suggested by Rozanski (1985) who studied deuterium and oxygen-18 in European groundwaters and the links to atmospheric circulation in the past. The general cooling during the Last Pleistocene age might be accompanied by a change in source of water vapor recharging the aquifer and the groundwaters with different deuterium excesses might have been formed (Figure 5.20). It is hard to reach a conclusion in the nature of the different vapor sources recharging the aquifer throughout the Pleistocene with the available limited data.

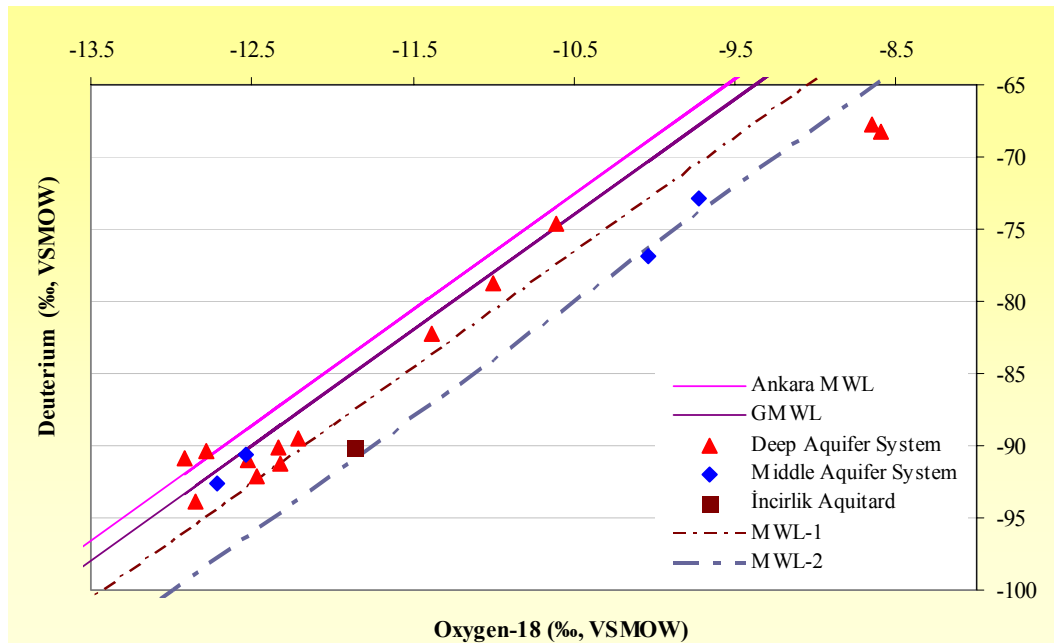


Figure 5.20 Deuterium versus oxygen-18 graph for middle and deep aquifer systems and different meteoric water lines representing different water vapor sources.

Different meteoric water lines can be constructed by using the stable isotope data of samples from the middle and deep aquifer systems as presented in Figure 5.20. These lines have the same slope as today's global meteoric water line but with different deuterium excess values which are substantially lower than presently observed value in the precipitation and infiltration waters in the area. The samples used to construct these lines together with their equations and coefficients of determinations are presented in Table 5.14. In this table all the meteoric water lines has the same slope as the GMWL but shifted to more negative trends which might be evidencing paleorecharge water as stated before. This is confirmed by the low ^{14}C activities which are very close to the detection limits. To further conclude about the past recharge conditions, additional noble gas data should be gathered and the noble gas temperatures should be recalculated by using more sophisticated methods like the iterative schemes and the inverse modeling method which were stated previously in this chapter. In addition, the ^{14}C data can be re-evaluated after collecting the necessary data about the $\delta^{13}\text{C}$ of the carbonates present in the study area.

Table 5.14. The different meteoric water lines and the samples used to construct these lines together with their equations and coefficient of determinations.

Name	Groundwater System	Samples used	Equation	Coefficient of Determination
AMWL	Deep	D-57A, D-33	$\delta^2\text{H}=8*(\delta^{18}\text{O})+12.23$	0.66
MWL-1	Deep	D-8, D-13, D-33, D-37, D-47, D-60A, D-63A, D-63B, D-68R	$\delta^2\text{H}=8*(\delta^{18}\text{O})+8$	0.96
MWL-2	Middle	M-65B and M-74C	$\delta^2\text{H}=8*(\delta^{18}\text{O})+4$	0.87

In order to better understand the flow regime and the state of stable isotopes in different aquifers, three cross-sections, which were oriented in N-S, NW-SE and NE-SW directions (Figure 5.22, 5.23 and 5.24 respectively) were prepared. The orientations of the cross sections were shown in Figure 5.21. In the cross sections oxygen-18, deuterium, carbon-13 and carbon-14 results were also presented whenever they are available. Cross section along line A-A' clearly shows that oxygen-18 and deuterium are not uniform throughout the deep aquifer system (Figure 5.22). These two isotopes should have been more or less identical in different parts of this aquifer because the recharge area is known. However this is not the case. SRK (2004) indicated in their conceptual model that deep aquifer system is mainly recharged along zones that outcrop in the ridges on the western side and by line sources. In the previous sections it has been proven that the depletion in the heavy isotopes of oxygen and hydrogen can not be explained with the elevation effect. In addition, the indication of recharge under different climatic conditions was also demonstrated. The line sources, mentioned by SRK (2004) should bring waters having diverse residence times. Actually, the most striking thing here is that there is a point (D-74B) with an unusually enriched oxygen-18 and deuterium content. This point can well be an indication of a line source bringing modern precipitation. When all the data points are considered, there is one another sample (D-53), plotting very close to D-74B in Figure 5.5. This particular well, D-53, is connected to the groundwater mound, observed in Figure 3.11. This mound was stated to be formed by the water coming with the NE-SW striking fault system at the western boundary of the Kazan Basin (SRK,

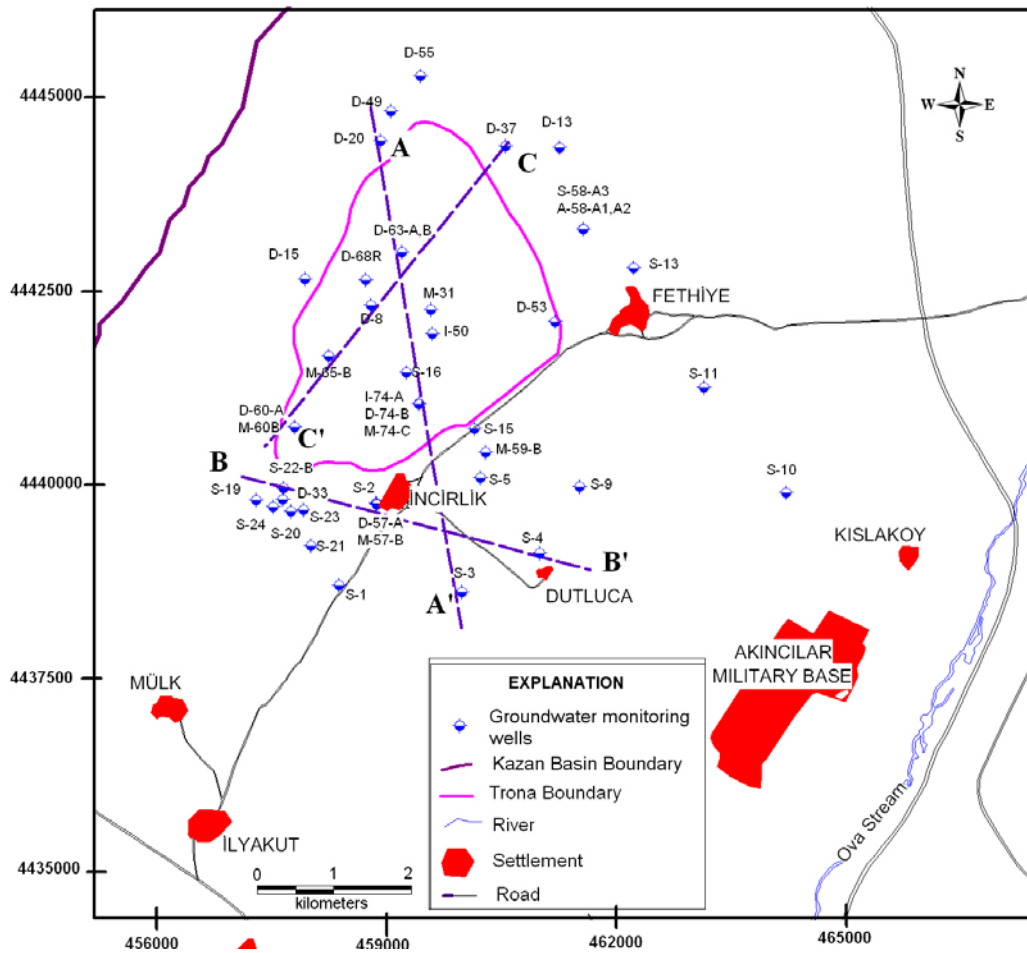


Figure 5.21 Map showing the lines of cross sections.

2004). Therefore, it is not unrealistic to assume that D-53 gives the stable isotope content of the water attributed to this system. These unusually enriched oxygen-18 and deuterium values might indicate that the water transported by the fault system is modern recharge water.

In cross section A-A', the upward flow of the deeper groundwater towards the shallower parts can also be seen (Figure 5.22). There are two points in which carbon-13 and carbon-14 measurements are available. The carbon-13 values of these two points are more or less the same however there is a huge difference between the radiocarbon activities. This indicates the decrease in the activities away from the outcrop area.

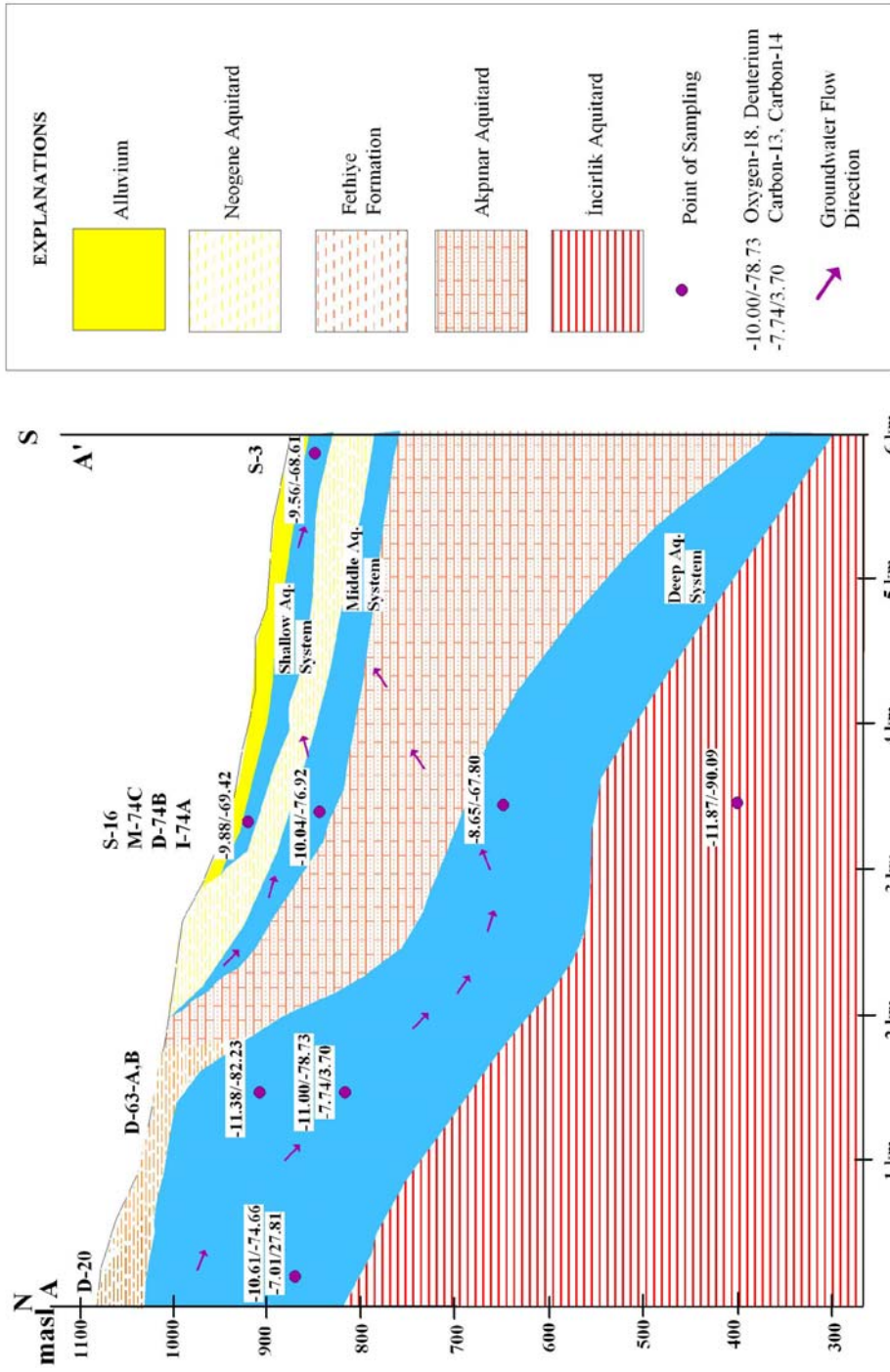


Figure 5.22 Cross-section along line A-A' also showing the results of oxygen-18, deuterium, carbon-13 and carbon-14 measurements.

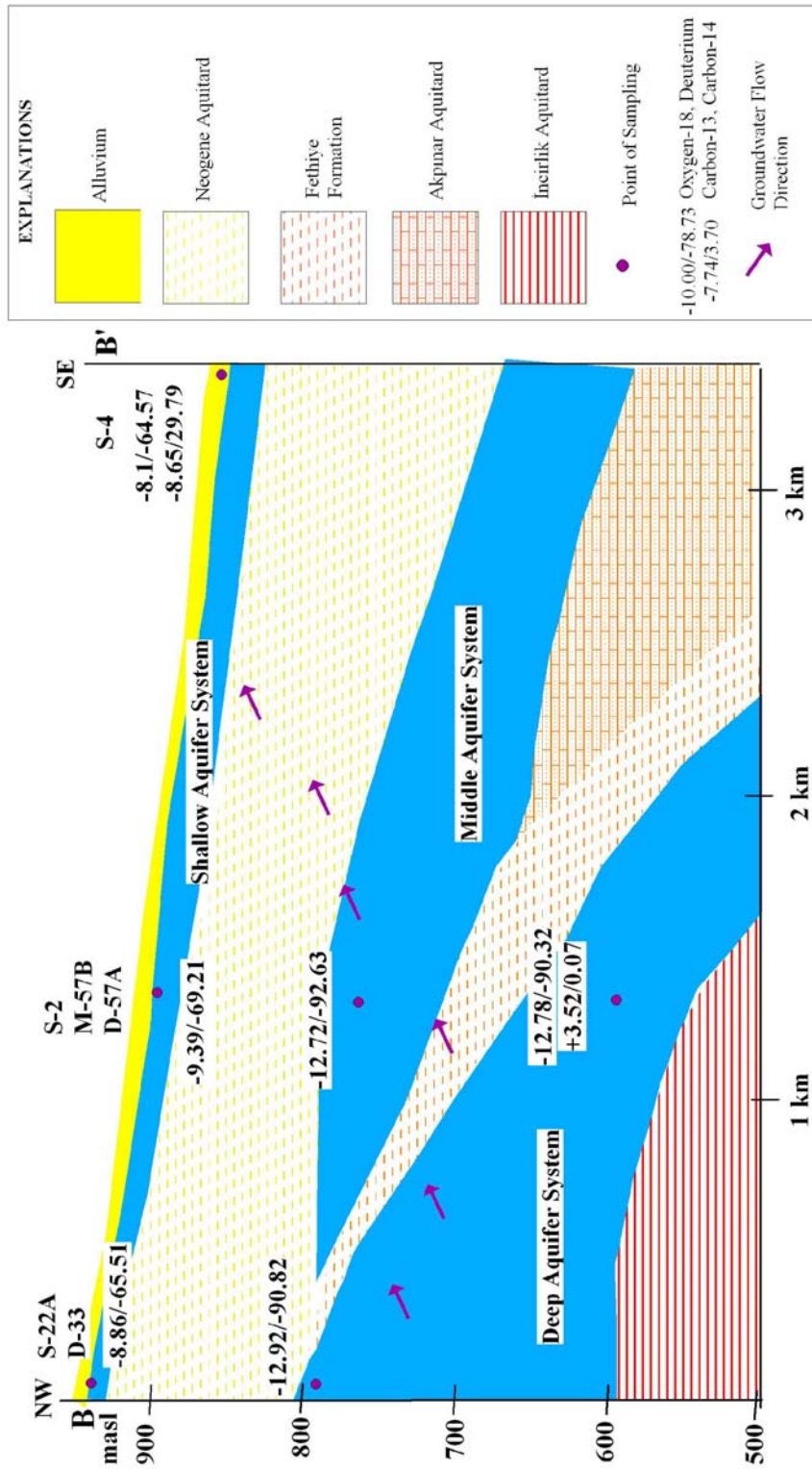


Figure 5.23 Cross-section along line B-B' also showing the results of oxygen-18, deuterium, carbon-13 and carbon-14 measurements.

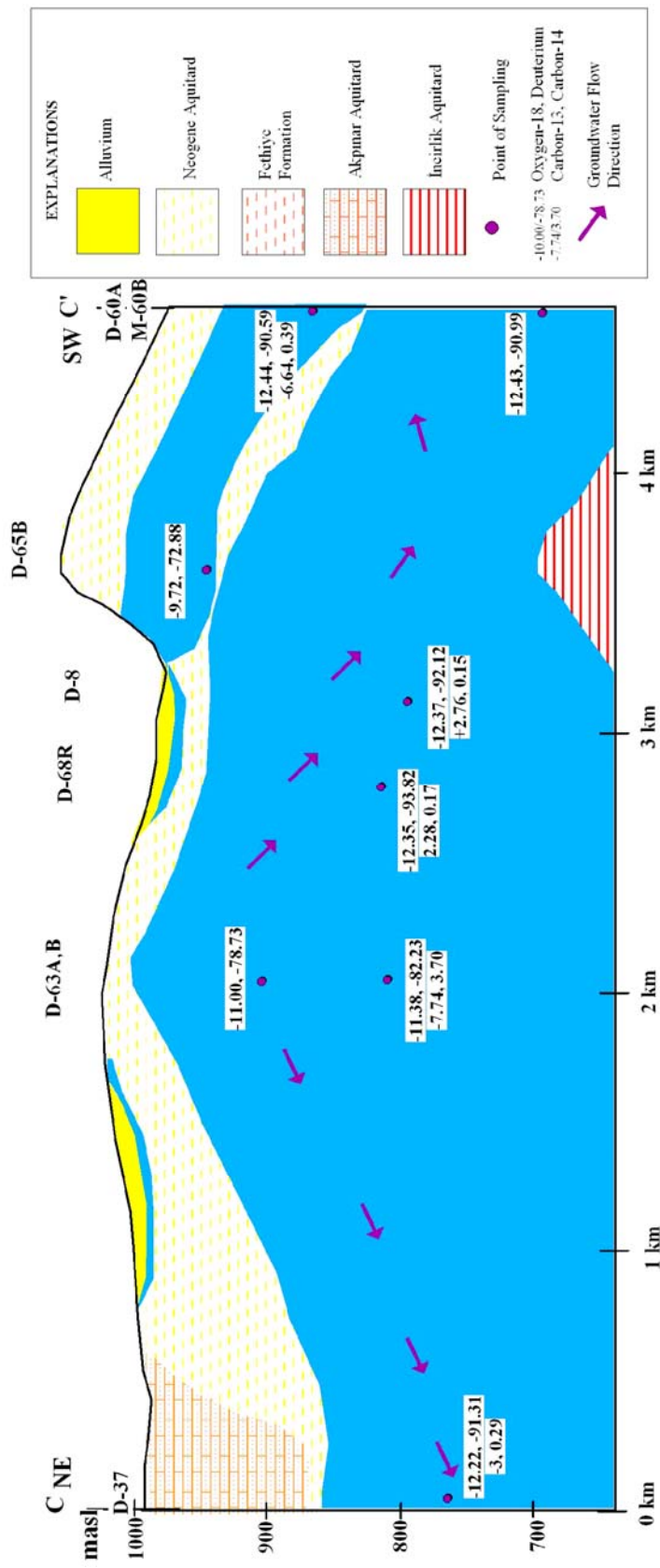


Figure 5.24 Cross-section along line C-C' also showing the results of oxygen-18, deuterium, carbon-13 and carbon-14 measurements.

Cross section B-B' shows a section where middle and deep aquifer systems are not separated by Akpınar Aquitard (Figure 5.23). In this particular part, the middle and deep aquifer systems have got similar stable isotope contents. In this cross-section, the stable isotope content of a point located downgradient (S-4) of the study area can also be seen. This point is characterized with the highest TDS, sulphate, chloride and sodium concentrations observed in the shallow groundwater system (Table 3.2). These elevated concentrations were attributed to the transport of these particular ions from the deeper groundwater to the shallow system. The stable isotope content at this particular point is enriched in heavy isotopes when compared to the ones presented in deep and the middle aquifer systems in the same cross section. This enrichment was concluded to be due to the evaporation effect. Unfortunately, there is no deep well in this downgradient site therefore it is very hard to reach a conclusion. It is impossible to decide on the exact nature of the mixing. There can be another line source recharging this particular point.

Cross section C-C' shows two different flow directions, away from the mound, one being towards NE and the other towards SW (Figure 5.24). The enrichment in the heavy isotopes along flow direction is again observed in NE direction. Towards SE direction, the water- rock interaction increases enormously and Dissolved Inorganic Carbon Content increases in the same manner. Two different points in the middle system show two extremely different stable isotope contents, one showing the affects of upward mixing therefore depleted in heavy isotopes; on the other hand the other shows a similar behavior to the water in the shallow aquifer system.

The existence of the line sources recharging the aquifer are also proven with the limited helium data. The helium results show that there is a remarkable mantle helium component surprisingly in a shallow well. It is known that fracturing is an important transport of mantle helium through fault zones to the upper crust and shallow groundwaters. Commonly, the atmospheric helium component, entering to the aquifer through infiltration, is expected to be the highest in the shallow-level groundwaters. This expectation is satisfied in only one well namely S-16. This well has high dissolved CFC concentration and does not have any chemical anomalies. It does not indicate mixing of shallow and deep groundwater. This confirms the validity of the results and the differences in the helium components of the shallow groundwater system can be

attributed to the existence of a deep buried fault bringing up high amounts of crustal and mantle helium to S-2, S-3, S-9 and S-11.

When the chemical and isotopic data is considered in an integrated manner it can be seen that whole data is in concordance with each other in the shallow aquifer system. This harmony can well be seen in Figure 5.25 and Figure 5.26. These two figures show the changes in the chemistry and isotope data with increasing distance from the recharge area in the shallow aquifer system. It should be stated that the data available is unfortunately not along a single flow path since the points are scattered throughout the area. Therefore Figure 5.25 and Figure 5.26 were drawn along an imaginary flow path in which the data points were projected to this path.

Figure 5.25 shows the change in deuterium content, sulphate, chloride and sodium ions in this imaginary flow path. The sulphate, chloride and sodium ion concentrations in the shallow groundwater system increase around 5 km away from the recharge area accompanied by enrichment in the heavy isotope of hydrogen. About 5.3 km away from the recharge area the increase in various ions is spectacular and the deuterium content did not show any enrichment of the heavy isotopes. When the deuterium change along the flow direction is considered it can be seen that although the deuterium content is more or less constant to some point in the shallow system there is depletion followed by again the same constant value. This depletion is consistent with the chemical data supporting the mixing of deeper groundwater with depleted stable isotope content.

In Figure 5.26, the changes in CFC-11 content, dissolved oxygen, sulphate, chloride and sodium concentrations along the flow direction, with increasing distance from the recharge area are presented along an imaginary flow path for the shallow aquifer system. In this graph, CFC-11 content of the shallow system and dissolved oxygen are in accordance with each other. Furthermore, there is one point, although located relatively upgradient the dissolved oxygen concentration and CFC-11 content is lower than expected. This situation was explained before with the help of helium data. Except for this point, the CFC-11 content decreases near to detection limits towards downgradient, about 5 km away from the recharge area, accompanied with the anomalies in various parameters.

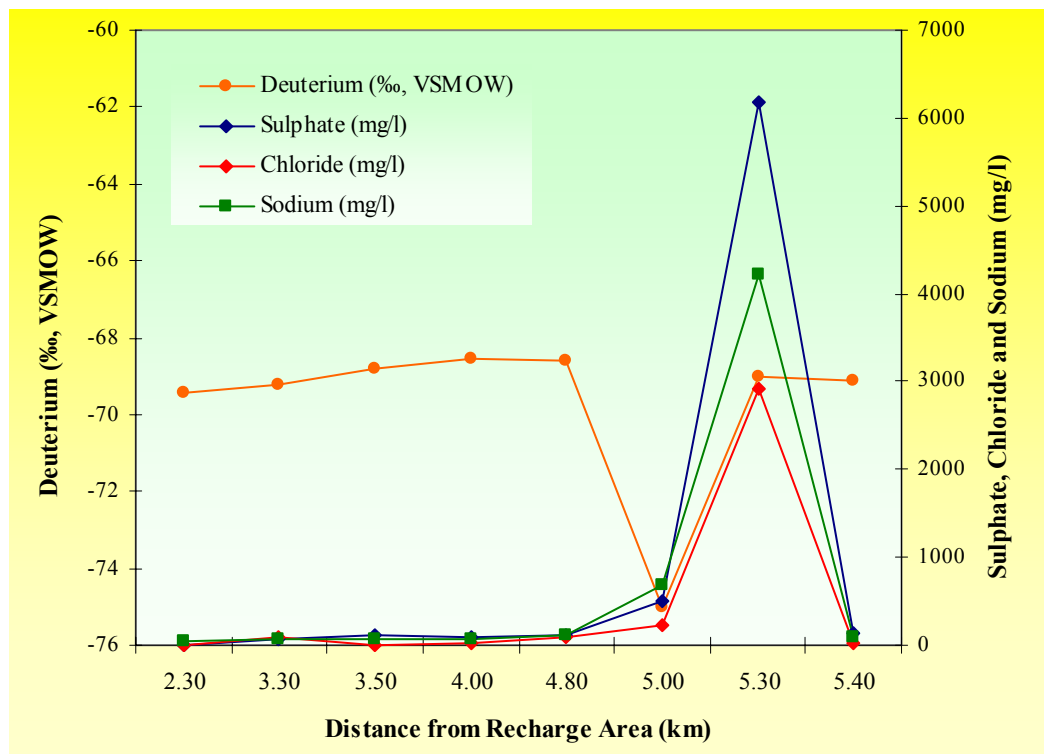


Figure 5.25 Deuterium content, sulphate, chloride and sodium concentration versus distance from the recharge area graph for shallow aquifer system.

Figures 5.25 and 5.26 indicate that the chemical and isotopic data matches each other all pointing the mixing of deeper groundwater to the shallower parts through a deep fault system. This mixing not only changes the chemistry of the groundwater in the shallow system but also affects the isotopic character of the water in those parts of this system. That is obvious that there are two completely different mixing conduits, affecting the chemistry and isotopes in different ways. One mixing system causes depletion in the heavy isotopes together with an increase in chloride, sulphate and sodium concentrations and a decrease in dissolved oxygen and CFC contents in the parts of the shallow system whenever mixing happens through this system. The other mixing outlet doesn't change the stable isotope content however alters the chemistry of the shallow water by increasing the sodium, chloride and sulphate concentrations. This conduit causes a decrease in the dissolved oxygen amounts and CFC contents. It is unfortunate that there isn't any deeper well available at the downgradient part of the shallow groundwater system. However, the

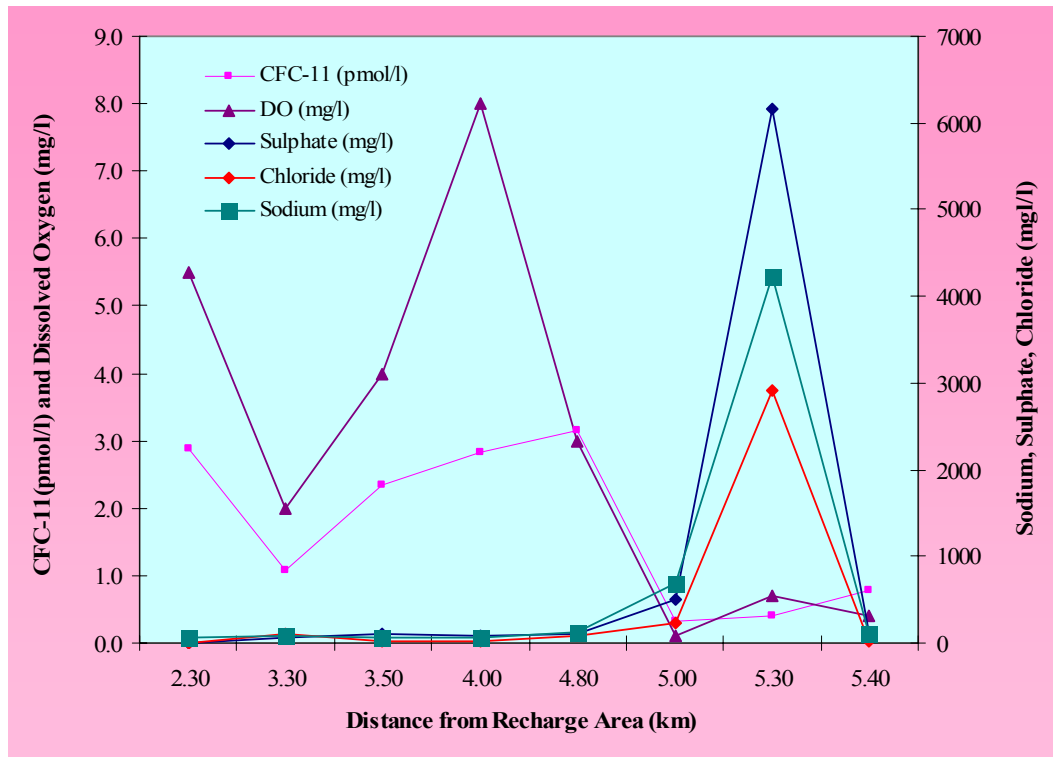


Figure 5.26 CFC-11, Dissolved Oxygen, sulphate, chloride and sodium concentration versus distance from the recharge area graph for shallow aquifer system.

heterogeneity of the system and the existence of various identified and unidentified fractures were proven once again herein with the help of the available isotope data.

The validity of the groundwater budget of the aquifer systems obtained from the calibration of the groundwater model by SRK (2004) can be tested by the stable isotope data. The budget elements presented in Table 3.3 by Yazıcıgil et al. (2007) are multiplied with corresponding oxygen-18 values. These values are selected carefully and presented in Table 5.15.

Assigning an oxygen-18 value to each component in the groundwater budget was not easy as there were uncertainties. According to Table 5.15, the recharge to the shallow aquifer system is from precipitation and from lower Neogene aquitard and from deep

aquifer. From the relationship between oxygen-18 and elevation, it is known that the recharge elevation for the shallow system is around 1100 m. The precipitation in this elevation should have an oxygen-18 value of -9.651‰ from Equation 5.4. Unfortunately, there is no information about the stable isotope content of Neogene aquitard so the stable isotope content of the middle system should be considered. The recharge from lower aquitard if occurs from M-74C then it should have a value of -10.04‰, however if occurs from M-57B then it should have a value of -12.72‰. Therefore the average of these two values can be taken as the value assigned to the oxygen-18 value of the recharge from the Neogene aquitard that is -11.38 ‰. The recharge from the deep aquifer system should have an oxygen-18 value close to -12.78.

The discharge from this shallow system occurs as discharge to Ova Stream and through evapotranspiration. SRK (2004) found that the composition of groundwater discharging to the stream should be similar to the chemical composition of S-3 and S-11, therefore the stable isotope contents of these two wells can be taken as the average oxygen-18 content of the groundwater discharging to the stream. This value is taken to be -9.56 ‰. The groundwater leaving the shallow system with evapotranspiration should have a value similar to the stable isotope content of the shallow wells, therefore an average of the oxygen-18 content of all the shallow wells were assigned as the multiplication coefficient which is -9.29 ‰.

Middle aquifer system recharges from deep aquifer, from lower and upper aquitards. If the recharge from deep aquifer should occur where Akpınar Aquitard does not exist the average oxygen-18 composition of this recharge should be around -12.78‰ (the oxygen-18 of D-57A). Recharge from Akpınar Aquitard should be assigned an oxygen-18 value of -11.55‰ as this aquitard is represented by A-58A2. Recharge from Neogene Aquitard is possible in the outcrop zones; therefore the recharging water should have an oxygen-18 value of -9.72 ‰. This value belongs to well M-65B containing water under unconfined conditions and located near outcrop zone. Discharge from this system is to upper and lower aquitards. The oxygen-18 composition of the discharge to Neogene Aquitard should be around -12.72 ‰ as can be seen in Figure 5.23, and the discharge to Akpınar aquitard is expected to be around -9.72 ‰ as it should be near outcrop zone.

Table 5.15 Groundwater budget of the aquifer systems obtained from the combination of calibration of the groundwater model (Yazıcıgil et al., 2007) and the isotope data.

Hydrogeologic Unit	Recharge	(m ³ /day)	δ ¹⁸ O (‰, VSMOW)	Discharge	(m ³ /day)	δ ¹⁸ O (‰, VSMOW)
Shallow Groundwater System	Precipitation	14,504	-9.651	Discharge to Ova Stream	14,822	-9.56
	Recharge from Lower Aquitard	5,018	-11.38	Springs (SP17, SP20 & SP21)	245	-9.88
	Recharge from Deep Aquifer	5,091	-12.78	Evapotranspiration	4,946	-9.29
				Surface Runoff	4,679	-9.651
Middle Groundwater System	Recharge from Deep Aquifer	3,015	-12.78	Discharge to Upper Aquifer	4,106	-12.72
	Recharge from Lower Aquitard	90	-11.55	Discharge to Lower Aquifer	12	-9.72
	Recharge from Upper Aquitard	994	-9.72			
				Discharge to Shallow Aquifer	5,091	-12.78
Deep Groundwater System	Precipitation	1,022	-10.531	Discharge to Middle Aquifer	3,015	-12.92
				Discharge to Upper Aquitard	1,056	-8.65
				Discharge to Lower Aquitard	14	-11.87
	Subsurface Inflow	9,812	-8.59	Surface Runoff (outcrop area)	671	-10.531
				Wells (K-17 & K-27)	487	-12.7

According to the Yazıcıgil et al. (2007) deep aquifer system receives 25% of its recharge from precipitation along the outcrop zones and the rest from the subsurface inflow. The existence of CFCs in the deep aquifer system proves that this system receives modern recharge however the exact amount can not be determined by using CFCs. Before arguing the accuracy of the amount of modern recharge to the deep system, the turnover time of this aquifer should be calculated. As a result of a rough estimate the reserve of this aquifer should be around $9600 \cdot 10^6 \text{ m}^3$. 25% of modern recharge makes $0.932 \cdot 10^6 \text{ m}^3/\text{year}$ of water entering to the aquifer each year (to simplify the situation subsurface inflow is totally ignored). Accordingly, the turnover time for this aquifer can be calculated as 10300 years. If this calculated turnover time is correct, then it would have

been impossible to sample any groundwater older than 10000 years old. This introduces a question: if this reservoir is completely flushed out with modern recharge in 10000 years how can the estimated radiocarbon ages be older than 10000 years old? The amount of this modern recharge should be evaluated again. If the amount of the modern precipitation is decreased to 10%, then the turnover time of the aquifer will be 26000 years that is a more reasonable estimation. Therefore herein, the modern recharge contribution to the deep system is decreased to 1022 m³/year and the contribution of the subsurface inflow is increased to 9,812 m³/year. This calculation will only be valid if the subsurface inflow does not bring modern groundwater to the deep system. If it is so, the calculations herein should be modified accordingly.

If the above calculations hold true, then the recharge elevation of the deep system should be around 1300 m and the oxygen-18 composition of the precipitation should be around -10.531 ‰ from Equation 5.4. The recharge in the form of subsurface inflow should be from the fault zone. It has been discussed earlier in this section that the oxygen-18 composition of the groundwater brought by the fault zone should be similar to the oxygen-18 composition of D-53; therefore the oxygen-18 composition of this subsurface inflow should be around -8.59‰. Discharge from the deep system is to middle aquifer and to Akpınar and İncirlik Aquitards and from wells. The oxygen-18 composition of the discharge to middle aquifer system should be similar to the one assigned to recharge from deep aquifer. For this reason it should be -12.78‰. Discharge to Akpınar aquitard can be assumed to have an isotopic composition of -8.65 ‰, the oxygen-18 content of D-74B, as from this point there is a direct upward gradient directly to this aquitard. Discharge to İncirlik Aquitard should have oxygen-18 content identical to the one observed in M-74A as this well is located in this aquitard. The wells discharging from this system should also be considered. According to SRK (2004), these wells discharge water flow all water bearing units therefore they should have an average oxygen-18 composition of -11.5‰. This is only estimation and since the water discharging from the wells is not a huge amount this estimation will not make great differences in the overall result.

When the recharge and discharge amounts are multiplied with the corresponding oxygen-18 values, the total discharge and recharge to the whole system can be calculated.

According to this calculation, the total discharges are about 1.9% higher than the total recharges (minus sign is ignored). This difference is most probably can well be due to the uncertainties in oxygen-18 value assigned to various budget components. There can be seasonal variations in the oxygen-18 content therefore the weighted mean values should be used which are indeed not available in this study. However, when overall calculations are considered, the groundwater budget presented in Table 5.15 can well be admitted as valid with the support of the stable isotope data.

After proving the validity of the groundwater budget obtained from the groundwater flow model of Yazıcıgil et al. (2007) there is one another finding that should be mentioned. For the two distinct wells, S-4 and S-9, the chemical anomalies points out existence of a buried fault as stated out by SRK (2004). Under the light of isotope data, there should be two different fault systems bringing water from the deeper parts to these wells. The first system should be related to the very deep line sources passing through S-3 and S-11 also as the helium data indicates although it is not supported by the major ion element data. In the previous sections, the formation of S-9 attributed to mixing of S-5 and D-57A was discussed. When the TDS amount measured in S-9 is considered, the high TDS is diluted by S-5 before reaching to S-9 (please refer to Table 3.1). The fractured system and the upward gradient help this mixing. The upward mixing is proven by the groundwater levels in deep and shallow aquifer systems and the existence of the fracture is proven by the existence of mantle and crustal helium. The other system should somehow affect the chemical composition of S-4 water. If there were a deep well near S-4 it would have been easier to reach further conclusions.

When the overall findings of SRK (2004) are considered, these findings are almost supported by isotope data. They were unable to find any evidence of past climates as they were concentrated on the flow through the whole system. They had no information about the residence times of groundwater inside these three systems. This study can be considered as a supplementary study to the study of SRK in which the available isotope techniques were utilized to a unique area where three complex aquifer systems are present.

CHAPTER 6

CONCLUSIONS

The results presented and discussed lead to the conclusions which will be presented herein.

1. The oxygen-18 and deuterium data showed a strong isotopic contrast between the shallow and deeper aquifer systems and even between the unconfined and confined parts of the middle and deep aquifers. There is approximately -3.3 ‰ depletion in oxygen-18 values and -26 ‰ in deuterium values from shallow to deep groundwater systems.
2. The relationship between oxygen-18 and elevation showed that it is not possible to explain the depletion of oxygen-18 and deuterium in the deeper aquifer systems as in terms of differences in recharge elevation the highest elevation in the area is not as high as the elevation corresponding to the depletion amount in heavy isotopes.
3. The Noble Gas Temperatures indicated the average yearly air temperatures in shallow aquifer system whereas the recharge temperatures came out to be around 4 °C lower than today's temperatures in two samples from deep groundwater system. This finding is also supported by the radiocarbon activities being close to the detection limits in those wells. These activities together with the stable isotope data showed that there might be evidence of recharge to the middle and deep aquifer systems under different climatic conditions, probably colder than present time.
4. Carbon-13 and extremely high dissolved inorganic carbon content data showed that there is extensive water-rock interaction in the deep aquifer system and there

is evolution of carbon-13 together with this interaction. Carbon-13 mixing method was utilized to correct the radiocarbon ages, affected by this interaction. The estimated radiocarbon ages came out to be around modern for a well located near recharge zone and up to 35000 years BP in the middle and deep aquifer systems.

5. Chlorofluorocarbon (CFC-11, CFC-12 and CFC-113) concentrations are high in the shallow aquifer system, indicating modern recharge, except for three points: S-4- S-9 and S-11 which came out to be very close to the detection limits just like the ones from the deep aquifer system. The CFC recharge years were calculated to be changing between 1987 and 1963 for the shallow aquifer system. The areal distribution of CFC's in the shallow aquifer system increases in the direction of flow, being highest in the most questionable wells: S-4, S-9 and S-11.
6. CFC concentrations were low in the deep system and the calculated CFC recharge years were between 1960 and before 1953. The existence of measurable amounts of CFCs in this system indicated modern recharge to the deep aquifer system.
7. The approximate hydraulic ages were calculated for two points in the deep aquifer system. According to the calculations, the water entering to the system from the recharge area will travel 1.7 km in 1.35 years if it passes through the high conductivity parts and in 1348 years if it travels through low conductivity zones. The time required for the water to reach 3.7 km away from the recharge area is only one year if this water travels through the fractured parts and if it travels through the matrix rock then 1.47 million years is required.
8. Helium components calculated by using the helium, helium-3/helium-4 ratio and neon data indicated that there is mantle-He component present in the shallow aquifer system. Mantle-He component is the highest in S-11, believed to be transported by a deep buried fault. The existence of this fault bringing water to

the wells S-3, S-9 and S-11 was demonstrated by the presence of mantle-He, whose escape to the surface was controlled by this fault system.

9. The groundwater mixing taking place between the aquifer systems were also revealed out by the help of stable isotopes. M-74C water composition was proven to be formed by 64.3% of D-74B groundwater and 35.7% of M-60B groundwater composition according to oxygen-18 data.
10. Different deuterium excess values lead to a conclusion that the general cooling during the Last Pleistocene age, proven by NGT's, should be accompanied by a change in source of water vapor recharging the aquifer and the groundwaters with different deuterium excesses should have formed. The deuterium excess values indicated different meteoric water lines, shifted from GMWL.
11. The groundwater budget prepared by Yazıcıgil et al. (2007) was checked by oxygen-18 data. Approximately 1.8% difference observed between discharges and recharges to the aquifer systems. However, in general, the budget components by Yazıcıgil et al. (2007) are consistent with the isotope data.

REFERENCES

- Aeschbach-Hertig, W., Peeters, F., Beyerle, U., and Kipfer, R., 1999, Interpretation of dissolved atmospheric noble gases in natural waters, *Water Resources Research*, 35 (9), 2779-2792.
- Aeschbach-Hertig, W., Schlosser, P., Stute, M., Simpson, H. J., Ludin, A., Clark, J. F., 1998, A $^3\text{H}/^3\text{He}$ Study of Ground Water Flow in a Fractured Bedrock Aquifer, *Ground Water*, 36 (4), 661-670.
- Aeschbach-Hertig, W., Stute, M., Clark, F.C., Reuter, R.F., Schlosser, P., 2002, A Paleotemperature Record Derived from Dissolved Noble Gases in Groundwater of the Aquia Aquifer (Maryland, USA), *Geochimica et Cosmochimica Acta*, 66 (5), 797-817.
- AFEAS, 1997, Production, Sales and Atmospheric Release of Fluorocarbons through 1995, Alternative Fluorocarbons Environmental Acceptability Study Program Office, Washington, DC, USA.
- Andrews, J.N., 1985, The Isotopic Composition of Radiogenic Helium and its Use to Study Groundwater Movement in Confined Aquifers, *Chemical Geology*, 49, 339-351.
- Andrews, J.N. and Lee D.J., 1979, Inert gases in groundwater from the Bunter Sandstone of England as indicators of age and palaeoclimatic trends, *Journal of Hydrology*, 41, 233-252.
- Apaydın, A. ,2004, Çakıloba- Karadoruk Akifer Sisteminin (Beypazarı Batısı- Ankara) Beslenme Koşullarının Araştırılması, Hacettepe Üniversitesi Fen Bilimleri Enstitüsü, Doktora Tezi, yayınlanmamış, p 147.
- ASTM D 5543-94, 1999, Low Level Dissolved Oxygen in Water, Test Method A.
- Ballentine C.J., and Hall, C.M., 1999, Determining palaeotemperature and other variables by using an error-weighted, nonlinear inversion of noble gas concentrations in water, *Geochimica et Cosmochimica Acta*, 63 (16), 2315-2336.

- Barka, A. A., 1984, Geology and Tectonic Evolution of Some Neogene-Quaternary Basins in the North Anatolian Fault Zone, Proceedings of Ketin Symposium, TJK, Ankara.
- Barka, A.A., and Gülen, L., 1988, New Constraints on Age and Total Offset of the North Anatolian Fault Zone: Implications for Tectonics of the Eastern Mediterranean Region, METU Journal of Pure and Applied Sciences, 21, 1-3, 39-63.
- Bayarı, C.S., Özyurt, N.N., Kilani, S., 2005, Konya Kapalı Havzası Yeraltısularında Karbon-14 Yaş Dağılımı, II. Ulusal Hidrolojide İzotop Teknikleri Sempozyumu Bildiri Kitabı, İzmir, .147-164.
- Begemann, F., Libby, F.W. ,1957, Continental Water Balance, Groundwater Inventory and Storage Times, Surface Ocean Mixing Rates, and Worldwide Water Circulation Patterns from Cosmic Ray and Bomb Tritium, Geochimica et Cosmochimica Acta, 12, 227-296.
- Benson, B.B., and Krause D. Jr., 1976, Empirical Laws for Dilute Aqueous Solutions of Nonpolar Gases, Journal of Chemical Physics, 64, 689- 709.
- Bu, X. and Warner, M.J., 1995, Solubility of Chlorofluorocarbon 113 in Water and Seawater, Deep-Sea Research, 42 (7), 1151- 1161.
- Bullister, J. L., 1984, Atmospheric Chlorofluoromethanes as Tracers of Ocean Circulation and Mixing: Studies in the Greenland and Norwegian Seas, Ph.D. Dissertation, unpublished, University of California, San Diego, La Jolla, p 172.
- Bullister, J. L., and Weiss, R. F., 1988, Determination of CFC₃F and CCl₂F₂ in Seawater and Air, Deep Sea Research, 35, 839-854.
- Busenberg, E. and Plummer, L. Niel, 1992, Use of Chlorofluorocarbons (CCl₃F and CCl₂F₂) as Hydrologic Tracers and Age-Dating Tools: The Alluvium and Terrace System of Central Oklahoma, Water Resources Research, 28 (9), 2257-2283.
- Busenberg, E., Weeks, E.P., Plummer, N.L., and Bartholomay, R.C., 1993, Age Dating Groundwater by Use Chlorofluorocarbons (CCl₃F and CCl₂F₂), and the Distribution of Chlorofluorocarbons in the Unsaturated Zone, Snake River Plain Aquifer. Idaho National Engineering Laboratory, Idaho, U.S. Geological Survey, Water Resources Investigation Report No. 93-4054, p 47.

- Busenberg E., and Plummer, L.N., 2000, Dating Young Ground Water with Sulfur Hexafluoride: Natural and Anthropogenic Sources of Sulfur Hexafluoride, *Water Resources Research*, 36 (10), 3011-3030.
- Clark, I., and Fritz, P., 1997, *Environmental Isotopes in Hydrogeology*, Lewis Publishers, CRC Press, Florida, p 328.
- Clarke, W.B., Jenkins, W.J., Top, Z., 1976, Determination of Tritium by Mass Spectrometric Measurement of ^3He , *International Journal of Applied Radiation Isotopes*, 27, 515- 522.
- Coplen, T.B., Herczeg, A.L., and Barnes, C., 2000, Isotope Engineering- Using Stable Isotopes of the Water Molecule to Solve Practical Problems, In *Environmental Tracers in Subsurface Hydrology*, Edited by Peter G. Cook and Andrew L. Herczeg, Kluwer Academic Publishers, Boston, 79-110.
- Cook, P.G., Solomon, D.K., Plummer, L.N., Busenberg, E., and Schiff, S.L., 1995, Chlorofluorocarbons as Tracers of Groundwater Transport Processes in a Shallow, Silty Sand Aquifer, *Water Resources Research*, 31 (3), 424-434.
- Cook, P.G., Solomon, D.K., 1997, Recent Advances in Dating Young Groundwater: Chlorofluorocarbons, $^3\text{H}/^3\text{He}$ and ^{85}Kr , *Journal of Hydrology*, 191, 245-265.
- Craig, H. 1961b, Isotopic Variations in Meteoric Waters, *Science*, 133, 1702-1703.
- Çakır, B., Bayarı, C.S., Tezcan, L., Özyurt, N.N., 1999, Kloroflorokarbonlar ile yeraltısuyu yaşının belirlenmesi: 3- Beydağları (Finike) karstik akiferi kaynaklarında uygulama, *Yerbilimleri Hacettepe Üniversitesi, Yerbilimleri Uygulama ve Araştırma Merkezi Yayını*, 21, 91-103
- Çamur, M. Z., Er, C., Yazıcıgil, H., 2007, Modeling of Lithology Induced Chemical Anomalies in the Aquifer Systems of the Kazan Trona Deposit Area, Ankara, Turkey, *Environmental Geology*, Published Online.
- Çetin, B., Unç, E., Uyar, G., 2002, The Moss Flora of Ankara- Kızılcahamam- Çamkoru and Çamlidere Districts, *Turkish Journal of Botany*, 26, 91- 101.
- Damon, P.E., Cheng, S., and Linick, T.W., 1989, Fine and Hyperfine Structure in the Spectrum of Secular Variations of Atmospheric ^{14}C , *Radiocarbon*, 31, 704- 718.

- Dansgaard, W., 1964, Stable Isotopes in Precipitation, *Tellus*, 16, 436- 468.
- Denovan, B.A., and Strand, S.E., 1992, Biological Degradation of Chlorofluorocarbons in Anaerobic Environments, *Chemosphere*, 24, 935- 940.
- Drimmie, R.J., Aravena, R., and Wassenaar, L.I., Fritz, P., Hendry, M.J., Hut, G., 1991, Radiocarbon and Stable Isotopes in Water and Dissolved Constituents, Milk River Aquifer, Alberta, Canada, *Applied Geochemistry*, 6 (4), 381-392.
- Drimmie, R.J., Shouakar-Stash, O., Walters, R., Heemskerk, A.R., 2001a, Hydrogen Isotope Ratio by Automatic, Continuous Flow, Elemental Analyses, and Isotope Ratio Mass Spectrometry, Technical Procedure 4.1 Rev 00 8 pages, Environmental Isotope Laboratory, Department of Earth Sciences, University of Waterloo.
- Drimmie, R.J. and Heemskerk, A.R. 2001b, Stable Oxygen Isotope Ratios by Carbon Dioxide Equilibration Automatic, Continuous Flow, Isotope Ratio Mass Spectrometry, Technical Procedure 13.1 Rev 00 7 pages, Environmental Isotope Laboratory, Department of Earth Sciences, University of Waterloo.
- DSİ, 1976, Hydrogeological Investigation Report for Mürted Plain, Ankara, Turkey, DSİ Genel Müdürlüğü, Ankara, Turkey.
- Dunkle, S.E.A., Plummer, L.N., Busenberg, E., Phillips, A.P.P., Denver, J.M., Hamilton, P.A., Michel, R.L., and Coplen, T.B., 1993, Chlorofluorocarbons (CCl₃F and CCl₂F₂) as Dating Tools and Hydrologic Tracers in Shallow Groundwater of the Delmarva Peninsula, Atlantic Coastal Plain, United States, *Water Resources Research*, 29 (12), 3837-3860.
- Ehleringer, J.R., Sage, R.F., Flanagan, L.B., and Pearcy, R., 1991, Climate Change and the Evolution of C₄ Photosynthesis, *Trends in Ecology and Evolution*, 6, 95- 99.
- Ekwurzel, B., Schlosser, P., Smethie, W.M., Plummer, L.N., Busenberg, E., Michel, R.L., Weppernig, R., and Stute, M., 1994, Dating of Shallow Groundwater: Comparison of the Transient Tracers ³H/ ³He, Chlorofluorocarbons, and ⁸⁵Kr, *Water Resources Research*, 30 (6), 1693-1708.
- Elkins, J.W., Thompson, T.M., Swanson, T.H., Butler, J.H., Hall, B.D., Cummings, S.O., Fisher D.A. and Raffo, A.G., 1993, Decrease in the Growth Rates of Atmospheric Chlorofluorocarbons 11 and 12, *Nature*, 364, 780-783.

- Elkins, J.W.(ed.), Butler, J.H., Thompson, T.M., Montzka, S.A., Myers, R.C., Lobert, J.M., Yvon, S.A., Wamsley, P.R., Moore, F.L., Gilligan, J.M., Hurst, D.F., Clarke, A.D., Swanson, T.H., Volk, C.M., Lock, L.T., Geller, L.S., Dutton, G.S., Dunn, R.M., Dicorleto, M.F., Baring, T.J., and Hayden, A.H., 1996, Nitrous Oxide and Halocompounds, Climate Monitoring and Diagnostics Laboratory No:23, Summary Report 1994-1995, eds. D.J. Hoffman, J.T. Peterson, and R.M. Rosson, U.S. Department of Commerce, NOAA Environmental Research Laboratories, 84-111.
- Elçi, B, Erik, S: Flora of Kirmir Valley (Güdül, Ankara), 2005, Turkish Journal of Botany, 29, 435- 461.
- Erol, O., 1960, Ankara Bolgesinin Hidrojeolojik Durumu, Rapor No.559, DSİ Jeoteknik Hizmetler ve Yeraltisuyu Dairesi Baskanligi, Ankara.
- Fisher, D.A., and Midgley, P.M., 1993, Production and Release to the Atmosphere of CFCs 113, 114, and 115, Atmospheric Environment, 27A, 271-276.
- Fontes, J.C., Garnier, J.M., 1979, Determination of the initial ¹⁴C activity of the total dissolved carbon, A review of the existing models and a new approach, Water Resources Research, 15, 399- 413.
- Fontes, J.C., Stute, M., Schlosser, P., and Broecker, W.S., 1993, Aquifers as Archives of Paleoclimate, EOS 74, 21-22.
- Fraser, P., Cunold, D., Alyea, F., Weiss, R., Prinn, R., Simmonds, P., Miller, B., and Langenfelds, R., 1996, Lifetime and Emission Estimates of 1,1,2-trichlorotrifluorethane (CFC-113) from Daily Global Background Observations June 1982- June 1994, Journal of Geophysical Research, 101 (D7), 12585-12599.
- Genç, Y., 2006, Genesis of the Neogene Interstratal Karst-type Pöhrenk Fluorite- Barite (±lead) Deposit (Kırşehir, Central Anatolia, Turkey), Ore Geology Reviews, 29, 105-117.
- Gilbert, T.W., Behymer, T.D., Castaneda, H.B., 1982, Determination of Dissolved Oxygen in Natural and Wastewaters”, American Laboratory, 119-134.

- Gooddy, D.C., Darling, W.G., Abesser, C., and Lapworth, D.J., 2006, Use of Chlorofluorocarbons (CFCs) and Sulphur Hexafluoride (SF₆) to Characterize Groundwater Movement and Residence Time in a Lowland Chalk Catchment. *Journal of Hydrology*, Volume 330, Issues 1-2, 44-52.
- Hancock, P. L. and Barka, A. A., 1983, Tectonic Interpretations of Enigmatic Structures in the North Anatolian Fault Zone, *Journal of Structural Geology*, 5, 217-220.
- Hayes J.M. and Thompson G.M., 1977, Trichlorofluoromethane in Groundwater - A Possible Indicator of Groundwater Age, Water Resources Research Center, Technical Report 90, Purdue University, NTIS Report PB 265 170, p 25.
- Heaton, T.H.E., and Vogel, J.C., 1981, 'Excess Air' in Groundwater, *Journal of Hydrology*, 50, 201- 216.
- Herzberg, O. and Mazor, E., 1979, Hydrological Applications of Noble Gases and Temperatures Measurements in Underground Water Systems: Examples from Israel, *Journal of Hydrology*, 41, 217- 231.
- Ho, D.T., Schlosser, P., 2000, Atmospheric SF₆ near a large area, *Geophysical Research Letters*, 27 (11), 1679-1682.
- Hydrolab, 1994, Operating Manual for Data Sonde 3 Multiparameter Water Quality Probe, Hydrolab Corp, Austin, Texas 78763, p 47.
- IAEA/WMO, 2004, Global Network of Isotopes in Precipitation, The GNIP Database (Online), <http://isohis.iaea.org>, last accessed: 1 February, 2008.
- Imbach, T., 1997, Geology of Mount Uludağ with Emphasis on the Genesis of the Bursa Thermal Waters, Northwest Anatolia, Turkey, In: C. Schindler and M. Pfister (editors), *Active Tectonics of Northwestern Anatolia – the Marmara Poly-Project*. Vdf Hochschulverlag AG an der ETH Zurich, 239-266.
- Kalin, R.M., 2000, Radiocarbon Dating of Groundwater Systems, In *Environmental Tracers in Subsurface Hydrology*, Edited by Peter G. Cook and Andrew L. Herczeg, Kluwer Academic Press, Boston, p 111-144.
- Kattan Z., 2001, Use of Hydrochemistry and Environmental Isotopes for Evaluation of Groundwater in the Paleogene Limestone Aquifer of the Ras Al-Ain Area (Syrian Jezireh), *Environmental Geology*, 41, 128-144.

- Katz B.G., Lee, T.M., Plummer, L.N., and Busenberg, E., 1995, Chemical Evolution of Groundwater near a Sinkhole Lake, Northern Florida, 1. Flow Patterns, Age of Groundwater, and Influence of Lake water Leakage, *Water Resources Research*, 31 (6) 1549- 1564.
- Katz, B.G., 2004, Sources of Nitrate Contamination and Age of Water in Large Karstic Springs of Florida. *Environmental Geology*, 46, 689-706.
- Kazancı, N., and Gökten, E., 1988, Lithofacies Features and Tectonic Environment of the Continental Paleocene Volcanoclastics in Ankara Region, *METU Journal of Pure and Applied Sciences*, 21, 1-3, 271-282.
- Kazemi, G.A., 1999, Groundwater Factors in the Management of Dryland and Stream Salinity in the Upper Macquarie Valley, New South Wales, Australia, unpublished Ph.D. Thesis, University of Technology, Sydney, Australia, p 252.
- Kazemi, G.A., Lehr, J. H., and Perrochet, P., 2006, *Groundwater Age*, John Wiley and Sons, Inc., Hoboken, New Jersey, p 325.
- Koçyiğit, A. and Lünel, A.T., 1987, Geology and Tectonic Setting of Alcı Region, Ankara, *METU Journal of Pure and Applied Sciences*, 20, 1, 35-57.
- Koçyiğit, A., Özkan, S., and Rojay, B., 1988, Examples from Fore-arc Basin Remnants of the Active Margin of Northern Neo-Tethys: Development and Emplacement Ages of the Anatolian Nappes, Turkey, *METU Journal of Pure and Applied Sciences*, 21, 1-3, 183-210.
- Koçyiğit, A., 1991a, An Example of an Accretionary Forearc Basin from Northern Central Anatolia and its Implications for the History of Subduction of Neo-Tethys in Turkey, *Geological Society America Bulletin*, 103, 22-36.
- Lesage, S., Brown, S., Hoster, K.R., 1992, Degradation of Chlorofluorocarbon-113 under Anaerobic Conditions, *Chemosphere*, 24, 1225- 1243.
- Libby, W.F., 1955, *Radiocarbon dating*, 2nd Edition, University of Chicago Press, Chicago.

- Lovley, D.R., and Wodward, J.C., 1992, Consumption of Freons CFC-11 and CFC-12 by Anaerobic Sediments and Soils, *Environmental Science and Technology*, 26, 925- 929.
- Mahlknecht, J., Gárfias-Solis, J., Aravena, R., and Tesch, R., 2006, Geochemical and Isotopic Investigations on Groundwater Residence Time and Flow in the Independence Basin, Mexico, *Journal of Hydrology*, 324, 1-4, 283-300.
- Mamyrin, B.A., Tolstikhin, I.N., 1984, *Helium Isotopes in Nature*, Elsevier, Amsterdam, Oxford, New York, Tokyo.
- Mazor, E., 1972, Paleotemperatures and Other Hydrological Parameters Deduced from Noble Gases Dissolved in Groundwaters, Jordal Rift Valley Israel, *Geochimica and Cosmochim. Acta* 36, 1321-1336.
- Mensch, M., Smethie, W.M., Schlosser, P., Weppernig, R., and Bayer, R., 1998, Transient Tracer Observations from the Western Weddell Sea During the Drift and Recovery of Ice Station Weddell, Ocean, ice and atmosphere: interactions at the Antarctic continental margin, Editors Jacobs S.S., Weiss, R., American Geophysical Union, Washington, DC, 75, 241- 256.
- Modica, E., Buxton, H.T., and Plummer, L.N., 1998, Evaluating the source and residence times of the groundwater seepage to streams, New Jersey Coastal Plain, *Water Resources Research*, 34, 2797- 2810.
- Nativ, R., Günay, G., Hötzl, H., Reichert, B., Solomon, D.K., Tezcan, L., 1999, Separation of groundwater-flow components in a karstified aquifer using environmental tracers, *Applied Geochemistry*, 14, 1001-1014.
- Oğuz, D., 2003, Remaining tree species from the indigenous vegetation of Ankara, Turkey, *Landscape and Urban Planning*, 68, 371- 388.
- O'Leary, M.H., 1988, Carbon Isotopes in Photosynthesis, *Bioscience*, 38, 238.
- Oster, H., Sonntag, C., and Münnich, K.O., 1996, Groundwater Age Dating with Chlorofluorocarbons, *Water Resources Research*, 32, 2989-3001.
- Ozima, M. and Podosek, F.A., 1983, *Noble Gas Geochemistry*, Cambridge University Press, Cambridge, p 367.

- Öztürk, A., İnan, S. and Tutkun, Z., 1985, Abant-Yeniçağa (Bolu) Bölgesinin Tektoniği, C.Ü. Mühendislik Fakültesi Dergisi, 2 (1) 35-52.
- Özyurt, N.N., 2005, Aladağ (Kayseri- Adana) Karstik Akiferinde Yeraltısuyu Geçiş Zamanı Dağılımının İncelenmesi, Hacettepe Üniversitesi Fen Bilimleri Enstitüsü, unpublished PhD thesis, p. 274.
- Özyurt, N.N., ve Bayarı, C.S., 1998, Kloroflorokarbonlar ile Yeraltısuyu Yaşının Belirlenmesi: 2- Aladağlar Karstik Akiferi Kaynakları, Yerbilimleri, Hacettepe Üniversitesi, Yerbilimleri Uygulama ve Araştırma Merkezi Yayını, 20, 139-154.
- Özyurt, N.N. ve Bayarı, C.S., 1999, Aladağ (Yahyalı- Kayseri) akiferinde fiziksel, kimyasal ve izotopik parametreler ile kloroflorokarbon yaşları arasında ilişkiler, Türkiye Jeoloji Bülteni, 42, 1, 97- 103.
- Pearson, F.J., 1965, Use of C-13/C-12 Ratios to Correct Radiocarbon Ages of Material Initially Diluted by Limestone, Proceedings of the 6th International Conference on Radiocarbon and Tritium Dating, Pulman, Washington, p 357.
- Pearson, F.J., and Hanshaw, B.B., 1970, Sources of Dissolved Carbonate Species in Groundwater and Their Effects on Carbon-14 Dating, Isotope Hydrology 1970, IAEA Symposium 129, Vienna, 271- 286.
- Phillips F.M., 1981, Noble Gases in Ground Water as Palaeoclimatic Indicators, unpublished Ph.D. thesis, University of Arizona.
- Plummer L.N., Busenberg E., Drenkard S., Schlosser P., McConnell J.B., Michel R.L., Ekwurzel B. and Weppernig R., 1998b, Flow of River Water into A Karstic Limestone Aquifer, Dating the Young Fraction in Groundwater Mixtures in the Upper Floridan Aquifer Near Valdosta, Georgia, Applied Geochemistry, 13-8-, 1017-1043
- Plummer, L.N. and Busenberg, E., 2000, Chlorofluorocarbons, In Environmental Tracers in Subsurface Hydrology, Edited by Peter G. Cook and Andrew L. Herczeg, Kluwer Academic Publishers, Boston, p 441-478.
- Plummer, L.N., Busenberg, E., Bohlke, J.K., Nelms, D.L., Michel, R.L., and Schlosser, P., 2001, Groundwater Residence Times in Shenandoah National Park, Blue Ridge Mountains, Virginia, USA: A Multi-Tracer Approach. Chemical Geology, 179, 93-111.

- Plummer, L.N., Prestemon, E.C., Parkhurst, D., 1994, An interactive code (NETPATH) for modeling net geochemical reactions along a flowpath: Version 2.0. U.S. Geological Survey Water- Resources Investigations Report 94- 4169, p 130.
- Poreda, R.J., Cerling, T.E., Solomon, D.K., 1988, Tritium and Helium Isotopes as Hydrologic Tracers in a Shallow Unconfined Aquifer, *Journal of Hydrology*, 103 (1), 1-9.
- Randall J.H. and Schultz T.R., 1976, Chlorofluorocarbons as Hydrologic Tracers: A New Technology, *Hydrology Water Resources Arizona Southwest*, 6, 189-195.
- Randall J.H., Schultz T.R. and Davis S.N., 1977, Suitability of Fluorocarbons as Tracers in Ground Water Resources Evaluation, Technical Report to Office of Water Research and Technology, U.S. Department of the Interior, NTIS PB 277 488, p 37.
- Rhodazine D method, ASTM Power Plant Manual, 1st ed., p.169.
- Rojay, B., Toprak, V., and Bozukrt, E., 2002, Core Sample Analysis in Kazan soda project area, Ankara, Turkey, Middle East Technical University.
- Rozanski, K., 1985, Deuterium and Oxygen-18 in European Groundwaters- links to Atmospheric Circulation in the Past, *Chemical Geology, Isotope Geoscience Section*, 52, 349-363.
- Rozanski, K., Araguas-Araguas, L. and Gonfiantini, R., 1993, Isotopic Patterns in Modern Global Precipitation, *Climate Change in Continental Isotopic Records*, P.K. Swart, K.C. Lohmann, J.McKenzie, and S. Savin, Editors, Geophysical Monograph 78, American Geophysical Union, 1-36.
- Rudolph, J., Rath, H.K., and Sonntag, C., 1984, Noble gases and stable isotopes in ¹⁴C-dated palaeowaters from central Europe and the Sahara, *Isotope Hydrology*, IAEA, Vienna, 467-477:
- Russel A.D. and Thompson G.M., 1983, Mechanism Leading to Enrichment of the Atmospheric Fluorocarbons CCl₃F and CCl₂F₂ in Groundwater, *Water Resources Research*, 19 (1) 57-60.

- Schlosser, P., Stute, M., Horr, C., Sonntag, C., and Munnich, K. O., 1988, Tritium/³He Dating of Shallow Groundwater, *Earth and Planetary Science Letters*, 89, 352-363.
- Schlosser, P., Stute, M., Sonntag, C., Munnich, K. O., 1989, Tritiogenic ³He in Shallow Groundwater, *Earth and Planetary Science Letters*, 94, 245- 254.
- Schultz T.R., Randall J.H., Wilson L.G. and Davis S.N., 1976, Tracing Sewage Effluent Recharge- Tucson, Arizona, *Ground Water*, 14, 463-470.
- Schultz T.R. ,1979, Trichlorofluoromethane as a Groundwater Tracer for Finite-state Models, Ph.D. Dissertation, University of Arizona, unpublished.
- Shapiro, S.D., Schlosser, P., Smethie, W.M. Jr., Stute, M., 1997, The Use of ³H and Tritiogenic ³He to Determine CFC Degradation and Vertical Mixing Rates in Framvaren Fjord, Norway, *Marine Chemistry*, 59, 141- 157.
- Solomon D.K., Hunt, A., Poreda, R.J., 1996, Sources of Radiogenic Helium 4 in Shallow Aquifers: Implications for Dating Young Groundwater, *Water Resources Research*, 32 (6) 1805-1813.
- SRK, 2001, Hydrogeology, Conceptual Understanding, Kazan Trona Project Ankara, Turkey.
- SRK, 2004, Hydrogeological Modeling Kazan Trona Project, Ankara, Turkey.
- Stute, M., Clark J.F., Schlosser P., Broecker W. S., 1995, A 30,000 Year Continental Paleotemperature Record Derived from Noble Gases Dissolved in Groundwater from the San Juan Basin, New Mexico, *Quaternary Research*, 43, 209-220.
- Stute, M., Deak, J., 1989, Environmental Isotope Study (¹⁴C, ¹³C, ¹⁸O, D, noble gases) on Deep Groundwater Circulation Systems in Hungary with Reference to Paleoclimate, *Radiocarbon*, 31 (3) 902- 918.
- Stute, M., Forster, M., Frischkorn, H., Serejo, A., Clark, J.F., Schlosser, P., Broecker, W.S., and Bonani, G., 1995a, Cooling of tropical Brazil (5°C) during the last glacial maximum, *Science*, 269, 379- 383.

- Stute, M., Schlosser, P., Clark, J.F., and Broecker, W.S., 1992, Paleotemperatures in the Southwestern United States Derived from Noble Gas Measurements in Groundwater, *Science*, 256, 1000-1003.
- Stute, M., and Schlosser, P., 1993, Principles and Applications of the Noble Gas Paleothermometer, *AGU Monograph on Climate Change in Continental Isotopic Records*, Geophysical Monograph, 78, 89-100.
- Stute, M and Schlosser, P., 2000, Atmospheric Noble Gases, In *Environmental Tracers in Subsurface Hydrology*, Edited by Peter G. Cook and Andrew L. Herczeg, Kluwer Academic Publishers, Boston, p 349-377.
- Szabo, Z., Rice, D.E., Plummer, L.N., Busenberg, E., Drenkard, S., and Schlosser, P., 1996, Age Dating of Shallow Groundwater with Chlorofluorocarbons, tritium/helium-3, and Flow Path Analysis, *Southern New Jersey Coastal Plain, Water Resources Research*, 32, 1023-1038.
- Şengör, A.M.C., Yılmaz, Y., 1981, Tethyan Evolution of Turkey: A Plate Tectonic Approach, *Tectonophysics*, 75, 181-241.
- Şengör, A.M.C., 1984, The Cimmeride Orogenic System and the Tectonics of Eurasia, *Geological Society of America Special Paper*, 195, p 82.
- Tamers, M.A., 1975, Validity of radiocarbon dates on groundwater, *Geophysical Surveys*, 2, 217- 239.
- Thompson G.M., Hayes J.M. and Davis S.N., 1974, Fluorocarbon Tracers in Hydrology, *Geophysical. Research Letters*, 1, 177-180.
- Thompson G.M., 1976, Trichloromethane: A New Hydrologic Tool for Tracing and Dating Groundwater. Ph.D. Dissertation, Department of Geology, Indiana University, Bloomington, Indiana, p 93.
- Thompson G.M. and Hayes J.M., 1979, Trichlorofluoromethane in Groundwater: A Possible Tracer and Indicator of Groundwater Age, *Water Resources Research*, 15 (3), 546-554.

- Tokay, M., 1973, Kuzey Anadolu Fay Zonunun Gerece ile Ilgaz Arasındaki Kisminda Jeolojik Gözlemler, Symposium on the North Anatolian Fault and Earthquake Belt, MTA, Ankara, 12-29.
- Tokay, M., 1982, Recently Active Breaks along the North Anatolian Fault Zone between Gerece and Ilgaz, Multidisciplinary Approach to Earthquake Prediction, Editors Işıkara, A.M., and Vogel, A., Wiesbaden, Friedrich, Vieweg and Sohn., 173-184.
- Tolstikhin, I.N., and Kamensky, I.L., 1969, Determination of Groundwater Age by the Tritium-³He method, *Geochemistry International*, 6, 810-811.
- Tominaga, T., 1992, Chlorofluorocarbons in the Atmosphere, Trends and Vertical Profiles, *Pure Applied Chemistry*, 64, 529- 536.
- Toprak, V., and Rojay, B., 2000, Geology Baseline Study for the Kazan Soda Project Area, Ankara, Turkey, Middle East Technical University.
- Toprak, V., and Rojay, B., 2001, Geological Investigation in Kazan Soda Project Area, Ankara, Turkey, Middle East Technical University.
- Verniani, F., 1966, Total Mass of the Atmosphere, *Journal of Geophysical Research*, 71, 835-891.
- Vogel, J.C., 1967, Investigation of groundwater flow with radiocarbon, *Isotopes in Hydrology*, International Atomic Energy Agency, Vienna, p. 255- 368.
- Vogel, J.C., 1970, Carbon-14 dating of groundwater, *Isotope Hydrology 1970*, IAEA Symposium 129, Vienna, 225- 239.
- Vogel, J.C., 1993, Variability of Carbon Isotope Fractionation During Photosynthesis, *Stable Isotopes and Plant Carbon- Water Relations*, Editors J.R. Ehleringer, A.E. Hall and G.D. Farquhar, Academic Press, San Diego, CA, 29- 38.
- Von Buttlar, H., 1959. Groundwater Studies in New Mexico Using Tritium as a Tracer, II, *Journal of Geophysical Research*, 64: 1031-1038.
- Warner, M.J., and Weiss, R.F., 1985, Solubilities of Chlorofluorocarbons 11 and 12 in Water and Seawater, *Deep-Sea Research*, 32, p. 1485- 1497.

- Weiss, R.F., 1970, The Solubility of Nitrogen, Oxygen and Argon in Water and Seawater, *Deep-Sea Research*, 17, 721-735.
- Weiss, R.F., 1971, Solubility of Helium and Neon in Water and Seawater, *Journal of Chemical and Engineering Data*, 16, 235-241.
- Weiss R.F., and Price, B.A., 1980, Nitrous oxide Solubility in Water and Seawater, *Marine Chemistry*, 8, 347- 359.
- Weissman, G.S., Zhang, Y., Labolle, E.M., and Fogg, G.E., 2002, Dispersion of groundwater age in an alluvial aquifer system, *Water Resources Research*, 38, 10, 1198.
- Wisegarver, D.P., and Gammon, R.H., 1988, A New Transient Tracer: Measured Vertical Distribution of $\text{CCl}_2\text{FCClF}_2$ (F-113) in the North Atlantic Subarctic Gyre, *Geophysical Research Letters*, 15, 188- 191.
- Woods Hole Oceanographic Institution (WHOI), 1989, National Ocean Sciences Accelerator Mass Spectrometry Facility (NOSAMS), <http://www.nosams.whoi.edu/>, last accessed: 1 February, 2008.
- Yazıcıgil, H., Doyuran, V., Çamur, M.Z., Duru, U., Şakıyan, J., Yılmaz, K.K., Toprak, F.Ö., Pusatlı, T., 2001, Hydrogeology- Hydrogeochemistry Baseline Study of the Kazan Trona Project Area, Ankara, Turkey, Middle East Technical University, Project No: 00-0309-02-00-08, p 355.
- Yazıcıgil, H., Er, C., Sakiyan Ates, J., Camur, M.Z., 2007, Effects of Solution Mining on Groundwater Quality in the Kazan Trona Field, Ankara- Turkey: Model Predictions, submitted to *Environmental Geology*.
- Yılmaz, Y., Tüysüz, O., Gözübol, A.M., and Yiğitbaş, E., 1981, Abant (Bolu)-Dokurcun (Sakarya) Arasındaki Kuzey Anadolu Fay Zonunun Kuzey ve Güneyinde Kalan Tektonik Birimlerin Jeolojik Evrimi, *İ.Ü. Yerbilimleri*, 1, 239-261.
- Zimmermann,U., Münnich, K.O. and Roether, W., 1967, Downward Movement of Soil Moisture Traced by Means of Hydrogen Isotopes, *Isotope Techniques in the Hydrologic Cycle*, Geophysical Monograph Series 11, American Geophysical Union.

CURRICULUM VITAE

PERSONAL INFORMATION

Surname, Name: Arslan, Sebnem

Nationality: Turkish (TC)

Date and Place of birth: 1 November 1979, Ankara

Marital Status: Married

Phone: +90 535 468 68 02

Fax: +90 312 210 57 50

E-mail: sebnem_okten@yahoo.com

EDUCATION

Degree	Institution	Year of Graduation
MS	METU Geological Engineering	2004
BS	METU Geological Engineering	2001
High School	Yukselis College, Ankara	1996

WORK EXPERIENCE

Year	Place	Enrollment
2008- Present	Ministry of Environment and Forestry	Engineer
2001- 2008	METU Department of Geological Engineering	Research Assistant
2000 July	General Directorate of Rural Services	Intern Student
1999 July	General Directorate of Mineral Research & Exploration	Intern Student

FOREIGN LANGUAGES

Advanced English, Fair French, Poor German

PUBLICATIONS

Okten, S. & Yazicigil, H., 2005, Investigation of Safe and Sustainable Yields for the Sandy Complex aquifer system in the Ergene River Basin, Thrace Region, Turkey, Turkish Journal of Earth Sciences, Vol: 14, 209-226 p.

Okten, S. & Yazicigil, H., 2004, Investigation of safe and sustainable yields for a complex aquifer system in Turkey, A short paper published in the proceedings of the International Conference on FEM_MODFLOW, 313- 316 p.

HOBBIES

Swimming, Literature, Traveling, Photography